UNIVERSITÀ
DEGLI STUDI
FIRENZE

DOTTORATO DI RICERCA IN SCIENZE CHIMICHE

CICLO XXXI

COORDINATORE Prof. PIERO BAGLIONI

STUDY OF DYNAMIC AND STRUCTURAL PROPERTIES OF COMPLEX FLUIDS FOR GREEN APPLICATIONS: EFFECTS OF AMBIENT CONDITIONS AND NATURE OF SOLUTES

STUDIO DELLE PROPRIETÀ DINAMICHE E STRUTTURALI DI FLUIDI COMPLESSI PER APPLICAZIONI ECOLOGICHE: EFFETTO DELLE CONDIZIONI AMBIENTALI E DELLA NATURA DEI SOLUTI

Settore Scientifico Disciplinare CHIM/02

Dottorando
Dott. Filippo Sarri

Tutore
Prof. Pierandrea Lo Nostro

Coordinatore
Prof. Piero Baglioni

Anni 2015/2018

Abstract:

This research project focused on the study of different complex fluid systems, formulated by using green chemical compounds and designed for potentially more environmental-sustainable applications. The study was performed mainly from a rheological and structural perspective, because these are two strictly connected aspects in complex fluids systems. Moreover, rheology represents an important parameter in both many industrial processes and quality of final manufactured products.

In the context of the wider subject of complex fluid, the present study mainly deals with polymer solutions, surfactants solutions, carbonaceous suspensions, and glassy forming liquid. More precisely, the project can be divided into three sub-topics of research: the study of salt/co-solute effects on aqueous polysaccharide systems; the modification of rheological behaviours, thermal properties, and responsivity to electrical treatment induced by specific additives and observed in polysaccharide formulations; and the examination of salt effects on the molecular association of glycerol carbonate, a structured glassy forming liquid.

Firstly, a systematic study on the interactions between ten distinct anions or two different neutral co-solutes and three polysaccharides was carried on with the purpose of examining how specific salt can significantly affect biopolymers rheological and thermal properties. The three polysaccharides investigated at the begin are guar gum (GG), sodium alginate (SA) and sodium hyaluronate (SH), while the added salts or co-solutes belong to the following list: NaF, NaCl, NaBr, NaI, Na_2SO_4,

$NaClO_4$, NaSCN, Na_3PO_4, Na_2HPO_4, NaH_2PO_4, trehalose and urea. From an applicative point of view, the study was aimed at evaluating the control over viscosity of polysaccharide-based green formulations through simple salt triggers. The results were discussed in terms of changes in the polymer chains hydration, conformation and structure of the network. Since the SA based dispersions revealed low viscosity values and unchanged rheological behaviours in response to the salt addition, we drove our research towards a fourth polysaccharide that is hydroxypropyl cellulose (HPC) as a replacement for SA. Successively, the polysaccharide aqueous systems were tested in high salinity conditions, obtained through a mixture of monovalent and bivalent ions in different concentrations, in order to acquire info about their resistance in high-salinity environment.

In the second topic of research, the polysaccharide aqueous systems were more deeply investigated through the analysis of the effects induced by specific additives on their mechanical, thermal, anti-scale precipitation and electro-responsive properties. More precisely, among the investigated additives, sodium citrate and the two bio-surfactants saponins ad rhamnolipids were evaluated as agents capable of modifying viscosity and rheology of GG, SH and HPC dispersions. Carbon Black (CB) was studied as a multifunctional additive that increases the viscosities, enhances the thermal stabilities and provides electro-responsive features to SH, GG and HPC formulations. Polyglutamate and polyaspartate were evaluated as anti-scale agents, able to reduce the precipitation of scales, constituted by $CaSO_4$ or $SrSO_4$, and modify the crystalline

structure of the observed precipitate. The effectiveness of additive inclusion in the network, and their consequent capability of modifying the polysaccharide properties, were evaluated through rheology, optical microscopy, and conductivity measurements.

Finally, in the third topic of research, it was investigated the solubility of various potassium salts in glycerol carbonate (GC, 4-hydroxymethyl-1,3-dioxolan-2-one), a structured organic solvent. More specifically, this study focused on the specific ion capability of significantly affecting the solvent-solvent molecular interactions, of promoting considerable changes in both molecular association mechanism and glassy liquid-forming tendency. The chronicle of this investigation began with the peculiar features observed on GC solutions of KF in a wide concentration range, varying from 10^{-3} M up to the saturation threshold. Indeed, the progressive addition of the salt promotes the formation of a glassy liquid by the solvent molecules, whose arrangement was evaluated through conductivity, rheology, differential scanning calorimetry (DSC) and infrared spectroscopy experiments. Successively, the study was extended to other seven potassium salts (K_3PO_4, KOCN, K_2CO_3, KCl, K_2SO_4, KBr and KI) and their effects on the GC structure were evaluated through NMR, DSC, solubility and ATR-FTIR experiments. From the combination of the results related to the two parts of the study, a dual mechanism of solvation, based on the cation and anion combined actions, was described.

Contents

PREFACE

This thesis was submitted to the University of Florence as a requirement to obtain the PhD degree. The work presented in this thesis was carried out in the years 2015-2018 at CSGI laboratories, Chemistry Department "Ugo Schiff", University of Florence. Besides myself, Professor Pierandrea Lo Nostro, supervisor of my PhD, was involved in the project.

THESIS OBJECTIVES

The final aim of this project is the dynamic and structural characterization of different complex fluid systems, formulated with green chemical compounds for environmental-safe applications. The objectives of this work are summarized as follow:

1. Study of salt-induced modification on the rheological behaviour of polysaccharide aqueous dispersions: evaluation of resistance in high salinity conditions and specific salt effect as a potential trigger to modify the viscosity of the systems.
2. Evaluation of two bio-surfactants and one green crosslinker as viscosity modifying agents for biopolymer-based systems.
3. Reduction of the scale precipitation in aqueous polysaccharide systems.

4. Inclusion of carbon black in aqueous complex fluids in order to improve their rheological properties and thermal resistance.
5. Application of an electrical treatment as a strategy to obtain a remote control over the fluid viscosity.
6. Study of the specific ion effects on the molecular association and glassy liquid-forming ability of an organic solvent glycerol carbonate.

THESIS OUTLINE

This thesis can be divided in different chapters which cover the different aspects of the work carried out during the project. The topics will be described through the following sections, in the chronological order shown here:

Chapter 1: Introduction – the chapter provides the motivation of the study and the overall pictures of each examined material, focusing on their origin and main properties.

Chapter 2: Materials & Methods - in this section are collected the info about the chemicals used in the study, the sample preparation methods, and the experimental conditions adopted.

Chapter 3: Results 1, Salt effect on polysaccharide aqueous solutions and dispersions – This is the first chapter of results and concerns the salt-induced effect, both specific ion effect and mixture of salts, on the polysaccharide aqueous systems behaviour.

1 Introduction

This first Chapter introduces the motivation of this study, explaining why a dynamic and structural investigation on the complex fluids is of great interest in different application fields, where the demand for greener and more environmental-friendly formulations generates a continuously increasing interest. A brief overview on the different materials examined in the light of propose innovative and green formulation is given, by focusing on their biological origin, physico-chemical properties and potential application fields; finally, the main targets of this work are discussed.

1.1 Intent of the study

Complex fluids are fluid systems characterized by an internal microstructure whose evolution affects the macroscopic dynamics of the material, especially the rheology [1]. Examples include polymer solutions, glassy liquids, foams, electro- and magneto-responsive suspensions, liquid crystals, gels, particulate suspensions, emulsions, and surfactant solutions [2]. As listed above, a large class of materials falls under the label of 'complex fluid'. But what do all these fluids have in common? Complex fluids can be considered homogeneous at the macroscopic, or bulk, scale but are disordered at the microscopic scale, and possess structure at an intermediate scale. The most attracting feature of complex fluids is that they exhibit many useful mechanical properties stemming from the variety of these

structures [3]. Moreover, such materials often have great practical utility since the microstructure can be manipulated via processing of the flow in order to produce useful mechanical, thermal and/or responsive properties.

In the study of complex fluids, rheology plays a key role in the characterization of these systems since the macroscopic flow behaviour of complex fluids is a strong function of the fluid microstructure. Furthermore, the rheological properties of complex fluids are an important operating parameter in many industrial processes and often affect the quality of the final product. For examples, in the formulation of inks and paints it is important to control the viscosity and the rheological behaviour of the fluid, that has to be of a shear-thinning type so that it can easily flow [4]. In the food industry, the science of rheology has many applications such as those in the fields of food acceptability, food processing, and food handling: sectors in which complex fluids are widely used [5,6]. Rheology covers a central role also in the preparation of cosmetic products: toothpaste, creams, nail products, lotions, hair products, and deodorant are only some examples of daily consumer goods whose performances are strongly determined by their rheological properties [7]. Rheology is crucially important also in pharmaceutical applications since it directly affects the way a drug is formulated and developed, the quality of the raw and finished product, the drug efficacy, the way a patient adheres to the prescribed drug, and the overall healthcare cost [8]. In addition, rheology plays a key role also in the shale gas extraction, where control over the rheological properties and the opportunity of modifying the viscosity of the fracturing fluid

during the different phases of the process are required. Indeed, in the initial stages, the fracturing fluids used in the shale gas procedures have to be sufficiently viscous in order to effectively carry the proppant (suspended solid particles of sands, glass/ceramic beads or sintered bauxite) downhole, while they have to be as less viscous as possible in the successive steps related to the recovery of gas and fluids [9].

Within this broad context, this study represents a contribution in the investigation of polymer solutions, glassy liquids and electro-responsive suspensions targeted for green formulations effective in reducing the environmental footprint. Consequently, the selection of materials was driven by the use of green chemicals, possibly of biological origins, such as polysaccharides, biosurfactants, environmentally-safe compounds, and biodegradable additives. Furthermore, the present study evaluates various additives and methods in order to significantly modify the rheological properties of the examined systems. In the line of investigating and proposing complex fluid formulations potentially suitable for a set of various applications, efforts were made to cover a wide range of viscosity, examine different materials, and provide responsive behaviour, always looking at environmentally-sustainable systems.

Since this work concerns with the study and formulation of green complex fluids, it will be provided in the next paragraphs an overview on each used material in order to better describe its ‘green nature’ and main properties.

1.2 Polysaccharides and Biopolymers

1.2.1 Guar Gum

Guar gum (GG) is a polysaccharide extracted from the seeds of *Cyamopsis tetragonolobus*, an agricultural crop belonging to the Leguminosae family which it is mainly cultivated in arid zones such as India, Pakistan, Sudan, and dry areas of United States [10]. The extraction is a multistep process during which the seeds are at first dried, then they are subject to one or more grinding and sieving operations, and subsequently separated from the husks. The achieved de-husked guar splits finally undergo to flaking and milling proceedings, at the end of which the commonly used guar gum powder is obtained [10,11].
GG chemical structure is characterized by a mannose backbone on which are grafted galactose side groups in a mannose-to-galactose ratio (M:G) that is approximately equal to 2:1 [12]. The backbone consists in a linear chain of mannose unities linked through ß (1,4) glycosidic bonds, where the galactose moieties are 1,6-linked and form short side branch every two molecules of mannose (see Figure 1). If on one side the galactose side branches favour the hydration and solubility of GG in water, on the other hand they play against the building of a robust and resistant intermolecular association, which is established through interactions between the unsubstituted mannose backbone unities [13]. Indeed, the galactose distribution along the mannose linear chain is not homogeneous, consequently, the GG chains are divided in “smooth” and “hairy” region, respectively poor and rich in galactose side branches [14]. The capacities of GG to

raise the system viscosity and to create a stable network in water are primarily due to the polysaccharide high molecular weight and to the extensive intermolecular association. This association, which is also known as “hyperentanglement”, is driven by both intra- and intermolecular hydrogen bonding of the mannose unsubstituted molecules that constitute the smooth regions of the polysaccharide chains [15]. Thus, the balance between the aggregation tendency, due to the “smooth” unsubstituted mannose regions, and the high solubility in water, provided by the “hairy” domains rich in galactose side branches, makes guar gum a hydrocolloidal system [16].

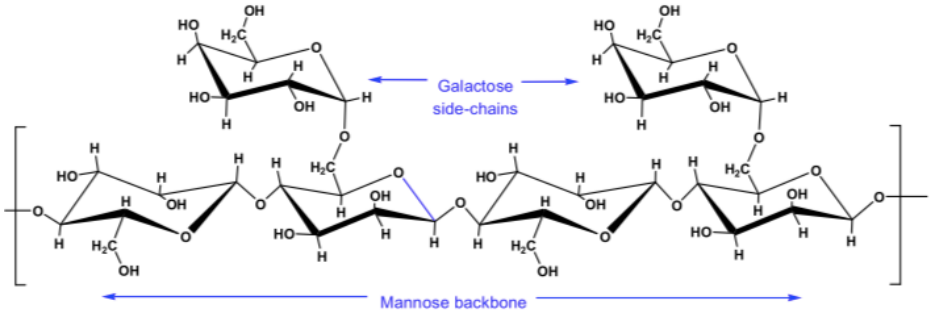

Figure 1: Guar gum chemical structure.

In the light of these properties, guar gum works well as thickening, emulsifying, and stabilizing agent. On the basis of such uses, GG finds application in many industrial sectors such as the food industry [17], animal feed [18], textile [19], cosmetics [20], pharmaceuticals [21], personal and health care [22,23], petroleum-contaminated water treatment [24], paper [25], mining [26], and oil & gas drills [27,28].

Moreover, thanks to its non-ionic nature, GG is substantially not affected by both pH and ionic strength; however, when temperature is raised up in parallel with a strong environment

acidification, the polysaccharide network degrades through a random scission process resulting in a system of lowered viscosity [29].

1.2.2 Sodium Hyaluronate

Sodium hyaluronate (SH) is the sodium salt of the hyaluronic acid, an anionic linear polysaccharide present in all body fluids and tissues, mainly epithelial, neural and connective ones, of higher animals like vertebrates and some bacteria [30]. Hyaluronic acid and sodium hyaluronate are often indicated with the more generic term hyaluronan which refers to both species, the acid and the conjugate base [31]. Hyaluronan belongs to the family of glycosaminoglycans, also known as mucopolysaccharides [32], which are long unbranched polysaccharides resulting from the repetition of disaccharide unities, usually consisting of an uronic acid and an amino sugar [33]. More specifically, in the case of sodium hyaluronate, the two saccharides involved in building the polymer chain are D-glucuronic acid and N-acetyl-D-glucosamine linked through ß (1,4) and ß (1,3) alternating glycosidic bonds, as it is shown in Figure 2 [34].

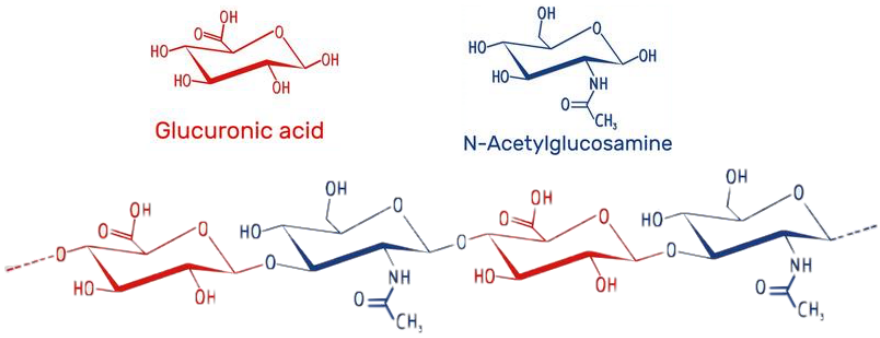

Figure 2: Hyaluronic acid disaccharide chemical structure.

Hyaluronic acid is biological synthesized in the plasma membrane by a membrane-bound class of proteins named hyaluronan synthase that, in the case of humans, gathers three enzymes identified by the acronym HAS1, HAS2, and HAS3 [35]. Each enzyme possesses different biological activity resulting in the synthesis of polysaccharide chains of various lengths and molecular weights. In details, HAS3 produced shorter chains of lower molecular mass, comprised between 10^5 - 10^6 Da; while, HS2 synthesis hyaluronan with the highest average molecular weight ($> 2 \cdot 10^6$ Da) [36]. In addition to the biological pathway, hyaluronic acid could be efficiently produced by microbial fermentation of specific bacterial strains, such as *Streptococcus* [37], or through a chemical synthesis, even if in the latter case it is possible to obtain only oligosaccharides up to ten sugar unities [38].

The industrial manufacturing of hyaluronan is carried out mainly through two processes: the extraction from waste tissues of animals and the fermentation brought about by cultures of specific microbial strains. However, the extraction technique is considerably affected by the hyaluronan degradation, which takes place as a consequence of the harsh extraction conditions

and the presence of endogenous hyaluronidase enzymes [39]. On the other hand, production of hyaluronic acid by bacterial fermentation exhibited constant significant progress in the last twenty years, as evidenced by the increasing numbers of publications on this topic [40–42]. Furthermore, a novel production technology, which allows a fine control over the length and molecular weight of the resulting hyaluronan chain, has recently been developed. More specifically, the strategy is based on the use of isolated hyaluronan synthase in order to catalyse the polymerization form the building sugars [43]. This third way, in addition to an easy modulation of the chain lengths, leads to the production of nearly monodisperse hyaluronan oligomers and polymers; however, in order to support a large industrial production, an upscale of the process is still missing [44].

When dissolved in water, hyaluronic acid assumes an expanded and stiffened random coil structure as a consequence of the disaccharide chemical structure, internal hydrogen bonds and the arising interactions between the solvent molecules and the hydrophilic patches of the chain. As a result of these features, hyaluronan attracts and retains significant amounts of water by binding water molecules through the large hydrophilic domains present along the chains, as shown in Figure 3 [45]. By trapping water molecules between the carboxylate and the aceto-amido groups, polymer chains expand their hydrodynamic volumes in a such way that hyaluronan individual molecules occupy essentially all the available solvent when the concentration reaches values around 3 mg/mL (0.3 wt.%) [46].

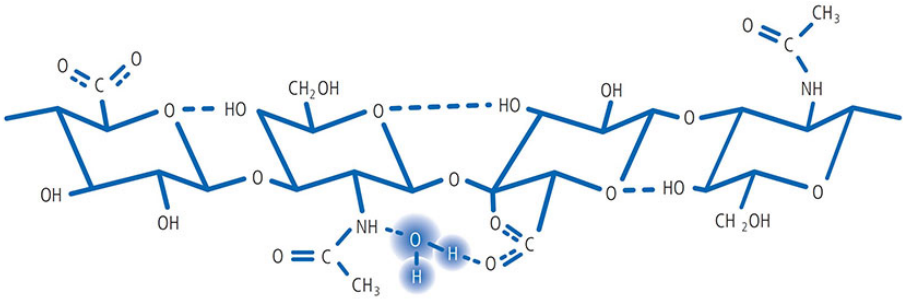

Figure 3: Hyaluronan binds water molecules thanks to its hydrophilic domains.

Hyaluronan chains in water can also move towards higher ordered structures, depending on parameters like temperature, pH, counterion type and hydration extent. Indeed, each disaccharide unity is twisted of about 180° with respect to the adjacent segments of the chain, as a consequence of the intramolecular hydrogen bonds arising from one saccharide with the next one: these hydrogen bonds, in addition to twisting the chain, impart higher stiffness to the network and create hydrophobic domains that favour the association between different hyaluronan chains [30]. The interaction between the hydrophobic patches is the driving force that makes possible the establishment of a stiff polymer network in spite of the negative charges present on the chains [47]. Therefore, the polymer coil can modify its conformation by adopting at first a single helix structure and, secondly, a higher ordered double-helix conformation, where the two single helices are antiparallel to each other as schematized in Figure 4 [48].

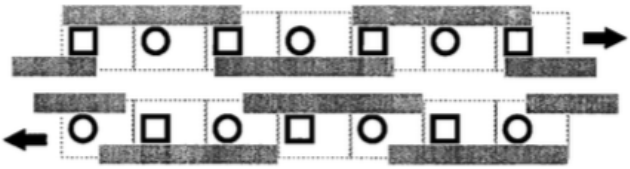

Figure 4: Double helix schematic representation of two hyaluronan chains: the dotted lines identify the areas of the different saccharides, the circles indicate aceto-amido groups, the squares represent carboxylate groups, and the rectangular grey bars depict the hydrophobic parts of the polysaccharide chains.

The strong affinity of hyaluronic acid towards water explains very well how this biopolymer plays important roles in the human body. Indeed, hyaluronan acts as a moisturizing agent able to keep collagen and eyes surfaces hydrated [49], even promoting both corneal and cartilage wounds healing [50,51]. In synovial fluid, hyaluronan contributes to lubricate, reduce the friction and absorb shocks in the joints [52]. Furthermore, hyaluronic acid is also abundant in the skin, where it plays a crucial role as a scavenger of free radicals derived from UV irradiation of the sun [53].

Although hyaluronan naturally occurs in human tissues and fluids, a flourishing biomedical and pharmaceutical market has developed from products based on this biopolymer. Indeed, hyaluronic acid mainly finds application in the fields of ophthalmology, both for eye care and surgery [54,55], rheumatology and orthopaedic surgery [56], dermatology and plastic surgery [57,58], otolaryngology [59], surgery and wounds healing [60], pharmacology and drug delivery [61].

1.2.3 Sodium Alginate

Sodium alginate (SA), frequently shortened to alginate, is the salt of the correspondent naturally occurrent polysaccharide, alginic acid. This biopolymer is mainly extracted from the cell walls of brown algae, a class of vegetal livings abundant in marine environments, especially along the shorelines of the Northern Hemisphere [62]. Furthermore, alginate is also present in some soil bacteria as capsular polysaccharide [63]. The biological function played by alginic acid in algae is primarily structural, in fact, the biopolymer imparts strength and flexibility to the cell walls where it is included [64].

Alginate chains are built up of two uronic acid residues, D-mannuronic (M) and L-guluronic (G) acids, which are linearly joined through ß (1,4) glycosidic linkages. As demonstrated in different papers [65–67], alginate does not possess a regular repeating unit and, consequently, the distribution of the two building monomers cannot be described through Bernoullian statistics. Indeed, the uronic unities do not follow a regular one-to-one pattern (i.e. -G-M-G-M-), rather, they tend to separate in M and G blocks along the chains, resulting in a linear copolymer characterized by the alternation of homopolymeric blocks, as it is shown in Figure 5 [68]. The proportion between the two building-blocks is usually indicated as MG ratio. This parameter can vary significantly depending on the specific vegetal or bacterial extraction source, the geographical location of a certain colony of algae, the season during which algae are harvested, and the age or type of different parts of the plants (new or old fronds, stipes, whole plants) [64]. The differences in chemical composition, considered in terms of MG ratio, are reflected in altered physical properties of the various alginates. Indeed, it was

demonstrated that the mannuronic to guluronic ration affects the alginates gel-forming ability [69], the ion exchange properties [70], and the tendency to dissociate in acid conditions [71].

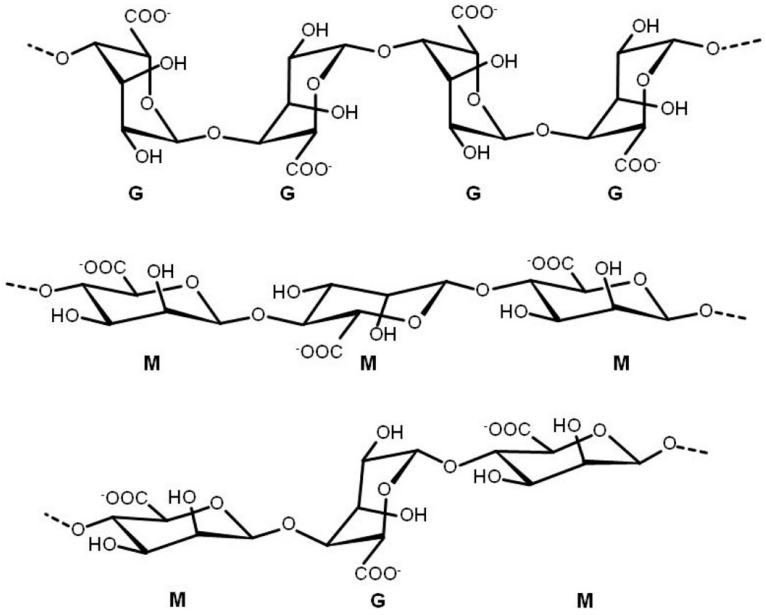

Figure 5: Sodium alginate chemical structure in different copolymer sequences.

The manufacture of sodium alginate starts from the alginic salts present in the algae cell walls and is aimed at the extraction of a dry powder. The manufacture can follow two distinct pathways, as resumed in Figure 6. The first one is based on the addition of a mineral acid (0.1-0.2 M), which lead to the formation of the insoluble alginic acid that is separated as a soft gel and partially dehydrated. Afterward, alcohol is added to alginic acid and, in a second step, the solution is neutralized through the addition of sodium carbonate. The carbonate converts alginic acid into the sodium salt and, since sodium alginate is insoluble in water/alcohol mixture, it can be removed from the mixture, dried and milled. The second strategy of recovering SA dry powder consists of the addition of calcium salt

to the initial extraction solution, in order to obtain a fibrous and insoluble texture of calcium alginate. Calcium alginate is suspended in water and converted to alginic acid by the addition of acid. At this point, alginic acid is easily separated and mixed, as in the previous extraction method, with alcohol and successively with sodium carbonate. The result of this process is the obtainment of a paste that is usually extruded in pellets, dried and milled [72].

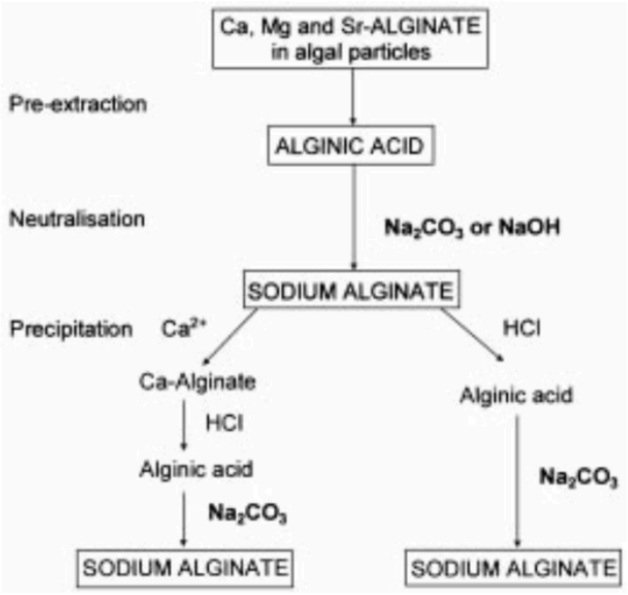

Figure 6: Schematized sodium alginate principal manufacturing processes

As mentioned before, the physical properties of alginates derived from different sources are strictly dependent on the polysaccharide chemical structure, or better on the MG ratio and on the spatial distribution of the G and M blocks. Nevertheless, it is possible to recognize some peculiar and characteristic properties that all the alginates possess in general terms, even if

each specific alginic sample can exhibit them in a more or less marked way.

Probably, the most interesting property of sodium alginate is the ability to form biocompatible hydrogels that find applications in really different fields, such as the biomedicine and the food industry. The most common and applied method to prepare alginate hydrogels is through the addition of divalent cations that, in the case of this biopolymer, play the role of effective crosslinking agents [73]. The concentration of divalent cation needed to form the gel depends on the ion introduced in the alginate water solution and affects the hydrogel stability and stiffness. More specifically, the required concentration of divalent ion to bring about gel formation increases following the series:

$$Ba < Pb < Cu < Sr < Cd < Ca < Zn < Ni < Co < Mn, Fe < Mg$$

The above series reflects the sensibility of alginate chains towards the gel formation in the presence of various divalent cation, however, it cannot be interpreted as an order of stability of the crosslinked species or as the biopolymer selectivity towards the specific ion [74]. The interactions established between alginate chains and divalent cations have been deeply investigated as it is demonstrated by a large number of publications in the literature [69,70,74,75]. The tendency to form a stable and stiff gel is due to the strong affinity of guluronic groups towards the divalent cations; whereas, mannuronic residues do not coordinate the ions with the same intensity [76]. Indeed, when two or more guluronate unities are close to each other, the alginate chain creates a pocket where the divalent ions are trapped by

interactions with the -COO^- and -OH groups of the G blocks, as evidenced in Figure 7. Moreover, the binding capacity of the alginate chains is cooperative, which means that the linkage of each ion prearranges the adjacent interactions pockets and facilitates the binding of the next ion [77]. According to the most reliable model that explains the divalent cation-alginate interactions, also known as "egg-box" model (see Figure 7), the coordinated divalent cation not only promotes the coordination of other ions by the next G blocks along the chains, but also attracts a second polysaccharide chain that contributes to create a two-filament array that encloses the ion between two chains [78].

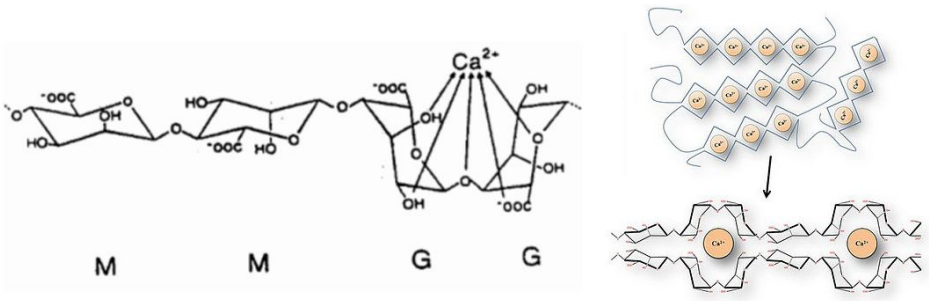

Figure 7: The egg-box model explains how Ca^{2+} ion is bonded by two guluronate bocks of different alginate chains.

However, ionically cross-linked alginates do not possess long-term stability in physiological conditions, because of ion exchange reactions that can take place and remove divalent cations from the availability of the guluronate residues [79]. When it is necessary to impart a greater stability to alginate networks, a covalent crosslinking is usually preferred; however, the reagents used in covalent crosslinking are often toxic and a further step consisting of the removal of the unreacted chemicals must be considered [73]. The mainly investigated crosslinking

agents to obtain covalent alginate networks are poly(ethylene glycol)-diamines of various molecular weights[80] and multi-functional cross-linking molecules such as poly(acrylamide-co-hydrazide) (PAH) or adipic acid dihydrazide (AAD) [81].
An alternative and fascinating route to obtain a crosslinked alginate gel is the use of a light sensitizer that can initiate the crosslinking reaction after the exposure to the appropriate light irradiation. This approach is of particular interest in the field of tissue engineering, as it is demonstrated by the papers present in literature where it is described the photo-crosslinking of methacrylate chemically modified-alginate through argon ion laser irradiation [82].
Due to its ability in absorbing water and forming hydrogels, sodium alginate finds application in various industrial sectors like the food industry, where it is known as additive E401 and it is mainly used as a protecting-film creator and thickening agent [83]; the production of paints and textile printing, where alginate plays the role of non-toxic thickening additive [84,85]; the biomedical area, where alginate represents a promising material in tissue engineering and wound dressing; the pharmaceutical industry, as film forming agent for the prevention of gastro-oesophageal reflux [86] or as a drug/protein delivery [73]; and the agriculture, where alginate hydrogels are used as releasing system able to nourish and protect plants [87,88].

1.2.4 Hydroxypropyl Cellulose

Hydroxypropyl cellulose (HPC) is a non-ionic derivative of cellulose that is usually synthesized through the reaction of a

cellulosic substrate, extracted from cotton and plants, with propylene oxide in alkaline ambient: the result is a cellulose backbone on which lateral chains containing a variable number of hydroxypropyl moieties are attached. Alternatively, cellulose substrate may be obtained through a bottom-up approach consisting of the synthesis from bacterial culture [89]. Since it is one of the main components of cell walls in the higher plants, cellulose is one of the most abundant raw natural material with an annual production that exceeds the 10^{11} tons [90]. Furthermore, cellulose attracts broad interest because it is cheap, biodegradable and renewable [91]. The molecular structure of cellulose and its derivatives is characterized by a linear homopolymer backbone consisting of ß (1,4) glycosidic linked D-glucose units, which are also called anhydroglucose units (see Figure 8).

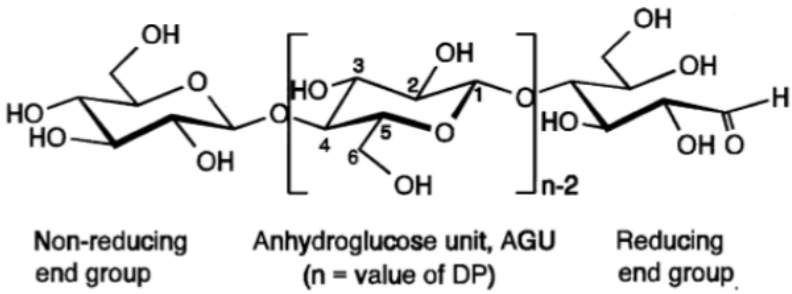

Figure 8: Cellulose chain chemical structure (n is the degree of polymerization, DP).

As a consequence of this linkages, the cellulose chain results in an alternate turning of 180° around its axis; thus, the repeating unit constituting the backbone is often considered as the combination of two anhydroglucose moieties and is called cellobiose [92]. The biopolymer exposes three reactive hydroxyl groups, two secondary and one primary at the positions C-2, C-

3 and C-6 respectively. These hydroxyl groups are accessible to substitution reactions that chemically modify the cellulose structure, leading to derivates with different physicochemical properties [93].

The linear conformation of the cellulose, combined with a large number of available hydroxyl groups, allows the reciprocal approach among the various polysaccharide chains and the establishment of both intra- and inter-chain hydrogen bonds, as schematized in Figure 9. Thus, these features create the opportune conditions thanks to which an extensive hydrogen bond network is built up, resulting in a structure of high cohesive energy [94]. Therefore, cellulose chains possess a very high tendency to self-order in different structural levels: at first the chains tend to organize in parallel arrangements, characterized by domains with varying order degree, called fibrils [95]; then, moving to an upper order level, the fibrils, in turn, organize themselves in higher structures consisting in pattern of layer of different density and texture [92].

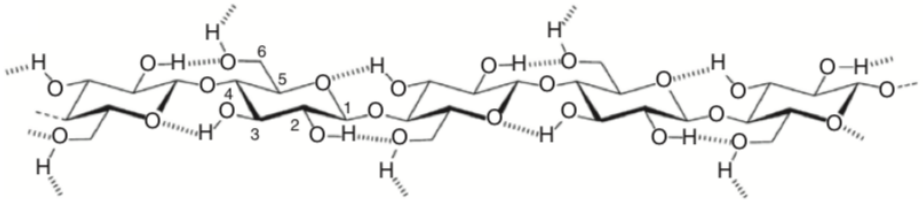

Figure 9: Hydrogen bond pattern of a singular cellulose chain.

The average oxygen number of the pristine cellulose repeating unit (i.e., glucose molecule) substituted by lateral groups is referred to as the degree of substitution (DS), and when a complete functionalization takes place this parameter reaches the value of 3 [96]. Moreover, in the case of HPC, the added

hydroxypropyl groups possess hydroxyl moieties that can undergo further substitution reaction, leading to the formation of etherified hydroxypropyl cellulose with extended lateral ramifications, as evidenced in Figure 10 [97]. However, the high cohesion exhibited by the fibrillar elements, that in turn constitute the cellulose fibres, markedly affects the accessibility and the chemical reactivity of the hydroxyl groups involved in substitution reactions [94]. Therefore, the cellulose tendency to associate in fibres plays against a complete substitution (DS=3) of the pristine chain. In addition, it must be considered that the reactions in which the hydroxyl groups are involved take place in heterogeneous conditions caused by the steric hindrances of the reacting agents and by the cellulose supramolecular structure [98]. The result of these heterogeneous conditions is similar to a chain made up of block copolymers. More precisely, the resulting polysaccharide is characterized by the alternation of anhydroglucose unities with different DS. Thus, the substituted chain exhibits domains that both carry no substituent and moieties totally substituted [94].

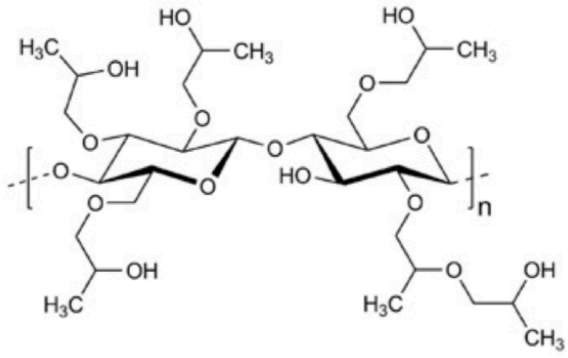

Figure 10: Schematic figure of hydroxypropyl cellulose with an averaged DS of 2.5.

Despite the substitution rarely reaches a DS of 3, the introduction of side hydroxypropyl groups is able to significantly affect the physicochemical properties of the cellulosic chains, even if the chemical modification is partial and heterogeneous. The main difference between the HPC and the unmodified cellulose is the solubility in water and organic solvents. Indeed, the pristine polysaccharide is insoluble in water and in many organic solvents, while it is soluble in water at extreme pHs, in ionic liquids and in solvents of 'intermediate properties' like N-methylmorpholine N-oxide [99]. This high insolubility of cellulose is ascribable to both the strong intermolecular hydrogen bonds and the hydrophobic interactions between cellulosic chains. The introduction of lateral hydroxypropyl moieties provides domains that weakens the interchain hydrophobic interactions and can be partially hydrated, despite their hydrophobic nature [100]. As a result of the substitution, the cellulosic backbone solubility is increased, and the macromolecule can be dissolved in water if the DS reaches the opportune grade [96]. Notwithstanding the hydroxyl groups impart a stronger hydrophilic behaviour to the cellulose backbone, the HPC chains show good solubility in water only under a certain temperature threshold, usually indicated as cloud point or lower critical solution temperature. Indeed, below this critical temperature the HPC chains hydrate and assume an expanded and solubilized structure; whereas, above this threshold, the polysaccharide chains dehydrate and collapse in shrunken insoluble structures [101]. Thus, when a solution of HPC is heated the lateral hydroxypropyl groups progressively lose the water molecules involved in their hydration and, consequently, the hydrophobic associations between cellulosic

backbones become favoured, leading to a contraction of the polymer network. The transition is often indicated as cloud point because the transparent solution becomes opaque when the temperature threshold is exceeded and, for this reason, is often examined through turbidimetry or optical absorbance methods [102]. In addition, it is important to stress that this threshold temperature is not fixed for all the hydroxypropyl cellulose water solution, but rather it is affected by the biopolymer specific polymorph and its concentration and can range between 36 and 65 °C as it is reported in the literature [96,103,104]. Moreover, it is possible to change the hydrophilic/hydrophobic balance and tune the LCST value of the HPC by including a co-monomer: if a hydrophilic co-monomer is incorporated the LCST is increased, whereas the inclusion of a hydrophobic one leads to a lower threshold value for the cloud point [105]. However, the features probably most captivating is that this phase transition is completely reversible because it is mainly due to a balance between hydrogen bonds and hydrophobic interactions that are promoted or inhibited by a temperature variation [106]. Thus, HPC attracted large interest for its possible applications as thermo-responsive macromolecule that, in comparison with the commonly synthesized polymers, has the advantage of been approved by the United States Food and Drug Administration [107]. The thermo-responsive behaviour of HPC mainly finds application in the biomedical field for the drug and gene delivery [108,109] or in the regenerative medicine sector [110].

Another peculiarity of HPC is the tendency to form lyotropic mesophases in highly concentrated water solutions, which exhibit a liquid crystalline behaviour and an iridescent range of colours.

This feature was accidentally discovered in the 1970s by Werbowyj and Gray when “a drop of fairly concentrated aqueous hydroxypropyl cellulose solution was placed between glass plates, and the water allowed to evaporate from the outer edges of the drop” [111]. The two scientists observed how HPC in solution, in concentrations ranging from 20% to 50 %, organizes itself in a lyotropic mesophase with a birefringent cholesteric (chiral nematic) structure. The formation of lyotropic liquid-crystalline phases by amphiphilic molecules is a well-known topic and it is possible to think to hydroxypropyl cellulose in the same light [111,112]. Indeed, as previously discussed HPC possesses both a hydrophilic and a hydrophobic character; thus, we can consider this cellulosic derivative as an amphiphilic molecule. The explanation provided by Webowyj and Gray is confirmed by successive scientific publications. In fact, aqueous solutions of HPC are isotropic at low polymer concentrations but, when the concentration is raised up, the lateral hydrophobic hydroxypropyl moieties promote the association in rigid rod-like micro-fibrils that, in turn, constitute the supra-molecular structure made up by stiff rod-like fragments linked through flexible polymer connections. [113,114]. Thus, when the polymer concentration is further increased, the rod-like fragments become more densely packed and tend to align parallel to each other, forming n this way a liquid crystal mesophase [115]. The liquid crystalline properties of HPC opened new prospects for potential applications of this cellulosic derivative in the preparation of film and fibres of high-modulus/high-strength comparable with the Kevlar fibre [116]. While on the one hand Kevlar performances are still far to be reached, on the other side HPC have already

been used for its film-forming capacity in different application such as, for examples, the cutaneous time-delayed drug release (both for oral ingestion and cutaneous administration) [117], products for the oral mucosal ulceration healing [118], or the production of ophthalmic inserts for the dry-eyes treatment [119]. In addition, thanks to its capacity to build up stiff and resistant polymer networks, HPC also finds application as a stabilizing and thickening agent in the food industry, where it is also known as additive E463 [120]; in the cosmetic industry, mainly as an oil-in-water emulsion stabilizing agent [121]; and as a consolidant in the textile and paper conservation [122,123].

1.3 Glycerol Carbonate

Glycerol carbonate (GC), also known in the IUPAC nomenclature as 4-hydroxymethyl-1,3-dioxolan-2-one, is a viscous, dense and water-soluble organic solvent, whose chemical structure consists in a five members dioxolane ring where both a carbonyl group and a hydroxyl pendant moiety are present (see Figure 11).

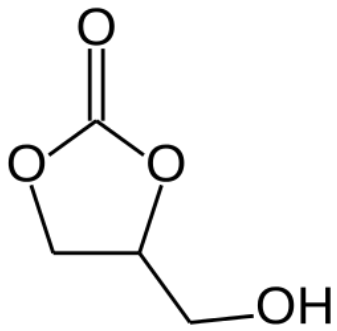

Figure 11: Glycerol carbonate chemical structure.

This organic solvent gained a lot of interest over the last two decades, and today the attention is still considerably increasing. The reasons behind this new attention and focus are ascribable to two main features: the wide reactivity of GC, that provides numerous possible applications, and the need to valorize glycerol, which is an over-supplied by-product in the bio-diesel production [124,125]. Indeed, glycerol can be used as a substrate for the synthesis of value-added glycerol derivates, such as glycerol carbonate, as it is widely documented in the literature [126,127]. More precisely, GC can be synthesized from different routes by using glycerol as the starting substrate and chemicals such as CO/O_2, organic carbonate, urea or carbon dioxide as carbonate source. Among the routes for GC synthesis, transesterification of glycerol with dimethyl carbonate (DMC) is one of the industrial most feasible pathways to produce GC in high yield [128]. At the moment, the only drawback that limits the GC production is the highly cost related to this process, as attested by the elevated market price around the 8141 US$/ton [124]. As a consequence, the use of GC in commercial applications has still not achieved a wide diffusion and, at the same time, major efforts of the scientific community have been devoted to reducing the production costs and enhancing the yields [129,130]. Thus, only few articles on the GC physicochemical properties have appeared in the literature in comparison to larger number of publications focused on innovative synthetic routes for the production of GC [131–133].

GC is characterized by high values of dielectric constant (ε = 109.7) and dipole moment (5.05 D), which make it an interesting solvent for electrolytes capable of promoting the electrolyte-

solvent interactions [134]. In addition, GC possesses a high boiling point (110–115 °C at 0.1 mmHg), an elevated flash point (190 °C) and low volatility (vapor pressure is 8 mbar at 177 °C), resulting in this way a potential low Volatile Organic Compound (VOC) solvents for many applications where bio-based alternatives to organic solvents are currently demanded [125].

Similarly to other cyclic carbonates such as ethylene and propylene carbonates, GC is an associated liquid that establishes strong intermolecular interactions, predominantly through hydrogen bonding and van der Waals forces. These interactions impart to GC a marked tendency to form the so-called glassy liquids, which are systems showing distinctly non-liquid like features and a soft glassy rheology [135].

As mentioned before, one of the peculiar features thanks to which GC gained interest is its wide reactivity due to the presence, on the same small molecule, of two reactive sites such as a primary hydroxyl group and a 2-oxo-1,3-dioxolane (ODO) group [125,128]. The consequence of this particular chemical structure is that GC has both one nucleophilic and three electrophilic sites, which are the oxygen atom of the hydroxyl group and the carbonyl carbon plus the two alkylene carbons of the ODO group, respectively [136]. Thanks to this rich reactivity, GC could play the role of bio-based building block in the synthesis of more complex chemicals in organic chemistry, acting both as nucleophile or electrophile (see Figure 12).

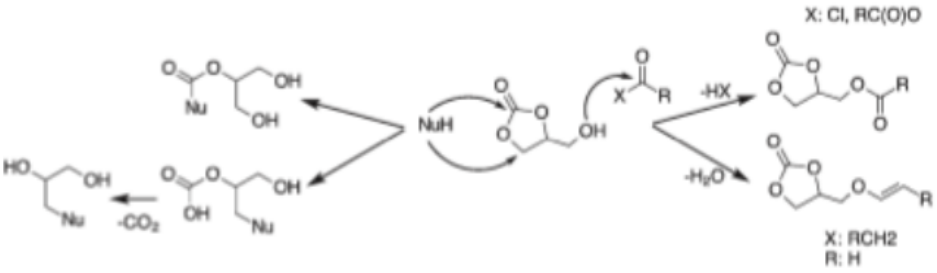

Figure 12: Reactivity of GC as a nucleophile or as an electrophile.

Indeed, the ODO group may be involved in reactions with various nucleophiles: aromatic and aliphatic alcohols, aromatic and aliphatic amines, carboxylic acids, ketone and isocyanates [126–128,137]. On the other hand, the hydroxyl group of glycerol carbonate enables the molecule to be linked with others without degrading the ODO group, providing in this way a strategy for introducing ODO functionality into a new molecule. However, chemicals and conditions have to be thoroughly selected because the ODO group may cause unwanted secondary reactions. Indeed, both functional groups can react with the same chemicals and under the same conditions. Selectivity towards one functional group or another is therefore a major concern in the case of glycerol carbonate reactivity [125].

As outlined before, the high cost of GC is still the crucial factor that limit its commercial usage, which currently do not exceed the worldwide threshold of few kt for year [124]. However, GC possesses really interesting properties that are between those of glycerol and those of the cyclic alkylene carbonates; therefore, it is proposed as a promising bio-based alternative in both indirect and direct applications. GC is attracting an ever-increasing interest in various application fields, as schematized in Figure

13, and may play a central role in the near future for the industrial-scale production of solvents, lubricants and surfactants from renewable carbon sources [138]. For example, GC is drawing attention for its wide window of applicability as electrolytes liquid carrier in lithium and lithium-ion batteries, where non-volatility and non-flammability of solvent are crucial features [139]. As a solvent, GC could find application also in NMR analysis, in the realization of soluble enzymatic systems, in ionic liquids for the fructose dehydration, or in other general purposes thanks to its peculiar properties [138,140,141]. Other potential applications involve GC as curing agent in cement and concrete industries, for the realization of self-compacting concrete [142]; as emulsifier, plasticizer, nail lacquer gel remover and humectant in cosmetic products [125]; as blowing agent or the realization of polyurethane foams [143]; as a gas separator (CO_2 from N_2) immobilized on liquid membranes [144]; as glycerol precursor in detergent formulations and as plant vitalizer [125].

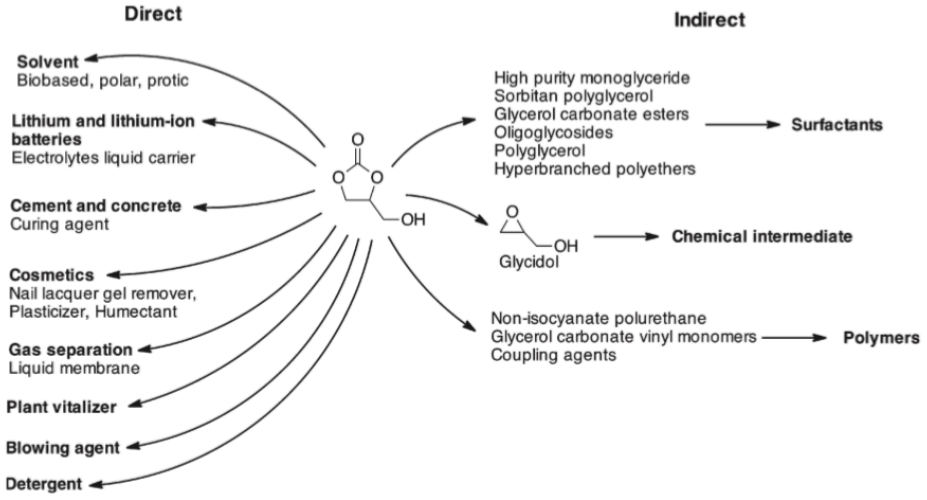

Figure 13: Direct and indirect applications of GC.

1.4 Additives

1.4.1 Saponins

Saponins are naturally occurring amphiphilic compounds that belong to the chemical class of the glycosides and whose name is due to their botanical origin and, specifically, to the soapwort plant Saponaria officinalis. When an aqueous solution of saponins, which are abundant in the roots of Saponaria officinalis, is shaken a soap-like effect is obtained; indeed, Saponaria was historically used to prepare soap [145]. As amphiphilic molecules saponins possess both hydrophilic domains, constituted by one or more carbohydrate chains, and hydrophobic moieties made up by a triterpenoid or steroid units, which are usually called aglycone or sapogenin units [146]. As a consequence, saponins are listed in two different classes usually referred to as triterpenoid and steroid (or saraponins) saponins, depending on the specific aglycone part (Figure 14).

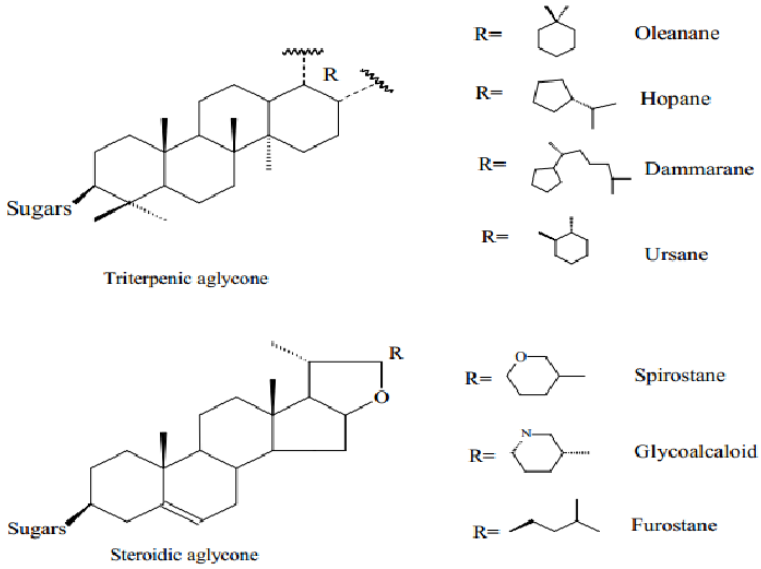

Figure 14: Triterpenic and steroidic structures of saponin aglycone (sapogenin) parts.

Moreover, depending on the number of saccharide chains linked to the aglycone part, saponins are further divided in monodesmoside/bidesmoside and so on when, respectively, one/two or more chains are attached to the hydrophobic sapogenin core. In addition, saponins can differ from each other in term of saccharide chain lengths and type of sugar unities, which constitute the chains. However, among the different possible classes, the in nature most frequently found saponins are constituted by D-glucose and D-galactose moieties and their saccharide chains usually range between 2 and 5 sugar unities [147]. Quillaja saponin, an example of a typical triterpene saponin molecule is shown in Figure 15 in the twelve most commonly found species.

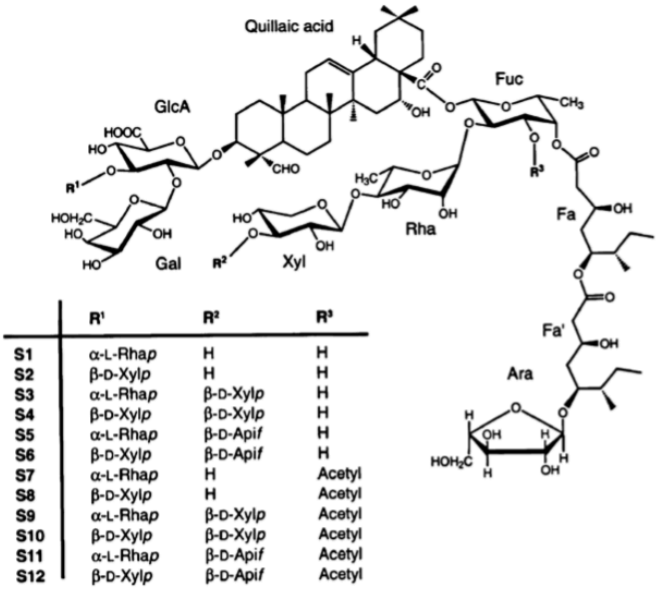

	R¹	R²	R³
S1	α-L-Rha*p*	H	H
S2	β-D-Xyl*p*	H	H
S3	α-L-Rha*p*	β-D-Xyl*p*	H
S4	β-D-Xyl*p*	β-D-Xyl*p*	H
S5	α-L-Rha*p*	β-D-Api*f*	H
S6	β-D-Xyl*p*	β-D-Api*f*	H
S7	α-L-Rha*p*	H	Acetyl
S8	β-D-Xyl*p*	H	Acetyl
S9	α-L-Rha*p*	β-D-Xyl*p*	Acetyl
S10	β-D-Xyl*p*	β-D-Xyl*p*	Acetyl
S11	α-L-Rha*p*	β-D-Api*f*	Acetyl
S12	β-D-Xyl*p*	β-D-Api*f*	Acetyl

Figure 15: Chemical structure of bidesmoside triterpenoid saponins, Quillaja saponins.

As a consequence of their complex and variable chemical structure, saponins are characterized by different physical, chemical and biological properties. In addition, among these properties, only a few are commonly shared by all the molecules belonging to this class. In spite of these differences, all the saponin species are surface-active compounds due to their amphiphilic nature characterized by similar behaviours as detergent, emulsifying, wetting and foaming agents [148,149]. Similarly to classic surfactants, saponins in aqueous solution tend to form micelles, which sizes and structures are dependent on the specific saponin class involved [150]. In some particular cases, as for Quillaja saponins (Figure 15), the critical micelle concentration and the aggregation number can be affected by ambient conditions like temperature, type of salts and their concentrations, and pH of the aqueous phase [151]. In addition

to the effects caused by a variation in the ambient conditions, properties and activities of saponins result altered by chemical modification occurring to the pristine compounds. Indeed, saponins are characterized by a complex structure that may undergo chemical reactions during the storage and processing phases, resulting in compounds of modified physico-chemical and biological properties. More precisely, both the glycosidic bonds, between aglycone core and the sugar chains, and the interglycosidic bonds, between the sugar unities within the same chain, can undergo hydrolysis in the presence of alkali/acids, which is in turn promoted by thermic effect (hydrothermolysis) or by enzymatic/microbial activity [147].

Saponins possess a wide range of biological activities that are linked to the broad variety of this class of compounds. Thus, in order to evaluate and investigate the specific biological behaviours of the different saponins, it is crucial to extract and isolate the single various species. [152]. Among these different activities, one of the most investigated and crosswise owned is the haemolysis activity, which consists of a rupture of the red blood cells (erythrocytes) membranes and the consequent release of their contents [153,154]. The mechanism through which saponins induce haemolysis in erythrocytes is not yet fully comprehended nowadays; nevertheless, it was demonstrated that the aglycone core is the part responsible for the haemolytic rupture, while the sugar hydrophilic moieties seem to play against this process [155,156]. Among the proposed mechanisms, the most plausible one consists in a two steps process: at first the saponin molecule adsorbs on the erythrocyte membrane through its hydrophobic sapogenin core, secondly, an enzyme-driven

(glycosidase) hydrolysis of the sugar chains takes place [157]. Indeed, this theory well explains why saponins characterized by the highest haemolytic activity are usually found bound to the red blood cells membranes and deprived of their carbohydrate chains. On the other hand, the above theory is lacking in clarifications about some cases where the saponins molecules showed a greater activity than the corresponding aglycone cores. This finding suggested the hypothesis that a second parallel haemolytic mechanism, probably linked to a reduction of the saponin surface activity, occurs in these cases [157].

In light of their haemolytic activity, saponins were historically classified as a toxic and considered as an 'anti-nutritional factors' [158]. However, this class of molecules results toxic for humans and other warm-blooded animals only if they are intravenously administered, while they show a low absorbance and reduced, or even negligible, haemolytic activity after oral assumption [150,152]. At the same time the saponin toxicity towards insects (insecticidal activity), parasite worms (anthelmintic activity), fish (piscidal activity), molluscs (antimolluscicidal activity), and their antifungal, antibacterial, antiviral activities are widely documented in literature [159–161].

Nevertheless, some recent researches have highlighted that saponins are the active components in many medicines of herbal origin and contribute to providing health benefits by the assumption through foods such as garlic or soybeans [162–164]. As a result, food and non-food sources of saponins have come into renewed light over the last years, primarily thanks to increasing evidence of their health benefits such as anticancer properties and a cholesterol-lowering effect [165,166]. Indeed,

saponins can significantly lower the cholesterol level by binding themselves in insoluble complexes with bile, which in turn is produced by the body with the use of cholesterol. In this way, the complexes are excreted, preventing the re-adsorption of bile back into the bloodstream [146]. Furthermore, it was observed by Matsuura that some saponins derived from garlic selectively bind the LDL cholesterol, commonly known as "bad" cholesterol, without affecting the HDL cholesterol levels [163].

The affinity of saponins towards cholesterol also provides anticancer properties which make them a potential candidate for the development of new anticancer drugs applicable both for the chemoprevention and chemotherapy, as in the case of ginseng sapogenins [152]. In particular, saponins may act on the cancer cell membranes, which are constituted by cholesterol-type compounds, as toxin able to slow down the growth of the cells or even induce their death [167,168].

As a consequence of the abovementioned antifungal and antimicrobial activities, saponins reveal to be effective also in boosting the immune system by fighting some harmful organisms such as the *Candida albicans* fungus and oral pathogens [169,170]. Other pharmaceutical/health applications that involve saponins are focused on the prevention and treatment of inflammations [171], infections [172], alcoholism [173], dementia [174], cardiovascular and cerebrovascular diseases related to coronary and hypertension [175], gastritis and gastric or duodenal ulcers [176]. Moreover, saponins are added as adjuvants to pharmaceutical formulations in order to enhance the absorption of pharmacologically active substances or drug [177,178].

Thanks to their surface-active properties, saponins are also utilized as natural surfactants in cosmetic formulations of cleansing and personal care products such as shampoos, liquid soaps/detergents, toothpaste, mouthwashes and baby care products [152,179,180]. In addition, saponins and their aglycone cores are marked as bioactive compounds in cosmetic formulations applied to prevent the acne and to delay the ageing-effect on the skin [181–183].

Finally, saponins find applications also in the food industry, especially the Quillaja, Liquorice and Yucca varieties that are classified as a food additive (as "Natural flavouring substances and natural substances used in conjunction with flavours") by the US Food and Drug Administration [107]. Indeed, quillaja saponins are mainly used as foaming agents in food and beverages or as emulsifying agents for lipophilic dye in the formulations of soft drinks; while, liquorice saponins are ingredients of beverages and food like candy, chewing gum, baked products, and mineral/vitamin dietary supplements [152]. Other saponins that are frequently present in foods are those derived from the soybean and the ginseng [152]. Moreover, due to their physico-chemical properties saponins are utilized in food processing applications. Indeed, the formation of complexes between saponins and cholesterol results to be useful in the removal of cholesterol from butter oil and dairy products [184,185], while the affinity of saponins towards the fat globule membranes is used to precipitate the cheese whey by increasing the hydrophobicity of the membranes and consequently facilitating the flocculation [186].

1.4.2 Rhamnolipids

Rhamnolipids belong to one of the most known classes of biosurfactants called glycolipids, which consist in carbohydrate unities linked to long-chain aliphatic or hydroxy aliphatic acids [187]. Rhamnolipids can rightfully be considered as a surfactant, indeed they possess rhamnose sugar moieties as hydrophilic head linked to the fatty acid chains, which in turn play the role of hydrophobic tails. More specifically, there are two main sub-classes of rhamnolipids, mono- and di-rhamnolipids which are constituted by one or two rhamnose moieties, respectively. [188]. In addition, the hydrophobic part of this biosurfactant can be composed by one or even two fatty acid chains of different lengths. Thus, just as can be conceivable, a wide diversity of rhamnolipids congeners and homologues exist in nature and, thanks to the development of more sensitive analytical techniques and more selective isolation procedures, about 60 distinct species were identified up to date [189]. Rhamnolipids were historically discovered by Bergström et al. in 1946, when they published two papers about an oily glycolipid produced by the Pseudomonas pyocyanea (now Pseudomonas aeruginosa), a rod-shaped pathogen bacterium that causes diseases in plants and animals, including humans [190,191]. The structure of this glycolipid, initially named as pyolipic acid, was successively identified as the combination of L-rhamnose and ß-hydroxydecanoic acid units. More precisely, Jarvis and Johnson provided a detailed description of the glycolipid structure, which results in two rhamnose moieties linked by 1,3-glycosidic bond to two ß-hydroxydecanoic acids, which are, in turn, linked

between themselves through an ester bond [192]. In subsequent decades, three additional congeners of Pseudomonas aeruginosa rhamnolipids were isolated: at first it was observed a kind of precursor, made up by a single rhamnose unit, of the initially discovered rhamnolipid [193]; afterwards, Syldatk et al. found two different species of mono- and do-rhamnolipids constituted by a single ß-hydroxydecanoic side chain [194]. Nevertheless, these two mono-lipidic congeners are usually produced in lower quantities in comparison with the di-lipidic ones. Indeed, as it was reported by Arino et al., the composition of rhamnolipid congeners produced by a P. aeruginosa batch culture approximately follows the sequent ratio: 67% di-rhamno- di-lipid (RL3), 22% mono-rhamno-di-lipid (RL1), 9% di-rhamno-mono-lipid (RL4), and less than 3% of mono-rhamno-mono-lipid (RL1) [195]. In Figure 16 are shown the four different congeners of rhamnolipid produced by Pseudomonas aeruginosa bacterium.

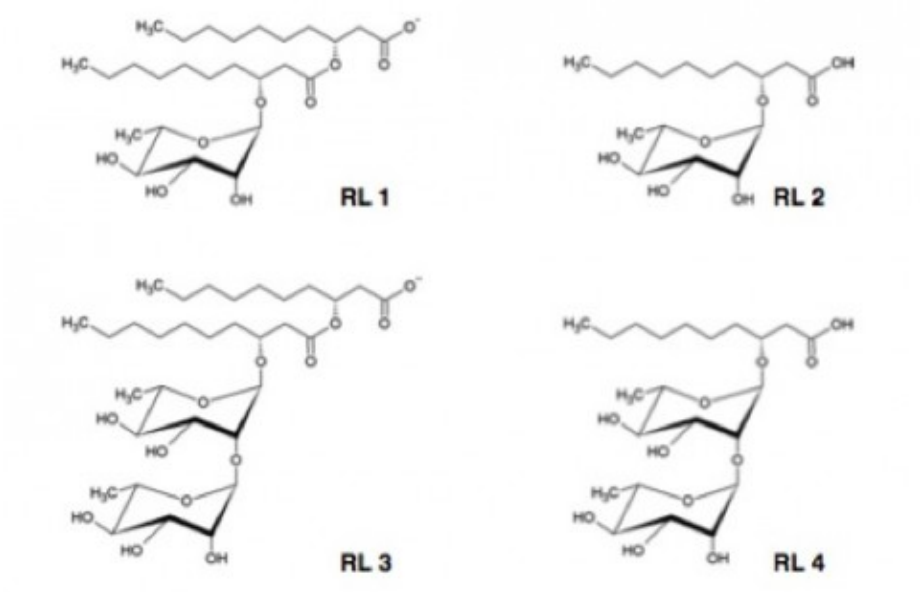

Figure 16: Rhamnolipids congeners produced by Pseudomonas aeruginosa: RL1 and RL3 belong to the di-rhamnolipid class, while RL2 and RL4 are examples of mono-

rhamnolipids. RL3 is the firstly discovered congeners, then were observed in chronological order RL1 and the couple RL2/RL4.

In the successive decades, with a particular focus on the last decade of the twentieth century, many different rhamnolipids species were revealed thanks to the development of analysis techniques and to the discovery of diverse rhamnolipid-producing bacteria which belong to the same family (Pseudomonas) [196], to different families (non-Pseudomonas, i.e. Burkholderia, Enterobacter, Pantoea, etc.) [197–199], and even to different phila (Actinobacteria, Firmicutes) [200,201].

Recently the biosurfactants have attracted an always increasing interest due to their low toxicity and biodegradable nature, which are two crucial parameters very suitable to meet the requirements of the European Surfactant Directive. Indeed, Regulation EC No. 648/2004 issued by the European Community established precise rules designed to achieve the free movement of detergents and surfactants in the European market, providing at the same time a guarantee of high protection of both environment and human health [202]. Thus, rhamnolipids are one of the most accredited candidates able to progressively substitute synthetic surfactants in the light of the fact that, besides satisfying both biodegradability and low toxicity requirements, they have the potential to cover a wide range of industrial and commercial applications [203]. The other side of the coin, however, is the high manufacturing cost of rhamnolipids that at the moment make them unsuitable for large-scale production. Indeed, the medium cost of synthetic surfactants is comprised between 1 and 3 $/kg, while rhamnolipids cost ranges from 20 to 25 $/kg depending on the volumetric productivity of

rhamnolipid fermentation [204]. In details, rhamnolipids are produced through a microbial fermentation carried on by hydrocarbon-degrading microorganisms; thus, hydrocarbons are needed as the carbon source to support the production [205]. Among the available strains, P. aeruginosa is the bacterium with highest rhamnolipid production yield; thus, it has historically been used as the model strain for the rhamnolipid manufacturing. However, the choice of P. aeruginosa as producing-rhamnolipid bacterium entails the drawback related to the opportunistic pathogen nature of the bacterium, requiring a restriction for a large-scale production due to the intrinsic health hazard of the process [206].

In broad outlines, the rhamnolipids production can be resumed in four steps: the seed preparation, the fermentation, the storage and, finally, the product purification (see Figure 17). The high costs of this procedure are mainly related to the fermentation step and, for some applications, to the product purification [204]. The cost involved in the rhamnolipid fermentation arise from the raw materials used as nitrogen and carbon sources for the microorganisms. Indeed, this cost for carbon source is particularly high because by using hydrophobic substrates higher product yields are achievable, and these substrates are usually more expensive than sugar-based substrates. The averaged expense for the raw materials used for the rhamnolipids fermentation was estimated to be about the 50 % of the total cost production [207]. Moreover, extensive purification steps are needed to obtain a pure product, with a consequent requirement of additional operating time and reagent costs. Obviously, the purification expense is strictly related to the desired product

purity, which in turn often depends on the particular targeted application [204].

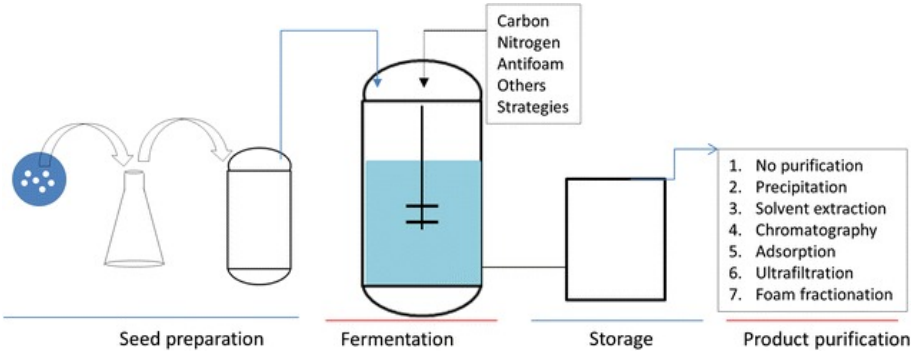

Figure 17: Flow chart of rhamnolipids production. A large scale rhamnolipid production contains the following steps: seed preparation, fermentation, storage and product purification.

Many efforts were made in order to lower the cost production of rhamnolipids and, consequently, make them economically competitive with synthetic surfactants; however, at the moment microbial fermentation to produce rhamnolipids on large scale is economically sustainable only for the realization of high-cost products like medicines and cosmetics [208,209]. Nevertheless, the biosurfactants and rhamnolipids demand is increasing annually and, as a consequence, new production strategies are explored to reduce the related costs [207]. More specifically, a deeply investigated strategy is the lowering of the fermentation cost by using cheaper substrates as carbon and nitrogen sources for the bacterial fermentation. A significant fermentation cost reduction could be achieved, for instance, by using mannitol, glucose or vegetable oils in place of the conventional hydrocarbons [210–212]. Among these alternative substrates, one green compound that has recently attracted an increasing interest is glycerol. Indeed, glycerol is a by-product of the trans-

esterification of vegetable oils and fats with methanol, reaction through which biodiesel is produced. The production of 1 ton of biodiesel leads to the generation of 100 kg of glycerol and, by considering only the European biodiesel industry, the annual glycerol production can easily overcome the value of 600 kton [203]. Moreover, due to the increase in biodiesel production, the glycerol price is constantly dropping down as a consequence of the achieved market oversupply. The projection of biodiesel demand is expected to reach 8 billion gallons in 2020, thus creating the necessity to find new outlets for the non-toxic, edible and biodegradable glycerol, such as the utilization in the biosurfactant production [213].

However, the choice of different organic substrates in place of the commonly used hydrocarbons is not the more effective strategy to reduce the rhamnolipid production cost, even if it can provide a precious contribute. In fact, the rhamnolipid yield is largely dependent on the selection of the specific producing-bacterium, apart from the fermentation conditions and the medium composition [209]. Therefore, obtaining a high-yield bacterial strain is the crucial step to limit the production cost and also to make easier the purification procedure. The widely applied strategy to obtain good producing-strains consists in the isolation of these bacteria from the fermentation environment, which results helpful in increasing the purity grade and cut-off many purification steps [204]. In addition, mutagenesis through radiation or chemical treatment can be applied to further increase the rhamnolipid yield, even if successively to an improvement in microbial production the mutants may lose its productivity after some time. [214,215]. Furthermore, a recently

examined method is the introduction of modified genes which result crucial for the rhamnolipids production. This metabolic engineering approach can be applied to both increase the production yield or to obtain non-pathogenic recombinant strains with the implicit benefit of easier and less expensive purification procedures [216,217].

As previously mentioned, rhamnolipids can find application in really various industrial sectors thanks to their surface-active properties combined with the non-toxic and biodegradable nature. Indeed, they can be used in the oil recovery and bioremediation to stabilize O/W emulsion, facilitate the oil recovery and remove crude oils from contaminated soils [218,219]; in agriculture as a bio-insecticide/pesticide, for the crop protection against phytopathogens agents, and to facilitate the absorption of nutrients and fertilizers through the roots [220,221]; in food industry as foaming agent, emulsifier, wetting agent, antimicrobial and antipathogenic agent to sanitize and prevent food spoilage [222,223]; in detergents and cleaners such as soaps, laundry products and shampoos [224]; in medicine and pharmaceutical industry as biofilm control to prevent medical device-related infections and as anticancer agent, able to inhibit the growth of many cancer cells [225,226]; and in the cosmetic and beauty industry as an active ingredient effective for several skin treatments like cure of burn shocks, wound healing and wrinkles reduction [227].

1.4.3 Sodium Citrate

Under the label of sodium citrate are sometimes commonly indicated all the three sodic salt of citric acid ($C_6H_8O_7$): trisodium citrate, sodium monohydrogen citrate, and sodium dihydrogen citrate. Citric acid is a naturally occurring weak organic acid whose name is derived from Latin word citrus, which in turn refers to trees of the genus citrus including lemon trees [228]. Citric acid is solid at room temperature and easily dissolve in water, originating colourless solutions made up of the different acid and basic species in a reciprocal ratio which depends on the pH value. Indeed, citric acid is a tribasic acid that possesses three carboxylic moieties (see Figure 18), which in turns dissociate with the pK_a values of 5.21, 4.28 and 2.92 at 25 °C [229]. As it is shown by the speciation curve in Figure 18, an aqueous solution of citric acid in a pH ranging between 2 and 8 is a buffer solution. In many biological systems, characterized by a pH value around 7, the only two existing species are tribasic citrate and monohydrogen citrate. When in solution the basic species are abundant, with a particular focus on the tribasic one, complexes with metal and alkali metal cations can be formed. The stability constants of these complexes usually reach high-value thanks to citrate ion structure, which can bind the metal cations through the chelate effect [230,231].

Due to their chelating capacity, citric acid and citrate anions have been investigated as green crosslinking agents, capable of improving the mechanical properties of polymers. More specifically, they attracted attention as crosslinking agents for biodegradable polymers applied in medical and pharmaceutical domains, where they are mainly used in fields like tissue and regenerative engineering [232], bioimaging application [233],

wound dressing [234], and drug delivery [235]. In the light of a sustainable development, citric acid has recently been evaluated as crosslinker and reinforcer agent for agriculture wastes and residues, leading to the creation of innovative products starting from low-cost raw-material such as starch, banana fibres and wheat gluten [236].

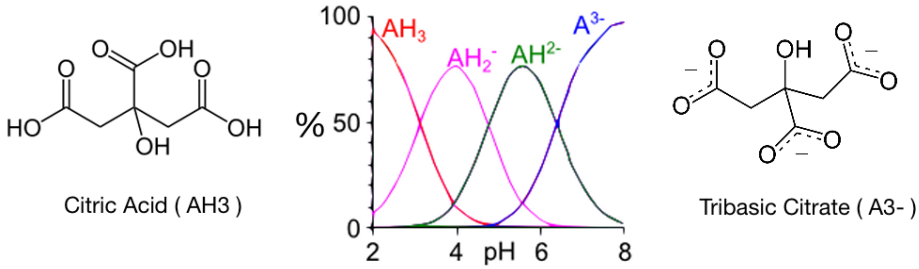

Figure 18: On the left, citric acid (AH_3) chemical structure; in the middle, speciation curve of citric acid; on the right, tribasic citrate (A^{3-}) chemical structure. The chemical structures of the intermediate species monohydrogen citrate (AH^{2-}) and dihydrogen citrate (AH^{-}) are not shown in the figure.

Citrate also plays a crucial role in biological processes linked to the metabolism of both aerobic and anaerobic organisms. Indeed, it is an intermediate product in the Krebs cycle, an aerobic metabolic pathway composed by a series of chemical reactions which follows the initial step of glycolysis and provides the fed for the successive metabolic process, the oxidative phosphorylation [237]. Moreover, sodium citrate plays an active role in controlling the glycolysis processes through the inhibitory mechanism of phosphofructokinase, the key enzyme in glycolysis regulation. The abundance of citrate in the cytosol indicates to phosphofructokinase that there is no need to accelerate the glycolysis since there is a more than sufficient supply of biosynthetic precursor molecules for the next metabolic

processes. Phosphofructokinase is the enzyme responsible for the catalysing of one rate-limiting step in glycolysis [238].

In addition, a citrate biological role that has recently attracted an increasing interest is the presence and the correlated function of this anion inside bones. Indeed, bones contain around 2% wt. of citrate, however, its role remains doubtful [239]. Despite the presence of citrate in bones is an accepted fact, one of the first attempt in rationalizing its biological function goes back just to 2010 and the question is still much-debated nowadays. Hu et al. proposed a surface interaction model according to which citrate anion strongly bind with calcium thanks to the abovementioned chelate effect and, in this way, it affects the apatite nanocrystals growth stabilizing crystals of small thickness that provide better mechanical properties to the bones [240]. Davies et al. deeply investigated the bones-citrate interactions, extending them also to the inner parts of bone and not only to the surfaces [239]. In their proposed model citrate is incorporated into the mineral structure, within hydrated layers, and acts as a bridge linking the mineral platelets present in bones [239]. Even though these papers represent a step forward in understanding the citrate role in bones, many questions remain unanswered still today, such as how it is controlled the citrate amount in the nanocrystals, in what stages of bones developments citrate appears and if in bone diseases it is possible to find some deviation from the typical conditions.

It is widely known that citric acid is a naturally occurring compound which is particularly abundant in citrus fruits, with a concentration in juices that ranges between 0.005 mol/L and 0.30 mol/L for oranges and lemons, respectively [241]. Indeed, both

citric acid and citrate anion were historically produced through the treatment of citrus fruit juices with calcium hydroxide, in order to precipitate the calcium citrate salt. Afterwards, citric acid was obtained by a reaction with diluted sulfuric acid able of protonating all the carboxylate groups [242]. Notwithstanding its natural abundance, sodium citrate produced exclusively by extraction from natural sources cannot longer match commercial needs, for this reason, the industrial-scale production has gradually turned itself from an extractive procedure into a fermentative process [228]. Citric acid fermentation was observed for the first time in 1893 as a fungal product by Wehmer; successively Currie, in 1916, discovered that various strains of the mould Aspergillus niger produced a considerable amount of citric acid, especially in a sugar-rich environment. Around the 30s of the twentieth century, the first citric acid fermentations were carried out through surface culture. Although new citric acid production methods were developed from the thirties, the submerged microbial fermentation is nowadays the worldwide most applied commercial process, and specifically the fermentation of A. niger in molasses [243]. As in the case of rhamnolipid (see previous paragraph 'Rhamnolipids'), also for the citric acid fermentation it is crucial to choose the best combination of fermenting agent/organic substrate in order to optimize the final yield. Over the years, a wide variety of microorganisms has been investigated for the citric acid production including bacteria, fungi and also yeasts [244–246]. In the attempt to answer the increasing citric acid demand, the improvement of citric acid fermentation yield is continuously studied through mutagenesis and selection, again in parallel to

what described for the rhamnolipid. Nowadays, A. niger still remains the organism of choice for commercial production because it provides the highest yield, it is easy-handling and can ferment with various cheap raw-materials substrates, which results in lower costs of production [243,247].

In recent years, a new technique for the citric acid production has been deeply investigated: the solid-state fermentation, otherwise known as 'Koji fermentation'. This process, which originated in Japan where there is a significant abundance of agro-industrial residues and wastes, consists in the cultivation of microorganisms in the absence of free liquid on moist solid materials [248]. The solid materials on which the fermentation is carried on play the double role of support and sources of nutrients for the microorganisms. To this end, many agro-industrial wastes can be used such as banana peel [249], kiwi fruit peel [250], cotton waste [251], orange peel waste [252], pineapple waste, apple pulp ultra-filtrated sludge and solid waste [248], dates pulp [253], wheat bran and soybean meal [254], potatoes and fresh *kumara* potatoes [255]. The main advantages related to this procedure are the use of inexpensive and widely available waste materials as substrates, the minimum consumption of water and the need for a simple equipment. All these features make the solid-state fermentation a more environmentally friendly and less expensive technique in comparison with the submerged fermentation [256]. On the other hand, the major drawback is represented by the reduced variety of microorganisms that can be used on the moist solid substrates [257].

Citric acid is worldwide accepted as GRAS (generally recognized and safe) and approved by the Joint FAO/WHO Expert Committee on Food Additives [258]. This status, combined with its non-toxicity, versatility, high solubility in water, pleasant tart taste, buffering and chelating properties and the recognized safety make citric acid and its derived salts widely used and active ingredients that can easily find application in many different sectors like food and beverages industry, cosmetic industry, agriculture, pharmaceutics, metal cleaning and various industrial processes [228,243,244].

1.4.4 Carbon Black

Carbon black (CB) is defined in the IUPAC gold book as "an industrially manufactured colloidal carbon material in the form of spheres and of their fused aggregates with sizes below 1000 nm" [259]. When discussing CB sizes, it is crucial to distinguish three different structures that are primary particles, aggregates and agglomerates [260]. More precisely, free primary particles are the primary spherical structure elements. They are not present in CB due to their high tendency to join in aggregates, which are the primary dispersible elements of CB, in response to the need of minimizing their high surface area to volume ratio and the related high surface energy. The aggregates can in turn associate in undispersed clusters of aggregates, called agglomerates, held together by van der Waals forces or any binders [260,261]. In Figure 19 are shown the typical structures of primary particles, aggregates and agglomerates accompanied by their average dimensions.

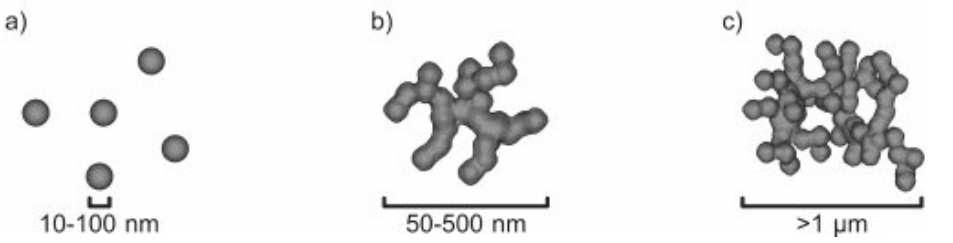

Figure 19: Carbon Black a) primary particles, b) aggregates, c) agglomerates.

More specifically, the spherical primary particles consist in both graphitic and amorphous parts. The graphitic domains are typically formed by the stacking of 3-4 turbostratic (basal planes slipped out with regard of the typical alignment) polyaromatic layers characterized by an average lateral extension of 3 nm and a plane-to-plane interlayer distance around 0.35 nm (see Figure 20) [262]. These graphitic-like domains are often indicated as BSU, which is the acronym of basic structural units [263,264]. The core of the sphere is mainly constituted by amorphous structures, while the BSU are almost concentrically oriented around the amorphous core. This peculiar arrangement of the carbon layers is responsible for the so-called onion like microtexture shown in Figure 20 [265].

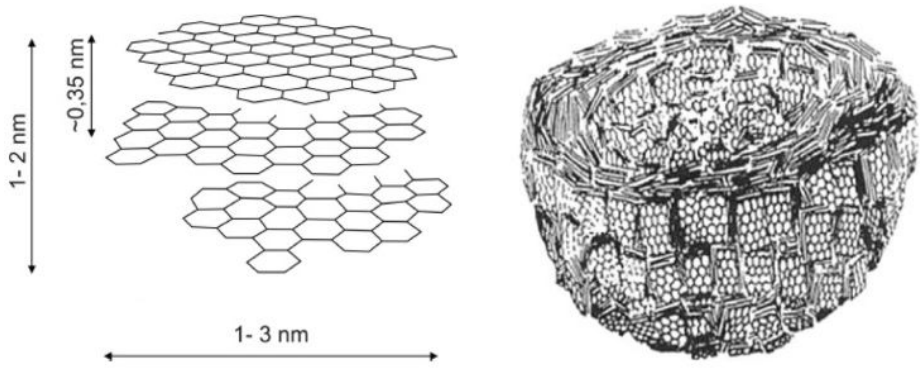

Figure 20: On the left, basic structural unit (BSU) consisting in turbostratic stacking of polyaromatic layers; on the right, concentrically arranged graphitic-like domains in 'onion microtexture' typical of carbon black primary particles.

The chemistry and physicochemical properties of CB are markedly affected by its large specific surface area, which provides a high tendency in adsorption of water, solvents, polymers or binders, depending on the specific surface chemistry [266]. Indeed, CB is invariably associated with varying amounts of oxygen and hydrogen and, depending on the adopted manufacturing process, with atoms of chlorine, nitrogen, and sulphur. These impurities are introduced mainly onto the CB surface area during the production steps because of their presence in the feedstock, reactor furnace, post-reactor chamber and become a part of the chemical structure [267]. In addition to these atoms, several oxygen-containing functional groups were detected on the CB surface such as carbonyl, carboxyl, pyrone, phenol, quinone, lactol and ether groups (see Figure 21) [268]. Moreover, CB tends to extend this layer of chemisorbed oxygen by decomposing certain oxidizing gases or aqueous solutions of salts, halogens hand acids [269–271]. In each case there is chemisorption of oxygen and a build-up of the oxide layer on the

carbon surface. However, the nature and the amount of the surface oxide formed depends upon the nature of the carbon black surface and the history of its formation, its surface area and the temperature of treatment [267]. Carbon-oxygen surface structures are by far the most important surface groups which influence the physicochemical properties such as wettability, catalytic, electrical and chemical reactivity of carbon blacks. Indeed, the presence of these surface groups provides the properties by which CB results a useful additive in many application fields [272].

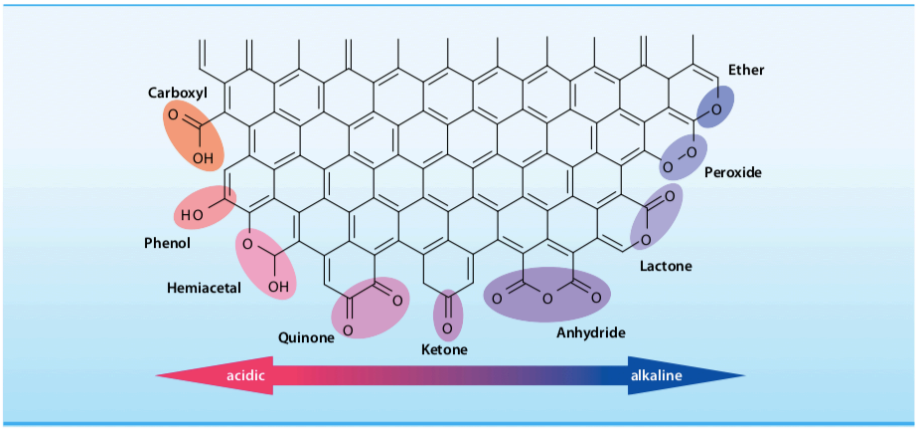

Figure 21: CB surface can bind oxygen functional groups in both acid and basic forms.

Therefore, even if CB is composed almost entirely of carbon, the attempt of describing it through using only the periodic table designator 'C' would provide a misleading picture that does not consider the functional groups mainly present on the CB surfaces, which in turn represent the causes of many interesting CB properties such as the electrical and thermal conductivities [273].

Indeed, CB is an electrically conductive material, characterized by a conductivity that usually falls in the range $10^{-1}/10^{2}$ $\Omega^{-1} \cdot cm^{-1}$. Due to its intrinsic conductive properties, CB can also impart good conductivity to normally insulating polymers, which can be turned in electrically conductive materials by exceeding a critical CB concentration to establish a continuous path in the polymer matrix. This critical concentration is usually indicated as percolation threshold, that is the point where the polymer composite makes a transition from insulating to conducting system (see Figure 22) [274].

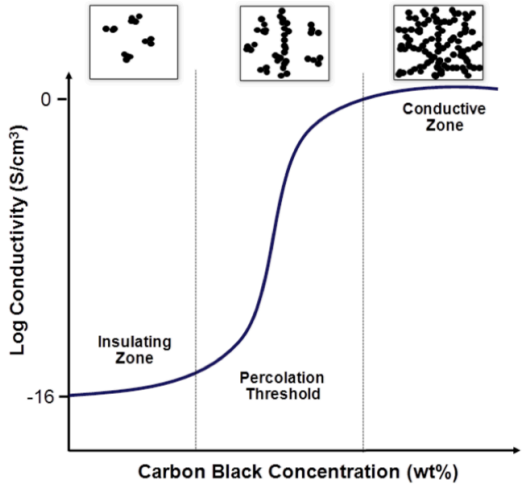

Figure 22: Schematic of Log conductivity versus CB concentration illustrating an S-shaped percolation curve.

The percolation theory hypothesizes that, when the filler threshold is reached and exceeded, an infinite cluster that connects the randomly dispersed conductive objects is formed. This infinite cluster has to be homogeneously located in the whole polymer matrix and, in this way, it allows the electron passage within the network [275,276]. Thus, in order to establish the conditions necessary for the electron passage, CB or other

conductive fillers have to be present in a sufficiently high content able to guarantee an adequate proximity of the particles. However, it is important to point out that the concept of proximity should not be interpreted solely as a direct contact between the interfaces of two carbon black particles. Indeed, the flux of electron can be established also when the interaggregate distance is small enough to allow an electron jump from one carbon black aggregate to another (i.e. tunnelling effect): it might as well be a physical contact as a contact via an insulating interface [277]. Indeed, as proven by numerous studies, the tunnelling electron conduction mechanism and the percolation theory result reliable and provide satisfying elucidation of how the electrical conduction is achieved in the CB polymer composites, depending on the filler dimensions and the experimental conditions [278–280]. For this reason, the conduction mechanism in CB-polymer matrices is often described as a combination of the two processes with a predominant character of one mechanism over the other related to the specific conditions [281,282].

Figure 23 provides a schematic picture of both electron percolation and tunnelling effect in CB-polymer composite matrix.

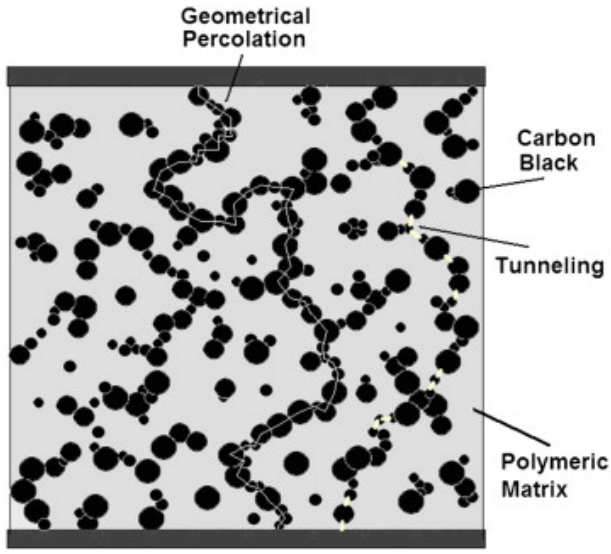

Figure 23: Electron conduction in a CB-polymer composite. Percolation by physical contact and through tunnelling effect.

The conductivity imparted to the polymer matrix is linked to the ability of the specific polymer to accept a sufficient load of CB to reach the percolation threshold. At the same time, the polymer should maintain an easy processability and a good balance between the mechanical and conductive properties. In order to lower the required CB content to exceed the percolation point, a series of carbon blacks have been developed for specific conductive applications, the so-called conductive, super-conductive and extra-conductive carbon blacks. Although, all carbon blacks can be used to produce conductive compounds, conductive blacks are designed to be used at low loading in most polymer types [267].

When added to a polymeric material, CB is also able to enhance the thermal conductivity of the resulting composite; however, in

this case, the parallelism with a metallic conductor is inappropriate: in metals heat transport occurs by the electric charge carriers, while in the case of amorphous materials like CB-polymer composite the transport mechanism is not fully understood. The thermal conductivity of such composite compound increases with CB concentration, however, the presence of a threshold could not be observed [283].

Furthermore, the feature of CB that attracts the broadest interest, from an applicative and industrial point of view, is its use as a reinforcing agent capable of enhancing the mechanical properties and the stability of the composite materials in which it is applied. For this reason, CB is widely used as filler in the manufacturing of plastic, rubber and various polymeric blends currently applied to many industrial areas: CB enriched tires show a longer lifetime, a lower thermal degradation and a higher resistance to abrasion and mechanical stresses [284,285]; in the rubber industry, CB leads to an improve in mechanical, thermal and tensile properties of natural rubbers and elastomers [286–288]; in the polymer industry, CB contributes to prevent the polymer degradation by increasing the resistance to thermal degradation, abrasion and tear and by playing an UV-shielding role thanks to its capacity of capturing those polymer-degrading wavelengths [289–291]; as a pigment in paints and inks, particularly those for ink-jet printing [292–294]. Moreover, the addition of carbon black in a rubber or polymer matrix deeply affects their mechanical properties and may impart viscoelastic behaviour to natural rubber and to polymeric materials such as polystyrene [295,296].

CB is popularly and erroneously considered as a type of soot, in spite of the fact that soot is produced through a randomly performed process while CB is manufactured under controlled conditions [259]. Indeed, CB is derived from substances that contain copious quantities of carbon, such as biomasses or hydrocarbons, mainly through two different categories of processes: incomplete combustion and thermal decomposition, which occur in the presence or absence of oxygen respectively [267]. Incomplete combustion processes, also known as thermal-oxidative processes, are further divided into furnace black, Degussa gas black, lamp black and channel black processes, depending on the particular process and refractory line adopted [267].

On the other hand, the main thermal decomposition processes are the thermal black and the acetylene black processes. Due to the reaction conditions and the particular feedstock properties, CB produce from acetylene differs from other carbon black grades, especially from the ones manufactured through incomplete combustion processes. Indeed, CB obtained from acetylene process exhibit a remarkable purity and a high degree of crystallization which make it extensively structured. Therefore, it is not possible to densify and handle it in pellets [267]. Due to this inherent physical constraint and because of their electrical properties, acetylene CB is used primarily as a conductive material in electric cells and conductive and antistatic rubber and plastic applications [297,298].

The low cost associated with the furnace black process justifies why this is still nowadays the most applied manufacturing technique for the production of commercial CB [266]. However,

the carbon yield achieved by the furnace black process strongly depends on the used feedstock and is usually moderate, ranging between 25 and 75 % of the carbon content in the liquid feedstock, as estimated by Rivin in 1986 [299,300]. Moreover, the legislation in different countries have become and will become more and more severe, encouraging in this way the CB industry in the application of new processes that also take into account environmental aspects related to the CB manufacturing [301]. In this light, new CB production and recovery methods are continuously evaluated like the thermal plasma processes and pyrolysis of scrap tires and biomass [302–305].

1.4.5 Anti-scale Agents

Mineral formation and scaling, widely occurring problems in various industrial processes, are currently solved by the use of inhibitors and dispersants such as polyacrylate and polycarboxylate homo- and copolymers. Most of these compounds are ultimately released to wastewater but they are usually poorly biologically degradable, if at all [306].
A multitude of organic molecules of biological origin and belonging to biological systems potentially interact with and modify inorganic crystallization. Among these molecules, one of the key compounds is a class of polyanionic proteins. The main constituents of these proteins are aspartic acid and phosphoserine. In aqueous solution, these polyanionic proteins can inhibit crystal nucleation and growth by altering the morphology of microscopically small crystals [307].

In the light of finding green biodegradable alternatives to the most actually used anti-scale agents, such as polyacrylates and polycarbonates, sodium salts of polyaspartate and polyglutamate were investigated as additives in the polysaccharide-based formulations.

1.4.5.1 Sodium Polyaspartate

Sodium polyaspartate (PAS) is the sodium salt of polyaspartic acid, a water soluble and biodegradable polymerized amino acid [308]. Indeed, the PAS polymer chain is made up by the repetition of aspartic acid molecules, a non-essential amino acid characterized by two carboxylic acid moieties at the opposite ends of the molecule. As a consequence, PAS results to be a polyelectrolyte with an anionic character when dissolved in aqueous solution.

In nature, PAS chemical structure exclusively consists of α-linked L-aspartic acid; whereas, the polyaspartate produced through a synthetic way can exist in four isomeric forms, which originate from the combination of two starting stereoisomers, L- and D- aspartic acid, with the specific synthetic pathway applied that may lead to a prevalence of α- or β- linkage between aspartic building blocks [309]. Figure 24 shows the chemical structure of aspartic acid with both α and β repeating units.

Thus, in the majority of cases, synthetically produced PAS shows a chemical structure where both α and β linkages are present, and whose respective percentages in the chains can markedly oscillate depending on the synthetic route adopted [310]. Indeed, numerous methods for the synthesis of polyaspartates have been

developed during the past decades. In addition, it was found that the applied synthetic method strongly affects the structure and properties of the resulting product [307].

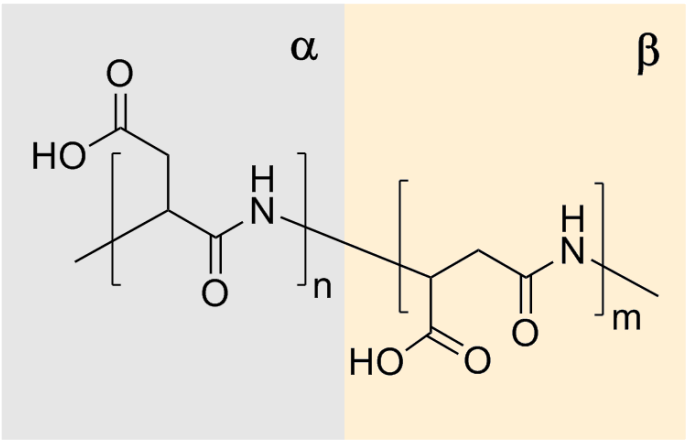

Figure 24: Polyaspartic acid chemical structure made up by both α and β repeating units.

The classic and widest used synthetic method is known as *thermal polycondensation*, and it was reported for the first time in the 19th century by Ugo Schiff [311,312]. The basic version of this method consists in a two-step procedure according to which, firstly, the amino acid precursor is heated and dehydrated resulting in the production of polysuccinimide; secondly, an alkaline treatment with sodium hydroxide leads to the formation of DL-(α,β)-poly(aspartate) with 30% α-linkages and 70% β-linkages [313]. In order to obtain PAS with the highest biodegradability capacity, the use of catalysts in the thermal polycondensation process has been investigated. More precisely, it was found that in the presence of acid catalysts, such as ortho-phosphoric, a less branched and consequently more biodegradable PAS is obtained.

However, all the mentioned synthetic routes start with L-aspartic acid, whose global production is still far from the worldwide demand for polycarboxylates, most of which are non-biodegradable. Therefore, a substitute should be available by a manufacturing process which can match that market. L-Aspartic acid is therefore not an adequate source for the production of all polyaspartates. Especially in the case of laundry detergents, dishwasher chemicals, and water treatment agents, the breakthrough of polyaspartates can only be achieved if large-scale production of tens of thousands of tons is possible. In this light, various chemical precursors of aspartic acid have been investigated as starting material for the thermal polycondensation procedure. Among these compounds, maleic acid ammonium salt, derivatives of the maleic acid anhydride with ammonia, and fumaric acid ammonium salt have aroused great interest [314,315]. More precisely, maleic anhydride is industrially produced in large volumes and consequently represents a source for the large-scale production of synthetic polyaspartates [307].

In addition to the thermal polycondensation processes, different synthetic methods in order to obtain pure homopolymers, such as D- or L- PAS with α- or β- linkages only. The synthetic routes applied for this purpose consist of the polymerization of aspartic acid esters, the polymerization of N-carboxyanhydride derivatives, and the enzymatic preparation through bacterial protease [316–318].

Chemically, PAS is assigned to the class of polycarboxylates, which refers to the repeating carboxylate units along the polymer chain (each monomer aspartate unit features one carboxylate

group). Consequently, PASs show some similar properties, effects, and eventually applications as the most representative of the polycarboxylates, namely the polyacrylates. However, the main difference is provided by the biodegradability of the PASs, which can be attributed to the potentially cleavable amid bonds in the molecule [307,308].

In addition to biodegradability, the main properties thanks to which PASs find application are described below. The first one is its dispersing capability, the phenomenon that allows preventing the agglomeration and subsequent settling of solid particles present in aqueous suspensions. Indeed, polyaspartate, due to its polyanionic character, adsorbs onto the highly polar particle surfaces, resulting in equally (negatively) charged particles, which undergo an electrostatic repulsion. PAS contributes in inhibiting the scale formation also through the crystal distortion: this means that the crystal shape is changed, consequently resulting in a loose, easy-removable precipitate. Polyaspartates, due to the presence of many carboxylate groups in the chains, may also act as complexing agents, especially towards metal ions such as ferric and calcium ions. Furthermore, PAS exerts a corrosion inhibiting effect, that can be attributed to an adsorption of the polymer onto the metal surface, forming a protective film [307].

Because of their interesting properties, polyaspartates could be used on a large scale in different applications. In particular, PAS results to be an effective dispersing agent for dirty particles in formulations of detergents and cleaners [319], and for pigments in leather and textile industries [307]; or as anti-scale and corrosion inhibiting agent in water treatment processes, in

mining, oil or shale gas recovery, and even in the wine production [320–322].

1.4.5.2 Sodium Polyglutamate

Sodium polyglutamate (PG) is the sodium salt of polyglutamic acid (PGA), which in turn is a naturally occurring biopolymer made up of repeating units of glutamic acid [323]. PG is an edible, non-immunogenic anionic homopolyamide with a high biodegradability, as in the case of polyaspartate [324].
PGA can be differentiated into two isoforms, α-PGA and γ-PGA, depending on the attachment of the carboxy group. As an example, Figure 25 shows the chemical structure of the α-PGA isoform.

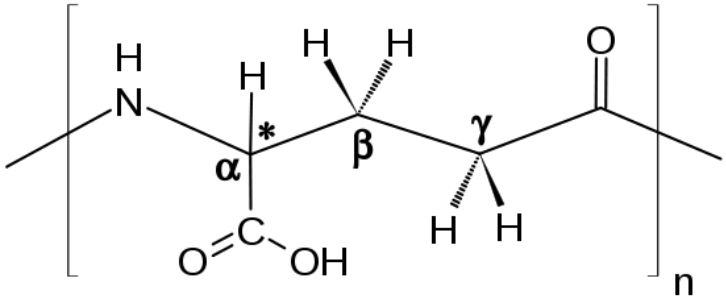

Figure 25: Chemical structure of α-PGA. The asterisk indicates the two possible isomers D- and L-PGA.

α-PGA is chemically synthesized by nucleophile-initiated polymerization of the γ-protected N-carboxyanhydride of L-glutamic acid. The difficulties in microbial production of α-PGA and the need to produce the polymer mainly through recombinant technology constitute an obstacle to the manufacturing of this specific isoform [325]. On the other hand,

γ-PGA has been produced extensively using bacteria, especially those of *Bacillus* species. Moreover, this synthetic method either allows to selectively produce only L-glutamic acid residues, only D-glutamic acid residues or both L- and D-glutamic acid residues [323]. For these reasons, γ-type PGA is the widest between the two species, so much so that the acronym PGA often refers to this the γ isoform only.

γ-PGA is widely present in many naturally occurring sources. Indeed, it was first discovered by Ivanovics and co-workers as a capsule of *Bacillus anthracis* which was released into the medium upon autoclaving or upon aging and autolysis of the cells [326]. Another naturally occurring source of γ-PGA is the mucilage of natto, which is a traditional Japanese food based on fermented soybeans and consisting of a mixture of γ-PGA and fructan produced by Bacillus subtilis Sawamura [327]. γ-PGA is produced mostly by Gram-positive bacteria; however, it has also been reported that at least one Gram-negative bacterium (*Fusobacterium nucleatum*), some archaea and eukaryotes have the ability to produce this macromolecule [323]. In addition, γ-PGA has also been found in neurons of mice [328].

Therefore, PGA is largely present in many living organisms and its function depends on the specific producing organism and on the environment the organism inhabits. Some pathogenic bacterial strains take advantages of PGA properties to escape phagocytosis and to protect themselves against antimicrobial agents and antibodies [329–331]. Differently, some soil bacteria release γ-PGA into the environment for the sequestration of toxic metal ions or the reduction of high local salt concentrations, increasing their resistance to adverse environments [332,333].

Furthermore, more complex organisms such as Cnidaria and mice uses PGA for prey capture, locomotion, protection or even regulation of the intracellular transport [334].

Although the microbial production of γ-PGA has since been established, the cost of production is still nowadays very high and this actually represents the major limitation to the widespread application of the biopolymer. Based on this, most research on the microbial production of PGA is focused on the optimization of growth conditions with the potential to produce a high yield, specific enantiomeric composition and desired molecular mass of PGA at a reduced cost. In spite of the high cost of production, PGA attracts an always increasing interest due to the combination of its unique properties. Moreover, PGA is biodegradable, edible and non-toxic for humans, which itself is a prerequisite for being used for human benefit broadens the potential application fields.

More precisely, γ-PGA results to be particularly attracting for medical applications related to tissue engineering [335], wound dressing [336], drug delivery [337], and calcium absorption for bone disorders treatment [338].

Logically, the edible character of PGA makes it an interesting ingredient in food industry, where it is mainly used as thermal and rheological enhancer in the wheat manufacturing [339], as oil-reducing agent that limits the oil uptake in deep-fat frying [340], or as a cryoprotectant due to its optimal antifreeze activity [341].

Moreover, the non-toxic nature of PGA allows its application in cosmetics as moisturizer for the formulation of skin care products

[342], in agriculture as biocontrol agent/fertilizer [343], in the realization of needle-tip glucose sensors [344].
However, the application field, which is the most strictly connected one to the investigation carried out in this project, is the water treatment sector. In this field, PGA effectively covers a broad set of functions. Indeed, PGA has been studied as anti-scale agent [345], biopolymer flocculant agent [324], heavy metal removal [346], and dye removing agent [347].

1.5 Aim of the research

The general purpose of this thesis is to characterize different green complex fluids designed for various potential applications. In particular, there were examined the effects exerted by salts, specific additives and operative conditions on both aqueous and organic solvents systems. The characterization was carried out mainly from a dynamic and structural perspective, searching for different strategies through which obtain a modification in the rheological behaviour of the systems.

The first phase of the research was focused on the study of simple polysaccharide aqueous dispersions, both pure and in the presence of salts. In particular, there were evaluated the effects arising from the presence of salts in the polysaccharide systems, mainly from a rheological and thermal perspective. Initially, it was analysed the specific ion effect on polysaccharide dispersions, induced by single salt individually considered; afterwards, the

response of the biopolymers was examined in more complex environment consisting of a mixture of salts. Thanks to the results arising from the first phase of the study, we acquired info about the salinity resistance of the various polysaccharide, that is a fundamental data for selecting the appropriate biopolymer for the desired applications.

In the further step, we moved towards more complex systems by the addition of specific additives capable of significantly affecting viscosity and rheological behaviour, remarkably reducing the precipitation of scales, enhancing the thermal resistance, and improving the system responsivity to the application of electrical treatment.

In a third phase, the study was finally extended to non-aqueous system. In detail, it was investigated how the presence of specific salts can affect the structural properties and the associative interactions of an organic solvent (glycerol carbonate), resulting in significant modifications of its conductivity and rheological behaviour.

2 Materials & Procedures

2.1 Materials

2.1.1 Salts & Co-Solutes

Sodium fluoride (NaF), sodium iodide (NaI), sodium perchlorate hydrate ($NaClO_4 \cdot H_2O$), sodium dihydrogen phosphate (NaH_2PO_4), and calcium chloride ($CaCl_2$) were purchased from Fluka (Milan, Italy). Sodium chloride (NaCl), sodium bromide (NaBr), sodium sulphate (Na_2SO_4), sodium phosphate tri-hydrate ($Na_3PO_4 \cdot 3H_2O$), sodium mono-hydrogen phosphate epta-hydrate ($Na_2HPO_4 \cdot 7H_2O$), trehalose ($C_{12}H_{22}O_{11}$), potassium fluoride (KF), potassium chloride (KCl), potassium bromide (KBr), potassium iodide (KI), potassium carbonate (K_2CO_3), potassium phosphate (K_3PO_4), potassium cyanate (KCN), and potassium sulfate (K_2SO_4) were supplied by Sigma-Aldrich (Milan, Italy). Strontium chloride esa-hydrate ($SrCl_2 \cdot 6H_2O$) and urea (CH_4N_2O) were purchased from Riedl de Haen (Germany), while Barium chloride di-hydrate ($BaCl_2 \cdot 2H_2O$) and sodium carbonate deca-hydrate were purchased from Merck (Germany). All the salts were reagent grade (purity $\geq$ 99%) and used as received, with the exception of the potassium salts applied in the study of glycerol carbonate properties which were purified, dried and stored under vacuum, accordingly to standard procedures [348].

2.1.2 Polysaccharides

Guar Gum and hydroxypropyl cellulose with corresponding weight averaged molecular weights (M_w) of 2000 kDa and 1600-1800 kDa were provided by Lamberti (Milan, Italy). Sodium alginate with a 0.44 mannuronate/guluronate ratio and M_w of 240 kDa was purchased from Sigma-Aldrich (Milan, Italy), while sodium hyaluronate with a M_w higher than 1800 kDa was supplied by Stanford Chemicals Company (California, USA).

2.1.3 Glycerol Carbonate

Glycerol carbonate, or 4-(Hydroxymethyl)-1,3-dioxolan-2-one), was purchased from Sigma-Aldrich (Milan, Italy).

2.1.4 Additives

Saponin with a sapogenin core fraction comprised between 8 and 25 wt.% and a CMC ranging between 0.001-0.01 wt.% was purchased from Sigma-Aldrich (Milan, Italy).
Rhamnolipid category R90 (purity ≥ 90 %, CMC 5-380 mg/L) was provided by AGAE Technologies (Oregon, USA). Sodium citrate tribasic dihydrate ACS reagent grade (purity ≥ 99.0%), poly-L-glutamic acid sodium salt with M_w comprised between 3000 and 15000 kDa, poly-L-glutamic acid sodium salt with M_w in the range 15000-50000 kDa, and poly-(α,β)-DL-aspartic acid sodium salt with a M_w between 2000 and 11000 kDa were supplied by Sigma-Aldrich (Milan, Italy). Conductive Carbon

Black VULCAN® XC-72R was provided by Cabot Corporation (Massachusetts, USA)

2.2 Sample Preparation

2.2.1 Polysaccharide Aqueous Dispersions

Pristine Polysaccharide in Water

GG, SA, HPC and SH 1 wt.% or 0.5 wt.% water mixtures were prepared by slowly adding a weighted amount of polysaccharide powder to water under constant stirring at room temperature. In these conditions complete dissolution occurs in about one hour for all the investigated biopolymers.

Polysaccharide in Salt Solutions

The samples containing the different salts or co-solutes (trehalose and urea) were prepared following the same procedure, replacing water with 0.5M aqueous solutions of the salts or co-solutes.

Polysaccharide in 'Shale Water' Solution

The samples containing polysaccharide in the so-called Shale Water (SW) solution were prepared following the same procedure, replacing water with an aqueous solution of the following composition: NaCl 1.000 M, $CaCl_2$ 0.200 M, KBr 0.014 M, $SrCl_2$ 0.010 M, and $BaCl_2$ 0.002 M.

Polysaccharide in Green Additive Solutions

The samples containing saponins, rhamnolipids or sodium citrate were prepared following the same procedure, replacing water with 0.05 wt.% aqueous solutions of the considered additive.

Anti-Scale Agents Solutions:
The precipitation of $CaSO_4$ (or $SrSO_4$) crystals was monitored after the mixing of two solutions, in the same aliquot, containing $CaCl_2$ (or $SrCl_2$) 0.5 M and Na_2SO_4 0.5 M. The anti-scale agents were added in each solution of salts in order to obtain a final concentration of 0.001 wt.%.
For the evaluation of the crystal precipitation in the polysaccharide systems, a weighted amount of polysaccharide powder was slowly added under magnetic stirring to each salt plus anti-scale agent solution, in order to achieve a final concentration of 0.5 wt.% of the polysaccharide.

2.2.2 Carbon Black Aqueous Dispersions

Dispersion of Carbon Black in Saponin Solutions
To effectively disperse Carbon Black (CB) in the aqueous-based system, a 2 wt.% saponin solution was firstly prepared. This solution was added to a weighted amount of CB powder in order to obtain a final CB concentration of either 1 wt.% or 3 wt.% and magnetically stirred for a few minutes. The mixture was successively sonicated for 1 hour at 40 kHz.

Inclusion of Carbon Black in Saponin Solutions
To effectively include CB in the polysaccharide network, CB was firstly homogenously dispersed as described above, then a

weighted amount of polysaccharide powder was slowly added under magnetic stirring to each dispersion in order to achieve a final concentration of 0.5 wt.%.

2.2.3 Glycerol Carbonate

2.3 Procedures

2.3.1 Rheology

Rheological measurements were performed on a Paar Physica UDS 200 rheometer working in the controlled shear-stress mode. For all samples a plate–plate geometry (diameter, 4.0 cm; gap, 300 µm) was used. All measurements were performed at 25.0 °C (Peltier control system). For each sample the flow curve was acquired in a torque range between 10^{-3} and 2000 mN m, after a 15 min soaking time to equilibrate at the set temperature.
For the evaluation of the thermal resistance of each polysaccharide systems, flow curves were acquired by applying the same parameters described above in a temperature range between 25 and 60 °C.

2.3.2 Differential Scanning Calorimetry

Differential Scanning Calorimetry (DSC) runs were carried out on a DSC-Q2000 from TA Instruments TA Instruments (Philadelphia, PA). The experiments were conducted under N_2 atmosphere with a flow rate of 50 mL/min.

Applied to Polysaccharide Systems

The samples were first cooled from 20 to -60 °C at 10 °C/min, then heated up to 50 °C at 5 °C/min. For the samples prepared with NaF and Na_2HPO_4 the deconvolution of endothermic peaks was performed by means of the Igor Pro 6.36 software, using a summation of exponentially modified Gaussian (EMG) functions [349]. The single EMG function is defined as:

$$f(T) = \sqrt{\frac{\pi}{2}}\frac{hw}{|s|}\exp\left[\frac{w^2}{2s^2}\left(\frac{T_0 - T}{s}\right)\right]\operatorname{erf}\left[\frac{T_0 - T}{2\left(w + \frac{w}{|s|}\right)}\right]$$

where h is the height, T_0 the center, w the width of the peak and s is the distortion factor (shape). For the deconvoluted peaks, the peak temperatures correspond to T_0, while the enthalpy changes are calculated using the total area under the peak.

Applied to Glycerol Carbonate Systems

The samples were first equilibrated at -30 °C, then cooled from -30 °C to -90 °C at 2 °C/min, and finally heated up to -30 °C at 2 °C/min. The thermograms were analysed by the TA Universal Analysis software. For all samples the glass transition temperatures (T_g) were obtained from the inflection point in the DSC signal.

2.3.3 Optical Microscopy

Nikon Eclipse Ti-S Inverted Microscope was used to obtain optical images of $CaSO_4$ (or $SrSO_4$) precipitated crystals and CB dispersions in saponin. All experiments were performed in

automatic mode using an objective with a 10x magnification at room temperature. At least three different regions for each sample were analyzed in order to obtain a statistically meaningful result.

2.3.4 Electric Conductivity Measurements

Polysaccharide Systems

Conductivities of polysaccharide systems were measured through a sensION™+EC7 conductivity platinum cell (HACH, error ≤ 5% in the measuring range between 0.2 and $2 \cdot 10^5$ μS/cm). For each sample at least five measurements were performed and averaged.

KF in Glycerol Carbonate Solutions

A Metrohm 712 conductimeter with a 0.83 cm^{-1} cell constant was used. Salt concentrations ranged between 0 and 1.5 M. The cell was immersed in a water bath with thermostatic control the temperature of the sample (25.0 ± 0.1 °C).

2.3.5 Electrical Responsiveness: Application of a Voltage

The electrical responsiveness of polysaccharide-based systems was assessed by applying a 30 V voltage for 1 hour through a Hewlett Packard Harrison 6112 A DC power supply. Two platinum wires of 1.0 mm diameter (Sigma-Aldrich) were dipped into the dispersions and used as electrodes.

2.3.6 Attenuated Total Reflection Fourier-Transform Infrared Spectroscopy

Attenuated Total Reflection Fourier-Transform Infrared spectroscopy (ATR-FTIR) spectra were acquired using a Thermo Nicolet Nexus 870 FT-IR spectrophotometer, equipped with a liquid nitrogen cooled MCT (mercury-cadmium-telluride) detector, by averaging on 128 scans at a resolution of 2 cm^{-1} and with CO_2-atmospheric correction. The spectra were acquired in the range 4000–900 cm^{-1}. For each spectrum the background was previously recorded and subtracted to the sample profile.

2.3.7 Nuclear Magnetic Resonance

1D- and 2D-Nuclear Magnetic Resonance (NMR) spectra were recorded with a Bruker 400 Ultrashield spectrometer operating at 400 MHz (for ^{1}H) and 100 MHz (for ^{13}C). All the experiments were carried out in vacuum-dried NMR coaxial tubes. $CDCl_3$ was used as external lock and reference material in the coaxial insert. NMR signals were referenced to nondeuterated residual solvent signals ($CDCl_3$, 7.26 ppm and 77.0 ppm for ^{1}H and ^{13}C, respectively).

2.3.8 Solubility of potassium salts in Glycerol Carbonate

The solubility of salts in GC was measured at different temperatures. A weighted amount of GC was transferred in a test tube and an excess of dry salt was added. The vial was sealed and kept under magnetic stirring for two days in a bath with a

thermostatic control of the temperature (±0.1 °C). The stirring was stopped, and the saturated solution was left to equilibrate in the presence of the salt for 24 h, before a certain amount (b, in grams) of solution was carefully taken from the top of the solution and transferred to a flask and diluted with water up to a volume V (in L). The aqueous mixture was than analyzed through Inductively Coupled Plasma Atomic Emission Spectrometer (ICP-AES) in order to measure the concentration of K+ (c, in mg/L). The calibration curve was built analysing five standard solutions of dry KCl using a water + GC mixture as a solvent with approximately the same composition of the sample under investigation. The calibration data were fitted with a quadratic curve with a correlation coefficient R2 of 0.99993.

Results Section

3 Salt effects on polysaccharide aqueous solutions and dispersions

This Chapter is reprinted with permission from "Specific ion effect in polysaccharide dispersions". Copyright 2017 Elsevier Ltd. The article is attached at the end of the thesis (Paper I)

The aim of the work presented in this chapter is the evaluation of the salt effect on polysaccharide dispersions and solutions. More precisely, the study was focused on a better comprehension of both specific salt effect and high-salinity conditions resistance of different biopolymer-based systems.

In the first phase, a systematic study on the interactions between ten distinct anions or two different neutral co-solutes and three polysaccharides was firstly carried on, in order to examine how specific salt can significantly affect biopolymers rheological and thermal properties. The three polysaccharides investigated in the paper are guar gum (GG), sodium alginate (SA) and sodium hyaluronate (SH), while the added salts or co-solutes belong to the following list: NaF, NaCl, NaBr, NaI, Na_2SO_4, $NaClO_4$, NaSCN, Na_3PO_4, Na_2HPO_4, NaH_2PO_4, trehalose and urea.

In line with the aim of describing the variations in thermal and rheological behaviours induced by specific salt/co-solute effect, a combination of Differential Scanning Calorimetry (DSC) experiments and flow curves with plate-plate geometry was used to characterize both the pristine polysaccharide aqueous mixtures and the analogous systems in the presence of all the

anions or neutral co-solute, whose effects were considered singularly (one by one?).

In addition to the abovementioned goals, this study was also aimed at evaluating the control over viscosity of polysaccharide-based green formulations through simple salt triggers. The results are discussed in terms of changes in the polymer chains hydration, conformation and structure of the network. In particular, it is possible to summarize the main obtained results as follows:

1. The addition of salt or co-solute can significantly modify the texture of the polysaccharide network by affecting the hydration of the chains and, consequently, their intermolecular interactions. These changes are reflected in remarkable variations in thermal properties, viscosity and rheological behaviours passing from the pure polysaccharide systems to the salt/co-solute added ones.

2. The addition of a certain salt (or co-solute) affects the thermal properties of all the examined polysaccharides in a similar way. Oppositely, the salt-induced modifications in viscosity and rheological behaviour are not analogous in the case of GG and SH, which are neutral and charged polysaccharides respectively.

3. The modifications induced can be interpreted in terms of Hofmesiter series. Indeed, a strongly hydrated (kosmotropic) ion effectively deprives the polysaccharide chain of water, remain confined in the bulk solution, and

enhance the interchain interactions in the case of the neutral GG, resulting in a remarkable strengthening of the system. On the other hand, with the negatively charged SH, kosmotropes induce a weakening in the interactions due to less water-mediated interactions between charged chains. The chaotropes (bromide, iodide, thiocyanate) do not significantly affect the rheological properties of the systems. Being almost unhydrated, these ions are assumed to adsorb at the polymer surface and partially deplete some water from the hydration layer. This phenomenon is supposed to favour the unfolding of the chain, increase its hydration and reduce the interchain interactions

4. Phosphate ions exhibited a peculiar effect both on GG and SH: PO_4^{3-} and $H_2PO_4^-$ lower the viscosity, while HPO_4^{2-} produces a significant increment in the viscosity. Such behaviour is probably related to a delicate balance between the different pH properties and the capacity of the three ions to strengthen the HB network.

5. The results specifically depend on the investigated polysaccharides; however, the thermodynamic interpretation of the interactions might be potentially extended to other neutral or charged macromolecules in aqueous mixtures, providing in this way a precious a-priori indication for the formulation of different polymer-water mixtures.

In the case of SA based system the examined dispersions revealed really low viscosity values and, furthermore, the addition of salt or co-solute did not lead to remarkable changes in rheological behaviours, notwithstanding the effect on the thermal properties is in line with the variations observed for GG and SH. Moreover, the necessity to extend the study to less concentred polysaccharide systems (from 1% to 0.5 %), in the attempt of cover a wider viscosity range and reduce the formulation costs, drove our research towards a fourth polysaccharide that is hydroxypropyl cellulose (HPC) as a replacement for SA.

In the second stage of the study, polysaccharide aqueous systems were tested in high salinity conditions, more precisely in a mixture of monovalent and bivalent salts in different concentrations. Since one of the possible applications of the examined polysaccharides is the formulation of fracturing fluids for the shale gas recovery, the mixture aimed at testing the salt resistance of the polysaccharide systems was prepared following the data related to the flowback water salinity content of some European shale basins, which can be found in literature [350,351]. Thus, we defined this mixed salt solution as 'shale water' (SW), which is composed by NaCl 1 M, CaCl2 0.2 M, KBr 0.014 M, SrCl2 0.01M and BaCl2 0.002 M. The assumption underpinning these experiments is that the salt composition and concentration of the SW should be not too dissimilar from real operative salinity conditions that can be found in environmental applications.

In Figure 26 are shown the flow curves acquired for GG, SH and HPC aqueous mixtures both pure and in the high salinity

conditions achieved with the SW. All the investigated polysaccharide formulations exhibit a good salt tolerance. In spite of the differences in the zero applied stress viscosities, the flow curves obtained in high salinity conditions show rheological profiles similar to those of their pristine counterparties, which are characterized by a viscosity plateau in the low applied stress range followed by a drop-in viscosity that begins at a critical stress (non-Newtonian behaviour). More specifically, sodium hyaluronate viscosity is lowered by the mix of salts present in the shale water; guar gum is only marginally affected by the rich in salts environment; while, on the other hand, hydroxypropyl cellulose shows a stiffening of the network which results in an increased viscosity. The observed trend seems to agree with the results reported in Paper I: charged polysaccharides suffer for the reduction in 'available water' and show weaker network interactions, while the interactions between the neutral polysaccharide chains are strengthen by the partial removal of water molecules in the hydration layer.

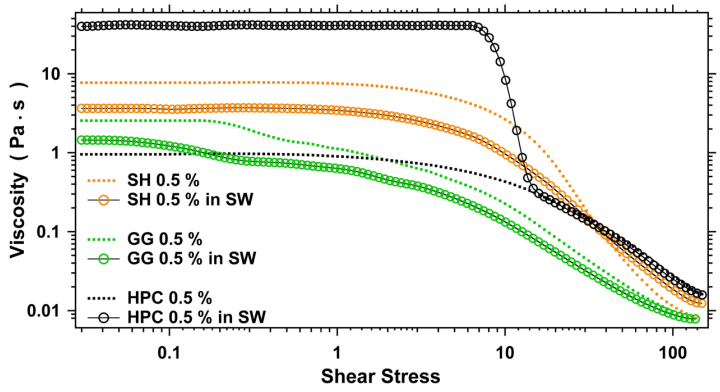

Figure 26: Flow curves of SH 0.5% pure (orange dotted line) and in SW (orange circles); GG 0.5% pure (green dotted line) and in SW (green circles); HPC 0.5% pure (black dotted line) and in SW (black circles).

4 Effect of specific additives on polysaccharide properties

The present chapter deals with the modification of viscosity, rheological behaviour, thermal resistance, electro-responsiveness and scales precipitation in polysaccharide aqueous systems based on GG, SH and HPC.

The chapter is divided into three sections, each of one describes the effects of different additives on the polysaccharide systems properties. More precisely, in the first paragraph, it is examined the modifications of the viscosity achieved through the inclusion of three bio-additive added singularly and one at a time: two surfactants, saponins and rhamnolipids, and sodium citrate as a crosslinker. In order to study the additive-induced modification on the viscosity and rheological properties, flow curves of the three polysaccharides systems were acquired both in the presence and in the absence of the specific additives.

In the second section, polyaspartate and polyglutamate were examined as green scale-limiting agents alternative to the commonly used polyacrylate. The anti-scale effects, on the precipitation of calcium/strontium/barium sulphate, was qualitatively investigated through the optical microscopy technique, carried out on both pure water solutions and SH-based model formulations.

Finally, the last paragraph deals with the multifunctional effect provided by the addition of carbon black (CB) to the investigated polysaccharide aqueous systems. More specifically,

it was examined the CB capability of strengthening the network, enhancing thermal resistance and improving electro-responsiveness. In order to characterize the different CB-polysaccharide systems and evaluate the effect imparted by the carbonaceous additive, rheology at different operating temperatures and before/after an electrical treatment, optical microscopy, and conductivity measurements were performed.

4.1 Saponins, Rhamnolipids and Sodium Citrate as viscosity modifiers

One of the most important practical aspects of polymer and surfactant systems is the possibility to modify and control rheology over very wide ranges. Indeed, surfactant molecules that bind to a polymer chain generally aggregate in clusters, which closely resemble the micelles formed in the absence of polymer [352]. This assembly is promoted when the polymer exhibits low polarity or contains hydrophobic domains, in this way an intimate contact between the micelles and the polymer chain becomes favoured. These aggregates, which are made up by surfactant molecules and hydrophobic groups/domains of polymer chains, are usually called ‘mixed micelles’ and they can significantly modify the network structure, leading to remarkable deviation of the rheological properties of the pristine systems in absence of surfactant [353].

Ionic surfactants may strongly interact with both non-ionic and ionic polymers, especially if polymer and hydrophilic head own opposite charges. On the other hand, non-ionic surfactants, significantly interact with polymer chains in the presence of

hydrophobic regions, as in block copolymers or so-called hydrophobically modified polymers (HMPs). In each case, the driving force that promotes surfactant self-assembly in polymer-surfactant systems is the hydrophobic interaction between the alkyl chains of the surfactant molecules, which in turn involves the hydrophobic parts of polymer chains.

The viscosity of a polymer with surfactant solution usually passes through a maximum, which is always just under the surfactants critical micelle concentration (CMC) [354]. Indeed, the increase in viscosity is attributed to the formation of mixed micelles, made up of surfactant and polymer hydrophobic regions, that act as crosslinkers between two distinct chains and strengthen the network [355–357]. However, when the surfactant concentration is further increased, the hydrophobic domains of two or more polymer chains are singularly solubilized by two or more micelles, resulting in the reduction of crosslink points and dissociation of the polymer network [358,359]. In Figure 27 it is schematized the surfactant-mediated polymer association and dissociation mechanism, which is strictly connected to the specific surfactant and its concentration in solution. At low surfactant concertation (region 1), few amphiphilic molecules are present and no significative effect on polymer network is observed; when the surfactant concentration is raised up without reaching the CMC (region 2), micellar bridging is established through mixed micelles structures and the network is enforced; finally, by further increasing surfactant concentration over the CMC (region 3), the dissociation of polymer chains is promoted and the hydrophobic domains are individually entangled in mixed micelles. Thus, the formation of mixed micelles is the onset of a

significant increase in viscosity. Most of the mixed micelles (in region 2) incorporate more than one hydrophobic region, which in turn means that a higher degree of overlap or links between separate chains is achieved.

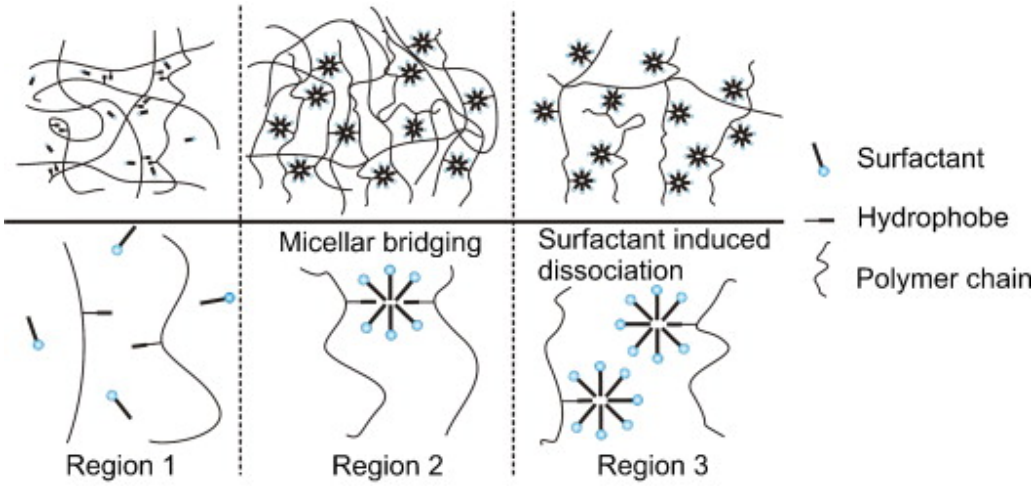

Figure 27: Surfactant-mediated polymer association and dissociation.

With the purpose of control and modify the viscosity and the rheology of the examined formulations, and always looking towards a more complete and functional fluid, the addition of green surfactants effective in enforcing/weakening the network was evaluated. In this light, saponins and rhamnolipids, two surfactants of biological origin, were added one at a time and in extremely small content, equal to 0.05 % in weight with respect to the total formulation, to the three investigated polysaccharide water systems.

More specifically, it was observed that saponin plays a constructive role in the formation of the polysaccharide network

both with GG and HPC, whereas with SH it enhances the viscosity of the systems only at lower stresses, then the flow curve of the pure hyaluronate and the profile of SH plus saponin in shale water exhibit a cross-over with increasing the applied stress (Figure 28a). Oppositely, rhamnolipids play against the structuring of the polysaccharide networks and, especially in the cases of GG and SH, move viscosity towards lower values. While the HPC solution is almost unchanged by the presence of rhamnolipid (Figure 28b).

These results can be interpreted in the light of the above-mentioned surfactant-mediated association/dissociation mechanism, even if deviations from the classic surfactant behaviour emerge. More precisely, it is possible to explain the opposite effects obtained by the addition of saponins and rhamnolipids in terms of surfactant nature and their tendency to establish crosslinking between chains. In both cases the surfactant concentration, equal to 0.05 wt.% (0.5 g/L) of the total formulation, exceeds the respective CMC (see 2.1.4 Additives) and, consequently, would be logical to expect a decrease in the viscosity of the two systems. If, on the one hand, rhamnolipids behave like classic surfactants, on the other saponins exhibit an atypical behaviour. This different attitude can be explained by considering the atypical nature of saponins as surfactants and its peculiar molecular structure (see Figure 14 and Figure 15). Indeed, saponins molecules possess a spatially restrained hydrophobic part combined with many hydrophilic segments oriented in diverse directions, which considerably extend the molecular volume and the capacity of interacting with distant chains. As a consequence of this extended molecular

structure, saponins can interact not only with the hydrophobic domains of the polymer chains but also with the hydrophilic segments, resulting in a further strengthening of the polymer network and an increase in viscosity. Moreover, the extended molecular volume of saponins provides a significantly high steric hindrance, which in turn makes unfavourable the individual solubilization of hydrophobic domains, as schematized in region 3, and the consequent polymer dissociation.

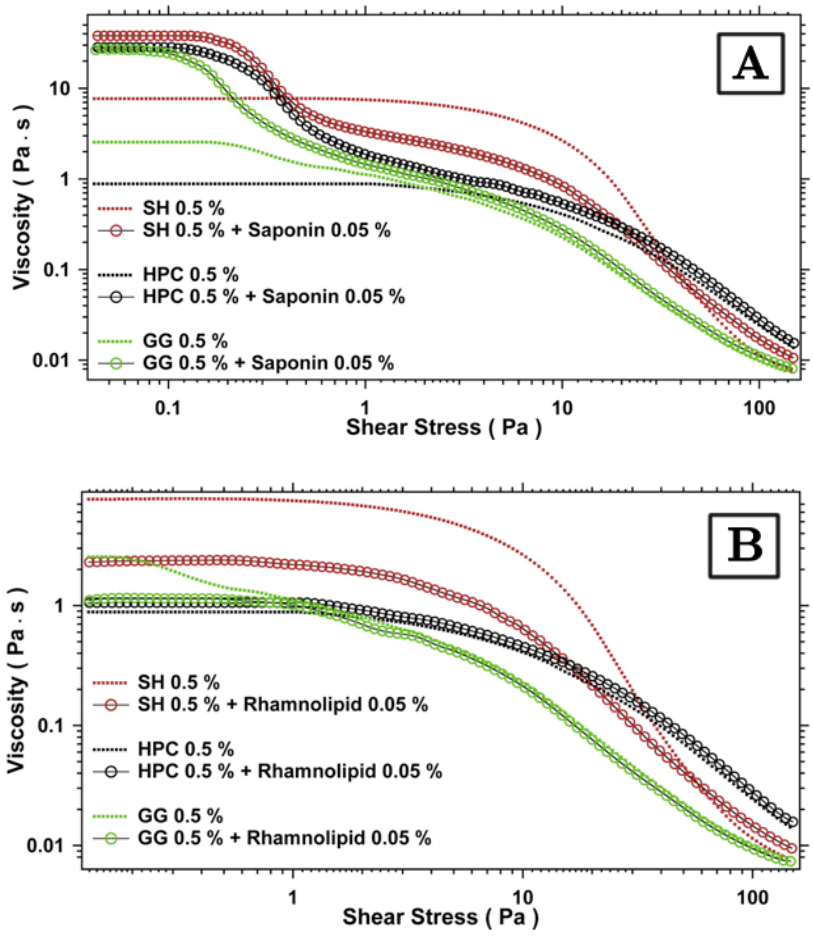

Figure 28: Flow curves acquired on GG, SH and HPC 0.5 % aqueous systems both in the absence and in the presence of A) Saponins 0.05 %, B) Rhamnolipids 0.05 %.

The last additive examined in the light of obtain significant viscosity modifications is sodium citrate. As in the cases of the two abovementioned biosurfactants, sodium citrate was added to the three polysaccharide systems in the amount of 0.05 wt.% of the total formulation.

Finally, by adding sodium citrate a more heterogeneous behaviour is observed, as evidenced in Figure 29: SH viscosity shows a noticeable reduction in terms of viscosity; guar gum exhibits a marked increment; and HPC reveals a remarkable surge in viscosity profile, with the zero stress viscosity that passes from 1 to 70 $Pa \cdot s$. The differentiated responses of the three polysaccharides demonstrate that sodium citrate can be used as an additive capable of both decreasing and enhancing the viscosity of the investigated formulations, depending on the specific polysaccharide used. Indeed, when added to neutral polysaccharide dispersions, such as those made up by GG or HPC, sodium citrate exhibits the behaviour of a crosslinking agent reported in the literature, thanks to which it finds applications in the role of crosslinker and reinforcer in different fields (see paragraph Sodium Citrate). More precisely, the outstanding upsurge exhibited by HPC is probably due to a combination of two effects: the crosslinking ability of citrate and a strengthening of the hydrophobic interactions through the hydroxypropyl side groups, which are brought closer by the action of citrate. Conversely, when sodium citrate is introduced in a negatively charged polymer network, like in the case of SH, the electrostatic repulsion arising from the interactions between the chains and the basic anions moves the polymer segments

away from each other, consequently resulting in a weakening of the network and a lower viscosity.

The rheological properties of sodium hyaluronate strongly depend on the specific pH [360]. Obviously, also the sodium citrate-polysaccharides interactions can be significantly altered by the specific pH conditions, which determine the most abundant citrate species passing from the tri-basic anion to the neutral citric acid, moving from high to low pH values respectively. In particular, when the tri-basic anion is increasingly protonated by a progressive acidification, it partially translates its donator into acceptor hydrogen-bonding character. This feature allows a closer distance with the negatively charged polymers in acid conditions but can also modify the interactions with neutral polysaccharides. Therefore, when sodium citrate is used as an additive for the modification of the polysaccharide viscosity it is crucial to consider the appropriate acid-base balance needed to obtain the desired effect, that can result in both a strengthening or a weakening of the network.

Anyway, the results obtained on the three investigated polysaccharide systems represent useful and easy-achievable strategies to control and modify the viscosity of the formulations, by simply adding low quantities of the appropriate additives.

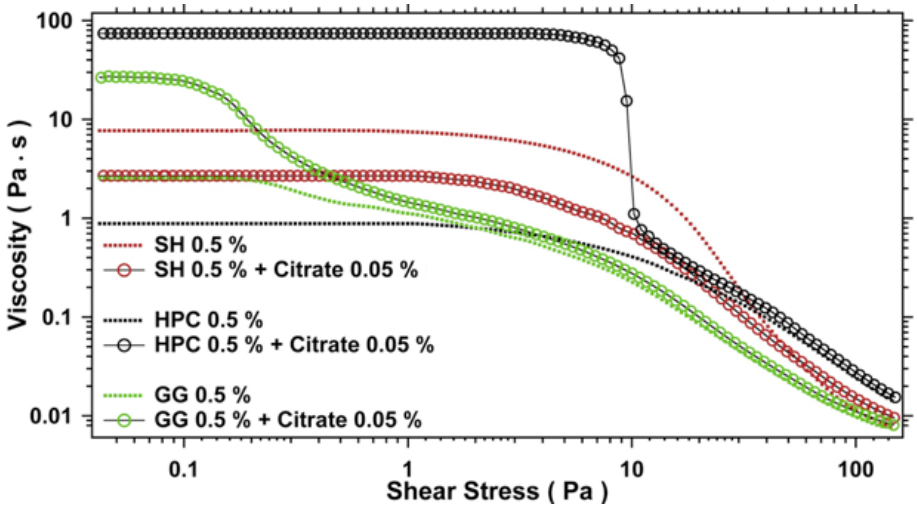

Figure 29: Flow curves acquired on GG, SH and HPC 0.5 % aqueous systems both in the absence and in the presence of Sodium Citrate 0.05 %.

4.2 Reduction of scales precipitation: Polyaspartate and Polyglutamate as anti-scale agents

The use of water can create several problems in many industrial applications, such as in the shale gas extraction, due to a massive precipitation of scales, especially when changes in temperature and/or pressure take place during the processes. In the light of limiting the scales formation, anti-scale agents are commonly included in various formulations.

In case of shale gas extraction, water used during the hydraulic fracture stimulation can form mineral scales when coming in contact with naturally occurring water in the producing well. To prevent this, a scale inhibitor is usually added to the

formulations in low dosages, that range between 0.0075% and 0.012% of the total fluid volume [361].

One of the most commonly used anti-scale agents, especially in shale gas applications, is the polyacrlylate (PAC) due to its resistance to chemical and biological breakdown. Thus, in our study PAC was chosen as a reference agent, in order to establish a comparison with polyaspartate (PAS) and polyglutamate (PG), the investigated green alternative anti-scale agents.

All the additives were used at a concentration of 10 mg/L (i.e., 0.001 wt% of the total formulation), in line with the data found in the literature [361,362].

First of all, we qualitatively evaluated their efficacy against calcium sulphate formation in pure water; tests were performed both at 25 and 60 °C to assess the performances of the scale inhibitors also at high temperatures achievable during various processes. Then, the behaviour of these additives was studied in a model polysaccharide formulation, consisting in sodium hyaluronate (0.5 wt%) plus sodium citrate (0.05 wt%) as physical cross-linker, in a content equal to 0.001 wt%. Finally, the effect of anti-scale agents on the precipitation of other insoluble salts, such as strontium sulphate, was investigated as well in order to gain information on their effectiveness against the precipitation of other sparingly soluble salts of alkali earth metals.

The choice of monitoring the anti-scale effect on the precipitation of calcium sulphate instead of other salts, such as carbonates, is based on the crystal morphology. Indeed, sulphates precipitate forming larger crystals with respect to carbonates, thus it is easier to observe eventual morphological variations induced by the presence of anti-scale agents through the optical microscopy

technique. For the same reason, results on barium salts in the presence of anti-scale agents are not reported since they precipitate immediately due to their very low solubility in water forming very small crystals, that are difficult to observe with a good resolution using optical microscope.

4.2.1 Effect in water

First of all, the performances of the studied anti-scale agents were assessed in pure water. Figure 30 shows $CaSO_4$ precipitates without and with the different studied anti-scale agents and the corresponding optical micrographs. In particular, we can observe a strong reduction of the amount of precipitated salt especially in the case of PAS (sample 1), PG-low M_w (sample 2) and PAC-medium and high M_w (sample 5 & 6).
Optical images reveal that, differently from the big floc crystals obtained when calcium sulphate is precipitated in neat water, the addition of the additives leads to the formation of less compact crystals for all the investigated molecules; however, the most remarkable effect on gypsum morphology is obtained for PAS and PAC-medium and high M_w.

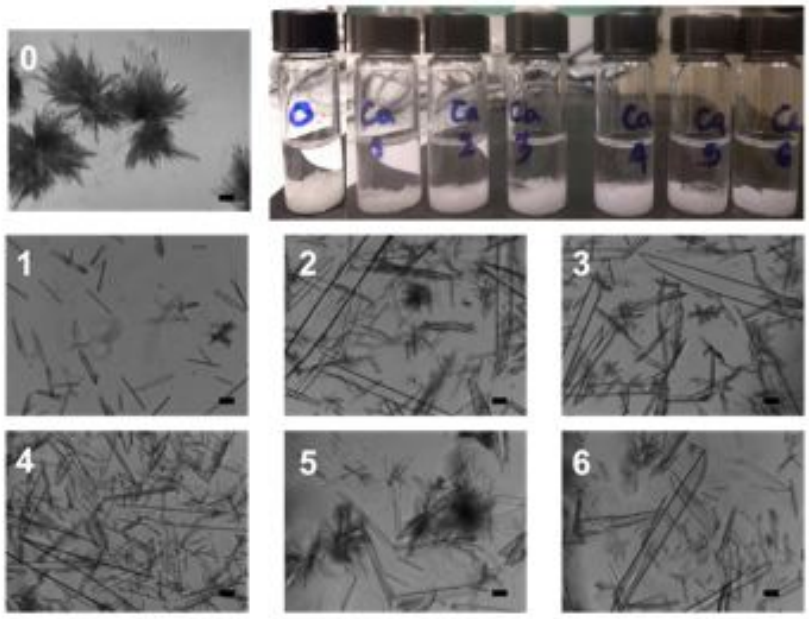

Figure 30: Effect of different anti-scale agents on the precipitation of calcium sulphate in water at 25 °C. Top: picture of the precipitates; bottom: corresponding optical micrographs. Scale bar: 100 µm. (0) no anti-scale agents; (1) PAS; (2) PG-low M_w; (3) PG-high M_w; (4) PAC-low M_w; (5) PAC-medium M_w; (6) PAC-high M_w.

Similar results were found in the case of $SrSO_4$ (see Figure 31).

Considering that scale inhibitors are added in a very small amount far from the stoichiometric concentration of the scaling species, scale suppression can be ascribed to physical mechanisms: the adsorption of anti-scale molecules on active growth sites of crystals leads to reduced nucleation and crystal growth rates and to the formation of distorted crystal structures. The crystal distortion weakens the tenacity of the scale and the highly irregular stressed crystals tend to slough off as crystal growth occurs. In addition, all the tested scale inhibitors possess negative charges in their chemical structure: the electrostatic

repulsion between approaching crystals is another possible mechanism to prevent the crystal growth. Considering that PAS possesses two negative charges while the other additives are monovalent salts, it is not surprising that it is one of the most performing agents.

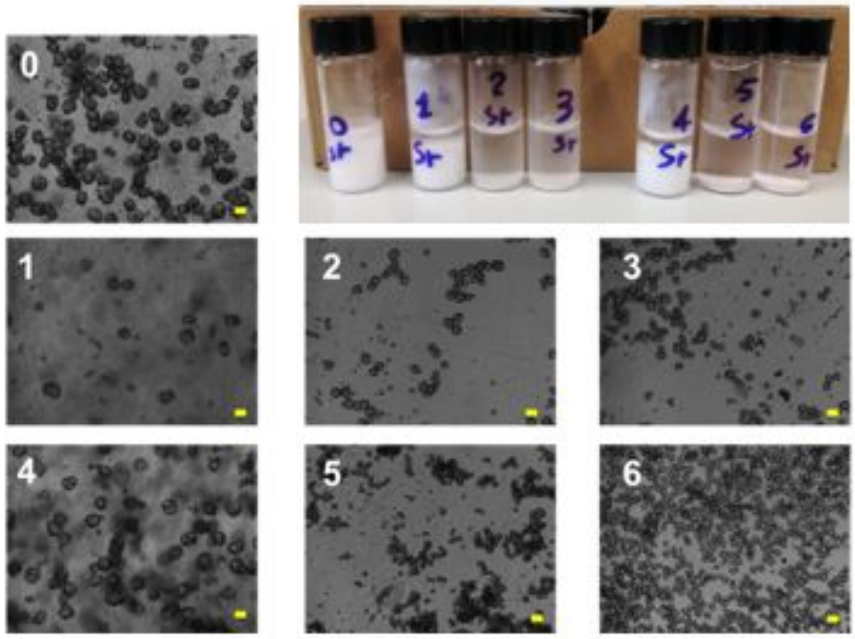

Figure 31: Effect of different anti-scale agents on the precipitation of strontium sulfate in water at 25 °C. Top: picture of the precipitates; bottom: corresponding optical micrographs. Scale bar: 100 μm. (0) no anti-scale agent; (1) PAS; (2) PG-low M_w; (3) PG-high M_w; (4) PAC-low M_w; (5) PAC-medium M_w; (6) PAC-high M_w.

Regarding the use of anti-scale agents with different molecular weights, the choice was done on the basis of previous literature reports. Indeed, it was proved that a minimum number of monomer units is required to have effective binding to the crystal surface that differs from mineral to mineral: for example, in the case of calcium sulphate in the presence of polyacrylates, it was found the optimum effectiveness with a molecular weight of

~2000 Da [363]. In another study on polyaspartate scale inhibitors, Ross et al. proved that polyaspartates in the range of 3000-4000 Da are the most effective for inhibition of calcium carbonate and barium sulphate, while, for calcium sulphate inhibition, the optimum molecular weight was found to be in the range of 1000-2000 Da [364].

In general, as the molecular weight increases, there might not be a proportional increase in binding effectiveness for a polymer. Additionally, the number of molecules in a given weight of polymer decreases, resulting in decreased activity. Finally, it has to be considered that larger molecules move in solution slower than smaller ones at the same temperature, as the adsorption on the surface of growing crystals is dependent on their diffusion coefficient in solution. Accordingly, the precipitation of larger crystals both in the case of $CaSO_4$ and $SrSO_4$ is observed in the case of the formulations containing high M_w PG and PAC. The effect of high temperature (60 °C) on the performances of anti-scale agents was also investigated. Tests were carried out just on calcium sulphate in water as an example and the obtained optical micrographs are shown in Figure 32.

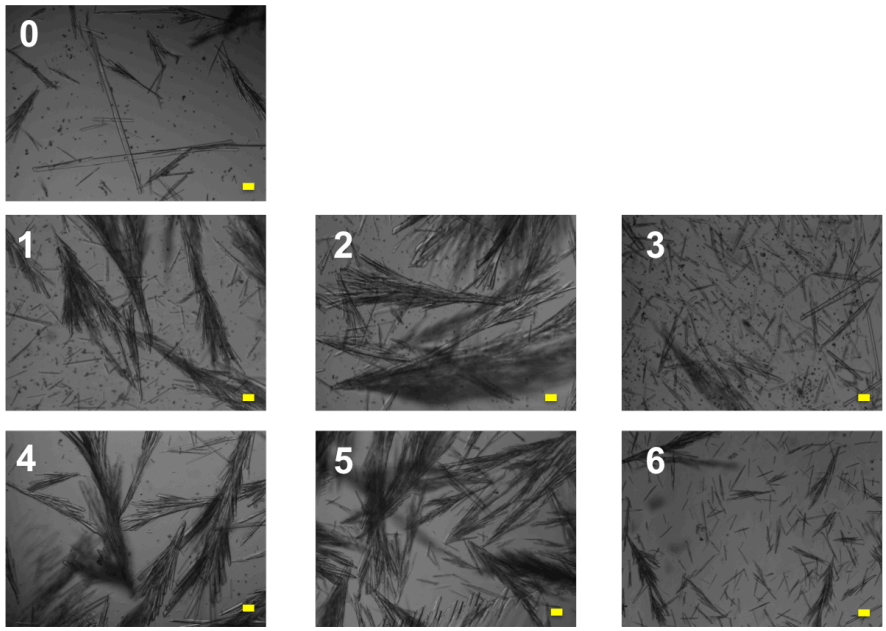

Figure 32: Optical micrographs showing the effect of different anti-scale agents on the precipitation of calcium sulphate in water at 60 °C. Scale bar: 100 µm. (0) no anti-scale agent; (1) PAS; (2) PG-low M_w; (3) PG-high M_w; (4) PAC-low M_w; (5) PAC-medium M_w; (6) PAC-high M_w.

By increasing temperature, the formation of bigger crystals is favored even in the presence of scale inhibitors since calcium sulfate solubility in water decreases in the same trend with room temperature. The worst performances of all the additives studied at 60 °C with respect to those observed at room temperature can be explained considering the enhancement of the thermal motion of anti-scale molecules, which probably reduces the rate of their adsorption on the forming crystalline nuclei. However, PG-low M_w and PAC-high M_w show very good performances in the reduction of precipitate amount.

4.2.2 Effect in polysaccharide-based formulations

Successively, the effectiveness of anti-scale agents was evaluated in the SH-based formulation, which was chosen as model formulation to observe the crystal precipitation for two reasons. The first one is the transparency and clearness of the SH system, analogously to the HPC formulation and differently to the GG dispersions. The second reason is that SH formulations do not produce bubbles when they are magnetically stirred, unlike what happens in the case of HPC systems. Figure 33 shows calcium sulphate precipitates and the corresponding optical micrographs, in the presence of scale inhibitors added to sodium hyaluronate-based formulation.

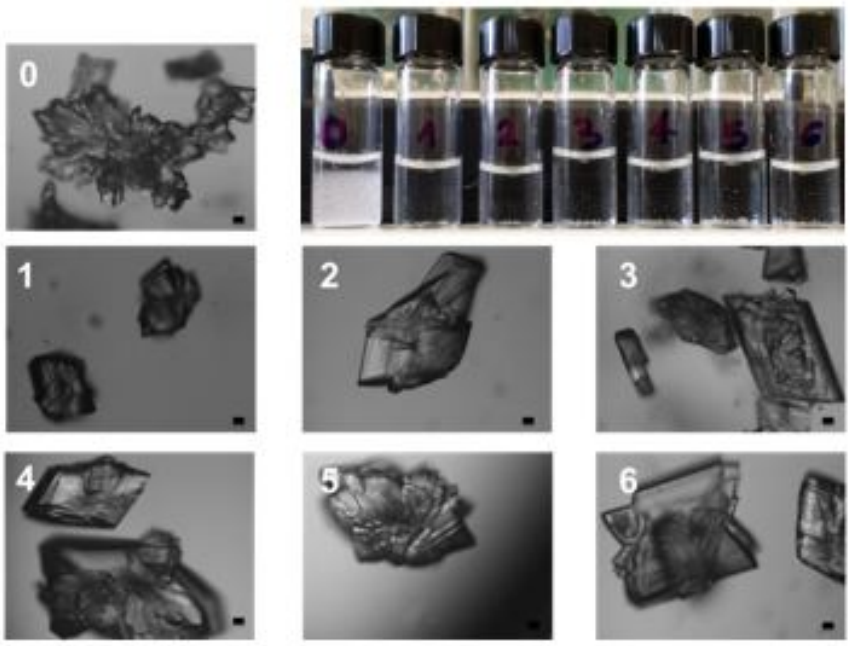

Figure 33: Effect of different anti-scale agents on the precipitation of calcium sulphate in SH-based formulation at 25 °C. Top: picture of the precipitates; bottom: corresponding micrographs. Scale bar: 100 µm. (0) no anti-scale agent; (1) PAS; (2)

PG-low M_w; (3) PG-high M_w; (4) PAC-low M_w; (5) PAC-medium M_w; (6) PAC-high M_w.

By observing the images, it is evident how crystal morphology completely changes from what was previously observed in pure water, both in the presence and in the absence of anti-scale additives. The formation of more ordered crystals with shorter needles suggests that the polysaccharide matrix acts as a 'templating agent'. By considering the high viscosity of polysaccharide aqueous systems, it reliable that crystalline nuclei move slower in comparison with pure water. In addition, the differences among the studied anti-scale agents are less remarkable if compared to that was observed in pure water: the amount of precipitate and the crystals morphology are more or less the same for all samples. However, all the anti-scale agents show very good performances, even better than those observed in water. An explanation of this unexpected result can be found in the sodium hyaluronate negatively charged chains, which make the polysaccharide itself a scale inhibitor. This, combined with the presence of anti-scale additives, ensures the stop of crystallites growth, thus significantly decreasing the amount of precipitate.

The obtained results are of great interest for real applications since it was demonstrated that the precipitation of scaling minerals can be inhibited by adding very small amounts of green additives, whose effectiveness results even enhanced in the polysaccharide formulations. In addition, it is possible to tune the effectiveness of these completely safe and degradable

additives against scales of different chemical composition simply varying the kind and molecular weight of the additives.

4.3 Carbon Black as a multifunctional additive

In this section are reported the results related to the effects on rheological properties, thermal resistance and electro-responsiveness induced by the addition of carbon black (CB). The results briefly described below are part of a paper recently submitted for publication that concerns the effect of CB as an additive in both polysaccharide and viscoelastic surfactant (VES) formulations. For the sake of coherence, the data listed here focus only on the three investigated polysaccharide GG, SH, and HPC; however, the full paper containing the results regarding both polysaccharide and VES systems is attached at end of the thesis (Paper II).

CB is an additive extensively used in the manufacturing of plastic, rubber and various polymer blends. This wide use is related to the peculiar properties that CB can provide to the host material in terms of longer lifetime, lower thermal degradation, electrical conductivity, improved resistance to mechanical stresses, viscoelasticity, microwave absorbance, and UV shielding effect [Paper II]. Although CB is mainly used in solids such as plastics and rubbers, its addition to liquid matrices is considerably increasing. This trend is related to the use of CB as a pigment in paints and inks, particularly those for ink-jet printing.

In the light of further study and characterize CB-enriched fluid systems, the addition of CB to polysaccharide-based formulations is explored with the aim of controlling and improving their thermal properties, rheological behaviour, conductivity and electrical responsiveness.
The investigation is carried out through rheology, electrical conductivity, and optical microscopy experiments. The results suggest that CB improves the performances of such water-based dispersions without affecting the 3D ordered network and the rheological behaviour. Set out below is a list of the most interesting results achieved on the polysaccharide-CB systems:

1. An amount of CB equal to 3 wt.% is successfully dispersed in aqueous systems thanks to the dispersing action of a 2 wt.% saponins solution. The examined dispersions result stable and, from the optical micrographs, it is possible to assert that the carbonaceous particulate appears homogeneously dispersed.

2. The addition of CB leads to an increase in the viscosity of at least an order of magnitude. This result is in line with the well-known thickening effect of CB and reflects the effective inclusion of the additive in the polysaccharide matrices. Moreover, in the presence of CB the rheological profiles are significantly modified with respect to the pure polysaccharides. In fact, besides the Newtonian region with a high viscosity value at low shear rates, a marked change in the slope of the curves is observed, for shear stress ranging be-tween 0.3 and 3 Pa, especially for GG

and SH based samples. This behaviour is probably related to the viscous drag between the polymer chains adsorbed on the CB particles and the bulk polymer.

3. The application of a voltage (30 V for 1 hour) to the formulations produces electrophoretic, polarization and osmotic effects, that result in the separation of a liquid and easy-flowing phase on one electrode, and of a viscous and sticky phase that concentrates at the opposite side. Taking advantage of their different viscosities, the two phases can be easily separated by simply turning the vessel. All pure polysaccharide dispersions, except for guar gum, exhibit this behaviour in response to the electrical treatment.

4. As expected, the addition of CB powder leads to a remarkable increase in the conductivity for all the polysaccharide systems, thus creating the conditions for the realization of smart molecular systems with enhanced electro-responsiveness.

5. When the CB-enriched polysaccharide dispersions are electrically treated different responses to the treatment were recorded, depending on the nature of the investigated polysaccharide. However, in all cases with the exception of guar gum, the split between the zero-shear viscosities related to the two phases obtained after the treatment, the easy-flowing phase and the sticky phase, results enhanced if compared to the pure polysaccharides. Thus,

the presence of CB in the SH and HPC polysaccharide matrices leads to an improved electro-responsiveness. This result suggests that CB can be successfully used as an additive to tune the response of polysaccharide formulations to an external treatment, such as the application of a voltage.

6. The rheological profiles acquired at different temperatures, ranging between 25 and 60 °C, confirm that when CB is added to polysaccharide matrices an enhancement in the formulation resistance to the temperature increase is achieved. At the same time, the rheological trend of each polysaccharide remains unchanged. More specifically, both SH and GG exhibit a downward shift in their flow curves, with a progressive lowering of the zero shear-viscosity, in response to the rise in temperature. Conversely, HPC shows an opposite trend characterized by an increase in both zero-shear viscosity and critical stress at which the system begins to disrupt. This latter apparently counterintuitive result is in line with the HPC lower critical solution temperature (LCST) described in the introduction.

5 Specific ion effects on glycerol carbonate

This Chapter is reprinted with permission from 'The curious case of potassium fluoride on glycerol carbonate. How salts can influence the structuredness of organic solvents' and 'Specific ion effects in non-aqueous solvents: the case of glycerol carbonate'. Copyright 2018 Elsevier Ltd. The articles are attached at the end of the thesis (Paper III and Paper IV).

5.1 The peculiar case of KF in Glycerol Carbonate

In this chapter the specific effects of different potassium salts on glycerol carbonate (GC, 4-hydroxymethyl-1,3-dioxolan-2-one) are discussed. The chronicle of this investigation began with the peculiar features observed on GC solutions of KF in a wide concentration range, varying from 10^{-3} M up to the saturation threshold. Indeed, the increasing addition of KF in GC progressively promotes the formation of a glassy liquid, which arrangement was evaluated through conductivity, rheology, differential scanning calorimetry (DSC) and infrared spectroscopy experiments.

GC is known to be an associated liquid, which is structured by strong intermolecular interactions. In addition, it possesses a remarkably high dielectric constant and an intense dipole moment which promotes the ion dissociation and the ion-solvent

interactions, resulting in this way an excellent solvent for electrolytes [paper III and IV]. Moreover, the presence of a terminal -OH moiety further contributes to extend the intermolecular association through hydrogen bonding (HB) interactions. In this scenario, the addition of a salt like potassium fluoride leads to remarkable changes in the solvent molecular organization and association, resulting in significant modification of the rheological and thermal properties. The main results achieved by examining the GC-KF interactions can be briefly outlined as follows:

1. In the dilute regime the specific conductivity (κ) raises with concentration (c) due to the increasing number of charge carriers. At moderate-to-high concentrations ($c > 1M$), as the ion-ion interactions strengthen and the viscosity of the medium increases, the curve shows a plateau due to the competition between the increase in the number of charge carriers and the decrease in ionic mobilities. For $c > 1.5$ M the solution becomes turbid, presumably due to the formation of larger particles and we observed the onset of an intense yellowing, that preludes to the degradation of GC.

2. From the molar conductivity (Λ) point of view, interesting insights into the solvent-solute interactions can be obtained. The curve shows a rapid increase in the dilute regime, then reaches a maximum around 0.15 M and progressively decreases when c further increases. The presence of a maximum is a behaviour that typically found

when the formation of ion pairs and triple ions (K_2F^+ and KF_2^- in the present case) occurs.

By the application of the Fuoss-Kraus model to the Λ data, the value of the association constants for ion pairs (K_I) and triple ions (K_T) were estimated to be $2.8 \cdot 10^6$ and 550, respectively. These values confirm the high tendency for K^+ and F^- to form ion pairs and the formation of triple ions in GC. Moreover, from the distribution curves derived from the association constants, it was found that KF ion pairs are always the most abundant species, they are accompanied by a very small fraction of free ions and the fraction of triple ions increases from as more KF is added. These data suggest that GC, despite its remarkably high dielectric constant, does not effectively solvate and separate K^+ and F^-, that rather remain associated in ion pairs (or triplets, at higher c). This behaviour can be explained in terms of the strong intermolecular interactions, on the 'structuredness' of the pure liquid, and on the asymmetry between the interactions of the terminal –OH moiety with anions and the carbonyl oxygen with cations in GC.

3. The viscosity of KF in GC solutions increases as a function of the solute concentration; however, when the KF content is further increased, the viscosity steeply grows and exceeds by >10 times the value found for the pure solvent. This suggests that KF induces a very significant change in the solvent ordering, by forcing the formation of a stronger and more viscous structure in the medium.

4. The fractions of triple ions, ion pairs and free ions obtained from the conductivity data were used in a modified Jones-Dole equation that describes the variation of the solution viscosity (η) as a function of the solute concentration c, by including two terms that consider the effect of free ion-solvent and ion pair-solvent interactions. By fitting the η values versus c with this modified equation, it was possible to attribute a positive and a negative contribution in strengthening the liquid structure to the ion pairs and charged species (free single or triple ions), respectively.

5. From the DSC experiments a glass transition temperature (T_g) was detected at – 70.8 °C for the pure GC and at – 61.3 °C for the KF saturated solution. The remarkable increment in the T_g of the liquid upon the addition of KF confirms a strong stiffening effect induced by the electrolyte on the solvent molecules structuredness.

6. The ATR-FTIR experiments indicate that an increment in the KF concentration brings about a shift in the O–H stretching band from 3420 cm^{-1} for pure GC, to 3370 cm^{-1} for the 0.68 M KF sample. This finding reflects the interaction between the hydroxyl moiety and the fluoride anion, that leads to a weakening in the O–H stretching mode. Further addition of KF results in a more significant shift of the band to lower wavenumbers. Importantly, the presence of KF does not modify the FTIR profile of pure

glycerol carbonate in correspondence of the other significative signals.

7. From the obtained results we proposed a hypothetical structure of the solution where the solvent molecules are organized in wormlike structures intercalated by KF ion pairs with which they interact through ion-dipole interactions (between K^+ and the C=O residue) and HB between F^- and the –OH moiety of GC. The dissolved KF salt mainly forms ion pairs that are responsible for the remarkable increase in the viscosity of the solution. A similar ordering was proposed by Jones for the dissolution of LiF in ethylene carbonate or propylene carbonate []. Free solvated K^+ and F^- and triple ions are present and contribute to the overall conductivity of the sample. In the side directions, along the main axis the solvent molecules are oriented in the opposite way, as required by the minimization of the dipoles energy. Such ordered structure would justify the conductivity and viscosity features of this glassy liquid system.

5.2 Specific ion effects in Glycerol Carbonate induced by various potassium salts

In a second step, the study was extended to other potassium salts like K_3PO_4, KOCN, K_2CO_3, KCl, K_2SO_4, KBr and KI. In this phase the effect of HB on the solubility of some salts, and more particularly on the thermodynamics and other physico-chemical

properties, was investigated through NMR, DSC and ATR-FTIR measurements. The set of the investigated salts ranges from potassium halides to phosphate, carbonate, sulphate and cyanate to study the effect of the anion's basicity and of the anion's capability to act as a donor/acceptor for hydrogen bonds. Since we operate either at the saturation limit or at a moderately high concentration, our results are both anion and solvent specific. The aim is to explore the nature of non-aqueous solvent Hofmeister effects systematically. Below the principal findings of the Paper III are recapped.

6 The solution of potassium phosphate, sulphate and carbonate behave similarly to the case of the aforementioned KF. The solvent can be easily oversaturated with these salts at all temperatures suggesting a behaviour analogous to one proposed for KF, where the formation of very stable ion pairs and triple ions occurs, while the free ions represent only a minor fraction of the entire distribution.

6 The NMR results show the change in the shift (δ) of the alcoholic proton that follows the series: KF > K_3PO_4 > KOCN > K_2CO_3 > KCl > K_2SO_4 > KBr > KI. These findings suggest that the major perturbation in the chemical shift of the –OH proton is produced by anions that behave as strong bases. The de-shielding of the hydrogen in the presence of these anions indicates an electron-poor environment around this nucleus. A quite strong interaction through hydrogen bonding between the

basic anion and the –OH group seems to take place in saturated solutions of KF, K_2CO_3, KCNO and K_3PO_4. Thus, the NMR results seem to confirm the hypothesis previously proposed for KF is reasonable also in the cases of phosphate, carbonate and cyanate. It is conceivable that also K_2CO_3 and K_3PO_4 ion pairs are intercalated between solvent molecules through ion-dipole interactions, involving the cation and the carbonyl moiety, and through hydrogen bond between the anion and the primary –OH residue.

On the other hand, other anions such as chloride, sulphate and bromide do not alter significantly the chemical environment around the alcoholic proton and/or the structuredness of the solvent. Remarkably, KI induces a strong decrement in the value of δ to lower ppm. Furthermore, potassium iodide lowered the chemical shifts of the non-hydroxyl protons, while the other investigated salts did not change the δ of the same nuclei respect to pure GC. Since HI is a very strong acid, and correspondingly iodide a very weak base, this behaviour is ascribable to the large polarizability of this anion and to the onset of significant dispersion interactions between the anion and the solvent molecules.

6 From the DSC curves acquired on the different GC solutions of the investigated potassium salts it is detected a significant increment in the glass transition temperature for K_3PO_4, KOCN and K_2CO_3 in comparison with the pure GC ($T_g = -70.8$ °C), while KCl, KBr and K_2SO_4 do not

modify T_g in a significant manner. Again, phosphate, carbonate and cyanate exhibit a behaviour similar to the before examined fluoride. The large increment in the T_g of the liquid upon the addition of KF, K_3PO_4, KOCN and K_2CO_3 confirms a strong stiffening effect induced by the electrolyte on the solvent molecules structuring and association as previously outlined.

6 The Attenuated ATR-FTIR experiments indicate a shift of the O–H stretching band from the pristine 3420 cm^{-1} for pure GC to lower wavenumber. The lowering in the frequency of the O–H signal induced by the presence of KF, K_3PO_4, KOCN and K_2CO_3 reflects the interaction between the hydroxyl moiety and the basic anion, that leads to a weakening in the O–H stretching mode. KI produces an effect comparable to that of KF with a significant shift (from 3420 to 3370 cm^{-1}) in the O–H stretching, indicating a weakening in the strength of the O–H bond. This result parallels the effect that we already recorded in NMR and DSC experiments on KI in GC samples and can be related to the partial adsorption of iodide ions near the GC ring.

6 Conclusions

The present work represents a contribution in the wide context of the complex fluids study. In particular, the project deals with systems based on polysaccharide solutions, surfactant solutions, electro-responsive suspensions, glassy-forming liquid, and biopolymer solutions. The selection of materials is driven by the choice of using green chemicals, possibly of biological origins, in order to design formulations potentially applicable in environmentally-safe frameworks. The formulations are investigated mainly from a rheological and structural perspective since complex fluids are systems characterized by an internal microstructure whose evolution affects the macroscopic dynamics of the material, especially the rheology.
The main objective of this work is the application of additives and strategies as triggers to modify the rheological, thermal, conductive, and responsive properties of the investigated systems. Indeed, the control over viscosity and other properties is an important operating parameter in many industrial processes that involve complex fluid formulations.

In order to pursue this goal, we started with the study of polysaccharide aqueous dispersions based on guar gum (GG), sodium hyaluronate (SH) and sodium alginate (SA). These systems were examined both pure and in the presence of different salts, with the purpose of evaluating the specific ion effects on their thermal properties and rheological behaviour. In details, the

investigation has shown that the presence of specific anions represents a feasible and easy-reproducible strategy to significantly modify the texture of the polysaccharide network by affecting the hydration of the chains and, consequently, their intermolecular interactions. These changes lead to remarkable variations in thermal properties, viscosity and rheological behaviours passing from the pure polysaccharide systems to the salt/co-solute added ones. More precisely, the salt/co-solute addition influences the thermal properties of all the polysaccharides in a similar way, whereas, in term of viscosity and rheological behaviour, it induces opposite changes in the cases of the neutral GG and the negatively charged SH. The modifications induced are interpreted in term of Hofmeister series. A strongly hydrated (kosmotropic) ion effectively deprives the polysaccharide chain of water, remain confined in the bulk solution, and enhance the interchain interactions. In the case of the neutral GG, this phenomenon leads to a remarkable strengthening of the system; while, when the negatively charged SH is involved, kosmotropic ions induce a weakening in the interactions due to less water-mediated interactions between charged chains. The chaotropic ions do not significantly affect the rheological properties of the systems since they remain almost dehydrated and tend to adsorb at the polymer. Therefore, the induced-changes specifically depend on the investigated polysaccharides; however, the thermodynamic interpretation of the interactions might be potentially extended to other neutral or charged macromolecules in aqueous mixtures, providing in this way a precious a- priori indication for the formulation of different polymer-water mixtures. Furthermore, knowing the

polysaccharide response to the presence of specific ions in advance allows the matching of the proper biopolymer with solutions of specific salt-composition and vice-versa.
The polysaccharide systems have also been tested in high salinity conditions, realized through a solution consisting of a mix of monovalent and divalent ions. All the examined formulations exhibit a great resistance in this environment, making feasible their usage also in applications where a good tolerance towards high salinity is required.

The second part of the work aims at evaluating different additives and strategies capable of modifying the viscosity, the rheological properties, the thermal resistance, the scale precipitation, the conductivity, and the electro-responsiveness nature of polysaccharide dispersions based on GG, SH and hydroxypropyl cellulose (HPC).
Firstly, one green crosslinker (sodium citrate) and two bio-surfactants as saponins and rhamnolipids have been tested in the role of viscosity modifying agents. Saponins and rhamnolipids affect the chain-chain interactions in the polysaccharide network through the so-called 'surfactant-mediated association/ dissociation mechanism'. Indeed, these surfactant molecules bind to the investigated polysaccharide and aggregate in clusters by incorporating the hydrophobic domains belonging to the macromolecule chains. These aggregates are known as mixed micelles and they can significantly modify the network structure, leading to remarkable changes in the rheological properties. The two bio-surfactants exhibit a considerable effect on the polysaccharide systems viscosity, even if added in low

concentration. More precisely, saponins strengthen the network and raise the viscosity, while rhamnolipids provide the opposite effect.

Even sodium citrate reveals to be an effective agent for the modification of viscosity. However, the addition of sodium citrate generates diverse effects on the rheological properties of the examined polysaccharide. More precisely, SH viscosity shows a noticeable reduction in terms of viscosity; GG exhibits a significant increment; and HPC reveals a remarkable surge in viscosity profile. The differentiated responses of the three polysaccharides demonstrate that sodium citrate can be used as an additive capable of both decreasing and enhancing the viscosity of the investigated formulations, depending on the specific polysaccharide used. Indeed, when added to neutral polysaccharide dispersions, such as those made up by GG or HPC, sodium citrate exhibits the behaviour of a crosslinking agent reported in the literature. Conversely, when sodium citrate is introduced in a negatively charged polymer network, like in the case of SH, the electrostatic repulsion arising from the interactions between the chains and the basic anions moves the polymer segments away from each other, consequently resulting in a weakening of the network and a lower viscosity. In each case, all the additive result effective in the modification of the viscosity and rheological properties of the polysaccharide aqueous dispersions.

With the aim of reducing the scales formation and precipitation in aqueous systems, polyglutamate and polyaspartate have been investigated as green biodegradable anti-scale agents. Their performances have been compared with the most commonly used

polyacrylates, which are non-biodegradable compounds. Both polyaspartate and polyglutamate reveal to be effective in modifying and limit the crystal growth and precipitation, making possible an use of these green alternatives in many application fields.

Another additive examined in the light of modifying the viscosity and other properties of polysaccharide-based systems is carbon black (CB). In our case, CB is homogeneously dispersed in aqueous solution of saponins and effectively included in the polysaccharide matrices in order strengthen the network, enhance the thermal resistance, and improve the response to the application of an electrical treatment. The optimized aqueous dispersion of CB in saponins results to be stable and homogeneous, making feasible the inclusion of carbonaceous particle in the polymer networks, whose viscosities result to be remarkably increased.

The application of a voltage to the pristine polysaccharide formulations produces electrophoretic, polarization and osmotic effects, that result in the separation of a liquid and easy-flowing phase on one electrode, and of a viscous and sticky phase that concentrates at the opposite side. Taking advantage of their different viscosities, the two phases can be easily separated by simply turning the vessel. All pure polysaccharide dispersions, except for guar gum, exhibit this behaviour in response to the electrical treatment. As expected, the addition of CB powder provides also a significant increase in the conductivity, thus creating the conditions for the realization of smart molecular systems with enhanced electro-responsiveness. More specifically, when a voltage is applied to the CB-enriched polysaccharide

dispersions, different responses were recorded, depending on the nature of the investigated polysaccharide. However, in all cases with the exception of guar gum, the split between the zero-shear viscosities related to the two phases obtained after the treatment results enhanced if compared to the pure polysaccharides. Thus, the presence of CB in the SH and HPC polysaccharide matrices leads to an improved electro-responsiveness. This result suggests that CB can be successfully used as an additive to tune the response of polysaccharide formulations to an external treatment, such as the application of a voltage.

Finally, the rheological profiles acquired at different temperatures, ranging between 25 and 60 °C, confirm that when CB is added to polysaccharide matrices an enhancement in the formulation resistance to the temperature increase is achieved. At the same time, the rheological trend of each polysaccharide remains unchanged. More specifically, both SH and GG exhibit a downward shift in their flow curves, with a progressive lowering of the zero shear-viscosity, in response to the rise in temperature. Conversely, HPC shows an opposite trend due to its LCST (lower critical solution temperature) and characterized by an increase in both zero-shear viscosity and critical stress at which the system begins to disrupt. This result further confirms that CB is effectively included in the polysaccharide matrix but, meantime, it does not modify the network structure.

Finally, in the last part of the work, the study is extended to the specific ion effects on glycerol carbonate (GC), an organic glassy-forming liquid solvent derived from glycerol. GC is known to be an associated liquid, which is structured by strong intermolecular

interactions. In addition, it possesses a remarkably high dielectric constant and an intense dipole moment which promotes the ion dissociation and the ion-solvent interactions, resulting in this way an excellent solvent for electrolytes. Moreover, the presence of a terminal -OH moiety further contributes to extending the intermolecular association through hydrogen bonding (HB) interactions. In this scenario, the addition of a salt leads to remarkable changes in the solvent molecular organization and association, resulting in significant modification of the rheological, structural and thermal properties.

The chronicle of this study begins with the investigation of the peculiar features observed on GC solutions of KF in a wide concentration range. The experimental results collected through conductivity, rheology, IR spectroscopy and DSC suggest a remarkable strengthening in the structure of liquid glycerol carbonate upon addition of potassium fluoride. This strengthening is ascribed to the hypothesized structure of the solution where the solvent molecules are organized in wormlike structures intercalated by KF ion pairs with which they interact through ion-dipole interactions (between K^+ and the C=O residue) and HB between F^- and the –OH moiety of GC. The dissolved KF salt mainly forms ion pairs that are responsible for the remarkable increase in the viscosity of the solution.

In order to better comprehend how different salts can affect the molecular association and the structuring of GC, an investigation has been extended to other potassium salts like K_3PO_4, KOCN, K_2CO_3, KCl, K_2SO_4, KBr and KI. In this phase, the effect of HB on the solubility of some salts, and more particularly on the thermodynamics and other physicochemical properties, was

investigated through NMR, DSC and ATR-FTIR measurements. In details, the results indicate that the dissolution of an electrolyte in glycerol carbonate occurs via two different solvation mechanisms. On one hand, the potassium cation interacts with the carbonyl group through simple electrostatic ion-dipole interactions. On the other hand, the role played by the anion greatly depends on its nature. If the anion has a strong basic nature, then it interacts with the hydroxyl moiety through hydrogen bonding. This would modify the structure of the solvent significantly. Instead, if the anion is not an acceptor, then its interaction with the solvent molecule is minimal.

In conclusion, this works represents an important contribution in the study of complex fluid and in the evaluation of alternative strategies to modify the structure and the rheological properties of these systems. Indeed, we have investigated the effect of several factors like the specific salt effects both on aqueous and organic systems, the resistance in high salinity conditions, the viscosity and rheological modifications through the use of biosurfactant and green crosslinker, the effective dispersion of carbon black in aqueous solutions and its inclusion in polysaccharide matrix, the application of a voltage as a strategy to achieve a remote control over the viscosity, and the reduction of the scale precipitation by using biopolymers as anti-scale agents. Furthermore, during this study, we have always taken into consideration the development of green and environmentally-safe formulations. This represents an added value for the investigated systems and for their potential usages

in green applications aimed at reducing the environmental footprint.

7 Bibliography

[1] J. Brannick, A. Kirshtein, C. Liu, Dynamics of Multi-Component Flows: Diffusive Interface Methods With Energetic Variational Approaches, in: Reference Module in Materials Science and Materials Engineering, Elsevier, 2016. doi:10.1016/B978-0-12-803581-8.03624-9.

[2] R.G. Larson, The structure and rheology of complex fluids, Oxford University Press, New York, 1999.

[3] P.E. Arratia, Viewpoint: Complex fluids at work, Physics. 4 (2011). https://physics.aps.org/articles/v4/9 (accessed October 22, 2018).

[4] A.J. Reuvers, Control of rheology of water-borne paints using associative thickeners, Progress in Organic Coatings. 35 (1999) 171–181. doi:10.1016/S0300-9440(99)00014-4.

[5] G.V. Barbosa-Cánovas, J.L. Kokini, L. Ma, A. Ibarz, The Rheology of Semiliquid Foods, Advances in Food and Nutrition Research. 39 (1996) 1–69. doi:10.1016/S1043-4526(08)60073-X.

[6] J.M.V. Blanshard, J.R. Mitchell, Polysaccharides in Food, Elsevier, 2013.

[7] D. Laba, Rheological Properties of Cosmetics and Toiletries, Routledge, 1993.

[8] D.J. Mastropietro, R. Nimroozi, H. Omidian, Rheology in Pharmaceutical Formulations-A Perspective, Journal of Developing Drugs. 02 (2013). doi:10.4172/2329-6631.1000108.

[9] J.K. Fink, ed., Chapter III - Fracturing Fluids, in: Water-Based Chemicals and Technology for Drilling, Completion, and Workover Fluids, Gulf Professional Publishing, Boston, 2015: pp. 115–178. doi:10.1016/B978-0-12-802505-5.00003-2.

[10] N. Thombare, U. Jha, S. Mishra, M.Z. Siddiqui, Guar gum as a promising starting material for diverse applications: A review, International Journal of Biological Macromolecules. 88 (2016) 361–372. doi:10.1016/j.ijbiomac.2016.04.001.

[11] R.L. Whistler, Industrial gums from plants: Guar and chia, Economic Botany. 36 (1982) 195–202. doi:10.1007/BF02858718.

[12] G.O. Philips, P.A. Williams, Gums and Stabilisers for the Food Industry 12, 2004. doi:10.1039/9781847551214.

[13] J.A. Casas, A.F. Mohedano, F. García-Ochoa, Viscosity of guar gum and xanthan/guar gum mixture solutions, Journal of the Science of

Food and Agriculture. 80 (n.d.) 1722–1727. doi:10.1002/1097-0010(20000915)80:12<1722::AID-JSFA708>3.0.CO;2-X.

[14] I.C.M. Dea, A.H. Clark, B.V. McCleary, Effect of galactose-substitution-patterns on the interaction properties of galactomannas, Carbohydrate Research. 147 (1986) 275–294. doi:10.1016/S0008-6215(00)90637-2.

[15] C. Sandolo, P. Matricardi, F. Alhaique, T. Coviello, Effect of temperature and cross-linking density on rheology of chemical cross-linked guar gum at the gel point - ScienceDirect, Food Hydrocolloids. 23 (2008) 210–220.

[16] D. Saha, S. Bhattacharya, Hydrocolloids as thickening and gelling agents in food: a critical review, J Food Sci Technol. 47 (2010) 587–597. doi:10.1007/s13197-010-0162-6.

[17] D. Mudgil, S. Barak, B.S. Khatar, Guar gum: processing, properties and food applications—A Review | SpringerLink, Journal of Food Science and Technology. 51 (2011) 409–418.

[18] A. Brinker, R. Reiter, Fish meal replacement by plant protein substitution and guar gum addition in trout feed, Part I: Effects on feed utilization and fish quality, Aquaculture. 310 (2011) 350–360. doi:10.1016/j.aquaculture.2010.09.041.

[19] J. Carrière, J.P. Jones, A.D. Broadbent, Decolorization Of Textile Dye Solutions, Ozone: Science & Engineering. 15 (1993) 189–200. doi:10.1080/01919519308552483.

[20] R.J. Chudzikowski, Guar gum and its applications, Journal of Society of Cosmetic Chemists. 22 (1971) 43–60.

[21] M. George, T.E. Abraham, pH sensitive alginate–guar gum hydrogel for the controlled delivery of protein drugs, International Journal of Pharmaceutics. 335 (2007) 123–129. doi:10.1016/j.ijpharm.2006.11.009.

[22] M.H. Pittler, E. Ernst, Guar gum for body weight reduction: meta-analysis of randomized trials, The American Journal of Medicine. 110 (2001) 724–730. doi:10.1016/S0002-9343(01)00702-1.

[23] E.G. Giannini, C. Mansi, P. Dulbecco, V. Savarino, Role of partially hydrolyzed guar gum in the treatment of irritable bowel syndrome, Nutrition. 22 (2006) 334–342. doi:10.1016/j.nut.2005.10.003.

[24] M.V.G. Paixão, R. de C. Balaban, Application of guar gum in brine clarification and oily water treatment, International Journal of Biological Macromolecules. 108 (2018) 119–126. doi:10.1016/j.ijbiomac.2017.11.166.

[25] D. McLean, V. Agarwal, K.R. Stack, J. Horne, D. Richardson,

Synthesis of gyar-gum-graft-poly(acrylamide-co-diallyldimethylammonium chloride) and its application in the pulp and paper industry, BioResources. 6 (2011) 4168–4180. doi:10.15376/biores.6.4.4168-4180.

[26] O. Bicak, Z. Ekmekci, D.J. Bradshaw, P.J. Harris, Adsorption of guar gum and CMC on pyrite, Minerals Engineering. 20 (2007) 996–1002. doi:10.1016/j.mineng.2007.03.002.

[27] A.M.A. Hasan, M.E. Abdel-Raouf, Applications of guar gum and its derivatives in petroleum industry: A review, Egyptian Journal of Petroleum. (2018). doi:10.1016/j.ejpe.2018.03.005.

[28] R. Beckwith, Depending On Guar For Shale Oil And Gas Development - OnePetro, Journal Of Petroleum Technology. 64 (2012). https://www.onepetro.org/journal-paper/SPE-1212-0044-JPT (accessed July 16, 2018).

[29] Q. Wang, P.R. Ellis, S.B. Ross-Murphy, The stability of guar gum in an aqueous system under acidic conditions, Food Hydrocolloids. 14 (2000) 129–134. doi:10.1016/S0268-005X(99)00058-2.

[30] Fraser J. R. E., Laurent T. C., Laurent U. B. G., Hyaluronan: its nature, distribution, functions and turnover, Journal of Internal Medicine. 242 (1997) 27–33. doi:10.1046/j.1365-2796.1997.00170.x.

[31] E.A. Balazs, T.C. Laurent, R.W. Jeanloz, Nomenclature of hyaluronic acid, Biochem J. 235 (1986) 903.

[32] W.A. Newman Dorland, Dorland's illustrated medical dictionary, 1890. https://www.google.it/search?ei=01VQW7SZE4mdkgWa847YBA&q=dorland+illustrated+medical+dictionary&oq=dorland+illustrated+medical+dicti&gs_l=psy-ab.3.0.0i203k1l5j0i22i30k1l3j0i22i10i30k1j0i22i30k1.17861.24537.0.25536.26.26.0.0.0.0.209.3391.0j25j1.26.0....0...1c.1.64.psy-ab..0.26.3386....0.3N5YBSZ3ACs (accessed July 19, 2018).

[33] R. Lanza, R. Langer, J. Vacanti, Principles of Tissue Engineering, Elsevier, 2014. doi:10.1016/C2011-0-07193-4.

[34] J.M. Guss, D.W.L. Hukins, P.J.C. Smith, W.T. Winter, S. Arnott, R. Moorhouse, D.A. Rees, Hyaluronic acid: Molecular conformations and interactions in two sodium salts, Journal of Molecular Biology. 95 (1975) 359–384. doi:10.1016/0022-2836(75)90196-5.

[35] K. Rilla, H. Siiskonen, A.P. Spicer, J.M.T. Hyttinen, M.I. Tammi, R.H. Tammi, Plasma Membrane Residence of Hyaluronan Synthase Is Coupled to Its Enzymatic Activity, J. Biol. Chem. 280 (2005) 31890–31897. doi:10.1074/jbc.M504736200.

[36] N. Itano, T. Sawai, M. Yoshida, P. Lenas, Y. Yamada, M. Imagawa, T. Shinomura, M. Hamaguchi, Y. Yoshida, Y. Ohnuki, S. Miyauchi, A.P. Spicer, J.A. McDonald, K. Kimata, Three Isoforms of Mammalian Hyaluronan Synthases Have Distinct Enzymatic Properties, J. Biol. Chem. 274 (1999) 25085–25092. doi:10.1074/jbc.274.35.25085.

[37] J.H. Sze, J.C. Brownlie, C.A. Love, Biotechnological production of hyaluronic acid: a mini review | SpringerLink, 3 Biotech. 6 (2016). https://link.springer.com/article/10.1007/s13205-016-0379-9 (accessed July 20, 2018).

[38] X. Lu, M.N. Kamat, L. Huang, X. Huang, Chemical Synthesis of a Hyaluronic Acid Decasaccharide - The Journal of Organic Chemistry (ACS Publications), The Journal of Organic Chemistry. 74 (2009) 7608–7617.

[39] C.G. Boeriu, J. Springer, F.K. Kooy, V.D. Broek, L.A. M, G. Eggink, Production Methods for Hyaluronan, International Journal of Carbohydrate Chemistry. 2013 (2013). doi:10.1155/2013/624967.

[40] L. Liu, Y. Liu, J. Li, G. Du, J. Chen, Microbial production of hyaluronic acid: current state, challenges, and perspectives, Microb Cell Fact. 10 (2011) 99. doi:10.1186/1475-2859-10-99.

[41] B.F. Chong, L.M. Blank, R. Mclaughlin, L.K. Nielsen, Microbial hyaluronic acid production, Appl Microbiol Biotechnol. 66 (2005) 341–351. doi:10.1007/s00253-004-1774-4.

[42] I.R. Amado, J.A. Vázquez, L. Pastrana, J.A. Teixeira, Microbial production of hyaluronic acid from agro-industrial by-products: Molasses and corn steep liquor, Biochemical Engineering Journal. 117 (2017) 181–187. doi:10.1016/j.bej.2016.09.017.

[43] P.L. DeAngelis, L.C. Oatman, D.F. Gay, Rapid Chemoenzymatic Synthesis of Monodisperse Hyaluronan Oligosaccharides with Immobilized Enzyme Reactors, J. Biol. Chem. 278 (2003) 35199–35203. doi:10.1074/jbc.M306431200.

[44] P.L. DeAngelis, Monodisperse Hyaluronan Polymers: Synthesis and Potential Applications, Current Pharmaceutical Biotechnology. 9 (2008). doi:info:doi/10.2174/138920108785161550.

[45] L. Lapcik, S. De Smedt, J. Demeester, P. Chabrecek, Hyaluronan: Preparation, Structure, Properties, and Applications, Chemical Reviews. 98 (1998) 2663–2684.

[46] V. Hascall, J.D. Esko, Hyaluronan, in: A. Varki, R.D. Cummings, J.D. Esko, P. Stanley, G.W. Hart, M. Aebi, A.G. Darvill, T. Kinoshita, N.H. Packer, J.H. Prestegard, R.L. Schnaar, P.H. Seeberger (Eds.),

Essentials of Glycobiology, 3rd ed., Cold Spring Harbor Laboratory Press, Cold Spring Harbor (NY), 2015. http://www.ncbi.nlm.nih.gov/books/NBK453025/ (accessed July 29, 2018).

[47] J.E. Scott, Supramolecular organization of extracellular matrix glycosaminoglycans, in vitro and in the tissues, FASEB J. 6 (1992) 2639–2645.

[48] J.E. Scott, C. Cummings, A. Brass, Y. Chen, Secondary and tertiary structures of hyaluronan in aqueous solution, investigated by rotary shadowing-electron microscopy and computer simulation., Biochemical Journal. 274 (1991) 699–705.

[49] S. Federico, U. Nöchel, C. Löwenberg, A. Lendlein, A.T. Neffe, Supramolecular hydrogel networks formed by molecular recognition of collagen and a peptide grafted to hyaluronic acid, Acta Biomaterialia. 38 (2016) 1–10. doi:10.1016/j.actbio.2016.04.018.

[50] J. Zhong, Y. Deng, B. Tian, B. Wang, Y. Sun, H. Huang, L. Chen, S. Ling, J. Yuan, Hyaluronate Acid-Dependent Protection and Enhanced Corneal Wound Healing against Oxidative Damage in Corneal Epithelial Cells, J Ophthalmol. 2016 (2016). doi:10.1155/2016/6538051.

[51] S.A. Unterman, M. Gibson, J.H. Lee, J. Crist, T. Chansakul, E.C. Yang, J.H. Elisseeff, Hyaluronic Acid-Binding Scaffold for Articular Cartilage Repair, Tissue Engineering Part A. 18 (2012) 2497–2506. doi:10.1089/ten.tea.2011.0711.

[52] T.M. Tamer, Hyaluronan and synovial joint: function, distribution and healing, Interdiscip Toxicol. 6 (2013) 111–125. doi:10.2478/intox-2013-0019.

[53] G. Kogan, L. Šoltés, R. Stern, P. Gemeiner, Hyaluronic acid: a natural biopolymer with a broad range of biomedical and industrial applications, Biotechnol Lett. 29 (2007) 17–25. doi:10.1007/s10529-006-9219-z.

[54] M.J. Rah, A review of hyaluronan and its ophthalmic applications, Optometry - Journal of the American Optometric Association. 82 (2011) 38–43. doi:10.1016/j.optm.2010.08.003.

[55] A. Maltese, A. Borzacchiello, L. Mayol, C. Bucolo, F. Maugeri, L. Nicolais, L. Ambrosio, Novel polysaccharides-based viscoelastic formulations for ophthalmic surgery: Rheological characterization, Biomaterials. 27 (2006) 5134–5142. doi:10.1016/j.biomaterials.2006.05.036.

[56] E.A. Balazs, J.L. Denlinger, Clinical Uses of Hyaluronan, in: Ciba

Foundation Symposium 143 - The Biology of Hyaluronan, Wiley-Blackwell, 1989: pp. 265–275. doi:10.1002/9780470513774.ch16.

[57] S.K. Kanchwala, L. Holloway, L.P. Bucky, Reliable Soft Tissue Augmentation: A Clinical Comparison of Injectable Soft-Tissue Fillers for Facial-Volume Augmentation, Annals of Plastic Surgery. 55 (2005) 30. doi:10.1097/01.sap.0000168292.69753.73.

[58] T. Pavicic, G.G. Gauglitz, P. Lersch, K. Schwach-Abdellaoui, B. Malle, H.C. Korting, M. Farwick, Efficacy of cream-based novel formulations of hyaluronic acid of different molecular weights in anti-wrinkle treatment., J Drugs Dermatol. 10 (2011) 990–1000.

[59] R.W. Chan, S.D. Gray, I.R. Titze, The Importance of Hyaluronic Acid in Vocal Fold Biomechanics , The Importance of Hyaluronic Acid in Vocal Fold Biomechanics, Otolaryngol Head Neck Surg. 124 (2001) 607–614. doi:10.1177/019459980112400602.

[60] R. Moseley, M. Walker, R.J. Waddington, W.Y.J. Chen, Comparison of the antioxidant properties of wound dressing materials–carboxymethylcellulose, hyaluronan benzyl ester and hyaluronan, towards polymorphonuclear leukocyte-derived reactive oxygen species, Biomaterials. 24 (2003) 1549–1557. doi:10.1016/S0142-9612(02)00540-9.

[61] E. Esposito, E. Menegatti, R. Cortesi, Hyaluronan-based microspheres as tools for drug delivery: a comparative study, International Journal of Pharmaceutics. 288 (2005) 35–49. doi:10.1016/j.ijpharm.2004.09.001.

[62] J.D. Wehr, 22 - BROWN ALGAE, in: J.D. Wehr, R.G. Sheath (Eds.), Freshwater Algae of North America, Academic Press, Burlington, 2003: pp. 757–773. doi:10.1016/B978-012741550-5/50023-4.

[63] P.A.J. Gorin, J.F.T. Spencer, Exocellular Alginic Acid from Azotobacter Vinelandii, Can. J. Chem. 44 (1966) 993–998. doi:10.1139/v66-147.

[64] F.A. Johnson, D.Q.M. Craig, A.D. Mercer, Characterization of the Block Structure and Molecular Weight of Sodium Alginates, Journal of Pharmacy and Pharmacology. 49 (1997) 639–643. doi:10.1111/j.2042-7158.1997.tb06085.x.

[65] O. Smidsrød, S.G. Whittington, Monte Carlo Investigation of Chemical Inhomogeneity in Polymers, Macromolecules. 2 (1969) 42–44. doi:10.1021/ma60007a008.

[66] T. Painter, O. Smidsrød, B. Larsen, A. Haug, J. Paasivirta, A Computer Study of the Changes in Composition-Distribution

Occurring during Random Depolymerization of a Binary Linear Heteropolysaccharide., Acta Chemica Scandinavica. 22 (1968) 1637–1648. doi:10.3891/acta.chem.scand.22-1637.

[67] B. Larsen, O. Smidsrød, T. Painter, A. Haug, S.E. Rasmussen, E. Sunde, N.A. Sørensen, Calculation of the Nearest-neighbour Frequencies in Fragments of Alginate from the Yields of Free Monomers after Partial Hydrolysis., Acta Chemica Scandinavica. 24 (1970) 726–728. doi:10.3891/acta.chem.scand.24-0726.

[68] A.I. Usov, Alginic acids and alginates: analytical methods used for their estimation and characterisation of composition and primary structure, Russ. Chem. Rev. 68 (1999) 957. doi:10.1070/RC1999v068n11ABEH000532.

[69] O. Smidsrød, A. Haug, B. Larsen, S. Gronowitz, R.A. Hoffman, A. Westerdahl, The Effect of Divalent Metals on the Properties of Alginate Solutions. I. Calcium Ions., Acta Chemica Scandinavica. 19 (1965) 329–340. doi:10.3891/acta.chem.scand.19-0329.

[70] A. Haug, J. Bjerrum, O. Buchardt, G.E. Olsen, C. Pedersen, J. Toft, The Affinity of Some Divalent Metals for Different Types of Alginates., Acta Chemica Scandinavica. 15 (1961) 1794–1795. doi:10.3891/acta.chem.scand.15-1794.

[71] A. Haug, S.E. Rasmussen, R.C. Sheppard, W.G. Terry, B. Sjöberg, J. Toft, Dissociation of Alginic Acid., Acta Chemica Scandinavica. 15 (1961) 950–952. doi:10.3891/acta.chem.scand.15-0950.

[72] K.I. Draget, 29 - Alginates, in: G.O. Phillips, P.A. Williams (Eds.), Handbook of Hydrocolloids (Second Edition), Woodhead Publishing, 2009: pp. 807–828. doi:10.1533/9781845695873.807.

[73] K.Y. Lee, D.J. Mooney, Alginate: properties and biomedical applications, Prog Polym Sci. 37 (2012) 106–126. doi:10.1016/j.progpolymsci.2011.06.003.

[74] A. Haug, O. Smidsrød, B. Larsen, S. Gronowitz, R.A. Hoffman, A. Westerdahl, The Effect of Divalent Metals on the Properties of Alginate Solutions. II. Comparison of Different Metal Ions., Acta Chemica Scandinavica. 19 (1965) 341–351. doi:10.3891/acta.chem.scand.19-0341.

[75] P. Sikorski, F. Mo, G. Skjåk-Bræk, B.T. Stokke, Evidence for Egg-Box-Compatible Interactions in Calcium−Alginate Gels from Fiber X-ray Diffraction, Biomacromolecules. 8 (2007) 2098–2103. doi:10.1021/bm0701503.

[76] H.H. Tønnesen, J. Karlsen, Alginate in Drug Delivery Systems, Drug Development and Industrial Pharmacy. 28 (2002) 621–630.

doi:10.1081/DDC-120003853.

[77] D.A. Rees, E.J. Welsh, Secondary and Tertiary Structure of Polysaccharides in Solutions and Gels, Angewandte Chemie International Edition in English. 16 (1977) 214–224. doi:10.1002/anie.197702141.

[78] G.T. Grant, E.R. Morris, D.A. Rees, P.J.C. Smith, D. Thom, Biological interactions between polysaccharides and divalent cations: The egg-box model, FEBS Letters. 32 (1973) 195–198. doi:10.1016/0014-5793(73)80770-7.

[79] G. Chan, D.J. Mooney, Ca2+ released from calcium alginate gels can promote inflammatory responses in vitro and in vivo, Acta Biomater. 9 (2013). doi:10.1016/j.actbio.2013.08.002.

[80] P. Eiselt, K.Y. Lee, D.J. Mooney, Rigidity of Two-Component Hydrogels Prepared from Alginate and Poly(ethylene glycol)−Diamines, Macromolecules. 32 (1999) 5561–5566. doi:10.1021/ma990514m.

[81] K.Y. Lee, K.H. Bouhadir, D.J. Mooney, Controlled degradation of hydrogels using multi-functional cross-linking molecules, Biomaterials. 25 (2004) 2461–2466.

[82] K.A. Smeds, A. Pfister-Serres, D. Miki, K. Dastgheib, M. Inoue, D.L. Hatchell, M.W. Grinstaff, Photocrosslinkable polysaccharides for in situ hydrogel formation, J. Biomed. Mater. Res. 54 (2001) 115–121.

[83] D.W.S. Wong, K.S. Gregorski, J.S. Hudson, A.E. Pavlath, Calcium Alginate Films: Thermal Properties and Permeability to Sorbate and Ascorbate, Journal of Food Science. 61 (1996) 337–341. doi:10.1111/j.1365-2621.1996.tb14189.x.

[84] R. Fijan, S. Šostar-Turk, R. Lapasin, Rheological study of interactions between non-ionic surfactants and polysaccharide thickeners used in textile printing, Carbohydrate Polymers. 68 (2007) 708–717. doi:10.1016/j.carbpol.2006.08.006.

[85] M.M. El-Molla, R. Schneider, Development of ecofriendly binders for pigment printing of all types of textile fabrics, Dyes and Pigments. 71 (2006) 130–137. doi:10.1016/j.dyepig.2005.06.017.

[86] L. Corvaglia, A. Aceti, E. Mariani, M.D. Giorgi, M.G. Capretti, G. Faldella, The efficacy of sodium alginate (Gaviscon) for the treatment of gastro-oesophageal reflux in preterm infants, Alimentary Pharmacology & Therapeutics. 33 (2011) 466–470. doi:10.1111/j.1365-2036.2010.04545.x.

[87] H.A.A. El-Rehim, Characterization and possible agricultural application of polyacrylamide/sodium alginate crosslinked hydrogels

prepared by ionizing radiation, Journal of Applied Polymer Science. 101 (2006) 3572–3580. doi:10.1002/app.22487.

[88] A.R. Kulkarni, K.S. Soppimath, T.M. Aminabhavi, A.M. Dave, M.H. Mehta, Glutaraldehyde crosslinked sodium alginate beads containing liquid pesticide for soil application, Journal of Controlled Release. 63 (2000) 97–105. doi:10.1016/S0168-3659(99)00176-5.

[89] C. Chen, Y. Huang, C. Zhu, Y. Nie, J. Yang, D. Sun, Synthesis and characterization of hydroxypropyl cellulose from bacterial cellulose, Chin J Polym Sci. 32 (2014) 439–448. doi:10.1007/s10118-014-1419-8.

[90] K.E. Perepelkin, Renewable Plant Resources and Processed Products in Chemical Fibre Production, Fibre Chemistry. 36 (2004) 161–176. doi:10.1023/B:FICH.0000037977.65328.4e.

[91] Suhas, V.K. Gupta, P.J.M. Carrott, R. Singh, M. Chaudhary, S. Kushwaha, Cellulose: A review as natural, modified and activated carbon adsorbent, Bioresource Technology. 216 (2016) 1066–1076. doi:10.1016/j.biortech.2016.05.106.

[92] K. Jedvert, T. Heinze, Cellulose modification and shaping – a review, Journal of Polymer Engineering. 37 (2017) 845–860. doi:10.1515/polyeng-2016-0272.

[93] T. Heinze, T. Liebert, Unconventional methods in cellulose functionalization, Progress in Polymer Science. 26 (2001) 1689–1762. doi:10.1016/S0079-6700(01)00022-3.

[94] D. Roy, M. Semsarilar, J.T. Guthrie, S. Perrier, Cellulose modification by polymer grafting: a review, Chem. Soc. Rev. 38 (2009) 2046–2064. doi:10.1039/B808639G.

[95] A.C. O'sullivan, Cellulose: the structure slowly unravels, Cellulose. 4 (1997) 173–207. doi:10.1023/A:1018431705579.

[96] S. Fortin, G. Charlet, Phase diagram of aqueous solutions of (hydroxypropyl)cellulose, Macromolecules. 22 (1989) 2286–2292. doi:10.1021/ma00195a050.

[97] S.N. Bhadani, D.G. Gray, Cellulose-Based Liquid Crystalline Polymers; Esters of (Hydroxypropyl) Cellulose, Molecular Crystals and Liquid Crystals. 99 (1983) 29–38. doi:10.1080/00268948308072026.

[98] P.J. Wakelyn, N.R. Bertoniere, A.D. French, D.P. Thibodeaux, B.A. Triplett, M.-A. Rousselle, W.R.J. Goynes, J.V. Edwards, L. Hunter, D.D. McAlister, G.R. Gamble, 9 - Cotton Fibers, in: Handbook of Fiber Chemistry (Edited by Menachem Lewin), Third Edition, CRC Press, New York, 1998.

[99] B. Medronho, A. Romano, M.G. Miguel, L. Stigsson, B. Lindman, Rationalizing cellulose (in)solubility: reviewing basic physicochemical

aspects and role of hydrophobic interactions, Cellulose. 19 (2012) 581–587. doi:10.1007/s10570-011-9644-6.

[100] E.D. Klug, Some properties of water-soluble hydroxyalkyl celluloses and their derivatives, Journal of Polymer Science Part C: Polymer Symposia. 36 (1971) 491–508. doi:10.1002/polc.5070360137.

[101] X. Lu, Z. Hu, J. Schwartz, Phase Transition Behavior of Hydroxypropylcellulose under Interpolymer Complexation with Poly(acrylic acid), Macromolecules. 35 (2002) 9164–9168.

[102] M. Bagheri, S. Shateri, Thermosensitive nanosized micelles from cholesteryl-modified hydroxypropyl cellulose as a novel carrier of hydrophobic drugs | SpringerLink, Iranian Polymer Journal. 21 (2012) 365–373.

[103] M.J. Seurin, J.M. Gilli, F. Fried, A.T. Bosch, P. Sixou, Liquid Crystalline Polymer Solutions and Mixtures, in: Polymeric Liquid Crystals, Springer, Boston, MA, 1985: pp. 377–387. doi:10.1007/978-1-4899-2299-1_24.

[104] D.-S. Lee, A.S. Perlin, 13C-N.M.R.-spectral and related studies on the distribution of substituents in O-(2-hydroxypropyl)cellulose, Carbohydrate Research. 106 (1982) 1–19. doi:10.1016/S0008-6215(00)80728-4.

[105] C. Porsch, S. Hansson, N. Nordgren, E. Malmström, Thermo-responsive cellulose-based architectures: tailoring LCST using poly(ethylene glycol) methacrylates, Polymer Chemistry. 2 (2011) 1114–1123. doi:10.1039/C0PY00417K.

[106] F.M. Winnik, Effect of temperature on aqueous solutions of pyrene-labeled (hydroxypropyl)cellulose, Macromolecules. 20 (1987) 2745–2750. doi:10.1021/ma00177a019.

[107] CFR - Code of Federal Regulations Title 21, United States Food and Drug Administration, 2017. https://www.accessdata.fda.gov/scripts/cdrh/cfdocs/cfcfr/CFRSearch.cfm?fr=172.870 (accessed August 7, 2018).

[108] D. Bielska, A. Karewicz, K. Kamiński, I. Kiełkowicz, T. Lachowicz, K. Szczubiałka, M. Nowakowska, Self-organized thermo-responsive hydroxypropyl cellulose nanoparticles for curcumin delivery, European Polymer Journal. 49 (2013) 2485–2494. doi:10.1016/j.eurpolymj.2013.02.012.

[109] F.J. Xu, Y. Ping, J. Ma, G.P. Tang, W.T. Yang, J. Li, E.T. Kang, K.G. Neoh, Comb-shaped copolymers composed of hydroxypropyl cellulose backbones and cationic poly((2-dimethyl amino)ethyl methacrylate) side chains for gene delivery., Bioconjug Chem. 20

(2009) 1449–1458. doi:10.1021/bc900044h.

[110] R. Liu, M. Fraylich, B.R. Saunders, Thermoresponsive copolymers: from fundamental studies to applications, Colloid Polym Sci. 287 (2009) 627–643. doi:10.1007/s00396-009-2028-x.

[111] R.S. Werbowyj, D.G. Gray, Liquid Crystalline Structure In Aqueous Hydroxypropyl Cellulose Solutions, Molecular Crystals and Liquid Crystals. 34 (1976) 97–103. doi:10.1080/15421407608083894.

[112] J.M. Seddon, Lyotropic Phase Behaviour of Biological Amphiphiles, Berichte Der Bunsengesellschaft Für Physikalische Chemie. 100 (1996) 380–393. doi:10.1002/bbpc.19961000324.

[113] Y. Geng, P.L. Almeida, S.N. Fernandes, C. Cheng, P. Palffy-Muhoray, M.H. Godinho, A cellulose liquid crystal motor: a steam engine of the second kind, Scientific Reports. 3 (2013) 1028. doi:10.1038/srep01028.

[114] G. Evmenenko, C.-J. Yu, S. Kewalramani, P. Dutta, Structural reorganization in films of cellulose derivatives in the presence of colloidal particles, Polymer. 45 (2004) 6269–6273. doi:10.1016/j.polymer.2004.07.015.

[115] A. Patra, P.K. Verma, R.K. Mitra, Slow relaxation dynamics of water in hydroxypropyl cellulose-water mixture traces its phase transition pathway: a spectroscopic investigation, J Phys Chem B. 116 (2012) 1508–1516. doi:10.1021/jp300428h.

[116] M.H. Godinho, D.G. Gray, P. Pieranski, Revisiting (hydroxypropyl) cellulose (HPC)/water liquid crystalline system, Liquid Crystals. 44 (2017) 2108–2120. doi:10.1080/02678292.2017.1325018.

[117] S. Borodkin, F.E. Tucker, Drug release from hydroxypropyl cellulose-polyvinyl acetate films, Journal of Pharmaceutical Sciences. 63 (1974) 1359–1364. doi:10.1002/jps.2600630904.

[118] B. Rodu, C.M. Russell, Performance of a hydroxypropyl cellulose film former in normal and ulcerated oral mucosa, Oral Surgery, Oral Medicine, Oral Pathology. 65 (1988) 699–703. doi:10.1016/0030-4220(88)90013-8.

[119] T. Nguyen, R. Latkany, Review of hydroxypropyl cellulose ophthalmic inserts for treatment of dry eye, Clin Ophthalmol. 5 (2011) 587–591. doi:10.2147/OPTH.S13889.

[120] S. Mezdour, G. Cuvelier, M.J. Cash, C. Michon, Surface rheological properties of hydroxypropyl cellulose at air–water interface, Food Hydrocolloids. 21 (2007) 776–781. doi:10.1016/j.foodhyd.2006.09.011.

[121] W.F. Bergfeld, D.C. Liebler, T.J. Slaga, Final Report of the Cosmetic Ingredient Review Expert Panel Amended Safety Assessment of Cellulose and Related Polymers as used in Cosmetics March 23 , 2009,

2009. /paper/Final-Report-of-the-Cosmetic-Ingredient-Review-of-%2C-Bergfeld-Liebler/d664a7f23cf41aab0d464b7b15071a508280a91a (accessed August 9, 2018).

[122] K. Gill, F. Boersma, Solvent reactivation of hydroxypropyl cellulose (Klucel G®) in textile conservation: Recent developments, The Conservator. 21 (1997) 12–20. doi:10.1080/01410096.1997.9995111.

[123] R.L. Feller, M. Wilt, G.C. Institute, Evaluation of cellulose ethers for conservation, Marina del Rey, Calif., USA : Getty Conservation Institute, 1990. https://trove.nla.gov.au/version/39879635 (accessed August 9, 2018).

[124] W.K. Teng, G.C. Ngoh, R. Yusoff, M.K. Aroua, A review on the performance of glycerol carbonate production via catalytic transesterification: Effects of influencing parameters, Energy Conversion and Management. 88 (2014) 484–497. doi:10.1016/j.enconman.2014.08.036.

[125] M.O. Sonnati, S. Amigoni, E.P.T. de Givenchy, T. Darmanin, O. Choulet, F. Guittard, Glycerol carbonate as a versatile building block for tomorrow: synthesis, reactivity, properties and applications, Green Chem. 15 (2013) 283–306. doi:10.1039/C2GC36525A.

[126] M. Pagliaro, R. Ciriminna, H. Kimura, M. Rossi, C. Della Pina, From Glycerol to Value-Added Products, Angewandte Chemie International Edition. 46 (2007) 4434–4440. doi:10.1002/anie.200604694.

[127] C.-H. (Clayton) Zhou, J.N. Beltramini, Y.-X. Fan, G.Q. (Max) Lu, Chemoselective catalytic conversion of glycerol as a biorenewable source to valuable commodity chemicals, Chem. Soc. Rev. 37 (2008) 527–549. doi:10.1039/B707343G.

[128] J.R. Ochoa-Gómez, O. Gómez-Jiménez-Aberasturi, C. Ramírez-López, M. Belsué, A Brief Review on Industrial Alternatives for the Manufacturing of Glycerol Carbonate, a Green Chemical, Org. Process Res. Dev. 16 (2012) 389–399. doi:10.1021/op200369v.

[129] P.U. Okoye, A.Z. Abdullah, B.H. Hameed, Stabilized ladle furnace steel slag for glycerol carbonate synthesis via glycerol transesterification reaction with dimethyl carbonate, Energy Conversion and Management. 133 (2017) 477–485. doi:10.1016/j.enconman.2016.10.067.

[130] P.U. Okoye, A.Z. Abdullah, B.H. Hameed, Glycerol carbonate synthesis from glycerol and dimethyl carbonate using trisodium phosphate, Journal of the Taiwan Institute of Chemical Engineers. 68 (2016) 51–58. doi:10.1016/j.jtice.2016.09.011.

[131] A. Behr, J. Eilting, K. Irawadi, J. Leschinski, F. Lindner, Improved

utilisation of renewable resources: New important derivatives of glycerol, Green Chem. 10 (2008) 13–30. doi:10.1039/B710561D.

[132] A. Corma, S. Iborra, A. Velty, Chemical Routes for the Transformation of Biomass into Chemicals, Chem. Rev. 107 (2007) 2411–2502. doi:10.1021/cr050989d.

[133] A. Takagaki, K. Iwatani, S. Nishimura, K. Ebitani, Synthesis of glycerol carbonate from glycerol and dialkyl carbonates using hydrotalcite as a reusable heterogeneous base catalyst, Green Chem. 12 (2010) 578–581. doi:10.1039/B925404H.

[134] Y. Chernyak, Dielectric constant, dipole moment, and solubility parameters of some cyclic acid esters, Journal of Chemical and Engineering Data. 51 (2006) 416–418. doi:10.1021/je050341y.

[135] U.R. Pedersen, P. Harrowell, Factors Contributing to the Glass-Forming Ability of a Simulated Molecular Liquid, J. Phys. Chem. B. 115 (2011) 14205–14209. doi:10.1021/jp205013w.

[136] M. Selva, M. Fabris, The reaction of glycerol carbonate with primary aromatic amines in the presence of Y- and X-faujasites: the synthesis of N-(2,3-dihydroxy)propyl anilines and the reaction mechanism, Green Chem. 11 (2009) 1161–1172. doi:10.1039/B904821A.

[137] J.H. Clements, Reactive applications of cyclic alkylene carbonates, Ind. Eng. Chem. Res. 42 (2003) 663–674.

[138] P. Lameiras, L. Boudesocque, Z. Mouloungui, J.-H. Renault, J.-M. Wieruszeski, G. Lippens, J.-M. Nuzillard, Glycerol and glycerol carbonate as ultraviscous solvents for mixture analysis by NMR, Journal of Magnetic Resonance. 212 (2011) 161–168. doi:10.1016/j.jmr.2011.06.021.

[139] D.P. Abraham, G. Cheng, Electrolyte compositions for lithium and lithium-ion batteries, US8936882B2, 2015. https://patents.google.com/patent/US8936882B2/en?q=patent&inventor=Abraham+D.&before=priority:20111231&after=priority:20110101&scholar&oq=us+patent+Abraham+D.+2011 (accessed October 8, 2018).

[140] G. Ou, B. He, Y. Yuan, Design of biosolvents through hydroxyl functionalization of compounds with high dielectric constant, Appl. Biochem. Biotechnol. 166 (2012) 1472–1479. doi:10.1007/s12010-012-9541-y.

[141] M. Benoit, Y. Brissonnet, E. Guélou, K.O.V. De, J. Barrault, F. Jérôme, Acid-catalyzed dehydration of fructose and inulin with glycerol or glycerol carbonate as renewably sourced co-solvent., ChemSusChem. 3 (2010) 1304–1309. doi:10.1002/cssc.201000162.

[142] J. Stark, Recent advances in the field of cement hydration and microstructure analysis, Cement and Concrete Research. 41 (2011) 666–678. doi:10.1016/j.cemconres.2011.03.028.

[143] H.R. Gillis, D. Stanssens, R.D. Vos, A.R. Postema, D. Randall, Polymeric foams, US5703136A, 1997. https://patents.google.com/patent/US5703136A/en (accessed October 8, 2018).

[144] A.S. Kovvali, K.K. Sirkar, Carbon Dioxide Separation with Novel Solvents as Liquid Membranes, Ind. Eng. Chem. Res. 41 (2002) 2287–2295. doi:10.1021/ie010757e.

[145] Cornell University Department of Animal Science, (n.d.). http://poisonousplants.ansci.cornell.edu/toxicagents/saponin.html (accessed August 18, 2018).

[146] G.P. Savage, Saponins, in: B. Caballero (Ed.), Encyclopedia of Food Sciences and Nutrition (Second Edition), Academic Press, Oxford, 2003: pp. 5095–5098. doi:10.1016/B0-12-227055-X/01050-6.

[147] K. Hostettmann, A. Marston, Saponins, Cambridge University Press, 1995. doi:10.1017/CBO9780511565113.

[148] Z.-W. Wang, M.-Y. Gu, G.-Z. Li, Surface Properties of Gleditsia Saponin and Synergisms of Its Binary System, Journal of Dispersion Science and Technology. 26 (2005) 341–347. doi:10.1081/DIS-200049604.

[149] C. Sarnthein-Graf, C. La Mesa, Association of saponins in water and water–gelatine mixtures, Thermochimica Acta. 418 (2004) 79–84. doi:10.1016/j.tca.2003.11.044.

[150] D. Oakenfull, G.S. Sidhu, Could saponins be a useful treatment for hypercholesterolaemia?, Eur J Clin Nutr. 44 (1990) 79–88.

[151] S. Mitra, S.R. Dungan, Micellar Properties of Quillaja Saponin. 1. Effects of Temperature, Salt, and pH on Solution Properties, J. Agric. Food Chem. 45 (1997) 1587–1595. doi:10.1021/jf960349z.

[152] Ö. Güçlü-Üstündağ, G. Mazza, Saponins: Properties, Applications and Processing, Critical Reviews in Food Science and Nutrition. 47 (2007) 231–258. doi:10.1080/10408390600698197.

[153] K. Oda, H. Matsuda, T. Murakami, S. Katayama, T. Ohgitani, M. Yoshikawa, Adjuvant and Haemolytic Activities of 47 Saponins Derived from Medicinal and Food Plants, Biological Chemistry. 381 (2005) 67–74. doi:10.1515/BC.2000.009.

[154] R. Bissinger, P. Modicano, K. Alzoubi, S. Honisch, C. Faggio, M. Abed, F. Lang, Effect of saponin on erythrocytes, Int. J. Hematol. 100 (2014) 51–59. doi:10.1007/s12185-014-1605-z.

[155] R. Segal, I. Milo-Goldzweig, On the mechanism of saponin hemolysis—II: Inhibition of hemolysis by aldonolactones, Biochemical Pharmacology. 24 (1975) 77–81. doi:10.1016/0006-2952(75)90317-2.

[156] R. Segal, M. Mansour, D.V. Zaitschek, Effect of ester groups on the haemolytic action of some saponins and sapogenins, Biochemical Pharmacology. 15 (1966) 1411–1416. doi:10.1016/0006-2952(66)90185-7.

[157] R. Segal, P. Shatkovsky, I. Milo-Goldzweig, On the mechanism of saponin hemolysis—I: Hydrolysis of the glycosidic bond, Biochemical Pharmacology. 23 (1974) 973–981. doi:10.1016/0006-2952(74)90027-6.

[158] L.U. Thompson, Potential health benefits and problems associated with antinutrients in foods, Food Research International. 26 (1993) 131–149. doi:10.1016/0963-9969(93)90069-U.

[159] G. Francis, Z. Kerem, H.P.S. Makkar, K. Becker, The biological action of saponins in animal systems: a review, Br. J. Nutr. 88 (2002) 587–605. doi:10.1079/BJN2002725.

[160] M.A. Lacaille-Dubois, H. Wagner, A review of the biological and pharmacological activities of saponins, Phytomedicine. 2 (1996) 363–386. doi:10.1016/S0944-7113(96)80081-X.

[161] J. Milgate, D.C.K. Roberts, The nutritional & biological significance of saponins, Nutrition Research. 15 (1995) 1223–1249. doi:10.1016/0271-5317(95)00081-S.

[162] S.M. Kerwin, Soy saponins and the anticancer effects of soybeans and soy-based foods, Curr Med Chem Anticancer Agents. 4 (2004) 263–272.

[163] H. Matsuura, Saponins in garlic as modifiers of the risk of cardiovascular disease, J. Nutr. 131 (2001) 1000S–5S. doi:10.1093/jn/131.3.1000S.

[164] C.B. Alice, V.M.F. Vargas, G.A.A.B. Silva, N.C.S. de Siqueira, E.E.S. Schapoval, J. Gleye, J.A.P. Henriques, A.T. Henriques, Screening of plants used in south Brazilian folk medicine, Journal of Ethnopharmacology. 35 (1991) 165–171. doi:10.1016/0378-8741(91)90069-P.

[165] D.M. Gurfinkel, A.V. Rao, Soyasaponins: the relationship between chemical structure and colon anticarcinogenic activity, Nutr Cancer. 47 (2003) 24–33. doi:10.1207/s15327914nc4701_3.

[166] S.-W. Kim, S.-K. Park, S.-I. Kang, H.-C. Kang, H.-J. Oh, C.-Y. Bae, D.-H. Bae, Hypocholesterolemic property of Yucca schidigera and Quillaja saponaria extracts in human body, Arch. Pharm. Res. 26 (2003) 1042–1046.

[167] A.V. Rao, M.K. Sung, Saponins as anticarcinogens, J. Nutr. 125 (1995) 717S-724S. doi:10.1093/jn/125.3_Suppl.717S.

[168] L.L. Yan, Y.J. Zhang, W.Y. Gao, S.L. Man, Y. Wang, In vitro and in vivo anticancer activity of steroid saponins of Paris polyphylla var. yunnanensis, Exp. Oncol. 31 (2009) 27–32.

[169] J.J. Coleman, I. Okoli, G.P. Tegos, E.B. Holson, F.F. Wagner, M.R. Hamblin, E. Mylonakis, Characterization of plant-derived saponin natural products against Candida albicans, ACS Chem. Biol. 5 (2010) 321–332. doi:10.1021/cb900243b.

[170] K.S. Jyothi, M. Seshagiri, In-Vitro Activity of Saponins of Bauhinia Purpurea, Madhuca Longifolia, Celastrus Paniculatus and Semecarpus Anacardium on Selected Oral Pathogens, J Dent (Tehran). 9 (2012) 216–223.

[171] A.D.P. Barbosa, Pharmacologically Active Saponins from the Genus Albizia (Fabaceae), International Journal of Pharmacy and Pharmaceutical Sciences. 6 (2014) 32–36.

[172] R.A. Forse, S. Chavali, Enternal formulations for treatment of inflammation and infection, US5674853A, 1997. https://patents.google.com/patent/US5674853A/en?oq=US+Patent+5%2c674%2c853 (accessed August 21, 2018).

[173] E. Bombardelli, B. Gabetta, Soya extract, process for its preparation and pharmaceutical composition, US6280777B1, 2001. https://patents.google.com/patent/US6280777B1/en?oq=US+Patent+6%2c280%2c777 (accessed August 21, 2018).

[174] B. Ma, J. Dong, B. Wang, Use of steroidal saponins for the prophylaxis or treatment of dementia, and novel steroidal saponin compounds, US6593301B1, 2003. https://patents.google.com/patent/US6593301B1/en?oq=US+Patent+6%2c593%2c301 (accessed August 21, 2018).

[175] M. Hidvegi, Process for the preparation of a pharmaceutical composition selectively lowering the blood-lipid level, US5277910A, 1994. https://patents.google.com/patent/US5277910/en (accessed August 21, 2018).

[176] D.-H. Kim, E.-A. Bae, M.-J. Han, M.-K. Choo, E.-K. Park, J.-H. Park, Novel use of the extract of processed Panax genus plant and saponin compound isolated therefrom, US20030190377A1, 2003. https://patents.google.com/patent/US20030190377A1/en?oq=US+Patent+Application+2003%2f0190377+A1 (accessed August 21, 2018).

[177] O. Tanaka, N. Yata, Promotion of absorption of drugs administered through the alimentary system, US4501734A, 1985.

https://patents.google.com/patent/US4501734A/en?oq=US+Patent+4%2c501%2c734 (accessed August 21, 2018).

[178] C.A. Kensil, S. Soltysik, D.J. Marciani, J. Recchia, Drug delivery enhancement via modified saponins, WO1996038161A1, 1996. https://patents.google.com/patent/WO1996038161A1/fr?oq=WO+Patent+96%2f38161 (accessed August 21, 2018).

[179] M.J. Olmstead, Organic toothpaste containing saponin, US6485711B1, 2002. https://patents.google.com/patent/US6485711B1/en (accessed August 21, 2018).

[180] V.R. Netala, S.B. Ghosh, P. Bobbu, D. Anitha, V. Tartte, Triterpenoid saponins: A review on biosynthesis, Applications and mechanism of their action, International Journal of Pharmacy and Pharmaceutical Sciences. 7 (2014) 24–28.

[181] E. Bombardelli, P. Morazzoni, A. Cristoni, R. Seghizzi, Pharmaceutical and cosmetic formulations with antimicrobial activity, US20010046525A1, 2001. https://patents.google.com/patent/US20010046525A1/en?oq=US+Patent+Application+2001%2f0046525+A1 (accessed August 21, 2018).

[182] F. Bonte, A. Meybeck, G. Massiot, Method of treatment for combatting the effects of aging on the condition of skin and hair, US5770223A, 1998. https://patents.google.com/patent/US5770223A/en (accessed August 21, 2018).

[183] B. Yoo, B. Kang, M. Yeom, D. Sung, S. Han, H. Kim, H. Ju, Nanoemulsion comprising metabolites of ginseng saponin as an active component and a method for preparing the same, and a skin-care composition for anti-aging containing the same, US20030175315A1, 2003. https://patents.google.com/patent/US20030175315A1/en?oq=US+Patent+Application+2003%2f0175315+A1 (accessed August 21, 2018).

[184] T. Richardson, R. Jimenez-Flores, Process to remove cholesterol from dairy products, US5326579A, 1994. https://patents.google.com/patent/US5326579A/en?oq=US+Patent+5%2c326%2c579 (accessed August 21, 2018).

[185] T.J. Micich, T.A. Foglia, V.H. Holsinger, Polymer-supported saponins: an approach to cholesterol removal from butteroil, Journal of Agricultural and Food Chemistry (USA). (1992). http:/agris.fao.org/agris-search/search.do?recordID=US9433371 (accessed August 21, 2018).

[186] D.C. (University of W. Hwang, S. Damodaran, Selective precipitation

of fat globule membranes of cheese whey by saponin and bile salt, Journal of Agricultural and Food Chemistry (USA). (1994). http://agris.fao.org/agris-search/search.do?recordID=US9601504 (accessed August 21, 2018).

[187] J.D. Desai, I.M. Banat, Microbial production of surfactants and their commercial potential., Microbiol Mol Biol Rev. 61 (1997) 47–64.

[188] R. Rahim, U.A. Ochsner, C. Olvera, M. Graninger, P. Messner, J.S. Lam, G. Soberón-Chávez, Cloning and functional characterization of the Pseudomonas aeruginosa rhlC gene that encodes rhamnosyltransferase 2, an enzyme responsible for di-rhamnolipid biosynthesis, Molecular Microbiology. 40 (2001) 708–718. doi:10.1046/j.1365-2958.2001.02420.x.

[189] A.M. Abdel-Mawgoud, F. Lépine, E. Déziel, Rhamnolipids: diversity of structures, microbial origins and roles, Appl Microbiol Biotechnol. 86 (2010) 1323–1336. doi:10.1007/s00253-010-2498-2.

[190] S. Bergström, H. Theorell, H. Davide, Pyolipic acid, a metabolic product of Pseudomonas pyocyanea, active against Mycobacterium tuberculosis - Request PDF, Archives of Biochemistry and Biophysiscs. 10 (1946) 165–166.

[191] S. Bergström, H. Theorell, H. Davide, On a metabolic product of Pseudomonas pyocyanea, pyolipic acid, active against Mycobacterium tuberculosis, Arkiv För Kemi, Mineralogi Och Geologi. 23A (1947) 1–12.

[192] F.G. Jarvis, M.J. Johnson, A Glyco-lipide Produced by Pseudomonas Aeruginosa, J. Am. Chem. Soc. 71 (1949) 4124–4126. doi:10.1021/ja01180a073.

[193] S. Ito, H. Honda, F. Tomita, T. Suzuki, Rhamnolipids produced by Pseudomonas aeruginosa grown on n-paraffin (mixture of C 12 , C 13 and C 14 fractions), J. Antibiot. 24 (1971) 855–859.

[194] C. Syldatk, S. Lang, F. Wagner, V. Wray, L. Witte, Chemical and physical characterization of four interfacial-active rhamnolipids from Pseudomonas spec. DSM 2874 grown on n-alkanes, Z. Naturforsch., C, Biosci. 40 (1985) 51–60.

[195] S. Arino, R. Marchal, J.-P. Vandecasteele, Identification and production of a rhamnolipidic biosurfactant by a Pseudomonas species, Appl Microbiol Biotechnol. 45 (1996) 162–168. doi:10.1007/s002530050665.

[196] T. Urakami, C. Ito-Yoshida, H. Araki, T. Kijima, K.I. Suzuki, K. Komagata, Transfer of Pseudomonas plantarii and Pseudomonas glumae to Burkholderia as Burkolderia spp. and description of

Burkholderia vandii sp. nov, International Journal of Systematic Bacteriology (USA). (1994). http://agris.fao.org/agris-search/search.do?recordID=US9446648 (accessed August 22, 2018).

[197] J. Howe, J. Bauer, J. Andrä, A.B. Schromm, M. Ernst, M. Rössle, U. Zähringer, J. Rademann, K. Brandenburg, Biophysical characterization of synthetic rhamnolipids, FEBS J. 273 (2006) 5101–5112. doi:10.1111/j.1742-4658.2006.05507.x.

[198] A.P. Rooney, N.P.J. Price, K.J. Ray, T.-M. Kuo, Isolation and characterization of rhamnolipid-producing bacterial strains from a biodiesel facility, FEMS Microbiol. Lett. 295 (2009) 82–87. doi:10.1111/j.1574-6968.2009.01581.x.

[199] E. Vasileva-Tonkova, V. Gesheva, Biosurfactant production by antarctic facultative anaerobe Pantoea sp. during growth on hydrocarbons, Curr. Microbiol. 54 (2007) 136–141. doi:10.1007/s00284-006-0345-6.

[200] M. Lee, M.K. Kim, M. Vancanneyt, J. Swings, S.-H. Kim, M.S. Kang, S.-T. Lee, Tetragenococcus koreensis sp. nov., a novel rhamnolipid-producing bacterium, Int. J. Syst. Evol. Microbiol. 55 (2005) 1409–1413. doi:10.1099/ijs.0.63448-0.

[201] N. Christova, B. Tuleva, Z. Lalchev, A. Jordanova, B. Jordanov, Rhamnolipid biosurfactants produced by Renibacterium salmoninarum 27BN during growth on n-hexadecane, Z. Naturforsch., C, J. Biosci. 59 (2004) 70–74.

[202] Regulation (EC) No. 648/2004 of the European Parliament and of the Council on detergents., n.d. https://www.ecolex.org/details/legislation/regulation-ec-no-6482004-of-the-european-parliament-and-of-the-council-on-detergents-lex-faoc042319/ (accessed August 23, 2018).

[203] K.K. Sekhon Randhawa, P.K.S.M. Rahman, Rhamnolipid biosurfactants—past, present, and future scenario of global market, Front Microbiol. 5 (2014). doi:10.3389/fmicb.2014.00454.

[204] H. Chong, Q. Li, Microbial production of rhamnolipids: opportunities, challenges and strategies, Microb Cell Fact. 16 (2017). doi:10.1186/s12934-017-0753-2.

[205] C.M. Chakrabarty, Genetically-manipulated microorganisms and their products in the oil service industries, Trends in Biotechnology. 3 (1985) 32–39. doi:10.1016/0167-7799(85)90056-3.

[206] J. Toribio, A.E. Escalante, G. Soberón-Chávez, Rhamnolipids: Production in bacteria other than Pseudomonas aeruginosa, European Journal of Lipid Science and Technology. 112 (2010) 1082–1087.

doi:10.1002/ejlt.200900256.

[207] T.B. Lotfabad, N. Ebadipour, R. RoostaAzad, Evaluation of a recycling bioreactor for biosurfactant production by Pseudomonas aeruginosa MR01 using soybean oil waste, Journal of Chemical Technology & Biotechnology. 91 (2016) 1368–1377. doi:10.1002/jctb.4733.

[208] M. Henkel, M. Geissler, F. Weggenmann, R. Hausmann, Production of microbial biosurfactants: Status quo of rhamnolipid and surfactin towards large-scale production, Biotechnol J. 12 (2017). doi:10.1002/biot.201600561.

[209] B. Kaskatepe, S. Yildiz, M. Gumustas, S.A. Ozkan, Biosurfactant production by Pseudomonas aeruginosain kefir and fish meal, Braz. J. Microbiol. 46 (2015) 855–859. doi:10.1590/S1517-838246320140727.

[210] M. Robert, M.E. Mercadé, M.P. Bosch, J.L. Parra, M.J. Espuny, M.A. Manresa, J. Guinea, Effect of the carbon source on biosurfactant production byPseudomonas aeruginosa 44T1, Biotechnol Lett. 11 (1989) 871–874. doi:10.1007/BF01026843.

[211] S. Nalini, R. Parthasarathi, Biosurfactant production by Serratia rubidaea SNAU02 isolated from hydrocarbon contaminated soil and its physico-chemical characterization, Bioresour. Technol. 147 (2013) 619–622. doi:10.1016/j.biortech.2013.08.041.

[212] N. Sakthipriya, M. Doble, J.S. Sangwai, Biosurfactant from Pseudomonas species with waxes as carbon source – Their production, modeling and properties, Journal of Industrial and Engineering Chemistry. C (2015) 100–111. doi:10.1016/j.jiec.2015.06.013.

[213] M. Ayoub, A.Z. Abdullah, Critical review on the current scenario and significance of crude glycerol resulting from biodiesel industry towards more sustainable renewable energy industry, Renewable and Sustainable Energy Reviews. 16 (2012) 2671–2686.

[214] Z.A. Raza, A. Rehman, M.S. Khan, Z.M. Khalid, Improved production of biosurfactant by a Pseudomonas aeruginosa mutant using vegetable oil refinery wastes, Biodegradation. 18 (2007) 115–121. doi:10.1007/s10532-006-9047-9.

[215] C. Giani, D. Wullbrandt, R. Rothert, J. Meiwes, Pseudomonas aeruginosa and its use in a process for the biotechnological preparation of L-rhamnose, 1996. https://patents.google.com/patent/US5501966A/en (accessed August 24, 2018).

[216] F. Zhao, Q. Cui, S. Han, H. Dong, J. Zhang, F. Ma, Y. Zhang, Enhanced rhamnolipid production of Pseudomonas aeruginosa SG by

increasing copy number of rhlAB genes with modified promoter, RSC Adv. 5 (2015) 70546–70552. doi:10.1039/C5RA13415C.

[217] A. Wittgens, T. Tiso, T.T. Arndt, P. Wenk, J. Hemmerich, C. Müller, R. Wichmann, B. Küpper, M. Zwick, S. Wilhelm, R. Hausmann, C. Syldatk, F. Rosenau, L.M. Blank, Growth independent rhamnolipid production from glucose using the non-pathogenic Pseudomonas putida KT2440, Microb. Cell Fact. 10 (2011) 80. doi:10.1186/1475-2859-10-80.

[218] S. Lang, D. Wullbrandt, Rhamnose lipids – biosynthesis, microbial production and application potential, Appl Microbiol Biotechnol. 51 (1999) 22–32. doi:10.1007/s002530051358.

[219] S.G.V.A.O. Costa, M. Nitschke, F. Lépine, E. Déziel, J. Contiero, Structure, properties and applications of rhamnolipids produced by Pseudomonas aeruginosa L2-1 from cassava wastewater, Process Biochemistry. 45 (2010) 1511–1516.

[220] I. Mnif, D. Ghribi, Glycolipid biosurfactants: main properties and potential applications in agriculture and food industry, J. Sci. Food Agric. 96 (2016) 4310–4320. doi:10.1002/jsfa.7759.

[221] D.P. Sachdev, S.S. Cameotra, Biosurfactants in agriculture, Appl. Microbiol. Biotechnol. 97 (2013) 1005–1016. doi:10.1007/s00253-012-4641-8.

[222] M. Nitschke, S.G.V.A.O. Costa, Biosurfactants in food industry, Trends in Food Science & Technology. 18 (2007) 252–259. doi:10.1016/j.tifs.2007.01.002.

[223] L. Magalhaes, M. Nitschke, Antimicrobial activity of rhamnolipids against Listeria monocytogenes and their synergistic interaction with nisin, Food Control. 29 (2013) 138–142. doi:10.1016/j.foodcont.2012.06.009.

[224] A. Parry, N. Parry, A. Peilow, P. Stevenson, Combinations of Rhamnolipids and Enzymes for Improved Cleaning, WO/2012/010406, 2012. https://patentscope.wipo.int/search/en/detail.jsf?docId=WO2012010406&recNum=207&docAn=EP2011061214&queryString=&maxRec=16643 (accessed August 24, 2018).

[225] M.A. Diaz De Rienzo, P.S. Stevenson, R. Marchant, I.M. Banat, Effect of biosurfactants on Pseudomonas aeruginosa and Staphylococcus aureus biofilms in a BioFlux channel, Appl. Microbiol. Biotechnol. 100 (2016) 5773–5779. doi:10.1007/s00253-016-7310-5.

[226] B.N. Paulino, M.G. Pessôa, M.C.R. Mano, G. Molina, I.A. Neri-Numa, G.M. Pastore, Current status in biotechnological production and

applications of glycolipid biosurfactants, Appl. Microbiol. Biotechnol. 100 (2016) 10265–10293. doi:10.1007/s00253-016-7980-z.

[227] T. Piljac, G. Piljac, Use of rhamnolipids as cosmetics, EP1056462B1, 2007. https://patents.google.com/patent/EP1056462B1/en (accessed August 24, 2018).

[228] P.L. Show, K.O. Oladele, Q.Y. Siew, F.A.A. Zakry, J.C.-W. Lan, T.C. Ling, Overview of citric acid production from Aspergillus niger, Frontiers in Life Science. 8 (2015) 271–283. doi:10.1080/21553769.2015.1033653.

[229] R.N. Goldberg, N. Kishore, R.M. Lennen, Thermodynamic Quantities for the Ionization Reactions of Buffers, Journal of Physical and Chemical Reference Data. 31 (2002) 231–370. doi:10.1063/1.1416902.

[230] B. Francis, C. Seebart, I. Kaiser, Citrate is an endogenous inhibitor of snake venom enzymes by metal-ion chelation, Toxicon. 30 (1992) 1239–1246. doi:10.1016/0041-0101(92)90440-G.

[231] C.G. Suhayda, A. Haug, Citrate chelation as a potential mechanism against aluminum toxicity in cells: the role of calmodulin, Can. J. Biochem. Cell Biol. 63 (1985) 1167–1175. doi:10.1139/o85-145.

[232] V. Rana, K. Babita, D. Goyal, A. Tiwary, Sodium citrate cross-linked chitosan films: optimization as substitute for human/rat/rabbit epidermal sheets, J Pharm Pharm Sci. 8 (2004) 10–17.

[233] J. Yang, Y. Zhang, S. Gautam, L. Liu, J. Dey, W. Chen, R.P. Mason, C.A. Serrano, K.A. Schug, L. Tang, Development of aliphatic biodegradable photoluminescent polymers, Proc Natl Acad Sci U S A. 106 (2009) 10086–10091. doi:10.1073/pnas.0900004106.

[234] R.T. Tran, J. Yang, G.A. Ameer, Citrate-Based Biomaterials and Their Applications in Regenerative Engineering, Annu Rev Mater Res. 45 (2015) 277–310. doi:10.1146/annurev-matsci-070214-020815.

[235] D. Gyawali, P. Nair, Y. Zhang, R.T. Tran, C. Zhang, M. Samchukov, M. Makarov, H. Kim, J. Yang, Citric acid-derived in situ crosslinkable biodegradable polymers for cell delivery, Biomaterials. 31 (2010) 9092–9105. doi:10.1016/j.biomaterials.2010.08.022.

[236] D. Nataraj, S. Sakkara, M. Hn, N. Reddy, Properties and applications of citric acid crosslinked banana fibre-wheat gluten films, Industrial Crops and Products. 124 (2018) 265–272. doi:10.1016/j.indcrop.2018.07.076.

[237] H.A. Krebs, W.A. Johnson, Metabolism of ketonic acids in animal tissues, Biochem J. 31 (1937) 645–660.

[238] J.M. Berg, J.L. Tymoczko, L. Stryer, 16.2 - The Glycolytic Pathway Is Tightly Controlled, in: Biochemistry. 5th Edition, 2002.

https://www.ncbi.nlm.nih.gov/books/NBK22395/ (accessed August 27, 2018).

[239] E. Davies, K.H. Müller, W.C. Wong, C.J. Pickard, D.G. Reid, J.N. Skepper, M.J. Duer, Citrate bridges between mineral platelets in bone, PNAS. (2014) 201315080. doi:10.1073/pnas.1315080111.

[240] Y.-Y. Hu, A. Rawal, K. Schmidt-Rohr, Strongly bound citrate stabilizes the apatite nanocrystals in bone, PNAS. 107 (2010) 22425–22429. doi:10.1073/pnas.1009219107.

[241] A.M. Duarte, D. Caixeirinho, M.G. Miguel, V. Sustelo, C. Nunes, M.M. Fernandes, A. Marreiros, ORGANIC ACIDS CONCENTRATION IN CITRUS JUICE FROM CONVENTIONAL VERSUS ORGANIC FARMING, Acta Horticulturae. (2012) 601–606. doi:10.17660/ActaHortic.2012.933.78.

[242] F. Ullmann, W. Gerhartz, Y.S. Yamamoto, F.T. Campbell, R. Pfefferkorn, J.F. Rounsaville, Ullmann's encyclopedia of industrial chemistry, VCH, 1992.

[243] C.R. Soccol, L.P.S. Vandenberghe, C. Rodrigues, A. Pandey, New perspectives for citric acid production and application, Food Technology and Biotechnology. 44 (2006) 141–149.

[244] H.S. Grewal, K.L. Kalra, Fungal production of citric acid, Biotechnol. Adv. 13 (1995) 209–234.

[245] L.P.S. Vandenberghe, C.R. Soccol, A. Pandey, J.-M. Lebeault, Microbial production of citric acid, Brazilian Archives of Biology and Technology. 42 (1999) 263–276. doi:10.1590/S1516-89131999000300001.

[246] I. Morgunov, S. Kamzolova, J. Lunina, I.G. Morgunov, S.V. Kamzolova, J.N. Lunina, Citric Acid Production by Yarrowia lipolytica Yeast on Different Renewable Raw Materials, Fermentation. 4 (2018) 36. doi:10.3390/fermentation4020036.

[247] M. Mattey, The Production of Organic Acids, Critical Reviews in Biotechnology. 12 (1992) 87–132. doi:10.3109/07388559209069189.

[248] Kareem, S. O., Akpan, I., Alebiowu, O. O., Production of citric acid by Aspergillus niger using pineapple waste, Malaysian Journal of Microbiology. 6 (2010) 161–165. doi:10.21161/mjm.19009.

[249] A. Karthikeyan, N. Sivakumar, Citric acid production by Koji fermentation using banana peel as a novel substrate, Bioresource Technology. 101 (2010) 5552–5556. doi:10.1016/j.biortech.2010.02.063.

[250] Y. Hang, B. Luh, E. Woodams, Microbial-Production of Citric-Acid by Solid-State Fermentation of Kiwifruit Peel, J. Food Sci. 52 (1987) 226–227. doi:10.1111/j.1365-2621.1987.tb14014.x.

[251] H. Kiel, R. Guvrin, Y. Henis, Citric-Acid Fermentation by Aspergillus-Niger on Low Sugar Concentrations and Cotton Waste, Appl. Environ. Microbiol. 42 (1981) 1–4.

[252] A. Maria Torrado, S. Cortes, J. Manuel Salgado, B. Max, N. Rodriguez, B.P. Bibbins, A. Converti, J. Manuel Dominguez, Citric Acid Production from Orange Peel Wastes by Solid-State Fermentation, Braz. J. Microbiol. 42 (2011) 394–409. doi:10.1590/S1517-83822011000100049.

[253] M. Mazaheri Asadi, M. Nikkhah, Production of Citric Acid from Date Pulp By Solid State Fermentation, Journal of Agricultural Science and Technology. 4 (2010) 119–125.

[254] M. Sauer, D. Porro, D. Mattanovich, P. Branduardi, Microbial production of organic acids: expanding the markets, Trends Biotechnol. 26 (2008) 100–108. doi:10.1016/j.tibtech.2007.11.006.

[255] Z.I.M. Arshad, A. Amid, F. Yusof, I. Jaswir, K. Ahmad, S.P. Loke, Bromelain: an overview of industrial application and purification strategies, Appl. Microbiol. Biotechnol. 98 (2014) 7283–7297. doi:10.1007/s00253-014-5889-y.

[256] G. Falony, J.C. Armas, J.C.D. Mendoza, J.L.M. Hernandez, Production of extracellular lipase from Aspergillus niger by solid-state fermentation, Food Technol. Biotechnol. 44 (2006) 235–240.

[257] M. Berovic, M. Legisa, Citric acid production, Biotechnol Annu Rev. 13 (2007) 303–343. doi:10.1016/S1387-2656(07)13011-8.

[258] L.P.S. Vandenberghe, C. Rodrigues, J.C. de Carvalho, A.B.P. Medeiros, C.R. Soccol, 25 - Production and Application of Citric Acid, in: A. Pandey, S. Negi, C.R. Soccol (Eds.), Current Developments in Biotechnology and Bioengineering, Elsevier, 2017: pp. 557–575. doi:10.1016/B978-0-444-63662-1.00025-7.

[259] S. Chalk, L. McEwen, The IUPAC Gold Book, Version 2.3.3, 2014. https://www.degruyter.com/view/j/ci.2017.39.issue-3/ci-2017-0307/ci-2017-0307.xml (accessed September 5, 2018).

[260] E.M. Dannenberg, L. Paquin, H. Gwinnell, Carbon Black, in: Kirk-Othmer Encyclopedia of Chemical Technology, American Cancer Society, 2000. doi:10.1002/0471238961.0301180204011414.a01.

[261] K. Gardiner, W.N. Trethowan, J.M. Harrington, I.A. Calvert, D.C. Glass, Occupational exposure to carbon black in its manufacture, Ann Occup Hyg. 36 (1992) 477–496. doi:10.1093/annhyg/36.5.477.

[262] A. Oberlin, High-resolution TEM studies of carbonization and graphitization, in: Chemistry & Physics of Carbon, CRC Press, 1989: pp. 1–143. https://www.crcpress.com/Chemistry--Physics-of-Carbon-

Volume-22/Thrower/p/book/9780824781132 (accessed September 14, 2018).

[263] E.S. Penev, V.I. Artyukhov, B.I. Yakobson, Basic structural units in carbon fibers: Atomistic models and tensile behavior, Carbon. 85 (2015) 72–78. doi:10.1016/j.carbon.2014.12.067.

[264] A. Oberlin, Carbonization and graphitization, Carbon. 22 (1984) 521–541. doi:10.1016/0008-6223(84)90086-1.

[265] M. Pawlyta, J.-N. Rouzaud, S. Duber, Raman microspectroscopy characterization of carbon blacks: Spectral analysis and structural information, Carbon. 84 (2015) 479–490. doi:10.1016/j.carbon.2014.12.030.

[266] M. Voll, P. Kleinschmit, Carbon, 6. Carbon Black, in: Ullmann's Encyclopedia of Industrial Chemistry, American Cancer Society, 2010. doi:10.1002/14356007.n05_n05.

[267] J.-B. Donnet, Carbon Black: Science and Technology, Second Edition, CRC Press, 1993.

[268] H.P. Boehm, Some aspects of the surface chemistry of carbon blacks and other carbons, Carbon. 32 (1994) 759–769. doi:10.1016/0008-6223(94)90031-0.

[269] A.S. Behrman, H. Gustafson, Behavior of Oxidizing Agents with Activated Carbon, Ind. Eng. Chem. 27 (1935) 426–429. doi:10.1021/ie50304a018.

[270] R.N. Smith, J. Swinehart, D. Lesnini, The Oxidation of Cardon by Nitric Oxide, J. Phys. Chem. 63 (1959) 544–547. doi:10.1021/j150574a023.

[271] J.B. Donnet, The chemical reactivity of carbons, Carbon. 6 (1968) 161–176. doi:10.1016/0008-6223(68)90300-X.

[272] M. Seredych, D. Hulicova-Jurcakova, G.Q. Lu, T.J. Bandosz, Surface functional groups of carbons and the effects of their chemical character, density and accessibility to ions on electrochemical performance, Carbon. 46 (2008) 1475–1488. doi:10.1016/j.carbon.2008.06.027.

[273] M.L. Studebaker, The Chemistry of Carbon Black and Reinforcement, Rubber Chemistry and Technology. 30 (1957) 1400–1483. doi:10.5254/1.3542764.

[274] G. Geuskens, J.L. Gielens, D. Geshef, R. Deltour, The electrical conductivity of polymer blends filled with carbon-black, European Polymer Journal. 23 (1987) 993–995. doi:10.1016/0014-3057(87)90047-4.

[275] I. Balberg, S. Bozowski, Percolation in a composite of random stick-

like conducting particles, Solid State Communications. 44 (1982) 551–554. doi:10.1016/0038-1098(82)90144-2.

[276] J.-P. Reboul, G. Moussalli, About Some D-C Conduction Processes in Carbon Black Filled Polymers, International Journal of Polymeric Materials and Polymeric Biomaterials. 5 (1976) 133–146. doi:10.1080/00914037608072394.

[277] F. Carmona, Conducting filled polymers, Physica A: Statistical Mechanics and Its Applications. 157 (1989) 461–469. doi:10.1016/0378-4371(89)90344-0.

[278] C.A. Nieves, I. Ramos, N.J. Pinto, N.A. Zimbovskaya, Electron transport mechanisms in polymer-carbon sphere composites, Journal of Applied Physics. 120 (2016) 014302. doi:10.1063/1.4955166.

[279] S.-G. Shin, Change of Percolation Threshold in Carbon Powder-Filled Polystyrene Matrix Composites, Korean Journal of Materials Research. 25 (2015) 119–124. doi:10.3740/MRSK.2015.25.3.119.

[280] M.J. da Silva, D.H.F. Kanda, H.N. Nagashima, Mechanism of charge transport in castor oil-based polyurethane/carbon black composite (PU/CB), Journal of Non-Crystalline Solids. 358 (2012) 270–275. doi:10.1016/j.jnoncrysol.2011.09.032.

[281] I. Balberg, A comprehensive picture of the electrical phenomena in carbon black–polymer composites, Carbon. 40 (2002) 139–143. doi:10.1016/S0008-6223(01)00164-6.

[282] F. Carmona, C. Mouney, Temperature-dependent resistivity and conduction mechanism in carbon particle-filled polymers, J Mater Sci. 27 (1992) 1322–1326. doi:10.1007/BF01142046.

[283] J. Wang, Q. Li, C. Wu, H. Xu, Thermal Conductivity and Mechanical Properties of Carbon Black Filled Silicone Rubber, Polymers & Polymer Composites. 22 (2014) 393–399.

[284] M.E. Semaan, C.A. Quartes, L. Nikiel, Carbon Black and silica as reinforcers of rubber polymers: Doppler broadening spectroscopy results, Polymer Degradation and Stability. 75 (2002) 259–266.

[285] S.-S. Choi, J.-C. Kim, Lifetime prediction and thermal aging behaviors of SBR and NBR composites using crosslink density changes, Journal of Industrial and Engineering Chemistry. 18 (2012) 1166–1170.

[286] C.S. Barrera, K. Cornish, High performance waste-derived filler/carbon black reinforced guayule natural rubber composites, Industrial Crops and Products. 86 (2016) 132–142. doi:10.1016/j.indcrop.2016.03.021.

[287] J.A.C. Harwood, A.R. Payne, Stress softening in natural rubber vulcanizates. Part III. Carbon black-filled vulcanizates, Journal of

Applied Polymer Science. 10 (1966) 315–324.

[288] N. Rattanasom, T. Saowapark, C. Deeprasertkul, Reinforcement of natural rubber with silica/carbon black hybrid filler, Polymer Testing. 26 (2007) 369–377. doi:10.1016/j.polymertesting.2006.12.003.

[289] N. Hayeemasae, H. Ismail, T.B. Khoon, S. Husseinsyah, H. Harahap, Effect of Carbon Black on the Properties of Polypropylene/ Recycled Natural Rubber Glove Blends, Progress in Rubber, Plastics and Recycling Technology. 32 (2015) 241–252.

[290] A.R. Horrocks, J. Mwila, M. Miraftab, M. Liu, S.S. Chohan, The influence of carbon black on properties of orientated polypropylene 2. Thermal and photodegradation, Polymer Degradation and Stability. 65 (1999) 25–36. doi:10.1016/S0141-3910(98)00213-4.

[291] H.S. Katz, J.V. Mileski, Handbook Of Fillers For Plastics, Springer Science & Business Media, 1987.

[292] J.A. Belmont, J.E. Johnson, C.E. Adams, Ink jet ink formulations containing carbon black products, 5571311, 1996. https://patents.google.com/patent/US5571311A/en (accessed February 22, 2018).

[293] K. Kordás, T. Mustonen, G. Tóth, H. Jantunen, M. Lajunen, C. Soldano, S. Talapatra, S. Kar, R. Vajtai, P.M. Ajayan, Inkjet printing of electrically conductive patterns of carbon nanotubes, Small. 2 (2006) 1021–1025. doi:10.1002/smll.200600061.

[294] S. Coppola, L. Mecozzi, V. Vespini, L. Battista, S. Grilli, G. Nenna, F. Loffredo, F. Villani, C. Minarini, P. Ferraro, Nanocomposite polymer carbon-black coating for triggering pyro-electrohydrodynamic inkjet printing, Appl. Phys. Lett. 106 (2015) 261603. doi:10.1063/1.4923469.

[295] Q. Cao, Y. Song, Y. Tan, Q. Zheng, Conductive and viscoelastic behaviors of carbon black filled polystyrene during annealing, Carbon. 48 (2010) 4268–4275. doi:10.1016/j.carbon.2010.07.036.

[296] L.B. Tunnicliffe, J. Kadlcak, M.D. Morris, Y. Shi, A.G. Thomas, J.J.C. Busfield, Flocculation and Viscoelastic Behaviour in Carbon Black-Filled Natural Rubber, Macromolecular Materials and Engineering. 299 (2014) 1474–1483. doi:10.1002/mame.201400117.

[297] J. Tang, J. Yang, X. Zhou, Acetylene black derived hollow carbon nanostructure and its application in lithium–sulfur batteries, RSC Adv. 3 (2013) 16936–16939. doi:10.1039/C3RA42835D.

[298] F. Cai, J. Liang, Z. Tao, J. Chen, R. Xu, Low-Pt-loading acetylene-black cathode for high-efficient dye-sensitized solar cells, Journal of Power Sources. 177 (2008) 631–636.

doi:10.1016/j.jpowsour.2007.10.096.

[299] P.-J. Tsai, H.-Y. Shieh, W.-J. Lee, S.-O. Lai, Characterization of PAHs in the atmosphere of carbon black manufacturing workplaces, Journal of Hazardous Materials. 91 (2002) 25–42. doi:10.1016/S0304-3894(01)00384-3.

[300] D. Rivin, Carbon Black, in: Anthropogenic Compounds, Springer-Verlag, Berlin Heidelberg, 1986: pp. 101–158. //www.springer.com/it/book/9783662161319 (accessed September 6, 2018).

[301] L. Fulcheri, N. Probst, G. Flamant, F. Fabry, E. Grivei, X. Bourrat, Plasma processing: a step towards the production of new grades of carbon black, Carbon. 40 (2002) 169–176. doi:10.1016/S0008-6223(01)00169-5.

[302] F. Fabry, G. Flamant, L. Fulcheri, Carbon black processing by thermal plasma. Analysis of the particle formation mechanism, Chemical Engineering Science. 56 (2001) 2123–2132. doi:10.1016/S0009-2509(00)00486-3.

[303] I. de Marco Rodriguez, M.F. Laresgoiti, M.A. Cabrero, A. Torres, M.J. Chomón, B. Caballero, Pyrolysis of scrap tyres, Fuel Processing Technology. 72 (2001) 9–22. doi:10.1016/S0378-3820(01)00174-6.

[304] M. Keiluweit, P.S. Nico, M.G. Johnson, M. Kleber, Dynamic Molecular Structure of Plant Biomass-Derived Black Carbon (Biochar), Environ. Sci. Technol. 44 (2010) 1247–1253. doi:10.1021/es9031419.

[305] H.P.S. Abdul Khalil, P. Firoozian, I.O. Bakare, H.M. Akil, A.M. Noor, Exploring biomass based carbon black as filler in epoxy composites: Flexural and thermal properties, Materials & Design. 31 (2010) 3419–3425. doi:10.1016/j.matdes.2010.01.044.

[306] R.J. Larson, E.A. Bookland, R.T. Williams, K.M. Yocom, D.A. Saucy, M.B. Freeman, G. Swift, Biodegradation of acrylic acid polymers and oligomers by mixed microbial communities in activated sludge, J Environ Polym Degr. 5 (1997) 41–48. doi:10.1007/BF02763567.

[307] T. Klein, R.-J. Moritz, R. Graupner, Polyaspartates and Polysuccinimide, in: Ullmann's Encyclopedia of Industrial Chemistry, American Cancer Society, 2008. doi:10.1002/14356007.l21_l01.

[308] T. Nakato, M. Yoshitake, K. Matsubara, M. Tomida, T. Kakuchi, Relationships between Structure and Properties of Poly(aspartic acid)s, Macromolecules. 31 (1998) 2107–2113. doi:10.1021/ma971629y.

[309] K.W. Rusenko, J.E. Donachy, A.P. Wheeler, Purification and Characterization of a Shell Matrix Phosphoprotein from the American

Oyster, in: Surface Reactive Peptides and Polymers, American Chemical Society, 1991: pp. 107–124. doi:10.1021/bk-1991-0444.ch008.

[310] S.M. Thombre, B.D. Sarwade, Synthesis and Biodegradability of Polyaspartic Acid: A Critical Review, Journal of Macromolecular Science, Part A. 42 (2005) 1299–1315. doi:10.1080/10601320500189604.

[311] H. Schiff, Ueber Polyaspartsäuren, Berichte Der Deutschen Chemischen Gesellschaft. 30 (1897) 2449–2459. doi:10.1002/cber.18970300316.

[312] P.R. Bahn, A. Pappelis, J. Bozzola, Protocell-like microspheres from thermal polyaspartic acid, Orig Life Evol Biosph. 36 (2006) 617–619. doi:10.1007/s11084-006-9044-3.

[313] K.C. Low, A.P. Wheeler, L.P. Koskan, Commercial Poly(aspartic acid) and Its Uses, in: Hydrophilic Polymers, American Chemical Society, 1996: pp. 99–111. doi:10.1021/ba-1996-0248.ch006.

[314] L.L. Wood, Preparation of salt of polyaspartic acid by high temperature reaction, US5288783A, 1994. https://patents.google.com/patent/US5288783A/en?oq=US+5288783+1994 (accessed October 18, 2018).

[315] G. Boehmke, Polyaspartic acid from maleic acid and ammonia, US4839461A, 1989. https://patents.google.com/patent/US4839461/en?oq=US+4839461+1989 (accessed October 18, 2018).

[316] V. Saudek, H. Pivcová, J. Drobník, Nmr study of poly(aspartic acid). II. α- and β-Peptide bonds in poly(aspartic acid) prepared by common methods, Biopolymers. 20 (1981) 1615–1623. doi:10.1002/bip.1981.360200805.

[317] V.S. Rao, P. Lapointe, D.N. McGregor, Synthesis of uniform poly(aspartic acids), Die Makromolekulare Chemie. 194 (1993) 1095–1104. doi:10.1002/macp.1993.021940405.

[318] Y. Soeda, K. Toshima, S. Matsumura, Sustainable Enzymatic Preparation of Polyaspartate Using a Bacterial Protease, Biomacromolecules. 4 (2003) 196–203. doi:10.1021/bm0200534.

[319] D.R. Karsa, Polymeric additives for high performance detergents, Paolo Zini ed. Technomic Publishing Co. Inc., Lancaster, USA, 1995., Polymer International. 38 (1995) 305–305. doi:10.1002/pi.1995.210380313.

[320] P. Kmec, D.E. Emerich, Scale and/or corrosion inhibiting composition, WO2000044677A1, 2000. https://patents.google.com/patent/WO2000044677A1/en?oq=WO+0

044677%2c+2000 (accessed October 18, 2018).

[321] W. Hater, Environmental Compatible Scale Inhibitor for the Mining Industry, in: NACE International, 1998. https://www.onepetro.org/conference-paper/NACE-98213?sort=&start=0&q=corrosion+98+hater&from_year=&peer_reviewed=&published_between=&fromSearchResults=true&to_year=&rows=50# (accessed October 18, 2018).

[322] A. Bosso, L. Panero, M. Petrozziello, M. Sollazzo, A. Asproudi, S. Motta, M. Guaita, Use of polyaspartate as inhibitor of tartaric precipitations in wines, Food Chem. 185 (2015) 1–6. doi:10.1016/j.foodchem.2015.03.099.

[323] A. Ogunleye, A. Bhat, V.U. Irorere, D. Hill, C. Williams, I. Radecka, Poly-γ-glutamic acid: production, properties and applications, Microbiology (Reading, Engl.). 161 (2015) 1–17. doi:10.1099/mic.0.081448-0.

[324] I. Bajaj, R. Singhal, Poly (glutamic acid) – An emerging biopolymer of commercial interest, Bioresource Technology. 102 (2011) 5551–5561. doi:10.1016/j.biortech.2011.02.047.

[325] J.M. Buescher, A. Margaritis, Microbial Biosynthesis of Polyglutamic Acid Biopolymer and Applications in the Biopharmaceutical, Biomedical and Food Industries, Critical Reviews in Biotechnology. 27 (2007) 1–19. doi:10.1080/07388550601166458.

[326] I.-L. Shih, Y.-T. Van, The production of poly-(γ-glutamic acid) from microorganisms and its various applications, Bioresource Technology. 79 (2001) 207–225. doi:10.1016/S0960-8524(01)00074-8.

[327] T. Candela, A. Fouet, Poly-gamma-glutamate in bacteria, Molecular Microbiology. 60 (2006) 1091–1098. doi:10.1111/j.1365-2958.2006.05179.x.

[328] B. Edde, J. Rossier, J.L. Caer, E. Desbruyeres, F. Gros, P. Denoulet, Posttranslational glutamylation of alpha-tubulin, Science. 247 (1990) 83–85. doi:10.1126/science.1967194.

[329] S. Mesnage, E. Tosi-Couture, P. Gounon, M. Mock, A. Fouet, The Capsule and S-Layer: Two Independent and Yet Compatible Macromolecular Structures in Bacillus anthracis, Journal of Bacteriology. 180 (1998) 52–58.

[330] K. Kimura, L.-S.P. Tran, I. Uchida, Y. Itoh, Characterization of Bacillus subtilisγ-glutamyltransferase and its involvement in the degradation of capsule poly-γ-glutamate, Microbiology. 150 (2004) 4115–4123. doi:10.1099/mic.0.27467-0.

[331] S. Kocianova, C. Vuong, Y. Yao, J.M. Voyich, E.R. Fischer, F.R.

DeLeo, M. Otto, Key role of poly-γ-dl-glutamic acid in immune evasion and virulence of *Staphylococcus epidermidis*, J Clin Invest. 115 (2005) 688–694. doi:10.1172/JCI23523.

[332] R.J.C. McLean, D. Beauchemin, L. Clapham, T.J. Beveridge, Metal-Binding Characteristics of the Gamma-Glutamyl Capsular Polymer of Bacillus licheniformis ATCC 9945, Appl. Environ. Microbiol. 56 (1990) 3671–3677.

[333] O. Kandler, H. König, J. Wiegel, D. Claus, Occurrence of Poly-γ-D-Glutamic Acid and Poly-α-L-Glutamine in the Genera Xanthobacter, Flexithrix, Sporosarcina and Planococcus, Systematic and Applied Microbiology. 4 (1983) 34–41. doi:10.1016/S0723-2020(83)80032-0.

[334] J. Weber, Poly(gamma-glutamic acid)s are the major constituents of nematocysts in Hydra (Hydrozoa, Cnidaria), J. Biol. Chem. 265 (1990) 9664–9669.

[335] C.-Y. Hsieh, S.-P. Tsai, D.-M. Wang, Y.-N. Chang, H.-J. Hsieh, Preparation of gamma-PGA/chitosan composite tissue engineering matrices, Biomaterials. 26 (2005) 5617–5623. doi:10.1016/j.biomaterials.2005.02.012.

[336] C.T. Tsao, C.H. Chang, Y.Y. Lin, M.F. Wu, J.L. Wang, T.H. Young, J.L. Han, K.H. Hsieh, Evaluation of chitosan/γ-poly(glutamic acid) polyelectrolyte complex for wound dressing materials, Carbohydrate Polymers. 84 (2011) 812–819. doi:10.1016/j.carbpol.2010.04.034.

[337] H. Ye, L. Jin, R. Hu, Z. Yi, J. Li, Y. Wu, X. Xi, Z. Wu, Poly(gamma,L-glutamic acid)-cisplatin conjugate effectively inhibits human breast tumor xenografted in nude mice, Biomaterials. 27 (2006) 5958–5965. doi:10.1016/j.biomaterials.2006.08.016.

[338] H. Tanimoto, T. Fox, J. Eagles, H. Satoh, H. Nozawa, A. Okiyama, Y. Morinaga, S.J. Fairweather-Tait, Acute effect of poly-gamma-glutamic acid on calcium absorption in post-menopausal women, J Am Coll Nutr. 26 (2007) 645–649.

[339] Y.-S. Shyu, J.-Y. Hwang, C.-K. Hsu, Improving the rheological and thermal properties of wheat dough by the addition of γ-polyglutamic acid, LWT - Food Science and Technology. 41 (2008) 982–987. doi:10.1016/j.lwt.2007.06.015.

[340] S.-M. Lim, J. Kim, J.-Y. Shim, B.-Y. Imm, M.-H. Sung, J.-Y. Imm, Effect of poly-γ-glutamic acids (PGA) on oil uptake and sensory quality in doughnuts, Food Sci Biotechnol. 21 (2012) 247–252. doi:10.1007/s10068-012-0032-2.

[341] M. Mitsuiki, A. Mizuno, H. Tanimoto, M. Motoki, Relationship between the Antifreeze Activities and the Chemical Structures of

Oligo- and Poly(glutamic acid)s, J. Agric. Food Chem. 46 (1998) 891–895. doi:10.1021/jf970797m.

[342] N. Ben-Zur, D. Goldman, γ-poly glutamic acid : a novel peptide for skin care, Cosmetics Toiletries. 122 (2007) 65–74.

[343] Q. Wang, S. Chen, J. Zhang, M. Sun, Z. Liu, Z. Yu, Co-producing lipopeptides and poly-gamma-glutamic acid by solid-state fermentation of Bacillus subtilis using soybean and sweet potato residues and its biocontrol and fertilizer synergistic effects, Bioresour. Technol. 99 (2008) 3318–3323. doi:10.1016/j.biortech.2007.05.052.

[344] M. Yasuzawa, K. Edagawa, T. Matsunaga, H. Takaoka, T. Yabutani, Highly Selective Needle-Type Glucose Sensors Prepared by the Immobilization of Glucose Oxidase on γ-Polyglutamic Acid Film, Analytical Sciences. 27 (2011) 337–337. doi:10.2116/analsci.27.337.

[345] S. Sarig, F. Kahana, R. Leshem, Selection of threshold agents for calcium sulfate scale control on the basis of chemical structure, Desalination. 17 (1975) 215–229. doi:10.1016/S0011-9164(00)84057-6.

[346] D. Bhattacharyya, J.A. Hestekin, P. Brushaber, L. Cullen, L.G. Bachas, S.K. Sikdar, Novel poly-glutamic acid functionalized microfiltration membranes for sorption of heavy metals at high capacity, Journal of Membrane Science. 141 (1998) 121–135. doi:10.1016/S0376-7388(97)00301-3.

[347] B.S. Inbaraj, C.P. Chiu, G.H. Ho, J. Yang, B.H. Chen, Removal of cationic dyes from aqueous solution using an anionic poly-gamma-glutamic acid-based adsorbent., J Hazard Mater. 137 (2006) 226–234. doi:10.1016/j.jhazmat.2006.01.057.

[348] N. Peruzzi, B.W. Ninham, P. Lo Nostro, P. Baglioni, Hofmeister phenomena in nonaqueous media: the solubility of electrolytes in ethylene carbonate, J Phys Chem B. 116 (2012) 14398–14405. doi:10.1021/jp309157x.

[349] D. Tatini, P. Tempesti, F. Ridi, E. Fratini, M. Bonini, P. Baglioni, Pluronic/gelatin composites for controlled release of actives, Colloids and Surfaces B: Biointerfaces. 135 (2015) 400–407. doi:10.1016/j.colsurfb.2015.08.002.

[350] M.M. Michel, L. Reczek, Pre-treatmet of flowback water to desalination, in: Membranes and Membrane Processes in Environmental Protection. Monographs of the Environmental Engineering., Committee Polish Academy of Sciences, 2014: pp. 309–321. https://www.researchgate.net/publication/264162613_PRE-TREATMENT_OF_FLOWBACK_WATER_TO_DESALINATION (accessed September 3, 2018).

[351] Q. Jiang, J. Rentschler, R. Perrone, K. Liu, Application of ceramic membrane and ion-exchange for the treatment of the flowback water from Marcellus shale gas production, Journal of Membrane Science. 431 (2013) 55–61. doi:10.1016/j.memsci.2012.12.030.

[352] B. Lindman, A. Carlsson, S. Gerdes, G. Karlström, L. Piculell, K. Thalberg, K. Zhang, Polysaccharide–Surfactant Systems: Interactions, Phase Diagrams, and Novel Gels, in: E. Dickinson, P. Walstra (Eds.), Food Colloids and Polymers, Woodhead Publishing, 2005: pp. 113–125. doi:10.1533/9781845698270.113.

[353] D.A.Z. Wever, F. Picchioni, A.A. Broekhuis, Polymers for enhanced oil recovery: A paradigm for structure–property relationship in aqueous solution, Progress in Polymer Science. 36 (2011) 1558–1628. doi:10.1016/j.progpolymsci.2011.05.006.

[354] S. Biggs, J. Selb, F. Candau, Copolymers of acrylamide N-alkylacrylamide in aqueous solution: the effects of hydrolysis on hydrophobic interactions, Polymer. 34 (1993) 580–591. doi:10.1016/0032-3861(93)90554-N.

[355] B. Magny, I. Iliopoulos, R. Zana, R. Audebert, Mixed Micelles Formed by Cationic Surfactants and Anionic Hydrophobically Modified Polyelectrolytes, Langmuir. 10 (1994) 3180–3187. doi:10.1021/la00021a047.

[356] E.D. Goddard, P.S. Leung, Studies of gel formation, phase behavior and surface tension in mixtures of a hydrophobically modified cationic cellulose polymer and surfactant, Colloids and Surfaces. 65 (1992) 211–219. doi:10.1016/0166-6622(92)80276-8.

[357] I. Iliopoulos, U. Olsson, Polyelectrolyte association to micelles and bilayers, Journal of Physical Chemistry. 98 (1994) 1500–1505. doi:10.1021/j100056a022.

[358] S. Biggs, J. Selb, F. Candau, Effect of Surfactant on the Solution Properties of Hydrophobically Modified Polyacrylamide, Langmuir. 8 (1992) 838–847. doi:10.1021/la00039a018.

[359] X. Xie, T.E. Hogen-Esch, Copolymers of N,N-dimethylacrylamide and 2-(N-ethylperfluorooctanesulfonamido)ethyl acrylate in aqueous media and in bulk. Synthesis and properties, Macromolecules. 29 (1996) 1734–1745.

[360] I. Gatej, M. Popa, M. Rinaudo, Role of the pH on Hyaluronan Behavior in Aqueous Solution, Biomacromolecules. 6 (2005) 61–67. doi:10.1021/bm040050m.

[361] J.L. Gidley, S.A. Holditch, D.E. Nierode, Fracturing Fluids and Additives, in: Recent Advances in Hydraulic Fracturing, Society of

Petroleum Engineers, 1989. https://store.spe.org/Recent-Advances-In-Hydraulic-Fracturing--P66.aspx (accessed October 15, 2018).

[362] D. Hasson, H. Shemer, A. Sher, State of the Art of Friendly "Green" Scale Control Inhibitors: A Review Article, Ind. Eng. Chem. Res. 50 (2011) 7601–7607. doi:10.1021/ie200370v.

[363] Z. Amjad, Calcium sulfate dihydrate (gypsum) scale formation on heat exchanger surfaces: The influence of scale inhibitors, Journal of Colloid and Interface Science. 123 (1988) 523–536. doi:10.1016/0021-9797(88)90274-3.

[364] R.J. Ross, K.C. Low, J.E. Shannon, Polyaspartate scale inhibitors -- Biodegradable alternatives to polyacrylates, Materials Performance. 36 (1997). https://www.osti.gov/biblio/460440-polyaspartate-scale-inhibitors-biodegradable-alternatives-polyacrylates (accessed October 16, 2018).

Appendix

List of Papers

Paper I

Carbohydrate Polymers 173 (2017) 344–352

Contents lists available at ScienceDirect

Carbohydrate Polymers

journal homepage: www.elsevier.com/locate/carbpol

Specific ion effects in polysaccharide dispersions

Duccio Tatini[a], Filippo Sarri[a], Piefrancesco Maltoni[a], Moira Ambrosi[a], Emiliano Carretti[a], Barry W. Ninham[a,b], Pierandrea Lo Nostro[a,*]

[a] Department of Chemistry "Ugo Schiff" and CSGI, University of Florence, 50019 Sesto Fiorentino, Firenze, Italy
[b] Department of Applied Mathematics, Research School of Physical Sciences and Engineering, Australian National University, Canberra, ACT 2600, Australia

ARTICLE INFO

Article history:
Received 17 March 2017
Received in revised form 22 May 2017
Accepted 24 May 2017
Available online 27 May 2017

Keywords:
Polysaccharide(s)
Guar gum
Sodium hyaluronate
Specific ion effect
Viscosity
Thermal properties

ABSTRACT

The specific effects induced by some strong electrolytes or neutral co-solutes on aqueous mixtures of guar gum (GG), sodium alginate (SA) and sodium hyaluronate (SH) were studied through rheology and DSC experiments. The results are discussed in terms of changes in the polymer conformation, structure of the network and hydration properties. This study is also aimed at controlling the viscosity of the aqueous mixtures for application in green formulations to be used as fracturing fluids for shale gas extraction plants.

1. Introduction

Hofmeister, or specific ion effects consist in changes induced in a measurable phenomenon or physico-chemical property by the addition of a specific salt. These effects usually take place at moderately high concentrations, e.g. above 10 mM. They occur in a large variety of systems and practically in all realms of nature: in bulk solutions, aqueous and non-aqueous systems, at interfaces and in self-assembled structures (Lo Nostro & Ninham, 2012; Lo Nostro & Ninham, 2016).

Compared to the pristine sequence found by Hofmeister in his studies on the precipitation of albumin dispersions, other systems may exhibit a different order. However, in general it is observed that as the ion changes, the measured properties are affected. Recently it has been found that the charge and polarity of the involved species and surfaces are crucial factors in determining whether the effectiveness of the salts follows the direct or reverse Hofmeister series (Schwierz, Horinek, Sivan, & Netz, 2016). In a dilute regime, electrostatics dominates the picture of ionic interactions, and Coulomb potential describes the behavior of the solution, with a substantial correct prediction of the ionic activity coefficient. However, electrostatic interactions are non ion-specific, while the surface charge density depends on the ion size. At high salt concentrations, non-electrostatic forces come into play, Coulomb interactions are screened, and ion specificity emerges.

The rheology and thermal behaviors of solutions and dispersions of biopolymers such as polysaccharides are examples of specific ion effects, in fact such features can be tuned by the proper choice of electrolytes at a suitable concentration. This topic has been fully investigated in the literature (see Hatakeyama, Tanaka, & Hatakeyama, 2010; Guan, Xu, & Huang, 2010; Kupská, Lapcík, Lapcíková, Záková, & Juríková, 2014, and references therein). One of the more interesting insights is the mechanism through which such effects take place. Norton studied the disorder-order transition and the helix–helix aggregation in κ-carrageenan in the presence of different salts, and concluded that these phenomena depend on the salt-induced modification of the solvent quality of water, and not on direct salt-polyelectrolyte interactions (Norton, Morris, & Rees, 1984). Along the same line, Xu explained the effect of salts on the sol-gel transition of methylcellulose in terms of the ability of individual ions to change water structure and of the strength of the interactions between water molecules (Xu, Wang, Tam, & Li, 2004).

As a final point regarding the application of the above theoretical model to salting-in and salting-out phenomena, we return to the fact that, in general, the surface of a macromolecule exposes sites

* Corresponding author at: Department of Chemistry Ugo Schiff, Via della Lastruccia 3, 50019 Sesto Fiorentino, Firenze, Italy.
E-mail addresses: duccio.tatini@unifi.it (D. Tatini), filippo.sarri@unifi.it (F. Sarri), pierfrancesco.maltoni@stud.unifi.it (P. Maltoni), moira.ambrosi@unifi.it (M. Ambrosi), emiliano.carretti@unifi.it (E. Carretti), barry.ninham@anu.edu.au (B.W. Ninham), pierandrea.lonostro@unifi.it (P. Lo Nostro).

http://dx.doi.org/10.1016/j.carbpol.2017.05.078
0144-8617/

(functional groups) which differ in their relative affinities to the components of the mixed solvent. (Piculell & Nilsson, 1989).

A more relevant study is that by Yin on the gelation of konjac glucomannan (KGM) and in particular on its rheological behavior in the presence of different salts. The increase in the viscosity upon addition of salting-out salts is explained in terms of (i) the modification of the water structure or (ii) by the change in the interactions between the ions and specific sites on the polymer chains (Yin, Zhang, Huang, & Nishinari, 2008). Finally, Singh investigated the gelling behaviour of agarose with Na_2SO_4, and found that the release of water from the gel is due to the water withdrawing action of sulfate ions (Singh, Meena, & Kumar, 2009).

In the present contribution we report a study on the effect induced by some strong electrolytes and neutral cosolutes on the rheology and thermal behavior of some polysaccharide aqueous dispersions and solutions. The results are discussed in terms of the Hofmeister series, ion-polymer and polymer-water interactions.

This investigation is relevant for the application of polysaccharides in green formulations for fracturing fluids used in shale gas extraction (Barati & Liang, 2014; Kelly, Khan, Leduc, Tayal, & Prud'homme, 2001; Legemah, Qu, Sun, Beall, & Zhou, 2013).

The basic ingredients that are commonly used in fracturing fluids comprise water, more or less chemically modified polysaccharides as gelling agents (guar gum, cellulose, xanthan gum and their derivatives), a large number of salts as formulation stabilizers or clay control agents, acids (e.g. HCl, H_3BO_3 and citric acid) and bases to adjust the pH, cross-linker initiators (potassium borate or metaborate, complexes of zirconium or titanium with organic chelators), naphtha derivatives and surfactants (Barati & Liang, 2014; Gandossi & Von Estorff, 2015; Li, Al-Muntasheri, & Liang, 2016; Montgomery, 2013).

Several scientists have discussed a number of possible environmental risks related to the production of shale gas. These include the accidental release of fracturing fluids, leaks of hydrocarbons, the uptake of Naturally Occurring Radioactive Materials (NORM), the introduction of foreign bacterial strains to the subsurface, and induced micro-seismicity (Arthur, Bohm, Coughlin, Layne, & Cornue, 2009; Holloway & Rudd, 2013, Chapter 11; Osborn, Vengosh, Warner, & Jackson, 2011; Vengosh, Jackson, Warner, Darrah, & Kondash, 2014). To limit some of these risks, we focus on "greener" formulations, which employ biocompatible and non-toxic ingredients.

2. Hypotheses

This study is aimed at demonstrating that the thermal and rheological properties of aqueous mixtures containing guar gum, sodium alginate and sodium hyaluronate can be significantly modified by using strong electrolytes, and that salt specific effects show up, following the Hofmeister series. The ions exhibit particular effects related to their structure and particularly to their capability to interfere with the polymer hydrogen bonding network and with the solvent properties of water. The results support our effort to formulate green alternatives to the currently used hydraulic fracturing fluids.

3. Experimental

3.1. Materials

All chemicals were reagent grade (≥99%) and used as received. NaF, NaI, NaSCN, $NaClO_4{\cdot}H_2O$, NaH_2PO_4 were purchased from Fluka (Milan, Italy). NaCl, NaBr, Na_2SO_4, $Na_3PO_4{\cdot}3H_2O$, $Na_2HPO_4{\cdot}7H_2O$, trehalose and sodium alginate (average molecular mass 240 kDa; mannuronate/guluronate ratio 0.44) were supplied by Sigma-Aldrich (Milan, Italy). Urea was purchased from Riedel de Haen (Germany). Guar gum (average molecular mass 2000 kDa) was supplied by Lamberti S.p.A. (Milan, Italy); high molecular weight (1800–2000 kDa) sodium hyaluronate was purchased from Stanford Chemicals Company (Fairbanks, CA). All solutions and dispersions were prepared with bidistilled Milli-Q water (resistivity>18 MΩ·cm at 25 °C).

3.2. Sample preparation

In general gelling agents for fracturing formulations are used up to 1% w/w (Couillet & Hughes, 2008; Kelly et al., 2001). The addition of a crosslinker lowers the concentration to 0.1–0.5% (Goel, Shah, & Grady, 2002). We chose a polysaccharide concentration of 1% to avoid the addition of a crosslinker; in this way we can focus exclusively on the effect of the salt on the polymer chains.

GG, SA and SH 1% w/w water mixtures were prepared by slowly adding a weighted amount of polysaccharide powder to water under constant stirring at room temperature. In these conditions complete dissolution occurs in about one hour for all the investigated biopolymers. The samples containing the different salts or co-solutes were prepared following the same procedure, replacing water with 0.5 M aqueous solutions of the salts or neutral co-solutes.

3.3. Rheology

Rheological measurements were performed on a Paar Physica UDS 200 rheometer working in the controlled shear-stress mode. For all samples a plate–plate geometry (diameter, 2.5 cm; gap, 300 μm) was used. Under these conditions the total amount of the sample in the cell was about 0.4 mL. All measurements were performed at 25.0 °C (Peltier control system). For each sample the flow curve was acquired in a torque range between 10^{-3} and 2000 mN m, after a 15 min soaking time to equilibrate at the set temperature.

3.4. Thermal properties

Differential Scanning Calorimetry (DSC) was performed by means of a DSC-Q2000 by TA Instruments (Philadelphia, PA). The samples were first cooled from 20° to −60 °C at 10 °C/min, then heated up to 50 °C at 5 °C/min. Measurements were conducted in N_2 atmosphere, with a flow rate of 50 mL/min. For the samples prepared with NaF and Na_2HPO_4 the deconvolution of endothermic peaks was performed by means of the Igor Pro 6.36 software, using a summation of exponentially modified Gaussian (EMG) functions (Tatini et al., 2015). The single EMG function is defined as:

$$f(T) = \sqrt{\frac{\pi}{2}}\frac{hw}{|s|}\exp\left[\frac{w^2}{2s^2}\left(\frac{T_0 - T}{s}\right)\right]\operatorname{erf}\left[\frac{T_0 - T}{2\left(w + \frac{w}{|s|}\right)}\right] \quad (1)$$

where h is the height, T_0 the center, w the width of the peak and s is the distortion factor (shape). For the deconvoluted peaks, the peak temperatures correspond to T_0, while the enthalpy changes are calculated using the total area under the peak.

4. Results and discussion

The thermal and rheological properties of the investigated polysaccharides were studied in their pure aqueous mixtures and after the addition of some sodium salts or neutral co-solutes (trehalose and urea). It may sound trivial, but it is important to underline that in the two experimental techniques used in this study the sample is treated in totally different manners. In DSC the specimen remains still and is heated/cooled above and below room temperature. On the other hand, during the acquisition of the

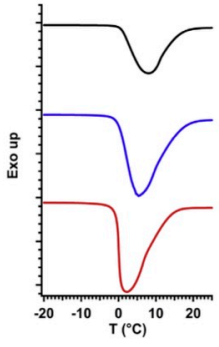

Fig. 1. From top to bottom: DSC heating curves of 1% aqueous mixtures of GG (black), SA (blue), and SH (red). Curves have been offset for graphical purposes. (For interpretation of the references to colour in this figure legend, the reader is referred to the web version of this article.)

flow curve the sample is mechanically stressed at constant temperature, its supramolecular texture is modified and its reaction to this perturbation recorded. The thermal behavior (studied through DSC) reflects the interactions between the cosolutes, the polymer chains and water; while the rheological behavior depends on the interactions between the polymer chains, and their distribution and entanglement in the matrix.

4.1. Thermal behavior

The thermograms of 1% aqueous mixtures of GG, SA and SH are reported in Fig. 1.

The endothermic peak, due to the melting of free water, is always centered slightly above 0 °C, presumably because of a kinetic effect (Hatakeyama et al., 2010; Naoi, Hatakeyama, & Hatakeyama, 2002). The melting peak temperatures (T_{mf}) and the corresponding enthalpy changes (ΔH_{mf}, in J/g) are listed in Table 1. GG shows the highest melting temperature, associated to the lowest melting enthalpy, while SH possesses the lowest peak temperature and the largest melting enthalpy. SA shows intermediate values.

The thermograms of GG in the presence of different 0.5 M solutions of sodium halides are shown in Fig. 2.

In the case of NaF the endothermic peak shows a bimodal behavior. The curve was deconvoluted by using an exponentially modified Gaussian function (EMG) according to Eq. (1). This approach is commonly implemented in the analysis of overlapping DSC peaks in drugs (Elsabee & Prankerd, 1992), paraffins (Anghel, Georgiev, Petrescu, Popov, & Constantinescu, 2014) and polymer composites characterization (Tatini et al., 2015). The fitting procedure provides the two T_0 values corresponding to the centers of the two Gaussian curves used for the deconvolution. T_0 are found to be 5.07 and −4.45 °C. This bimodal behavior is increased with increasing halide atomic number: in the case of NaCl, NaBr and NaI two distinct peaks appear in the DSC curve whose distance increases moving down in the group. The higher temperature peak corresponds to the melting of free water (T_{mf} in Table 1) and is similar to the peak produced by the salt-free GG dispersion. The lower temperature peak located between −30 and −5 °C relates to the melting of freezable bound water (T_{mb} in Table 1), that freezes below 0 °C and has a reduced enthalpy of fusion (Chaplin, 2012).

For the samples containing pure GG, SA and SH the peak related to the melting of freezable bound water is not observed. Presumably the freezable bound and the free water melting peaks overlap together in the broad endothermic signal which is centered around 0 °C in the heating scans (see Fig. 1). A similar behavior was reported by Nakamura in the case of cellulose with different amounts of adsorbed water (Nakamura et al., 1981). The addition of a salt modifies the interactions between water and the polysaccharide chains, and changes the distribution of water between the two states: freezable bound and free water. This effect induces a separation of the two overlapping peaks, which is strictly dependent on the salt nature.

The melting point and the enthalpy change for the bound freezable water depend on the interactions between the polymer chains and water (Guan et al., 2011).

As proposed by De Andres-Santos for 1% aqueous solutions of sodium hyaluronate, we assume that the lower T_{mb}, the higher the number of water and polysaccharide molecules that remain closely associated to each other, i.e., the more hydrated the chains (De Andres-Santos, Velasco-Martin, Hernández-Velasco, Martín-Gil, & Martín-Gil, 1994). On the other hand, a higher T_{mb} indicates an increment in the interchain hydrogen bonding (HB) interactions within the polysaccharide, thus suggesting a sort of de-hydration of the polymer.

The results obtained for the samples containing the sodium halides show no remarkable variation in T_{mf} and ΔH_{mf} with the exception of NaF. Instead, the values of T_{mb} decrease from −4.45 (NaF) to −29.65 °C (NaI), while ΔH_{mb} decreases from 125.8 (NaF) to 15.07 J/g (NaI). These trends suggest the presence of a specific anion effect on the conformational structure and intermolecular interactions of GG. In particular, the more chaotropic the anion, the lower the value of T_{mb} and hence the lower the number of interacting sites between the polysaccharide chains. We argue that strongly hydrated kosmotropic anions like fluoride and sulfate compete with the polysaccharide chains for water molecules, thus lowering the hydration of the chains (Yin et al., 2008). This effect promotes the formation of interchain HB and eventually leads to the aggregation of polysaccharide molecules.

On the other hand, the presence of chaotropic anions, like iodide, modifies the dimensions of the polysaccharide coils and increases their solvent-accessible surface area (ASA) (Curtis, Steinbrecher, Heinemann, Blanch, & Prausnitz, 2002). These ion hydration effects that lead to the salting-in processes induced by chaotropes and salting-out by kosmotropes on proteins have been extensively studied (López-Arenas, Solís-Mendiola, Padilla-Zúñiga, & Hernández-Arana, 2006). The ruling mechanism by which chaotropes increase the solvation of the polymer surface seems to be a direct interaction of the ions with the weakly hydrated portions of the polysaccharide chain, as already found and reported in the case of proteins (Arakawa & Timasheff, 1982; Collins, 2004; Lo Nostro & Ninham, 2012).

The presence of urea produces a second endothermic peak in the thermogram, related to the melting of freezable bound water. At this concentration urea usually acts as an enhancer of the solvation of the polysaccharide chains (Winkworth-Smith, MacNaughtan, & Foster, 2016) by promoting their unfolding.

In the case of the other additives (Na_2SO_4, NaSCN, $NaClO_4$, Na_3PO_4, Na_2HPO_4, NaH_2PO_4 and trehalose) only a broad endothermic peak around 0 °C is clearly detected (see Table 1, and Figs. S1 and S2 in Supplementary material). The presence of these cosolutes does not induce a separation between the freezable bound and the free water melting peaks, resulting in a DSC profile which is similar to those of pure GG, SA and SH samples (Fig. 1). The case of Na_2SO_4 is peculiar as it shows a value of ΔH_{mf} (318.4 J/g) which is close to that of pure water (333.5 J/g). The sulfate ions strongly interact with the water molecules inducing a de-hydration of the polysaccharide

Table 1
Melting temperature and enthalpy change of free water (T_{mf} and ΔH_{mf}, in °C and J/g) and of the freezable bound water (T_{mb} and ΔH_{mb}, in °C and J/g) in 1% aqueous mixtures of guar gum, sodium alginate, and sodium hyaluronate, in the presence of different salts or neutral cosolutes. The concentration of all cosolutes is always 0.5 M, unless otherwise specified.

additive	T_{mf}	ΔH_{mf}	T_{mb}	ΔH_{mb}	T_{mf}	ΔH_{mf}	T_{mb}	ΔH_{mb}	T_{mf}	ΔH_{mf}	T_{mb}	ΔH_{mb}
Guar Gum 1%					Sodium Alginate 1%				Sodium Hyaluronate 1%			
none	7.88	307.3			5.36	336.4			2.18	353.0		
NaF	5.07	155.5	−4.45	125.8	1.16	273.7	−4.11	56.39	0.66	300.8	−5.23	40.46
NaCl	1.05	245.2	−19.98	22.11	1.33	241.8	−19.82	21.50	−0.03	260.1	−20.43	23.77
NaBr	1.80	249.7	−26.03	16.58	0.05	267.3	−26.34	17.78	−0.16	268.8	−26.71	19.18
NaI	1.62	256.2	−29.65	15.07	0.07	267.6	−29.73	16.40	−0.57	272.4	−29.99	16.54
Na_2SO_4	4.24	318.4			2.61	334.1			2.49	331.8		
NaSCN	1.54	282.7			−0.22	276.3			−0.13	289.4		
$NaClO_4$	2.58	278.2			−0.35	293.6	−33.23	12.28	−0.22	299.6	−33.19	5.678
Na_3PO_4	1.28	58.88			4.42	294.8			0.64	317.6		
Na_2HPO_4	5.13	293.5			1.50	331.9			1.79	274.5		
NaH_2PO_4	3.00	291.5			−0.23	295.8			−0.32	307.5		
Urea	3.48	247.9	−10.62	8.342	2.03	254.1	−11.11	11.68	0.00	268.8	−11.83	13.67
Trehalose	1.56	255.2			0.59	279.9			0.07	261.9		

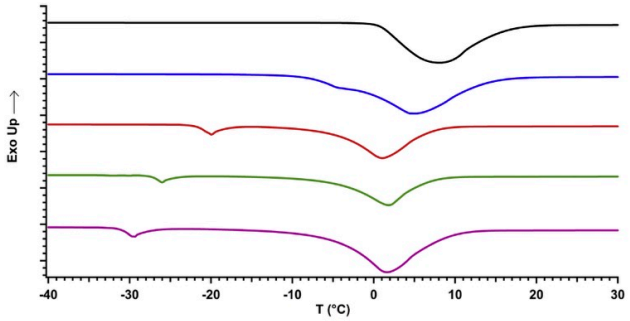

Fig. 2. From top to bottom: DSC heating curves of 1% aqueous mixtures of GG pure (black) and in the presence of 0.5 M solutions of NaF (blue), NaCl (red), NaBr (green) and NaI (magenta). Curves have been offset for graphical purposes. (For interpretation of the references to colour in this figure legend, the reader is referred to the web version of this article.)

chains, reducing the amount of freezable bound water in favour of the free water, and resulting in an overlap of the two DSC signals.

The effect induced by Na_2HPO_4 is peculiar and deserves an in-depth analysis. The DSC curve (Fig. S3 in Supplementary material) shows a shoulder at about 20 °C. This phenomenon can be related to a liquid crystalline-to-isotropic liquid state transition (Hatakeyama, Naoi, & Hatakeyama, 2004; Nakamura, Hatakeyama, & Hatakeyama, 1991). Since this transition is observed both for GG and SA samples, we argue that the presence of Na_2HPO_4 preserves the liquid crystalline phase in the guar and sodium alginate network, whereas all the other examined salts and co-solutes destabilize this state.

In order to separate the two endothermic contributions and calculate the enthalpy for this transition, EMG deconvolution was performed and the fitting parameters (T_{ph} and ΔH_{ph}) are shown in Table S1 (see the Supplementary material). For GG the liquid crystalline-to-isotropic liquid state transition occurs at T_{ph} = 19.3° C, with a corresponding enthalpy change of 24.68 J/g.

Aqueous solutions of SA and SH in the presence of salts and cosolutes show an identical thermal behavior to that previously described for GG dispersions. The values of T_{mf}, ΔH_{mf}, T_{mb} and ΔH_{mb} extracted from the thermograms are reported in Table 1. SH and SA samples show analogous DSC curves to the corresponding GG samples, with the exception of perchlorate. For both SA and SH systems, the thermograms of perchlorate containing sample show two peaks instead of one, as in the GG/perchlorate sample. An extra peak appears at about −33 °C and can be ascribed to the freezable bound water melting. This peak may reflect polymer-salt interactions similar to those occurring with other chaotropic ions. In the GG sample this peak is not shown, indicating that a different mechanism occurs. It is worthwhile to mention that ClO_4^- may act as an oxidizer and it is extensively used as gel breaker in guar-based formulations (Hall, Szemenyei, & Gupta, 1991; Schnoor, Singh, & Russel, 2016; Schultheiss, 2015). Presumably perchlorate partially oxidizes the polysaccharide chains, inducing a structural modification and a change in the polymer-water interactions, and the peak for the melting of freezing bound water disappears. This mechanism does not take place with the partially anionic chains of SA and SH.

4.2. Rheology

4.2.1. Fitting of the flow curves

All the flow curves show a similar profile (see Fig. 3). At low shear rate all mixtures exhibit a Newtonian plateau. For stronger perturbations a shear thinning region is shown.

We applied the Bird–Carreau–Yasuda (BCY) rheological model to the flow curves. This model, sometimes referred to as Carreau–Yasuda or Carreau model (Barnes, Hutton, & Walters, 1989), was empirically developed to describe the mechanical

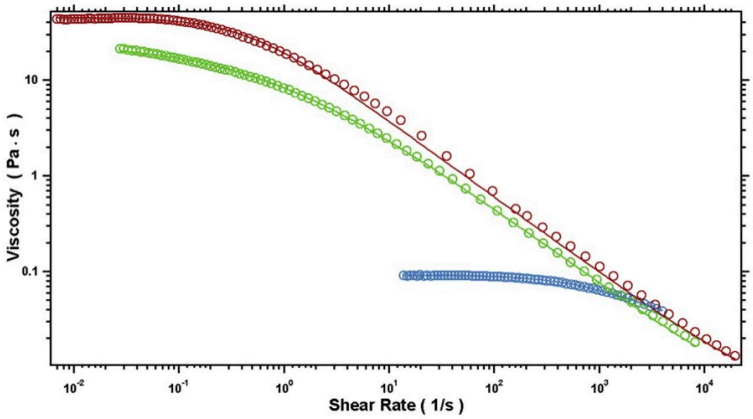

Fig. 3. From bottom to top: Flow curves for 1% w/w SA (light blue), GG (green), and SH mixtures (red). The solid lines represent the fitting of the experimental curves. (For interpretation of the references to colour in this figure legend, the reader is referred to the web version of this article.)

behavior of systems that exhibit both a Newtonian and a shear thinning region (Osswald & Rudolph, 2015). In particular it is used to study the rheology of polymeric water-based dispersions and solutions, e.g. those from polyacrylamide (Escudier et al., 2005), polypropylene (Lertwimolnun & Vergnes, 2006), and polysaccharides such as SH (Haward, Jaishankar, Oliveira, Alves, & McKinley, 2013), GG (Nandhini Venugopal & Abhilash, 2010), xanthan gum and carboxymethylcellulose (Escudier, Gouldson, Pereira, Pinho, & Poole, 2001; Escudier et al., 2005; García, Alfaro, Calero, & Muñoz, 2014).

In the BCY model the following equation describes the dependence of the viscosity value η:

$$\eta = \eta_\infty + (\eta_0 - \eta_\infty) \cdot [1 + (\lambda\dot{\gamma})^a]^{(n-1)/a} \quad (2)$$

where η, η_0, η_∞, $\dot{\gamma}$, λ, n, and a are the viscosity, the zero shear rate viscosity, the viscosity at infinite shear, the applied shear rate, the yield of shear rate above which the system shows a shear thinning behavior, the power law index, and the Yasuda parameter indicating the width of the transition region between η_0 and η_∞, respectively (Carreau, 1972; Osswald & Rudolph, 2015; Yasuda, Armstrong, & Cohen, 1981).

Almost all flow curves containing GG and SH are well fitted (as shown by the χ^2, see Table 2) by the BCY model with the sole exceptions of SH in the presence of Na_3PO_4 and of the SA solutions, which show a very low variability in the whole shear range examined. Table 2 lists the values of $\boldsymbol{\eta_0}$, $\boldsymbol{\lambda}$, a and n extracted from the fitting of the flow curves, according to Eq. (2).

4.2.2. Flow curves

In order to check the effect of different salts on the viscosity of polysaccharide mixtures, we mainly focussed our attention on the trend of η_0 value.

Fig. 3 shows the flow curves for the 1% aqueous mixtures of SA, GG and SH. All samples exhibit a specific non-Newtonian behavior: the zero shear viscosity of SH and GG water-based systems are in the order of tens of Pa s (η_0 = 44.66 and 24.41 Pa s, respectively), while the alginate system shows a low value, about 0.11 Pa s in the whole explored torque range. On the other hand, the addition of salts or neutral co-solutes induces remarkable changes in the rheological properties of GG and SH (see Table 2).

Fig. 4 illustrates the effect of trehalose, Na_2SO_4 and NaF on the profile of the flow curve of SH and GG. For SH the presence of trehalose led to an increase of the strength of the tridimensional network, as indicated by the increase of η_0 (from 44.66 up to 159.25 Pa s) and by a shift of the yield value of $\dot{\gamma}$, λ. On the other hand, sulfate and fluoride lower both the η_0 (21.01 and 28.05 Pa s respectively) and the λ values.

A similar trend is obtained for trehalose and GG, while the addition of Na_2SO_4 and NaF to GG induces an opposite effect, as indicated by the raise in the zero shear viscosity (from 24.41 up to 43.53 and 33.30 Pa s, respectively), and by the shift of λ to higher values. These results suggest a synergistic interaction between trehalose and the polysaccharide molecules, which is more significant for SH. We argue that trehalose establishes crosslinking intra- and intermolecular interactions, resulting in a strengthening of the system.

Indeed, trehalose is known as a kosmotrope or water-structure maker: this disaccharide is able to break the tetrahedral HB network of water and re-order the water molecules in the hydration layer (Branca et al., 2005; Lerbret et al., 2005). However, experiments conducted by us on a 0.5 M solution of trehalose in water show neither an increase in the viscosity, nor a modification in the rheological response.

The competition for water molecules between trehalose and the polysaccharide chains leads to partial de-hydration of the macromolecules (Jain & Roy 2008). It has been shown that trehalose can modify the hydration layer of biomolecules (Kawai, Sakurai, Inoue, Chujo, & Kobayashi, 1992; Magazù, Migliardo, Musolino, & Sciortino, 1997), stabilizing their HB network. This picture is commonly known as *preferential exclusion theory*. The *water replacement theory* instead argues that the hydration layer of the macromolecules is substituted by trehalose, which directly forms HB and stabilizes the structure. A third approach, the *vitrification theory*, can be applied only at higher concentration of trehalose and envisages that it creates a glassy matrix which acts as a protective cocoon, shielding and stabilizing the macromolecules from external stresses (Jain & Roy 2008). Since in our case the concentration of tre-

Table 2
The zero shear rate viscosity (η_0, in Pa s), power law index (n), the reciprocal of the critical shear rate at which the viscosity begins to drop down (λ, in s), the width of the transition region between η_0 and η_∞ (a), and the χ^2 extracted from the fitting of the flow curves for 1% aqueous mixtures of guar gum and sodium hyaluronate, in the presence of different salts or neutral cosolutes. The concentration of all cosolutes is always 0.5 M, unless otherwise specified.

additive	$\eta_0 \pm 2.5\%$	n ± 4%	λ ± 5%	a ± 3%	χ^2	$\eta_0 \pm 1.5\%$	n ± 15%	λ ± 9%	a ± 4%	χ^2
	Guar Gum 1%					Sodium Hyaluronate 1%				
none	24.41	0.20	1.36	0.58	6.96	44.66	0.20	2.22	1.21	51.71
NaF	33.30	0.19	1.64	0.65	13.29	28.05	0.19	0.87	0.57	7.12
NaCl	25.23	0.22	1.19	0.58	7.28	44.84	0.21	2.14	1.00	72.92
NaBr	23.68	0.22	1.24	0.57	3.64	40.95	0.26	2.07	0.93	98.98
NaI	19.70	0.24	1.11	0.51	6.88	46.23	0.15	1.22	0.55	6.25
Na_2SO_4	43.53	0.21	3.14	0.67	32.67	21.01	0.22	0.76	0.59	3.75
NaSCN	28.27	0.16	1.12	0.42	7.05	40.96	0.27	2.11	0.68	39.50
$NaClO_4$	23.87	0.22	1.47	0.67	10.10	53.09	0.28	2.93	0.84	32.18
Na_2HPO_4	30.07	0.20	2.02	0.80	16.01	77.68	0.22	2.58	1.18	26.14
NaH_2PO_4	20.44	0.19	1.01	0.63	3.50	19.75	0.30	1.22	0.70	12.07
Na_3PO_4	19.90	0.24	1.29	0.64	5.36					
Urea	33.68	0.23	2.16	0.66	10.45	46.21	0.26	1.98	0.78	3.83
Trehalose	37.65	0.21	2.60	0.66	38.32	159.25	0.20	6.07	0.90	73.50

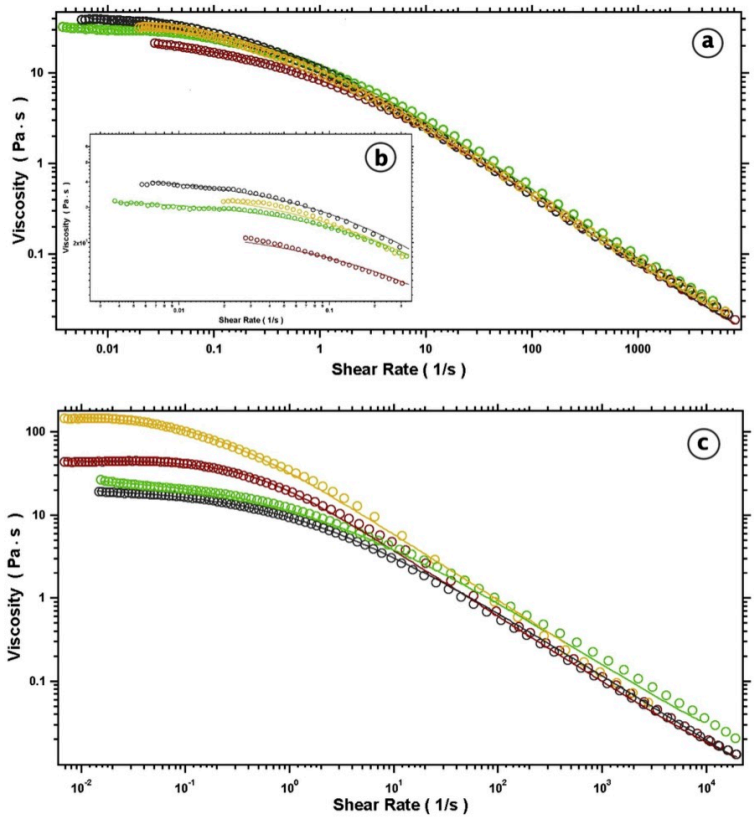

Fig. 4. Flow curves of (a) GG and SH (c) 1% w/w mixtures (red) and in the presence of 0.5 M trehalose (yellow), NaF (green) and Na_2SO_4 (grey). The inset (b) shows the flow curves of GG zoomed at low shear stress. The solid lines represent the fitting of the experimental curves. (For interpretation of the references to colour in this figure legend, the reader is referred to the web version of this article.)

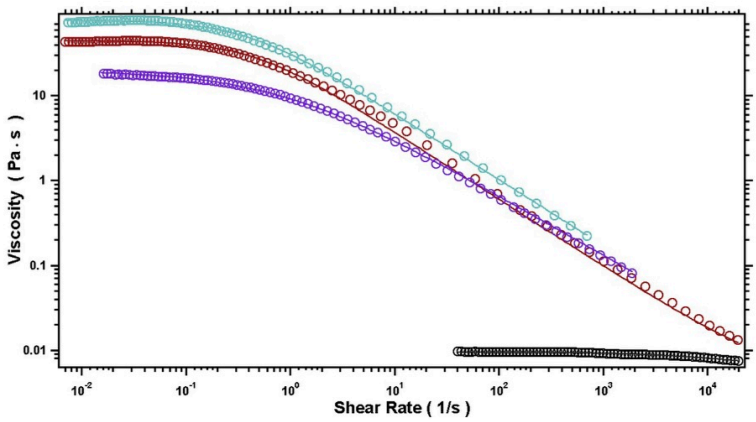

Fig. 5. Flow curves of SH 1% w/w pure solution (red), in the presence of 0.5 M NaH_2PO_4 (violet), Na_2HPO_4 (turquoise) and Na_3PO_4 (black). The solid lines represent the fitting of the experimental curves. (For interpretation of the references to colour in this figure legend, the reader is referred to the web version of this article.)

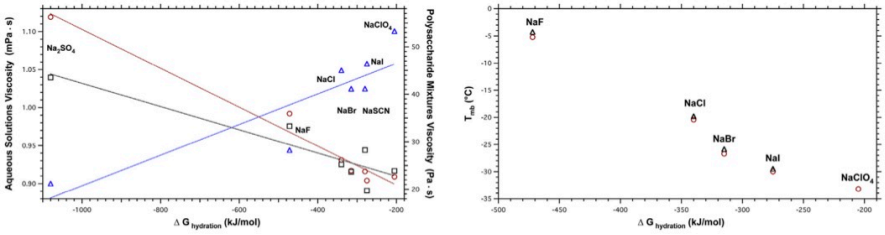

Fig. 6. Left panel: viscosity values for GG (black), SH (blue) and water (red) in the presence of the different sodium salts as a function of the $\Delta G_{hydration}$ of the anion. The left axis refers to the red line, while the right axis refers to black and blue lines. The dotted lines are only a guide for the eye. Right panel: T_{mb} for GG (black) and SH (red) in the presence of different sodium salts as a function of the $\Delta G_{hydration}$ of the anion. (For interpretation of the references to colour in this figure legend, the reader is referred to the web version of this article.)

halose is relatively low, we can exclude the latter hypothesis. In the case of sulphate we propose two different mechanisms, depending on the investigated polysaccharide. The SO_4^{2-} ion is a kosmotrope, which subtracts water from the macromolecule hydration layer. In the case of SH, where negatively charged $-COO^-$ groups are distributed along the chains, the addition of sulfate brings about a weakening in the polymeric network, that results in a decrease of the strength of the polymeric network. Conversely for GG the reduction of water molecules in the hydration layer promotes the formation of interchain interactions, due to the non-ionic nature of the polysaccharide. Therefore, the strength of the polymeric network increases, as indicated by the trend of both the viscosity and the λ values.

Moreover, also the effect of fluoride supports this argument. Indeed, kosmotropic ions like fluoride and sulfate strongly modify the rheology of the systems. At the same time, the addition of the other halides to GG and SH does not affect significantly the values of η_0 and λ.

A further peculiar case concerns the three phosphate anions (Fig. 5). In fact, the rheological profiles show that HPO_4^{2-} increases the viscosity of the SH solution to 77.68 Pa·s, while $H_2PO_4^-$ lowers (19.75) and PO_4^{3-} dramatically breaks down the flow curves.

We recall that the rheological properties of hyaluronate strongly depend on the pH in a non-linear correlation (Gatej, Popa, & Rinaudo, 2005; Gibbs, Merrill, & Smith, 1968; Gura, Hückel, & Müller, 2003; Maleki, Kjøniksen, & Nyström, 2008). In particular for hyaluronic acid the complex viscosity reaches a maximum value at about pH = 2.5, sided by two remarkable drops in acid (pH = 1.6) and mid-acid conditions (pH = 3.34) (Gatej et al., 2005). The stiffening of the hyaluronic network is attributed to a critical balance between attractive and repulsive forces. These forces that involve ionized or neutral carboxylic and amino groups are mainly electrostatic (Gibbs et al., 1968). Moreover, above pH = 12 the viscosity dramatically breaks down, leading to a Newtonian-like behavior. Finally, in a wide range of pH (between 2.8 and 12) the rheological properties and viscosity remain unchanged (Gatej et al., 2005; Maleki, 2008). Furthermore, Maleki investigated the dilute (0.05% w/w) and semi-dilute (0.5% w/w) regimes of HA solutions, with the pH set between 1 and 13 by adding 0.1 M phosphate buffers (Maleki et al., 2008).

The results show that the presence of these buffers does not affect the pH responsivity.

The 0.5 M Na_3PO_4 solution provides an extremely high pH (13) that can at least partly deprotonate the —OH groups of the hyaluronate chain, breaking the cooperative HB network of the polysaccharide chains. On the other hand, our results for 0.5 M NaH_2PO_4 and Na_2HPO_4 solutions (pH = 4.7 and 9.9, respectively) differ from those reported in the literature. Presumably in these pH conditions mono-hydrogenphosphate acts as a soft cross-linker, strengthening the HB network and increasing the viscosity. We argue that the increment in viscosity is due to a combination of two cooperating effects: the basic pH promotes the deprotonation, enhancing the HB network, and at the same time the higher SH concentrations shrink the polysaccharide network where HPO_4^{2-} anions bridge different chains and re-enforce the HB network.

In the presence of di-hydrogenphosphate the pH is lower. The mid-acid environment weakens the network by reducing the number of active sites available for HB. Moreover, in $H_2PO_4^-$ the number of acceptor sites for hydrogen bonding is reduced and thus the ion contribution to the strengthening of the system is reduced.

Moreover, the power law index parameter n reflects how the systems respond to an applied stress. Indeed, both GG dispersions and SH solutions exhibit only small fluctuations of n around the value of 0.2 for all samples. Thus, the scalar law that describes the shear thinning behavior above the λ critical value, is almost independent on the chemical nature of the added salt. After the disruption of the HB network in both cases we observed the same shear thinning effect.

In order to correlate the rheological and thermal behaviors to the thermodynamic properties of the investigated salts, we report in Fig. 6 the viscosities for GG, SH and water (on the left) and the T_{mb} values for GG and SH (on the right) in the presence of Na_2SO_4, NaF, NaCl, NaBr, NaSCN, NaI, $NaClO_4$ as functions of the $\Delta G_{hydration}$ of the anion.

The viscosity values of aqueous salt solutions and $\Delta G_{hydration}$ are taken from literature and reported in Table S2 in the Supplementary Material (Abdulagatova et al., 2005; Goldsack & Franchetto, 1977; Galmarini et al., 2011; Hood, 1933; Janz et al., 1969; Marcus, 1991; Wolf, 1966). In the case of T_{mb}, the samples containing Na_2SO_4, NaSCN and $NaClO_4$ (only for GG) are not reported since no bound freezable water melting peak was detected in the DSC thermograms.

The viscosity plot (left panel in Fig. 6) shows that the addition of a salt to GG (black) and to water (red) produces a similar trend, in agreement to the direct Hofmeister sequence: Na_2SO_4 > NaF > NaCl > NaBr > NaSCN > NaI > $NaClO_4$. Thus, we conclude that the addition of a salt induces a similar modification in the viscosity for both pure water and GG dispersion. On the other hand, the trend recorded for SH differs remarkably, showing the opposite behavior and following a reverse Hofmeister series.

The added salt produces an identical effect on the T_{mb} for the two polysaccharides, resulting in a decrease of the freezable bound water melting temperature moving along the series: NaF > NaCl > NaBr > NaI > $NaClO_4$.

These results confirm that the salt affects in the same way the hydration of the GG and SH by modifying the interactions between the water molecules and the polysaccharides, regardless of the different charge of their chains. Despite this, the GG dispersions and SH solutions show a diametrically opposite trend in terms of viscosities.

Kosmostropic anions induce a partial de-hydration of the polysaccharide chains, while the less hydrated chaotropic ions adsorb to the polymer chains, promote their unfolding and enhance the polymer–water interactions. The magnitude of the anion effect, both on the thermal and the rheological behaviors, is considerably higher in the case of the kosmotropic ions, whereas in the presence of chaotropic ions the behaviors are practically the same as those of the pure polysaccharide solutions.

These findings apparently point out that the degree of hydration of the polymer chains is the crucial factor that leads to a significant variation in the strength of the polysaccharide network, and that this phenomenon is ion specific. In the case of a neutral polysaccharide (guar gum) the decrease in the number of the water molecules that interact with the polysaccharide chains leads to a strengthening of the network, due to stronger inter-chain interactions. Vice versa, for a charged polysaccharide (sodium hyaluronate), electrostatic repulsive forces come into play with a greater impact, as a result of the reduced number of water molecules that can screen the charges. The overall effect is a weakening of the chain–chain interactions and, consequently the softening of the network.

5. Conclusions

The thermal and rheological behavior of 1% aqueous mixtures of guar gum (GG), sodium hyaluronate (SH) and sodium alginate (SA) were investigated in the presence of different salts or neutral co-solutes at constant concentration. The results suggest that the added solutes can remarkably modify the texture of the polysaccharide network by perturbing the hydration of the chains and changing their intermolecular interactions. The effect of the ions is apparently related to their hydration properties and their propensity to adsorb at the polymer interface. As a matter of fact a strongly hydrated (kosmotropic) ion is expected to deprive the polysaccharide chain of water, remain confined in the bulk solution, and enhance the interchain interaction in the case of the neutral GG. This results in a remarkable strenghtening of the system. On the other hand with the negatively charged SH, kosmotropes induce a weakening in the interactions. The chaotropes (bromide, iodide, thiocyanate) do not change the rheological properties of the mixtures. Being almost unhydrated, these ions are assumed to adsorb at the polymer surface and partially deplete some water from the hydration layer. This phenomenon is supposed to favor the unfolding of the chain, increase its hydration and reduce the interchain interactions. Phosphate ions deserve a special comment, in fact PO_4^{3-} and $H_2PO_4^-$ lower the viscosity, while HPO_4^{2-} produces a significant increment in the viscosity, both for GG and SH. Such behavior is probably related to a delicate balance between the different pH properties and the capacity of the three ions to strengthen the HB network.

These results are relevant for the formulation of greener frac fluids to be used in shale gas exploitation. More work is necessary to modify the behavior of more diluted polysaccharide solutions and dispersions (e.g. 0.5%), to study the effect of more concentrated salt solutions, to check the effect of temperature and pressure, and of other physico-chemical triggers for controlling the viscosity of the frac fluid in the different stages of the life of a basin.

Acknowledgments

The authors acknowledge funding from the European Union Horizon 2020 research and innovation programme under grant agreement No. 640979.

Appendix A. Supplementary data

Supplementary data associated with this article can be found, in the online version, at http://dx.doi.org/10.1016/j.carbpol.2017.05.078.

References

Anghel, E. M., Georgiev, A., Petrescu, S., Popov, R., & Constantinescu, M. (2014). Thermo-physical characterization of some paraffins used as phase change materials for thermal energy storage. *Journal of Thermal Analysis and Calorimetry, 117*, 557–566.

Arakawa, T., & Timasheff, S. N. (1982). Preferential interactions of proteins with salts in concentrated solutions. *Biochemistry, 21*, 6545–6552.

Arthur, J. D., Bohm, B. K., Coughlin, B. J., Layne, M. A., & Cornue, D. (2009). Evaluating the environmental implications of hydraulic fracturing in shale gas reservoirs. *Society of Petroleum Engineers, 121038*, 1–15.

Barati, R., & Liang, J.-T. (2014). A review of fracturing fluid systems used for hydraulic fracturing of oil and gas wells. *Journal of Applied Polymer Science, 131*(16).

Barnes, H. A., Hutton, J. F., & Walters, K. (1989). *An introduction to rheology*. Elsevier.

Branca, C., Maccarrone, S., Magazù, S., Maisano, G., Bennington, S. M., & Taylor, J. (2005). Tetrahedral order in homologous disaccharide-water mixtures. *The Journal of Chemical Physics, 122*, 174513.

Carreau, P. J. (1972). Rheological equations from molecular network theories. *Journal of Rheology, 16*(1), 99–127.

Chaplin, M. (n.d.). *Polysaccharide hydration*. Retrieved March 16, 2017, from http://www1.lsbu.ac.uk/water/polysaccharide_hydration.html.

Collins, K. D. (2004). Ions from the Hofmeister series and osmolytes: Effects on proteins in solution and in the crystallization process. *Methods, 34*, 300–311.

Couillet, I., & Hughes, T. (2008). Aqueous fracturing fluid. US Patent 7,427,583B2, Retrieved: March 16, 2017.

Curtis, R. A., Steinbrecher, C., Heinemann, M., Blanch, H. W., & Prausnitz, J. M. (2002). Hydrophobic forces between protein molecules in aqueous solutions of concentrated electrolyte. *Biophysical Chemistry, 98*(3), 249–265.

De Andres-Santos, A. I., Velasco-Martin, A., Hernández-Velasco, E., Martín-Gil, J., & Martín-Gil, F. J. (1994). Thermal behaviour of aqueous solutions of sodium hyaluronate from different commercial sources. *Thermochimica Acta, 242*, 153–160.

Elsabee, M., & Prankerd, R. J. (1992). Solid-state properties of drugs. II: Peak shape analysis and deconvolution of overlapping endotherms in differential scanning calorimetry of chiral mixtures. *International Journal of Pharmaceutics, 86*, 211–219.

Escudier, M. P., Gouldson, I. W., Pereira, A. S., Pinho, F. T., & Poole, R. J. (2001). On the reproducibility of the rheology of shear-thinning liquids. *Journal of Non-Newtonian Fluid Mechanics, 97*, 99–124.

Escudier, M. P., Poole, R. J., Presti, F., Dales, C., Nouar, C., Desaubry, C., et al. (2005). Observations of asymmetrical flow behaviour in transitional pipe flow of yield-stress and other shear-thinning liquids. *Journal of Non-Newtonian Fluid Mechanics, 127*, 143–155.

Gandossi, L., & Von Estorff, U. (2015). *An overview of hydraulic fracturing and other formation stimulation technologies for shale gas production—Update 2015. JRC technical report*. EUR 26347.

García, C., Alfaro, C., Calero, N., & Muñoz, J. (2014). Influence of polysaccharides on the rheology and stabilization of α-pinene emulsions. *Carbohydrate Polymers, 105*, 177–183.

Gatej, I., Popa, M., & Rinaudo, M. (2005). Role of the pH on hyaluronan behavior in aqueous solution. *Biomacromolecules, 6*, 61–67.

Gibbs, D. A., Merrill, E. W., & Smith, K. A. (1968). Rheology of hyaluronic acid. *Biopolymers, 6*, 777–791.

Goel, N., Shah, S. N., & Grady, B. P. (2002). Correlating viscoelastic measurements of fracturing fluid to particles suspension and solids transport. *Journal of Petroleum Science and Engineering, 35*(1–2), 59–81.

Guan, L., Xu, H., & Huang, D. (2010). The investigation on states of water in different hydrophilic polymers by DSC and FTIR. *Journal of Polymer Research, 18*, 681–689.

Gura, E., Hückel, M., & Müller, P.-J. (2003). Specific degradation of hyaluronic acid and its rheological properties. *Polymer Degradation and Stability, 59*, 297–302.

Hall, B. E., Szemenyei, C. A., & Gupta, D. V. S. (1991). *Breaker system for aqueous fluids containing xanthan gums.*. Retrieved: March 16, 2017, from http://www.google.ch/patents/US5054552.

Hatakeyama, T., Naoi, S., & Hatakeyama, H. (2004). Liquid crystallization of glassy guar gum with water. *Thermochimica Acta, 416*, 121–127.

Hatakeyama, T., Tanaka, M., & Hatakeyama, H. (2010). Thermal properties of freezing bound water restrained by polysaccharides. *Journal of Biomaterials Science, Polymer Edition, 21*, 1865–1875.

Haward, S. J., Jaishankar, A., Oliveira, M. S. N., Alves, M. A., & McKinley, G. H. (2013). Extensional flow of hyaluronic acid solutions in an optimized microfluidic cross-slot device. *Biomicrofluidics, 7*(4).

Holloway, M. D., & Rudd, O. (2013). *Fracking: The operations and environmental consequences of hydraulic fracturing*. John Wiley & Sons.

Jain, K. N., & Roy, I. (2008). Effect of trehalose on protein structure. *Protein Science, 18*, 24–36.

Kawai, H., Sakurai, M., Inoue, Y., Chujo, R., & Kobayashi, S. (1992). Hydration of oligosaccharides: Anomalous hydration ability of trehalose. *Cryobiology, 29*, 599–606.

Kelly, R. M., Khan, S. A., Leduc, P., Tayal, A., & Prud'homme, R. K. (2001). *Methods and compositions for fracturing subterranean formations.*. Retrieved: March 16, 2017, from http://www.google.com/patents/US5421412.

Kupská, I., Lapcík, L., Lapcíková, B., Záková, K., & Juríková, J. (2014). The viscometric behaviour of sodium hyaluronate in aqueous and KCl solutions. *Colloids and Surfaces A: Physicochemical and Engineering Aspects, 454*, 32–37.

López-Arenas, L., Solís-Mendiola, S., Padilla-Zúñiga, J., & Hernández-Arana, A. (2006). Hofmeister effects in protein unfolding kinetics: Estimation of changes in surface area upon formation of the transition state. *Biochimica Et Biophysica Acta (BBA): Proteins and Proteomics, 1764*, 1260–1267.

Legemah, M., Qu, Q., Sun, H., Beall, B., & Zhou, J. (2013). Alternative polysaccharide fracturing fluids for harsh reservoir conditions. *Presented at the SPE unconventional resources conference and exhibition-Asia pacific, society of petroleum engineers*.

Lerbret, A., Bordat, P., Affouard, F., Guinet, Y., Hedoux, A., Paccou, L., et al. (2005). Influence of homologous disaccharides on the hydrogen-bond network of water: complementary Raman scattering experiments and molecular dynamics simulations. *Carbohydrate Research, 340*, 881–887.

Lertwimolnun, W., & Vergnes, B. (2006). Effect of processing conditions on the formation of polypropylene/organoclay nanocomposites in a twin screw extruder. *Polymer Engineering and Science, 46*, 314–323.

Li, L., Al-Muntasheri, G. A., & Liang, F. (2016). A review of crosslinked fracturing fluids prepared with produced water. *Petroleum, 2*(4), 313–323.

Lo Nostro, P., & Ninham, B. W. (2012). Hofmeister phenomena: An update on ion specificity in biology. *Chemical Reviews, 112*, 2286–2322.

Lo Nostro, P., & Ninham, B. W. (2016). Editorial: Electrolytes and specific ion effects. New and old horizons. *Current Opinion in Colloid & Interface Science, 23*, A1–A5.

Magazù, S., Migliardo, P., Musolino, A. M., & Sciortino, M. T. (1997). α,α-Trehalose-water solutions. 1. Hydration phenomena and anomalies in the acoustic properties. *Journal Physical Chemistry B, 101*, 2348–2351.

Maleki, A., Kjøniksen, A.-L., & Nyström, B. (2008). Effect of pH on the behavior of hyaluronic acid in dilute and semidilute aqueous solutions. *Macromolecular Symposia, 274*, 131–140.

Marcus, Y. (1991). Thermodynamics of solvation of ions. Part 5. Gibbs free energy of hydration at 298.15 K. *Journal of the Chemical Society, Faraday Transactions, 87*(18), 2995–2999.

Montgomery, C. (2013). Fracturing fluid components. In R. Jeffrey (Ed.), *Effective and sustainable hydraulic fracturing* (pp. 25–45). InTech.

Nakamura, K., Hatakeyama, T., & Hatakeyama, H. (1991). Formation of the liquid crystalline state in the water–sodium alginate system. *Sen'i Gakkaishi, 47*, 421–423.

Nandhini Venugopal, K., & Abhilash, M. (2010). Study of hydration kinetics and rheological behaviour of guar gum. *International Journal of Pharma Sciences and Research, 1*(1), 28–39.

Naoi, S., Hatakeyama, T., & Hatakeyama, H. (2002). Phase transition of locust bean gum-, tara gum- and guar gum-water systems. *Journal of Thermal Analysis and Calorimetry, 70*, 841–852.

Norton, I. T., Morris, E. R., & Rees, D. A. (1984). Lyotropic effects of simple anions on the conformation and interactions of kappa-carrageenan. *Carbohydrate Research, 134*, 89–101.

Osborn, S. G., Vengosh, A., Warner, N. R., & Jackson, R. B. (2011). Methane contamination of drinking water accompanying gas-well drilling and hydraulic fracturing. *Proceedings of the National Academy of Sciences, 108*(20), 8172–8176.

Osswald, T., & Rudolph, N. (2015). Polymer rheology. In *Understanding plastics rheology*. Hanser.

Picullell, L., & Nilsson, S. (1989). Anion-specific salt effects in aqueous agarose systems. 1. Effects on the coil-helix transition and gelation of agarose. *Journal of Physical Chemistry, 93*, 5596–5601.

Schnoor, E. A., Singh, D., & Russel, A. G. (2016). *Aldehydes as a catalyst for an oxidative breaker*. Retrieved: March 16, 2017, from http://www.google.it/patents/WO2016099502A1.

Schultheiss, N. C. (2015). *Multi-component materials for breaker activity control.*. Retrieved: March 16, 2017, from http://www.google.it/patents/WO2015020670A1.

Schwierz, N., Horinek, D., Sivan, U., & Netz, R. R. (2016). Reversed Hofmeister series—The rule rather than the exception. *Current Opinion in Colloid & Interface Science, 23*, 10–18.

Singh, T., Meena, R., & Kumar, A. (2009). Effect of sodium sulfate on the gelling behavior of agarose and water structure inside the gel networks. *Journal of Physical Chemistry B, 113*, 2519–2525.

Tatini, D., Tempesti, P., Ridi, F., Fratini, E., Bonini, M., & Baglioni, P. (2015). Pluronic/gelatin composites for controlled release of actives. *Colloids and Surfaces B: Biointerfaces, 135*, 400–407.

Vengosh, A., Jackson, R. B., Warner, N., Darrah, T. H., & Kondash, A. (2014). A critical review of the risks to water resources from unconventional shale gas development and hydraulic fracturing in the United States. *Environmental Science & Technology, 48*(15), 8334–8348.

Winkworth-Smith, C. G., MacNaughtan, W., & Foster, T. J. (2016). Polysaccharide structures and interactions in a lithium chloride/urea/water solvent. *Carbohydrate Polymers, 149*, 231–241.

Xu, Y., Wang, C., Tam, K. C., & Li, L. (2004). Salt-assisted and salt-duppressed sol–gel transitions of methylcellulose in water. *Langmuir, 20*, 646–652.

Yasuda, K., Armstrong, R. C., & Cohen, R. E. (1981). Shear flow properties of concentrated solutions of linear and star branched polystyrenes. *Rheologica Acta, 20*(2), 163–178.

Yin, W., Zhang, H., Huang, L., & Nishinari, K. (2008). Effects of the lyotropic series salts on the gelation of konjac glucomannan in aqueous solutions. *Carbohydrate Polymers, 74*, 68–78.

Supplementary Information.

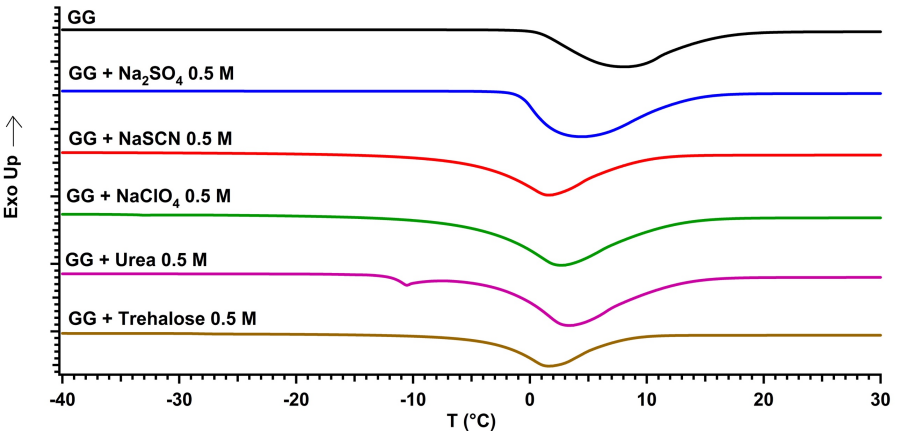

Figure S1 Stacked DSC heating curves of 1% aqueous dispersions of GG pure (black) and in the presence of 0.5 M solutions of Na_2SO_4 (blue), NaSCN (red), $NaClO_4$ (green), urea (magenta) and trehalose (brown).

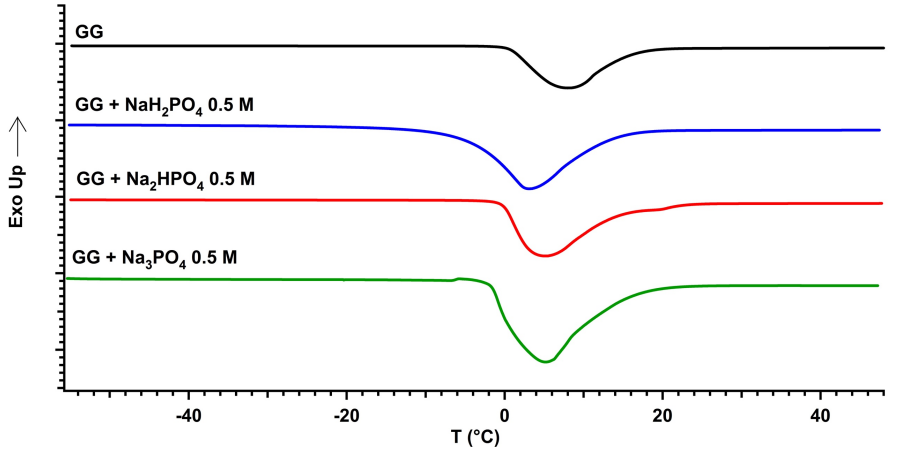

Figure S2. Stacked DSC heating curves of 1% aqueous dispersions of GG pure (black) and in the presence of 0.5 M

solutions of NaH_2PO_4 (blue), Na_2HPO_4 (red) and Na_3PO_4 (green)

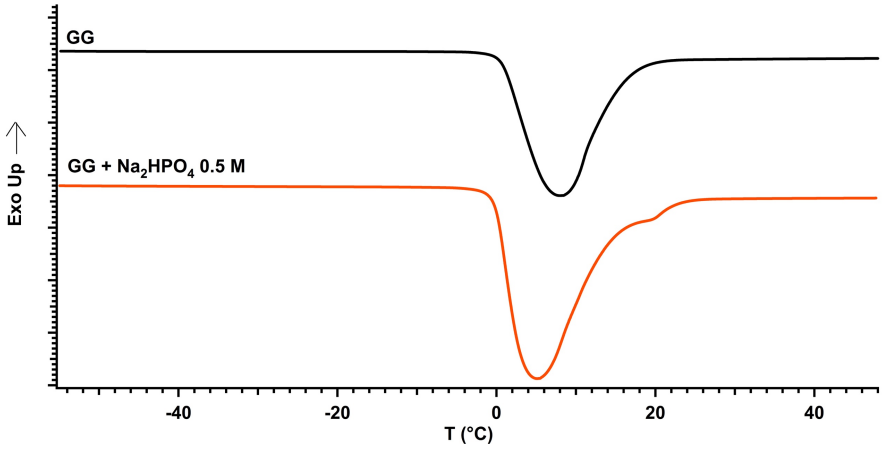

Figure S3. DSC curves of 1% aqueous dispersions of GG pure (black) and in the presence of 0.5 M NaH_2PO_4 (orange).

Table S1. Temperature and enthalpy change for the transition between the liquid crystalline and the isotropic liquid state in the presence of Na_2HPO_4 0.5 M for the three investigated polysaccharides.

polysaccharide	T_{ph} (°C)	ΔH_{ph} (J/g)
guar gum 1%	19.32	24.68
sodium alginate 1%	14.41	7.10
sodium hyaluronate 1%	19.02	67.14

Table S2. Dynamic viscosities (, in mPa · s) of aqueous salt solutions at concentration c (in molar units) and temperature T (in °C), Gibbs free energy of hydration ($\Delta G_{hydration}$, in kJ/mol) and molar surface tension increment (, in $N \cdot m^2/mol$) for the investigated anions.

salt	c	T	η	$\Delta G_{hydration}$[a]
none		25°	0.8902	
NaF	0.50	25°	0.992[b]	- 465
NaCl	0.50	25°	0.931[c]	- 340
NaBr	0.50	25°	0.917[b]	- 315
NaI	0.50	25°	0.904[b]	- 275
Na_2SO_4	0.49	25°	1.119[d]	- 1080
NaSCN	0.50	25°	0.916[c]	- 280
$NaClO_4$	0.50	25°	0.909[c]	- 205
NaH_2PO_4	0.52	20°	1.223[e]	- 465
Na_2HPO_4	0.41	20°	1.286[e]	
Na_3PO_4	0.50	20°	1.662[e]	- 2765
Trehalose	0.58	27°	1.90[f]	
Urea	0.54	25°	0.909[g]	

a: from Refs. 1 and 2; b: from Ref. 3; c: from Ref. 4; d: from Ref. 5; e: from Ref. 6; f: from Ref. 7; g: from Ref. 8.

References.

1. Marcus, Y. (1991). Thermodynamics of Solvation of Ions. Part 5. – Gibbs free energy of hydration at 298.15 K. Journal of the Chemical Society, Faraday Transactions; 87(18), 2995-2999.

2. Brown G. M. & Gu, B. (2006). The Chemistry of Perchlorate in the Environment. In Perchlorate: Environmental Occurrence, Interactions and Treatment; Eds.; Springer US: Boston, MA.

3. Goldsack, D. E., & Franchetto, R, (1977). The viscosity of concentrated electrolyte solutions. II. Temperature dependence, Canadian Journal of Chemistry, 55(6), 1062-1072.

4. Janz, G. J., Oliver, B. G., Lakshminarayanan, G. R., & Mayer, G. E. (1969). Electrical Conductance, Diffusion, Viscosity, and Density of Sodium Nitrate, Sodium Perchlorate, and Sodium Thiocyanate in Concentrated Aqueous Solutions, The Journal of Physical Chemistry, 74 (6), 1285.

5. Abdulagatov, I. M., Zeinalova, A., Azizov, N. D. (2005). Viscosity of aqueous Na_2SO_4 solutions at temperatures from 298 to 573 K and at pressures up to 40 MPa, Fluid Phase Equilibria, 227, 57–70.

6. Wolf, A. V. (1966). Aqueous Solutions and Body Fluids, Hoeber.

7. Galmarini, M. V., Baeza, R., Sanchez, V., Zamora, M. C., & Chirife, J. (2011). Comparison of the viscosity of trehalose and sucrose solutions at various temperatures: Effect of guar gum addition, LWT - Food Science and Technology, 44, 186 -190.

8. Hood, G. R. (1933). The Viscosity of Urea in Aqueous Solution, Physics, 4, 211.

Paper II

CARBON BLACK INDUCES ELECTRICAL RESPONSIVENESS IN GREEN BIOPOLYMERS AND VISCOELASTIC FORMULATIONS

Filippo Sarri[a], Duccio Tatini[a], Martina Raudino[a], Moira Ambrosi[a], Emiliano Carretti[a], Pierandrea Lo Nostro[a,b]*

a: Department of Chemistry "Ugo Schiff" & CSGI, University of Florence, 50019 Sesto Fiorentino (Firenze), Italy

b: Enzo Ferroni Foundation, 50019 Sesto Fiorentino (Firenze), Italy

* Email: pierandrea.lonostro@unifi.it

KEYWORDS: green frac fluid; carbon black; electrical responsiveness; rheology; smart device; viscoelastic.

ABSTRACT. In this work carbon black is added to green aqueous viscoelastic dispersions based on sodium oleate, or guar gum, sodium hyaluronate or hydroxypropyl cellulose gels, in order to obtain higher viscosities and conductivities, enhance the thermal properties and provide electrical responsiveness to the final formulations. Rheology, optical microscopy, SAXS and conductivity measurements are performed to test and compare the properties of carbon black-enriched samples to those of the original dispersions. The results indicate that even small amounts of carbon black lead to an enhanced stability against mechanical and thermal stresses, and imparts a significant electrical responsiveness to an external voltage. This work shows that the addition of carbon black to viscoelastic systems or to polysaccharide gels imparts interesting technological features that significantly expand the horizon of their potential applications, for example in situations where the remote control of their physico-chemical properties is necessary, not easily obtained with other systems, and does not require the addition of toxic or potentially dangerous chemicals.

ABSTRACT GRAPHIC

SYNOPSIS

Electrical responsiveness is imparted to green viscoelastic aqueous dispersions used as fracturing fluids by small amounts of carbon black.

INTRODUCTION

The use of carbon black (CB) as an additive in the manufacturing of plastic, rubber and various polymeric blends currently applies to many industrial areas.[1] This wide use is related to the peculiar properties that the carbon powder imparts to the rubber blend. For example, CB enriched tires show a longer lifetime, a lower thermal degradation and a higher resistance to abrasion and mechanical stresses.[2,3]

Another remarkable fraction of the annual CB production, close to 20%, is used in the rubber industry, where CB is added as a filler to improve mechanical, thermal and tensile properties of natural rubbers and elastomers.[4–6] The addition of carbon black in a rubber matrix deeply affects its mechanical properties and may impart viscoelastic behavior to natural rubber.[7] However, the rubber's mechanical responses can be further modified through an appropriate functionalization of the carbonaceous particles with, e.g., phenol, carboxyl or lactone functional groups as reported by Park.[8]

CB also finds a remarkable use in the polymer industry, especially in the production of polypropylene, polyvinyl chloride, polyester and polyethylene.[9–12] In fact, CB is able to capture the UV wavelengths that largely contribute to the polymer degradation.[13] The benefits of CB for plastics are not limited just to the UV shielding effect. The presence of carbonaceous particles grants the plastic matrix a greater electric conductivity and an increased resistance to thermal degradation, abrasion and tear.[14,15] Moreover, the addition of carbon black powder imparts viscoelastic properties to polymeric materials such as polystyrene.[16] Moreover, the addition of CB brings about another advantage, i.e. the reduction of polymeric materials with no significant modification of their mechanical properties.

More recently, CB has attracted some attention for the production of specifically designed nanocomposites. According to Bagavathi, CB can be combined to Fe_3O_4 and used in dye-sensitized solar cells (DSSC) as a better performing and low cost alternative material to conventional platinum counter electrodes.[17] Battista reports on the coupling of CB and $LiNbO_3$ crystals for the production of devices for the accumulation of solar power based on the pyroelectric effect.[18] The coupling of polyaniline and CB leads to the production of microwave absorbing materials,[19] while the combination of CB and a suitable polymer can lead to the production of a portable sensor for the detection of volatile organic compounds (VOCs), i.e. a portable electronic nose system.[20] Zhang et al. produced regenerated cellulose/graphene films through a green procedure.[21]

Although CB is mainly used in solids such as plastics and rubbers, its addition to liquid matrices is considerably increasing. This trend is related to the use of CB as pigment in paints and inks, particularly those for ink-jet printing.[22–25]

In normal field operations, the viscosity of frac fluids used for the extraction of shale gas must be high when the fluid is pumped downhole and must carry the proppant underground. Later on, typically after 6 hours after the injection, the viscosity needs to be remarkably lowered. This viscosity change is reached by using cross-linking agents, such as borates and Ti(IV), Zr(IV), and Al(III) chemicals.[26,27]

The demand for green alternatives, where the use of toxic and polluting controlled substances is avoided, the use of water[28] is at least limited and the presence of NORM (naturally occurring radioactive material) is strictly controlled, prompts several researchers to explore new innovative formulations. In this line we developed a system for changing the viscosity of the frac fluid through a physical trigger such as an electrical stimulus. In this paper we present the electroresponsive effect of relatively small amounts of carbon black added to different frac fluid formulations. The application of a moderately low voltage results in a prompt collapse of the gel structure and therefore in a significant drop of its viscosity. The process is reversible as the frac fluids can be recovered and recycled.

In this contribution we explore the potential use of carbon black in liquid systems such as polysaccharide or viscoelastic surfactants (VES) based green formulations for the control and improvement of their thermal properties, rheological behavior, conductivity and electrical responsiveness. The investigation was conducted through rheology, electrical conductivity, optical microscopy and small angle X-ray scattering (SAXS) experiments. The results suggest that CB improves the performances of such water-based dispersions without affecting the 3D ordered network and its rheological behavior. CB was added in small amounts, 3% and 10% w/w for polysaccharides and VES, respectively. Such contents are much lower than 20% w/w, the common amount of CB or of carbon nanotubes (CNT) that is necessary in order to modify the properties of most composites.[29] The formation of fluid systems that contain relatively moderate amounts of CB paves the way to new potential applications in so far unexplored fields, such as the formulation of fluids for hydraulic fracturation involved in the extraction of shale gas.

MATERIALS AND METHODS

Materials. Sodium oleate (NaOL, ACS grade) was purchased from Riedel-De Haën (Seelze, Germany). Carbon Black VULCAN® XC-72R was provided by Cabot Corporation (Boston, USA), KCl (≥ 99%) and saponin (≥ 99%) were purchased from Sigma-Aldrich (Milan, Italy), guar gum and hydroxypropyl cellulose (average molecular mass 2000 and 1600-1800 kDa, respectively) were supplied by Lamberti S.p.A. (Milan, Italy), and high molecular weight (1800 – 2000 kDa) sodium hyaluronate was purchased from Stanford Chemicals Company (Fairbanks, CA). All solutions and dispersions were prepared with Milli-Q water (resistivity > 18 MΩ·cm at 25 °C).

Polysaccharide Sample Preparation. 0.5% w/w water dispersions of guar gum (GG), hydroxypropyl cellulose (HPC) and sodium hyaluronate (SH) were prepared by slowly adding a weighted amount of the polysaccharide powder to MilliQ water under constant stirring at room temperature. In these conditions homogeneous dissolution occurs in about 30 minutes for all the investigated biopolymers.

VES Sample Preparation. 2% and 13% w/w VES samples were prepared by dissolving under magnetic stirring the proper amount of sodium oleate in MilliQ water or in a 0.5 M KCl aqueous solution.

Preparation of Samples Containing Carbon Black. Carbon black was added to the polysaccharide or to the VES samples following two different procedures: a) To effectively include CB in the polysaccharide matrices, a 2% w/w saponin solution was first prepared. This solution was added to a weighted amount of CB in order to obtain a final CB concentration of either 1% or 3% w/w and magnetically stirred for a few minutes. The mixture was sonicated for 1 hour at 40 kHz and the polysaccharide was added under magnetic stirring. b) In the case of the VES systems, no additive was necessary for the dispersion of CB, as sodium oleate itself is able to disperse the carbonaceous particulate. Hence, the VES solution was simply added to a weighted amount of CB (1, 3 or 10% w/w), then the mixture was sonicated for 30 minutes.

Optical Microscopy. Nikon Eclipse Ti-S Inverted Microscope was used to obtain optical images of CB dispersions in saponin and sodium oleate. All experiments were performed in automatic mode using an objective with a 10x magnification at room temperature. At least three different regions for each sample were analyzed in order to obtain a statistically meaningful result.

Flow Curves of Polysaccharide and VES Systems. Rheological measurements were performed by a Paar Physica UDS 200 rheometer working in the controlled shear-stress mode. For all samples a plate–plate geometry (diameter 4.0 cm; gap 300 μm) was used. In these operating conditions, the total amount of the sample in the cell was about 0.5 mL. Rheological measurements were performed at 25, 30, 40, 50 and 60 °C (Peltier control system). For each sample, the flow curve was acquired in a torque range between 10^{-3} and 2000 mN·m, after a 15 min soaking time to equilibrate at the set temperature.

Frequency Sweep on VES Formulations. Frequency sweep measurements were carried out within the linear viscoelastic range determined by means of an amplitude sweep test. The storage (G') and loss (G") moduli were measured over the frequency range of 0.001 to 100 Hz.

Conductivity Measurements. Conductivities of both polysaccharide and VES systems were measured through a sensION™+EC7 conductivity platinum cell (HACH, error $\leq$ 5% in the measuring range between 0.2 and $2 \cdot 10^5$ μS/cm). For each sample at least five measurements were performed and averaged.

Electrical Responsiveness. The electrical responsiveness of VES and polysaccharide-based systems was assessed by applying a 30 V voltage for 1 hour through a Hewlett Packard Harrison 6112 A DC power supply. Two platinum wires of 1.0 mm diameter (Sigma-Aldrich) were dipped into the dispersions and used as electrodes (See Figure 1).

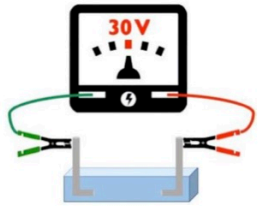

Figure 1. Schematic representation of the setup for the electrical treatment.

SAXS Experiments. SAXS experiments were carried out using a HECUS S3-Micro (Kratky camera) equipped with two position-sensitive detectors (PSD-50M) containing 1024 channels of 54-µm width. Cu Kα radiation of wavelength 1.542 Å was provided by a GeniX X-ray generator (Xenocs, Grenoble) working with a microfocus sealed-tube operating at 50 W. The sample to detector distance was 281 mm. The volume between the sample and the detector was kept under vacuum during the measurements to minimize scattering from the air. The Kratky camera was calibrated using silver behenate, which is known to have a well-defined lamellar structure (d = 58.38 Å)[30]. Scattering curves were monitored in a q-range from 0.02 to 0.55 $Å^{-1}$. Liquid samples were analyzed in a borosilicate glass capillary tube. For all measurements the temperature was kept constant at 25 °C controlled by a Peltier element, with an accuracy of ± 0.1 °C. All scattering curves were corrected for the empty capillary contribution considering the relative transmission factors. Desmearing of the SAXS curves was not necessary because of the sophisticated point microfocusing system.

RESULTS AND DISCUSSION

Dispersibility of carbon black. Optical micrographs of carbon black (CB) dispersions in saponin and sodium oleate (see Figure 2) were acquired to assess the dispersibility of CB as a function of the additive amount and in the presence of two dispersing agents (saponin or sodium oleate). Indeed, it was proved that the structure of carbon black, the nature of the polymer, and the processing history of the sample affect the electrical conductivity of the composite.[31,32]

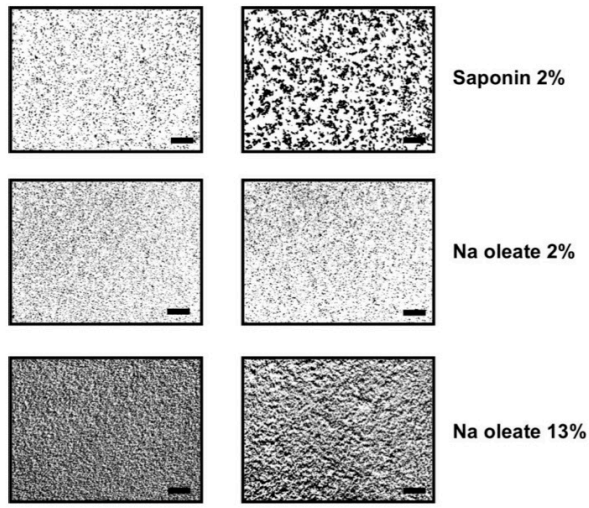

Figure 2. Optical images of carbon black 1% (left) and 3% w/w (right) dispersions in saponin 2% and sodium oleate 2% and 13% w/w. Scale bar: 300 μm.

Our results show that stable aqueous dispersions of CB with saponin or sodium oleate were obtained. Carbonaceous aggregates form when the amount of carbon black increases from 1% to 3% w/w. The carbonaceous particulate appears homogeneously dispersed also in the presence of the higher amount of CB. Therefore, any effect on the electro-responsiveness due to samples inhomogeneity can be disregarded.

This result is of particular interest for practical applications since several efforts were made in the past to find an easy way to disperse hydrophobic carbonaceous materials, such as fullerenes or carbon nanotubes in aqueous media, especially for biomedical applications.[33,34] Some works report the encapsulation of CB in silica[35,36] or polymer particles,[37] while others suggest the use of surfactant molecules, such as sodium oleate and saponin, that can provide both electrostatic and steric stabilization, depending on the nature of the hydrophilic head.[38,39]

In particular, saponin can adsorb by exposing its hydrophobic triterpene or steroid moiety to the CB surface, while the glucoside hydrophilic head faces the aqueous phase.[40] In the case of sodium oleate, we expect that its adsorption on the CB surface occurs through the C=C double bond in the chain, as suggested by Wang,[41] while the negatively charged carboxylate provides an electrostatic stabilizing effect.

Rheology behavior. Rheological flow curves were acquired on both pure and carbon black-enriched polysaccharides or VES formulations. The different rheological profiles (Figure 3) reflect the viscosity changes and network stiffening induced by CB. For the sake of brevity, we discuss the results obtained

for the samples showing the most significant changes, i.e. polysaccharides and VES formulations containing 3 and 10% of CB, respectively.

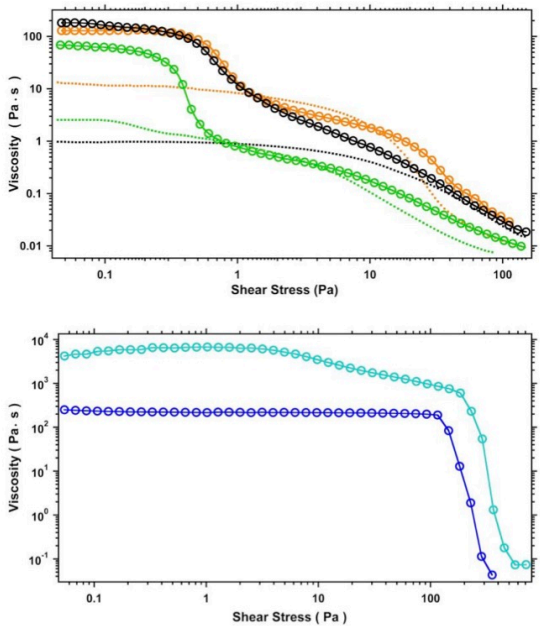

Figure 3. Top: Flow curves of 0.5% w/w pure (dotted lines) and containing 3% w/w of CB (empty circles) GG (green), HPC (black), and SH (orange) dispersions. Bottom: Flow curves of NaOL 13% + KCl 4% (dark blue) and NaOL 13% + KCl 4% + CB 10% (light blue).

The pure polysaccharide dispersions exhibit a non-Newtonian behavior with the zero stress viscosity ranging between 1 and 13 Pa·s moving from HPC to SH.[42] The addition of CB leads to an increase in the viscosity of at least an order of magnitude. This result is in line with the well known thickening effect of CB,[43] and reflects the effective inclusion of the additive in the polysaccharide matrices. Moreover, in the presence of CB the rheological profiles are significantly modified with respect to the pure polysaccharides. In fact, besides the Newtonian region with a high viscosity value at low shear rate, a marked change in the slope of the curves is observed, for shear stress ranging between 0.3 and 3 Pa, especially for GG and SH based samples. This behavior is probably related to the viscous drag between the polymer chains adsorbed on the CB particles and the bulk polymer, as described by Barrie in the study of the interaction between CB and an acrylic resin.[44]

Regarding the VES formulations (Figure 3), the pristine system NaOL 13% + KCl 4% shows the typical non-Newtonian behavior of ionic surfactants' aqueous dispersions: in particular, the sample displays a Newtonian plateau with a high viscosity value (η_0 = 230 Pa·s) followed by a shear-thinning region

above a critical stress (around 115 Pa) that reflects the different alignment of the self-assembled structures in the shear flow direction.[45,46] When CB is added to the VES system up to 10% w/w, we observed a strong increase in the zero-stress viscosity, from 230 to 5400 Pa·s, indicating that the carbonaceous particulate acts as a reinforcing agent for the network. Furthermore, we observed that the shear-thinning behavior starts at a higher value of the critical stress, suggesting a structuring effect for the CB particles. Despite the addition of CB strongly affects the stiffness of the VES network, the rheological profile with or without CB remains essentially unaltered. We argue that the structure of the NaOL micellar network is not significantly modified by the presence of the carbonaceous particles. In order to understand the effect of CB on the mechanical properties of NaOL dispersions and to obtain insights on their relaxation dynamics, oscillatory frequency sweep tests were carried out on VES systems before and after the addition of 10% of carbon black (see Figure 4).

At high frequency the samples behave as elastic systems (G' shows a plateau and dominates over G"), whereas at low frequency they show a viscous behavior (G" > G').

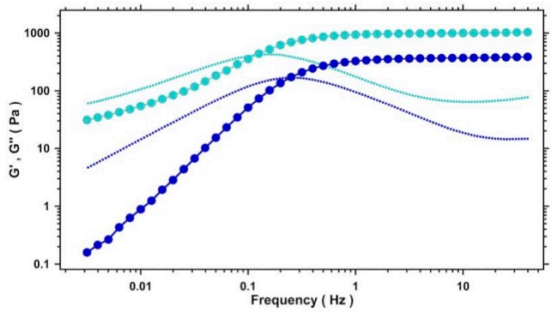

Figure 4. Storage (circles) and loss (dotted lines) moduli of pristine (dark blue) and 10% w/w CB-enriched (light blue) NaOL 13% + KCl 4% VES formulations. All the measurements were carried out in the linear viscoelastic regime (strain amplitude = 1.0 %).

At high frequency the samples behave as elastic systems (G' shows a plateau and dominates over G"), whereas at low frequency they show a viscous behavior (G" > G'). The dynamics of the studied systems cannot be described according to the single-element Maxwell model, hence G' and G" are used to calculate the time-weighted relaxation spectra H(τ) reported in Figure 5.[47] The CB-enriched VES formulation shows a higher relaxation time, confirming the reinforcing role of the particulate in the stabilization of the matrix. Moreover, considering that the numbers of interconnections in the self-assembled structure is directly related to the values of the elastic plateaus in the oscillatory frequency sweep tests (Figure 4),[48] we argue that carbon black leads to the formation of a more entangled network, as suggested by the higher value of the G' modulus associated to the CB-enriched sample.

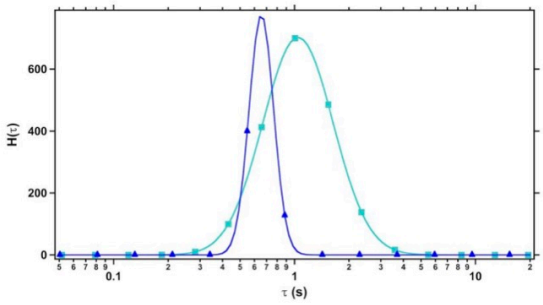

Figure 5. H(τ) relaxation spectra of pristine (dark blue) and CB-enriched (light blue) NaOL 13% + KCl 4% VES formulations.

A further confirmation of the negligible effect of CB on the micellar structure of NaOL arises from the SAXS data analysis (see Figure 6). The scattering curves of the samples before and after the addition of CB are similar, except for the strong contribution to the scattering intensity in the low q-region (q < 0.005 $Å^{-1}$) due to the CB particles. This result indicates that the addition of CB does not affect the size and the intermicellar interactions among the charged aggregates.

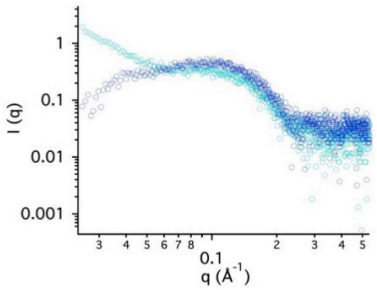

Figure 6. SAXS curves of VES formulations: NaOL 13 % + KCl 4 % (dark blue circles) and 10 % CB enriched samples (light blue circles).

According to the literature,[49,50] the observed scattering profile is associated to the presence of polydispersed core-shell elongated objects interacting via a screened Coulomb potential in solution.

Electrical treatment. The electroresponsivity of polymers is a widely known phenomenon that involves a large set of biomolecules.[51–53] The application of a voltage (30 V for 1 hour) to the formulations produces electrophoretic, polarization and osmotic effects, that result in the separation of a liquid and easy-flowing phase on one electrode, and of a viscous and sticky phase that concentrates at the

opposite side. Taking advantage of their different viscosities, the two phases can be easily separated by simply turning the vessel. The measured weight gives a rough estimation of the percentage of recovered liquid phase squeezed out from the sample after the electrostimulation (Table 1).

Table 1. Zero stress viscosities (η_0 ± 5%, in Pa·s) and mass percentage of liquid (L, %) and sticky (S, %) phases recovered after the application of a voltage (30 V for 1 hour).

Sample	η_0	L	η_0 (L)	S	η_0 (S)
GG	2.1	-	1.1	-	1.1
HPC	1.3	60	0.55	40	40
SH	13	52	0.15	48	43
NaOL 13% + KCl 4%	230	34	390	66	4.4
GG+CB 3%	67	-	22	-	22
HPC+CB 3%	120	50	20	50	$4.5 \cdot 10^3$
SH+CB 3%	130	30	63	70	$1 \cdot 10^3$
NaOL13% + KCl 4% + CB 10%	$5.4 \cdot 10^3$	-	$3.6 \cdot 10^5$	-	$3.6 \cdot 10^5$

All pure polysaccharide dispersions, except for guar gum, exhibit this behavior in response to the electrical treatment. Figure 7 shows the flow curves in the case of sodium hyaluronate. The electrical treatment effect on the flow curves for the GG and HPC dispersions are reported in the Supporting Information (Figure S1). By comparing the profiles of the pristine SH sample (black) and those of the "liquid" and "sticky" phases (red and green, respectively), we figured out that the rheological response is affected by the application of the voltage. Indeed, the red profile shows a two order of magnitude lower η_0, whereas the green curve shows a noticeable increase in η_0.

Despite this difference in the viscosity values, the three rheological profiles are similar. This suggests that all the samples possess the same structure and no modification in the polysaccharide network is induced by the electrical stimulation. Thus, we argue that the changes in viscosity are simply due to the electrically induced differences in the polysaccharide/water ratio. Indeed, the applied voltage leads to the contraction of both SH and HPC networks and results in the reduction of the mesh size and in the partial removal of water from the polysaccharidic network. As expected the amount of the liquid portion recovered at the end of the electrical stimulation depends on the nature of the polysaccharide (see Table 1).

The electrical treatment imparts an effect also on the NaOL-based formulations, leading to the formation of two phases with different flow curves (Figure 7). Both phases show lower profiles and the curve obtained from the sticky and more viscous portion is not shown. Moreover, unlike the case of polysaccharide formulations, the two collected phases exhibit a rheological profile significantly different from that of the sample before the treatment. This result suggests that the application of the voltage partially breaks the micellar entanglement and the homogeneity of the sample, leading to irregular and more indented profiles in comparison to the typical VES flow curve.

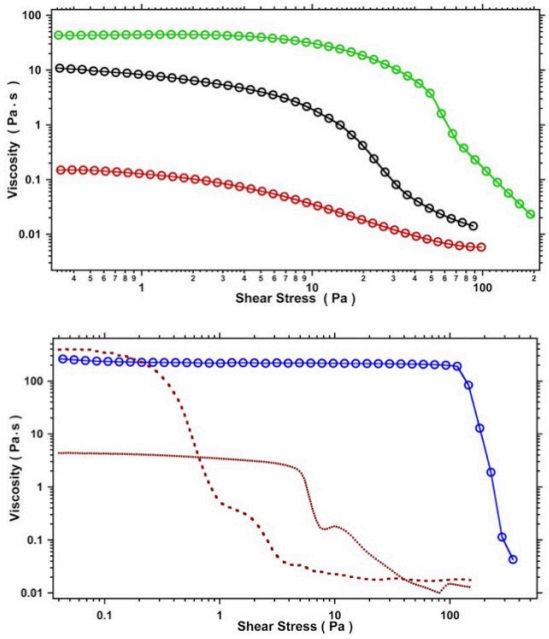

Figure 7. Top: Flow curves of 0.5% w/w SH dispersion before the application of the electrical treatment (black) and of the two phases separated at the end of the process (viscous phase in green, fluid phase in red). Bottom: Flow curves of NaOL 13% + KCl 4% VES formulation before the application of the electrical treatment (blue circles) and of the two phases separated at the end of the process (brown lines).

Considering that both pure VES and polysaccharides show a remarkable responsiveness upon the application of a voltage, their electro-responsiveness was checked after the addition of the conducting CB in different amounts: from 1 to 3% for the polysaccharides and up to a maximum of 10% for the VES formulation. As expected, the addition of CB powder leads to a remarkable increase in the conductivity for polysaccharide and VES systems, as resumed in Table S1 in the Supporting Information. This result could inspire the production of smart molecular devices with enhanced electroresponsiveness.

The flow curves of the two phases collected after the application of the electrical stimulation in the presence of CB are reported in Figure 8.

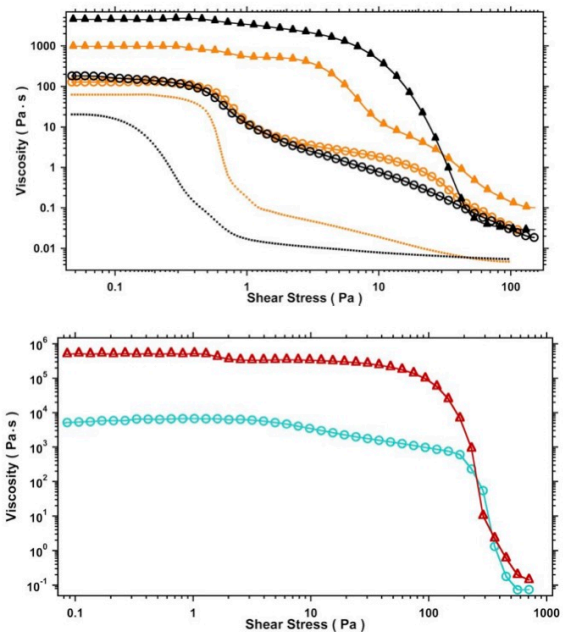

Figure 8. Top: Flow curves of 0.5% w/w HPC (black) and SH (orange) dispersion containing CB 3 wt% before the application of the electrical treatment (empty circles) and of the two phases separated at the end of the process (viscous, triangles and liquid, dotted lines). Bottom: Flow curves of sodium oleate 13% + KCl 4% VES formulation containing CB 10 % before the application of the electrical treatment (light blue circles) and at the end of the process (red triangles).

For the polysaccharide matrices, we recorded different responses to the electrical treatment depending on the nature of the investigated polysaccharide (Figure 8 top). However, in all cases with the exception of guar gum, the change in the zero-shear viscosities of the different phases after the treatment is enhanced compared to the pure polysaccharides. This result suggests that CB can be successfully used as an additive to tune the response of polysaccharide formulations to an external treatment, such as the application of a voltage.

When the CB-enriched VES formulation is electrically treated, the zero-stress viscosity of the formulation increases of about two orders of magnitude, indicating the formation of a more rigid network, probably due to the shrinking of the self-assembled network. However, as for the pristine formulation before the addition of CB, we did not observe the formation of two different phases, presumably because CB acts as a reinforcing agent. In addition, the rheological profile of the sample before and after the stimulation does not change significantly, showing the typical non-Newtonian behavior of the VES formulations. This result confirms the view that, in the presence of carbon black,

the application of a voltage can be used as a trigger to effectively increase the strength and stiffness of the matrix without changing the viscoelastic network of sodium oleate-based formulations.

Effect of temperature. To evaluate the increased thermal resistance of our formulations after the addition of carbon black, the flow curves were acquired at 25, 30, 40, 50, and 60 °C. For the sake of comparison, the measurements were performed on polysaccharide- and VES-based formulations both with and without CB powder.

Figure 9 shows the rheological behavior of GG dispersions before and after the addition of CB (3% w/w). As expected, the raise in temperature causes a downward shift in the polysaccharide flow curve, with a progressive lowering of the zero shear-viscosity value moving from 25 to 60 °C. More specifically, the viscosity of pristine polysaccharide system ranges between 2.2 and 0.34 Pa·s, while the GG+CB samples exhibit a wider and higher spectrum between 67 and 10 Pa·s. Thus, the presence of CB enhances the thermal resistance of the GG polysaccharide network with higher viscosity profiles in comparison to the pure GG sample. Moreover, the two systems exhibit quite different profiles in the lower stress region, while they flow in the same way. This feature seems to suggest that an additional structural order is granted by the carbonaceous particles, that are responsible for the higher viscosity in the GG+CB system. However, when the applied stress increases, this higher structuring breaks down and the difference is canceled out. Despite this effect, the flow curves remain unchanged within each series. Thus, the intermolecular interactions of the two systems are weakened as temperature raises, resulting in a softer network where the chains slide one over the other with a progressively lower friction. However, the similarities among the profiles in each polysaccharide set of curves confirm that the structures of the network are only weakened but not modified in different arrangements.

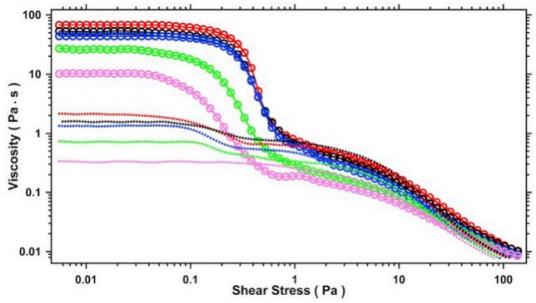

Figure 9. Flow curves of GG 0.5% (dotted lines) and GG 0.5% + CB 3% (circles) at 25 (red), 30 (black), 40 (blue), 50 (green) and 60 (pink) °C.

For SH and SH+CB we recorded a similar rheological behavior (Figure 10). Indeed, sodium hyaluronate exhibits the same trend observed for guar gum with a progressive lowering of the zero-stress plateau as temperature increases. The presence of CB does not modify this behavior but the response to the increase in temperature is enhanced. More in detail, the pristine SH system shows only a limited decrease in the viscosity, between 13 and 4.9 Pa·s, while the SH+CB sample shows a wider gap, from

129 to 1.7 Pa·s. In comparison to guar gum the addition of carbonaceous particles affects the SH network thermal resistance in a slightly different manner: the system is strengthened below 50 °C, while at higher temperatures the presence of CB seems to promote the chains disentanglement. As with guar gum, the CB-enriched system shows a double plateau and a double drop in its profile. Instead, the pure polysaccharide exhibits a single plateau associated to a single fall in viscosity. This difference reflects the second level structure, originating from the reinforcement of the polysaccharide network due to the CB particles, that is responsible for the overall increased rigidity and viscosity. Moving along the temperature series, we note the shift of the critical stress at which the higher viscosity plateau starts to decrease. The highly ordered structure loses its stability: in fact, passing from 25 to 50 °C, the gap between the first and the second plateau progressively becomes less pronounced, until it is barely visible in the profile recorded at 60 °C.

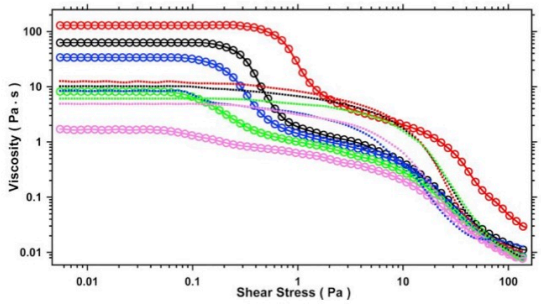

Figure 10. Flow curves of SH 0.5% (dotted lines) and SH 0.5% + CB 3% (circles) at 25 (red), 30 (black), 40 (blue), 50 (green) and 60 (pink) °C.

On the other hand, HPC 0.5 % shows an opposite trend, as reported in Figure 11. Both in the case of HPC and HPC+CB, the zero-shear viscosity increases with temperature, as the polysaccharide network becomes more viscous and rigid. Moreover, also the critical stress values corresponding to the collapse of the network are shifted to higher rates. This counterintuitive behavior does not represent an absolute novelty in the literature. Indeed, a similar case concerns another cellulosic derivative, the extracellular polysaccharide produced by some bacterial strains of Xanthomonas Campestris.[35,54] This biomolecule shows a viscosity trend that follows in parallel the temperature profile: the higher the temperature, the greater the zero stress viscosity of the system. In our case, this response to the thermal stress is presumably due to the partially hydrophobic nature of the HPC side-chain. When temperature is raised the hydrating water molecules are depleted from the hydroxypropyl side groups, and lead to the formation of ”stronger aggregation of interpolymer complexes” stabilized by hydrogen bonding and hydrophobic interactions.[55] The final result is an increase in the network crosslinking degree and a strengthening in the viscosity and stiffness of the system. A further increase of the temperature up to 120 °C leads to the gelation of HPC.

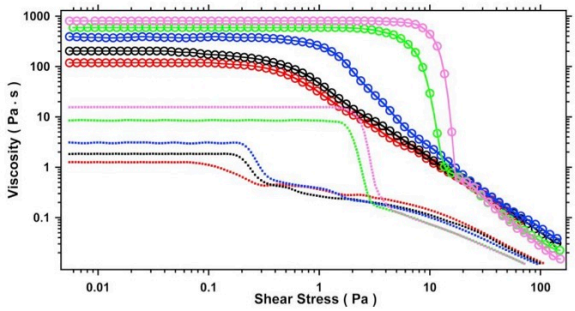

Figure 11. Flow curves of HPC 0.5% (dotted lines) and HPC 0.5% + CB 3% (circles) at 25 (red), 30 (black), 40 (blue), 50 (green) and 60 °C (pink).

In summary, the rheological profiles confirm that when CB is added to polysaccharide matrices, the result is an enhancement in the formulation resistance to the temperature increase, while the rheological trend of each polysaccharide remains unchanged.

Regarding the NaOL-based formulations, Figure 12 shows the flow curves acquired at the different temperatures on both systems before and after the addition of CB.

In the absence of CB, the temperature increase induces the breaking in the entangled micellar network with a rapid drop in the viscosity of the system. In the case of the CB-enriched formulations, the zero-shear viscosities are about two orders of magnitude higher, confirming the reinforcement of the network due the addition of CB.

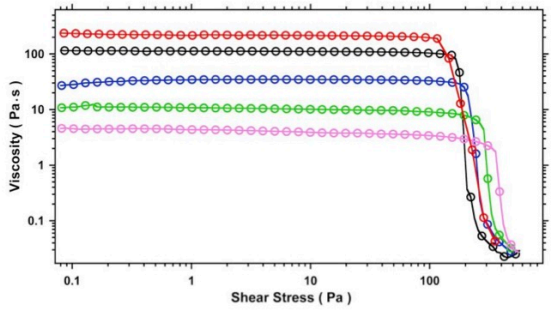

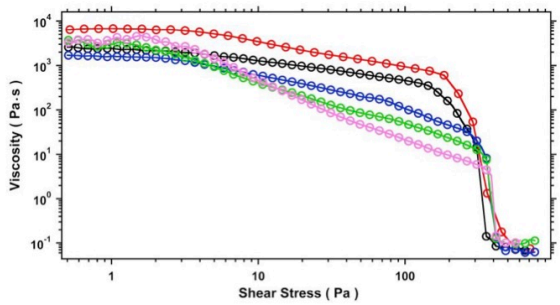

Figure 12. Top: Flow curves of NaOL 13% + KCl 4% acquired at 25 (red), 30 (black), 40 (blue), 50 (green) and 60 (pink) °C. Bottom: Flow curves of the same VES systems containing CB 10% w/w at different temperatures.

Furthermore, the rheological profile is quite different if compared to the pristine samples, with two different regions before the shear-thinning behavior. We argue that for low values of the shear stress both the assembled objects and the CB particles move together with the typical Newtonian behavior. When higher shear stresses are applied to the system, the viscous force between sodium oleate micelles and the carbonaceous particles arises, producing a second region where the system behaves as a shear-thinning material.[44]

It is worth noting that the system seems to have a more pronounced shear-thinning behavior as the temperature increases, as suggested by the value of critical stress that corresponds to the onset of the second region. For shear stresses higher than 100 Pa, the rapid drop of viscosity is similar to that observed for the pristine samples without CB, indicating the total break of the entangled micellar network even in the presence of the reinforcing agent.

The low-stress plateau region can be investigated at different temperatures in terms of an activated mechanism that can be interpreted accordingly to a modified Arrhenius equation (see Table S2 and Figure S2 in the Supporting Information).[56] The extracted Gibbs free energy of activation ($\Delta G^{\neq}$) for the pure VES formulation (91.5 ± 5.1) kJ·mol^{-1}, reflecting a tight entanglement of the chains that hinders the flow. The obtained value is in line with those reported in the literature.[57,58] In the presence of the carbonaceous additive, the VES system exhibits a different response to the temperature raise. Indeed, the viscosity decreases in the range between 25 and 40 °C, as observed in the case of pure VES, whereas it shows a higher plateau when the temperature is further increased up to 50 and 60 °C. Thus, in this case $\Delta G^{\neq}$ cannot be estimated with an Arrhenius plot.

For the polysaccharide systems the results are listed in the Supporting Information (Table S3 and Figures S3 and S4). In the case of pure aqueous dispersions of SH and GG, we obtained values for $\Delta G^{\neq}$ of (20.8 ± 1.1) and (38.8 ± 5.1) kJ·mol^{-1}, respectively. The calculated $\Delta G^{\neq}$ values of the two polysaccharide dispersions fall in the range reported in literature for polymers.[59] A similar analysis cannot be extended to HPC because of the temperature-induced gelation process. As we already

noted, when CB is added to the polysaccharide systems, we observed different responses to a temperature increment. In the case of GG (a neutral polymer), we calculated almost the same $\Delta G^{\neq}$ value obtained before the addition of CB, (38.9 ± 7.3) kJ·mol^{-1}. Instead in the case of the anionic SH, the addition of CB induces a significant change in $\Delta G^{\neq}$, that increases up to (92.4 ± 9.6) kJ·mol^{-1}.

The CB-polymer intermolecular interactions are usually interpreted in terms of a tunneling effect,[60] a percolation phenomenon[61] or through a combination of the two models.[62,63] Both models assume a close contact between the chains and the CB particles. Probably, the different charge on the polysaccharide chains is the key factor that affects the CB-polymer interaction mechanism and how the system answers in response to the application of various stimuli. Anyway, the obtained results seem to indicate a complex behavior of the mixed CB-polysaccharide systems and further experiments are needed in order to describe the different mechanisms of interactions.

CONCLUSIONS

In conclusion, carbon black (CB) was added and dispersed uniformly in different green aqueous polysaccharide or viscoelastic (VES) dispersions stabilized by saponin and sodium oleate. The rheological, thermal and electrical properties of the samples showed significant changes upon the addition of CB. In particular, carbon black brings about a greater viscosity and a larger threshold of the network collapse, an improvement in the thermal properties, and imparts a remarkable electrical responsiveness to an external voltage. Moreover, all these improved performances are achieved at a quite low CB content (3% for the polysaccharide dispersions and 10% for the VES formulations), much lower than the common amounts needed to obtaining significant results.[29]

Most composite systems that contain CB as a filler possess a solid matrix which implies that the system is rigid and arrested and the components are in direct contact, without the mediation of a medium. Steric, electrostatic, excluded volume, hydrogen bonding interactions rule over the thermal, mechanical and rheological behavior of such systems. These solid systems are usually well described in terms of the tunneling and percolation models.

In our case the presence of a dispersing continuous phase (aqueous solutions) totally changes the scenario as the dispersed ingredients diffuse through the medium. This participates in the intermolecular interactions that involve the single components, for example through solvation, hydrophobic effects, depletion forces, etc. A very preliminary and rough speculation may favor the percolative model over the tunneling effect. In fact, the presence of a dispersing agent (i.e. sodium oleate or saponin) may increase the CB-polymer distance and deplete the short range interactions that are required in the tunneling effect. Definitely further experiments are needed to investigate this topic more thoroughly.

The addition of carbon black to viscoelastic or polysaccharide aqueous formulations can significantly widen the horizon of their potential applications, for example in situations where the remote control

of the physico-chemical properties of a water-based gel is necessary and not easily obtained with other systems.

ASSOCIATED CONTENT

Supporting Information

The conductivity of VES and polysaccharide systems, with and without CB (Table S1); the flow curves of pure GG and HPC before and after the electrical treatment (Figure S1); Arrhenius plot of polysaccharide and VES systems (Tables S2 and S3, Figures S2, S3 and S4). The following file is available free of charge: Electro-resp_ESI.pdf

AUTHOR INFORMATION

Corresponding Author

* Phone: +39 055 457-3010. Email: pierandrea.lonostro@unifi.it

Author Contributions

The manuscript was written through contributions of all authors. All authors have given approval to the final version of the manuscript.

ACKNOWLEDGMENT

The authors acknowledge funding from the European Union Horizon 2020 research and innovation program “Shale for Environment” (SXT) under grant agreement Nr. 640979.

ABBREVIATIONS

CB, carbon black; VES, viscoelastic; NaOL, sodium oleate; GG, guar gum; HPC, hydroxypropyl cellulose; SH, sodium hyaluronate; SAXS, small angle X-ray scattering.

REFERENCES

(1) Speight, J. G. Handbook of Petroleum Product Analysis, 2nd Edition; Wiley, 2015.

(2) Semaan, M. E.; Quartes, C. A.; Nikiel, L. Carbon Black and Silica as Reinforcers of Rubber Polymers: Doppler Broadening Spectroscopy Results. Polymer Degradation and Stability 2002, 75 (2), 259–266.

(3) Choi, S.-S.; Kim, J.-C. Lifetime Prediction and Thermal Aging Behaviors of SBR and NBR Composites Using Crosslink Density Changes. Journal of Industrial and Engineering Chemistry 2012, 18 (3), 1166–1170.

(4) Barrera, C. S.; Cornish, K. High Performance Waste-Derived Filler/Carbon Black Reinforced Guayule Natural Rubber Composites. Industrial Crops and Products 2016, 86, 132–142.

(5) Rattanasom, N.; Saowapark, T.; Deeprasertkul, C. Reinforcement of Natural Rubber with Silica/Carbon Black Hybrid Filler. Polymer Testing 2007, 26 (3), 369–377.

(6) Harwood, J. A. C.; Payne, A. R. Stress Softening in Natural Rubber Vulcanizates. Part III. Carbon Black-filled Vulcanizates. Journal of Applied Polymer Science 1966, 10 (2), 315–324.

(7) Tunnicliffe, L. B.; Kadlcak, J.; Morris, M. D.; Shi, Y.; Thomas, A. G.; Busfield, J. J. C. Flocculation and Viscoelastic Behaviour in Carbon Black-Filled Natural Rubber. Macromolecular Materials and Engineering 2014, 299 (12), 1474–1483.

(8) Park, S.-J.; Cho, K.-S.; Ryu, S.-K. Filler–elastomer Interactions: Influence of Oxygen Plasma Treatment on Surface and Mechanical Properties of Carbon Black/Rubber Composites. Carbon 2003, 41 (7), 1437–1442.

(9) Liu, M.; Horrocks, A. R. Effect of Carbon Black on UV Stability of LLDPE Films under Artificial Weathering Conditions. Polymer Degradation and Stability 2002, 75 (3), 485–499.

(10) Zhao, J.; Dai, K.; Liu, C.; Zheng, G.; Wang, B.; Liu, C.; Chen, J.; Shen, C. A Comparison between Strain Sensing Behaviors of Carbon Black/Polypropylene and Carbon Nanotubes/Polypropylene Electrically Conductive Composites. Composites Part A: Applied Science and Manufacturing 2013, 48, 129–136.

(11) Wypych, G. PVC Degradation & Stabilization; 2015.

(12) Harrison, D. A.; Davis, P. J. Carbon Black Reheat Additive for Polyester and Polypropylene. WO/2006/052572, November 1, 2005.

(13) Horrocks, A. R.; Mwila, J.; Miraftab, M.; Liu, M.; Chohan, S. S. The Influence of Carbon Black on Properties of Orientated Polypropylene 2. Thermal and Photodegradation. Polymer Degradation and Stability 1999, 65 (1), 25–36.

(14) Katz, H. S.; Mileski, J. V. Handbook Of Fillers For Plastics; Springer Science & Business Media, 1987.

(15) Hayeemasae, N.; Ismail, H.; Khoon, T. B.; Husseinsyah, S.; Harahap, H. Effect of Carbon Black on the Properties of Polypropylene/ Recycled Natural Rubber Glove Blends. Progress in Rubber, Plastics and Recycling Technology 2015, 32 (4), 241–252.

(16) Cao, Q.; Song, Y.; Tan, Y.; Zheng, Q. Conductive and Viscoelastic Behaviors of Carbon Black Filled Polystyrene during Annealing. Carbon 2010, 48 (15), 4268–4275.

(17) Bagavathi, M.; Ramar, A.; Saraswathi, R. Fe3O4–carbon Black Nanocomposite as a Highly Efficient Counter Electrode Material for Dye-Sensitized Solar Cell. Ceramics International 2016, 42 (11), 13190–13198.

(18) Battista, L.; Mecozzi, L.; Coppola, S.; Vespini, V.; Grilli, S.; Ferraro, P. Graphene and Carbon Black Nano-Composite Polymer Absorbers for a Pyro-Electric Solar Energy Harvesting Device Based on LiNbO3 Crystals. Applied Energy 2014, 136, 357–362.

(19) Wu, K. H.; Ting, T. H.; Wang, G. P.; Ho, W. D.; Shih, C. C. Effect of Carbon Black Content on

Electrical and Microwave Absorbing Properties of Polyaniline/Carbon Black Nanocomposites. Polymer Degradation and Stability 2008, 93 (2), 483–488.

(20) Kim, Y. S.; Ha, S.-C.; Yang, Y.; Kim, Y. J.; Cho, S. M.; Yang, H.; Kim, Y. T. Portable Electronic Nose System Based on the Carbon Black–polymer Composite Sensor Array. Sensors and Actuators B: Chemical 2005, 108 (1), 285–291.

(21) Zhang, T.; Zhang, X.; Chen, Y.; Duan, Y.; Zhang, J. Green Fabrication of Regenerated Cellulose/Graphene Films with Simultaneous Improvement of Strength and Toughness by Tailoring the Nanofiber Diameter. ACS Sustainable Chem. Eng. 2018, 6 (1), 1271–1278.

(22) Donnet, J.-B. Carbon Black: Science and Technology, Second Edition; CRC Press, 1993.

(23) Belmont, J. A.; Johnson, J. E.; Adams, C. E. Ink Jet Ink Formulations Containing Modified Carbon Products. 5630868, March 20, 1997.

(24) Kordás, K.; Mustonen, T.; Tóth, G.; Jantunen, H.; Lajunen, M.; Soldano, C.; Talapatra, S.; Kar, S.; Vajtai, R.; Ajayan, P. M. Inkjet Printing of Electrically Conductive Patterns of Carbon Nanotubes. Small 2006, 2 (8–9), 1021–1025.

(25) Coppola, S.; Mecozzi, L.; Vespini, V.; Battista, L.; Grilli, S.; Nenna, G.; Loffredo, F.; Villani, F.; Minarini, C.; Ferraro, P. Nanocomposite Polymer Carbon-Black Coating for Triggering Pyro-Electrohydrodynamic Inkjet Printing. Appl. Phys. Lett. 2015, 106 (26), 261603.

(26) Li, L.; Al-Muntasheri, G. A.; Liang, F. A Review of Crosslinked Fracturing Fluids Prepared with Produced Water. Petroleum 2016, 2 (4), 313–323.

(27) Barati, R.; Liang, J.-T. A Review of Fracturing Fluid Systems Used for Hydraulic Fracturing of Oil and Gas Wells. Journal of Applied Polymer Science 2014, 131 (16).

(28) Lin, W.; Bergquist, A. M.; Mohanty, K.; Werth, C. J. Environmental Impacts of Replacing Slickwater with Low/No-Water Fracturing Fluids for Shale Gas Recovery. ACS Sustainable Chem. Eng. 2018, 6 (6), 7515–7524.

(29) Lopez Manchado, M. A.; Valentini, L.; Biagiotti, J.; Kenny, J. M. Thermal and Mechanical Properties of Single-Walled Carbon Nanotubes–polypropylene Composites Prepared by Melt Processing. Carbon 2005, 43 (7), 1499–1505.

(30) Blanton, T. N.; Huang, T. C.; Toraya, H.; Hubbard, C. R.; Robie, S. B.; Louër, D.; Göbel, H. E.; Will, G.; Gilles, R.; Raftery, T. JCPDS—International Centre for Diffraction Data Round Robin Study of Silver Behenate. A Possible Low-Angle X-Ray Diffraction Calibration Standard. Powder Diffraction 1995, 10 (2), 91–95.

(31) Huang, J.-C. Carbon Black Filled Conducting Polymers and Polymer Blends. Adv. Polym. Technol. 2002, 21 (4), 299–313.

(32) Bigg, D. M. An Investigation of the Effect of Carbon Black Structure, Polymer Morphology, and

Processing History on the Electrical Conductivity of Carbon-Black-Filled Thermoplastics. Journal of Rheology 1984, 28 (5), 501–516.

(33) Liang, F.; Chen, B. A Review on Biomedical Applications of Single-Walled Carbon Nanotubes. Curr. Med. Chem. 2010, 17 (1), 10–24.

(34) Medicinal Chemistry and Pharmacological Potential of Fullerenes and Carbon Nanotubes; Cataldo, F., Ros, T. da, Eds.; Carbon Materials: Chemistry and Physics; Springer Netherlands, 2008.

(35) Morris, E. R.; Rees, D. A.; Young, G.; Walkinshaw, M. D.; Darke, A. Order-Disorder Transition for a Bacterial Polysaccharide in Solution. A Role for Polysaccharide Conformation in Recognition between Xanthomonas Pathogen and Its Plant Host. Journal of Molecular Biology 1977, 110 (1), 1–16.

(36) Tiarks, F.; Landfester, K.; Antonietti, M. Silica Nanoparticles as Surfactants and Fillers for Latexes Made by Miniemulsion Polymerization. Langmuir 2001, 17 (19), 5775–5780.

(37) Tiarks, F.; Landfester, K.; Antonietti, M. Encapsulation of Carbon Black by Miniemulsion Polymerization. Macromol. Chem. Phys. 2001, 202 (1), 51–60.

(38) Sis, H.; Birinci, M. Effect of Nonionic and Ionic Surfactants on Zeta Potential and Dispersion Properties of Carbon Black Powders. Colloids and Surfaces A: Physicochemical and Engineering Aspects 2009, 1–3 (341), 60–67.

(39) Das, D.; Panigrahi, S.; Senapati, P. K.; Misra, P. K. Effect of Organized Assemblies. Part 5: Study on the Rheology and Stabilization of a Concentrated Coal–Water Slurry Using Saponin of the Acacia Concinna Plant. Energy Fuels 2009, 23 (6), 3217–3226.

(40) Das, D.; Panigrahi, S.; Misra, P. K.; Nayak, A. Effect of Organized Assemblies. Part 4. Formulation of Highly Concentrated Coal–Water Slurry Using a Natural Surfactant. Energy Fuels 2008, 22 (3), 1865–1872.

(41) Wang, W.; Efrima, S.; Regev, O. Directing Oleate Stabilized Nanosized Silver Colloids into Organic Phases. Langmuir 1998, 14 (3), 602–610.

(42) Tatini, D.; Sarri, F.; Maltoni, P.; Ambrosi, M.; Carretti, E.; Ninham, B. W.; Lo Nostro, P. Specific Ion Effects in Polysaccharide Dispersions. Carbohydrate Polymers 2017, 173, 344–352.

(43) Yang, S.-Y.; Ling, W.-N.; Huang, Y.-L.; Tien, H.-W.; Wang, J.-Y.; Ma, C.-C. M.; Li, S.-M.; Wang, Y.-S. Synergetic Effects of Graphene Platelets and Carbon Nanotubes on the Mechanical and Thermal Properties of Epoxy Composites. Carbon 2011, 49 (3), 793–803.

(44) Barrie, C. L.; Griffiths, P. C.; Abbott, R. J.; Grillo, I.; Kudryashov, E.; Smyth, C. Rheology of Aqueous Carbon Black Dispersions. J Colloid Interface Sci 2004, 272 (1), 210–217.

(45) Kalur, G. C.; Raghavan, S. R. Anionic Wormlike Micellar Fluids That Display Cloud Points: Rheology and Phase Behavior. J. Phys. Chem. B 2005, 109 (18), 8599–8604.

(46) Förster, S.; Konrad, M.; Lindner, P. Shear Thinning and Orientational Ordering of Wormlike Micelles. Phys. Rev. Lett. 2005, 94 (1), 017803.

(47) Carretti, E.; Matarrese, C.; Fratini, E.; Baglioni, P.; Dei, L. Physicochemical Characterization of Partially Hydrolyzed Poly(Vinyl Acetate)–borate Aqueous Dispersions. Soft Matter 2014, 10 (25), 4443–4450.

(48) Schubert, B. A.; Kaler, E. W.; Wagner, N. J. The Microstructure and Rheology of Mixed Cationic/Anionic Wormlike Micelles - Langmuir (ACS Publications). Langmuir 2003, 19 (10), 4079–4089.

(49) Flood, C.; Dreiss, C. A.; Croce, V.; Cosgrove, T.; Karlsson, G. Wormlike Micelles Mediated by Polyelectrolyte. Langmuir 2005, 21 (17), 7646–7652.

(50) Dreiss, C. A. Wormlike Micelles: Where Do We Stand? Recent Developments, Linear Rheology and Scattering Techniques. Soft Matter 2007, 3 (8), 956–970.

(51) Nasri-Nasrabadi, B.; Kaynak, A.; Nia, Z. K.; Li, J.; Zolfagharian, A.; Adams, S.; Kouzani, A. Z. An Electroactive Polymer Composite with Reinforced Bending Strength, Based on Tubular Micro Carbonized-Cellulose. Chemical Engineering Journal 2015, 334, 1775–1780.

(52) Alvarez-Lorenzo, C.; Blanco-Fernandez, B.; Puga, A. M.; Concheiro, A. Crosslinked Ionic Polysaccharides for Stimuli-Sensitive Drug Delivery. Advanced Drug Delivery Reviews 2013, 65 (9), 1148–1171.

(53) Kennedy, S.; Bencherif, S.; Norton, D.; Weinstock, L.; Mehta, M.; Mooney, D. Rapid and Extensive Collapse from Electrically Responsive Macroporous Hydrogels. Advanced Healthcare Materials 2014, 3 (4), 500–507.

(54) Holzwarth, G. Conformation of the Extracellular Polysaccharide of Xanthomonas Campestris. Biochemistry 1976, 15 (19), 4333–4339.

(55) Filip, D.; Macocinschi, D.; Paslaru, E.; Munteanu, B. S.; Dumitriu, R. P.; Lungu, M.; Vasile, C. Polyurethane Biocompatible Silver Bionanocomposites for Biomedical Applications. J Nanopart Res 2014, 16 (11), 2710.

(56) Chandler, H. D. Activation Energy and Entropy for Viscosity of Wormlike Micelle Solutions. J Colloid Interface Sci 2013, 409, 98–103.

(57) Kuryashov, D. A.; Philippova, O. E.; Molchanov, V. S.; Bashkirtseva, N. Y.; Diyarov, I. N. Temperature Effect on the Viscoelastic Properties of Solutions of Cylindrical Mixed Micelles of Zwitterionic and Anionic Surfactants. Colloid J 2010, 72 (2), 230–235.

(58) Angelescu, D.; Khan, A.; Caldararu, H. Viscoelastic Properties of Sodium Dodecyl Sulfate with Aluminum Salt in Aqueous Solution. Langmuir 2003, 19 (22), 9155–9161.

(59) Desbrieres, J. Viscosity of Semiflexible Chitosan Solutions: Influence of Concentration, Temperature, and Role of Intermolecular Interactions. Biomacromolecules 2002, 3 (2), 342–349.

(60) Sichel, E. K.; Gittleman, J. I.; Sheng, P. Transport Properties of the Composite Material Carbon-Poly(Vinyl Chloride). Phys. Rev. B 1978, 18 (10), 5712–5716.

(61) Reboul, J.-P.; Moussalli, G. About Some D-C Conduction Processes in Carbon Black Filled Polymers. International Journal of Polymeric Materials and Polymeric Biomaterials 1976, 5 (1–2), 133–146.

(62) Balberg, I. A Comprehensive Picture of the Electrical Phenomena in Carbon Black–polymer Composites. Carbon 2002, 40 (2), 139–143.

(63) Carmona, F.; Mouney, C. Temperature-Dependent Resistivity and Conduction Mechanism in Carbon Particle-Filled Polymers. J Mater Sci 1992, 27 (5), 1322–1326.

Supporting Information

CARBON BLACK INDUCES ELECTRICAL RESPONSIVENESS IN GREEN BIOPOLYMERS AND VISCOELASTIC FORMULATIONS

*Filippo Sarri[a], Duccio Tatini[a], Martina Raudino[a], Moira Ambrosi[a], Emiliano Carretti[a], Pierandrea Lo Nostro[a,b]**

a: Department of Chemistry "Ugo Schiff" & CSGI, University of Florence, 50019 Sesto Fiorentino (Firenze), Italy

b: Enzo Ferroni Foundation, 50019 Sesto Fiorentino (Firenze), Italy

* Email: pierandrea.lonostro@unifi.it

SUPPORTING INFORMATION

Conductivity Data

Table S1. Conductivity measurements (κ, μS·cm) on polysaccharide and VES formulations, both with and without the addition of carbon black.

	κ ± Std. Dev.	
	no CB	with CB
GG 0.5 %	75.6 ± 1.6	2964 ± 16[a]
SH 0.5 %	928 ± 6.6	2965 ± 16[a]
HPC 0.5 %	124.9 ± 1.4	2440 ± 28[a]
NaOL 13 % + KCl 4%		5944 ± 234[b]

a: 3% w/w CB; b: 10% w/w CB .

Flow Curves of Electrically Stimulated Polysaccharides

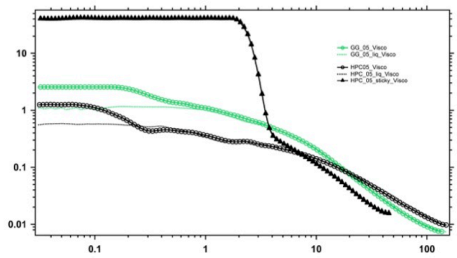

Figure S1. Flow curves acquired on HPC (black) and GG (green), before and after the electrical stimulation. The responses of the polysaccharide systems before the stimulation are represented by circles, the liquid and sticky parts obtained after the application of a voltage are indicated by dotted lines and triangles, respectively. The application of the voltage leads to a separation in two rheological profiles for HPC, as in the case of SH. Instead, GG shows an overall reduction of its viscosity profile only, without any phase separation.

Arrhenius plots

The initial plateau region at low stress, characteristic of the Newtonian behaviour of worm-like micelles, can be analysed as a function of temperature according to the modified Arrhenius equation, as proposed by Chandler,[1,2] to obtain the Gibbs free energy of activation representing the strength of flow objects in solution:

$$\eta_N = \eta_{\infty N} exp\left(\frac{\Delta G_N}{RT}\right)$$

plotting $\ln(\eta_N)$ versus $1/T$ we obtain ΔG_N from the slope and $\ln(\eta_{\infty N})$ from the intercept, respectively.

Table S2. Zero-stress viscosity values η_0 (in Pa·s) measured for the NaOL 13 % + KCl 4 % green formulation at two different concentrations of CB as a function of temperature (T, in ° C).

T	η_0	
	no CB	10% w/w CB
25°	230	6740
30°	150	2420
40°	36	1627
50°	11	2985
60°	4.1	3914

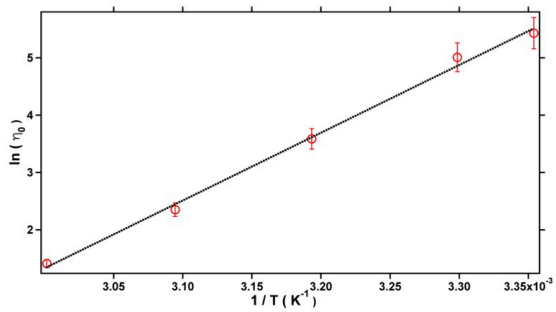

Figure S2. Arrhenius plot for the CB-free NaOL 13 % + KCl 4 % sample. The linear regression gives $\Delta G_N = 91.5 \pm 5.1$ kJ·mol^{-1}.

Table S3. Zero-stress viscosity values η_0 (in Pa·s) measured for polysaccharide green fluids at two different concentrations of CB as a function of temperature (T, in °C). GG: guar gum, SH: sodium hyaluronate and HPC: hydroxypropyl cellulose.

	η_0					
T	GG		SH		HPC	
	no CB	3% CB	no CB	3% CB	no CB	3% CB
25°	2.2	67	13	129	1.3	118
30°	1.6	53	10	67	1.9	203
40°	1.3	44	8.4	34	3.1	390
50°	0.73	26	6.1	8.1	8.4	594
60°	0.34	10	4.9	1.7	16	805

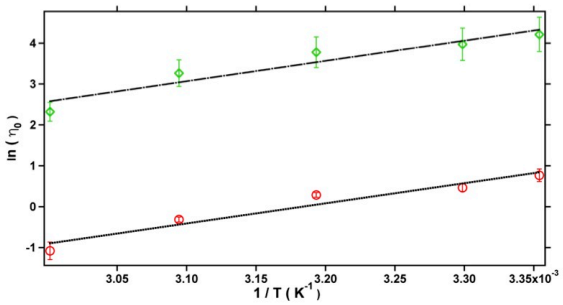

Figure S3. Arrhenius plot for GG formulations with (green diamonds) and without (red circles) CB 3 %. The linear regression provides ΔG_N = (38.9 ± 7.3) and (38.8 ± 5.1) kJ·mol^{-1} with and without CB, respectively.

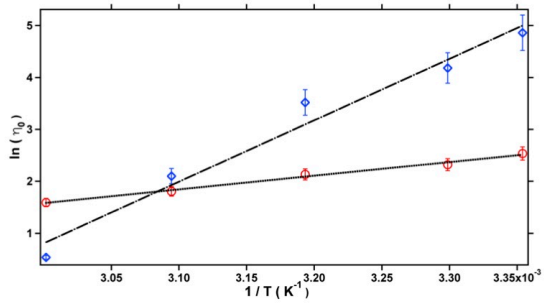

Figure S4. Arrhenius plot for SH formulations with (blue diamonds) and without (red circles) CB 3 %. The linear regression provides ΔG_N = (92.4 ± 9.6) and (20.8 ± 1.1) kJ·mol^{-1} with and without CB.

REFERENCES

(1) Alvarez-Lorenzo, C.; Blanco-Fernandez, B.; Puga, A. M.; Concheiro, A. Crosslinked Ionic Polysaccharides for Stimuli-Sensitive Drug Delivery. *Advanced Drug Delivery Reviews* **2013**, *65* (9), 1148–1171.

(2) Chandler, H. D. Activation Energy and Entropy for Viscosity of Wormlike Micelle Solutions. *J Colloid Interface Sci* **2013**, *409*, 98–103.

Paper III

Journal of Molecular Liquids 255 (2018) 397–405

Contents lists available at ScienceDirect

Journal of Molecular Liquids

journal homepage: www.elsevier.com/locate/molliq

The curious effect of potassium fluoride on glycerol carbonate. How salts can influence the structuredness of organic solvents

Filippo Sarri [a], Duccio Tatini [a], Moira Ambrosi [a], Emiliano Carretti [a], Barry W. Ninham [b], Luigi Dei [a], Pierandrea Lo Nostro [a,*]

[a] Department of Chemistry "Ugo Schiff", University of Florence, Via della Lastruccia 3, 50019 Sesto Fiorentino (Firenze), Italy
[b] Department of Applied Mathematics, Research School of Physical Sciences and Engineering, Australian National University, Canberra, ACT 0200, Australia

ARTICLE INFO

Article history:
Received 7 December 2017
Received in revised form 23 January 2018
Accepted 25 January 2018
Available online 31 January 2018

Keywords:
Glassy liquid
Structuredness
Ion pairs
Glycerol carbonate
Potassium fluoride

ABSTRACT

Glycerol carbonate (4-hydroxymethyl-1,3-dioxolan-2-one, shortly GC) is a dense, viscous, water soluble solvent. The high dielectric constant and dipole moment make it a suitable non-aqueous green solvent for several salts in different applications. GC dissolves significant amounts of inorganic salts such as KF. The saturation of GC with KF leads to the formation of a viscous liquid at room temperature. In this paper, we report on conductivity, rheology, differential scanning calorimetry and infrared spectroscopy experiments that indicate the formation of a glassy liquid where GC molecules and KF ion pairs are intercalated in a firm and ordered tridimensional structure, stabilized by hydrogen bonding and strong ion-dipole interactions.

1. Introduction

Cyclic carbonates, such as glycerol carbonate (GC), propylene carbonate (PC) and ethylene carbonate (EC) are associated liquids with strong intermolecular interactions, as suggested by their structural features (see Scheme 1), the large value of the Trouton constants $\Delta_{vap}S/R$ and the Kirkwood parameter g (see Table 1) [1,2].

These liquids find remarkable applications in several industrial fields [3,4]. In particular they are excellent solvents for electrolytes, due to their very high dielectric constant and dipole moment that determine the dissociation of ions and promote ion-solvent interactions, respectively. Moreover, in the case of GC a terminal primary –OH residue further increases the structuredness of the solvent and can assist in the ion solvation through hydrogen bonding (HB). In glass-forming liquids molecules are disordered though strongly interacting. PC and glycerol are examples of low-molecular-weight organic glass formers [5].

Molecular liquids like GC, usually show an excellent glass-forming ability, which is related to the strength of the intermolecular interactions (van der Waals forces and hydrogen bonds) [6,7]. These materials exhibit distinctly non-liquid-like features, a soft glassy rheology, which make them very attractive for technological applications and intriguing systems in terms of physics of condensed matter [8,9]. Indeed, several technical applications take advantage of GC physico-chemical properties. These include the technology of lithium and lithium-ion batteries, cement and concrete industries, sugar cane treatment, cosmetics and detergents [1,10–12].

In spite of the increasing interest in innovative synthetic routes for the production of GC [13,14], aimed at reducing the costs and enhancing the yield, only few articles on the GC physico-chemical properties have appeared in the literature.

While studying the solubility of some electrolytes in different cyclic carbonates in terms of the Hofmeister series [1], we came across a peculiar behavior of saturated solutions of KF in GC. In this paper we report our results from conductivity, viscosity, calorimetric and infrared measurements that reflect the formation of a dense and viscous glassy liquid at room temperature.

2. Experimental

2.1. Materials

Glycerol carbonate and potassium fluoride (99%) were purchased from Sigma-Aldrich (Milan, Italy). The salt was purified, dried and stored under vacuum, according to the standard procedures [1a,b]. Glycerol carbonate was used as received and kept under inert atmosphere to avoid water contamination.

2.2. Electric conductivity measurements

A Metrohm 712 conductimeter with a 0.83 cm^{-1} cell constant was used. Salt concentrations ranged between 0 and 1.5 M. The cell was

* Corresponding author.
E-mail address: pierandrea.lonostro@unifi.it (P. Lo Nostro).

https://doi.org/10.1016/j.molliq.2018.01.152
0167-7322/

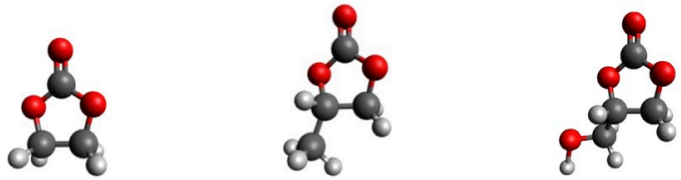

Scheme 1. From left to right: minimized chemical structures of EC, PC and GC. Grey, red and white spheres represent carbon, oxygen and hydrogen atoms, respectively.

Table 1
Physico-chemical properties of glycerol, propylene and ethylene carbonate at 25 °C.

Property	GC	PC	EC[a]
Dielectric constant, ε	109.7	64.9	89.8
Dipole moment, μ (D)[b]	5.05	5.36	4.81
Viscosity, η (cP)	85.4[c]	2.53	1.90
Density, ρ (g/mL)	1.3969[d]	1.200	1.321
Trouton constant, $\Delta_{vap}S/R$	34.6	11.6	12.1
Kirkwood parameter, g	8.18	1.23	1.60

[a] At 40 °C.
[b] From Ref. [4].
[c] From Ref. [3].
[d] This work.

immersed in a thermostatted water bath to control the temperature of the sample (25.0 ± 0.1 °C).

2.3. Rheology measurements

Rheology measurements were acquired with a Paar Physica UDS 200 rheometer working in the controlled shear-stress mode. For all samples a plate–plate geometry (diameter, 4 cm; gap, 300 μm) was used. All measurements were performed at (25.00 ± 0.01) °C. For each sample the flow curve was acquired in a torque range from 10^{-3} to 2000 mNm. The sample equilibrated for 15 min at the set temperature before running the measurement.

2.4. Differential scanning calorimetry

Differential Scanning Calorimetry (DSC) runs were carried out on a DSC-Q2000 from TA Instruments (Milan, Italy). The samples were first equilibrated at −30 °C, then cooled from −30 °C to −90 °C at 2 °C/min, and finally heated up to −30 °C at 2 °C/min. The experiments were conducted under N_2 atmosphere with a flow rate of 50 mL/min. The thermograms were analyzed by the TA Universal Analysis software. For all samples the glass transition temperatures (T_g) were obtained from the inflection point in the DSC signal.

2.5. Attenuated total reflection Fourier-transform infrared spectroscopy

Attenuated total reflection Fourier-transform infrared spectroscopy (ATR-FTIR) spectra were acquired using a Thermo Nicolet Nexus 870 FT-IR spectrophotometer, equipped with a liquid nitrogen cooled MCT (mercury-cadmium-telluride) detector, by averaging on 128 scans at a resolution of 2 cm^{-1} and with CO_2-atmospheric correction. The spectra were acquired in the range 4000–900 cm^{-1}. For each spectrum the background was previously recorded and subtracted to the sample profile.

3. Results and discussion

3.1. Electric conductivity measurements

The conductivity of KF + GC samples was measured at 25.0 °C as a function of the salt concentration (c). Fig. 1 shows the specific conductivity κ and the molar conductivity Λ of KF + GC solutions as a function of c. The data of κ and Λ were fitted according to the Casteel-Amis equation [15], and to the Fuoss-Kraus model, respectively (see Appendix A) [16].

In the dilute regime κ raises with c due to the increasing number of charge carriers. At moderate-to-high concentrations ($c > 1$ M), as the ion-ion interactions strengthen and the viscosity of the medium increases, the curve shows a plateau due to the competition between the increase in the number of charge carriers and the decrease in ionic mobilities [17]. For $c > 1.5$ M the solution becomes turbid presumably

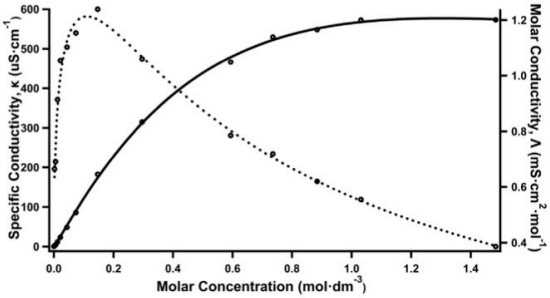

Fig. 1. Specific conductivity κ (solid line) and molar conductivity Λ (dashed line) for KF solutions in GC as a function of the molar concentration of the salt (c). The lines serve as a guide to the eyes.

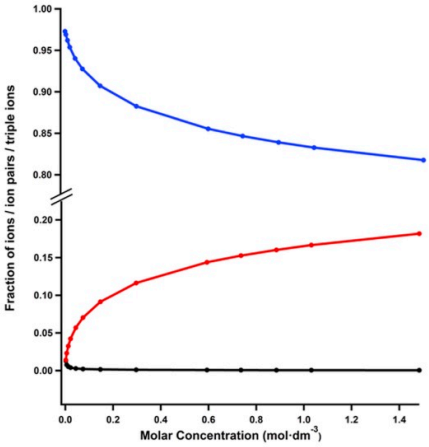

Fig. 2. Calculated fractions for triple ions (red), ion pairs (blue) and free ions (black) for KF in GC at 25 °C. (For interpretation of the references to colour in this figure legend, the reader is referred to the web version of this article.)

due to the formation of larger particles and we observed the onset of an intense yellowing, that preludes to the degradation of GC [18].

The Casteel-Amis model fits the experimental data with good agreement. The trend recorded for κ confirms that at moderate-to-high concentrations stronger ion-ion interactions come into play and rule over other forces in setting the ionic conductivity [19].

The plot of Λ vs. c (Fig. 1) provides interesting insights into the solvent-solute interactions. The curve shows a rapid increase in the dilute regime, then reaches a maximum at about 0.15 M and progressively decreases when c further increases. The presence of a maximum is a typical behavior that suggests the formation of ion pairs and triple ions (K_2F^+ and KF_2^-) [20]. In most cases the maximum is preceded by a minimum, corresponding to the onset of triple ions formation [12]. In our system this minimum is not observed, indicating that the ion association is predominant and the formation of charged triplets already occurs at very low c values. The Λ data were analyzed in terms of the Fuoss-Kraus model (see Fig. A1 in Appendix A) from which the association

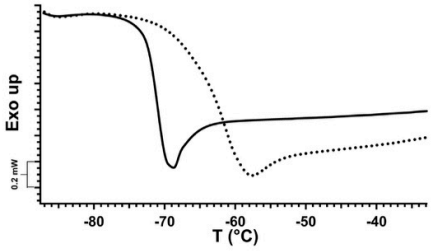

Fig. 4. DSC runs for pure GC (solid line) and for the KF saturated solution (dotted line).

constants for ion pairs (K_I) and for triple ions (K_T) can be estimated (see Appendix A) [16,21].

K_I is about $2.8 \cdot 10^6$, confirming the high tendency for K^+ and F^- to form ion pairs, while K_T is about 550, that reflects the formation of triple ions in GC. While the formation of ion pairs is typical for solutions of salts in polar organic solvents, the creation of triple ions at the extent recorded here was unexpected. From these values the fraction of triplets, ion pairs and free ions (α_T, α_P, and α_I, respectively) can be calculated as described in Appendix A [16,21].

The distribution curves for α_T, α_P, and α_I are reported in Fig. 2. KF ion pairs are always the most abundant species ($\alpha_P > 0.8$), with a very small fraction of free ions ($\alpha_I < 0.02$). The fraction of triple ions increases from 0.01 to 0.18 as more KF is added.

These findings lead to two important conclusions: (i) The lack of a minimum in the Λ/c plot is due to the high concentration of the non-conductive ion pairs even at very low contents of KF, and to the decrease in their fraction as triple ions are formed. Thus, the major contribution to the conductivity is provided by the triple ions, and this results in the maximum in the Λ/c curve. (ii) These data suggest that GC, despite its remarkably high dielectric constant, does not effectively solvate and separate K^+ and F^-, that rather remain associated in ion pairs (or triplets, at higher c). This can be explained in terms of the strong intermolecular interactions, on the structuredness of the pure liquid, and on the asymmetry between the interactions of the terminal –OH moiety with anions and the carbonyl oxygen with cations in GC.

3.2. Rheology measurements

Rheology measurements were performed at 25.0 °C. The flow curve for pure GC (see Fig. A2 in Appendix B) shows a remarkable hysteresis in

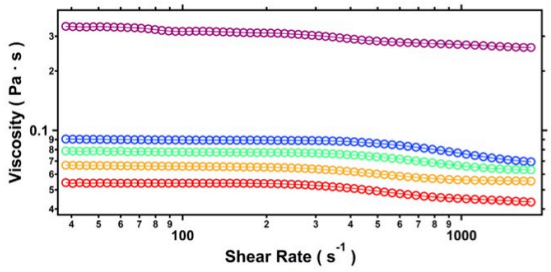

Fig. 3. Flow curves acquired on pure GC (red) and on KF + GC solutions at different salt concentrations: $7 \cdot 10^{-3}$ M (yellow), $7 \cdot 10^{-2}$ M (light blue), 0.21 M (blue), and 0.68 M (purple). (For interpretation of the references to colour in this figure legend, the reader is referred to the web version of this article.)

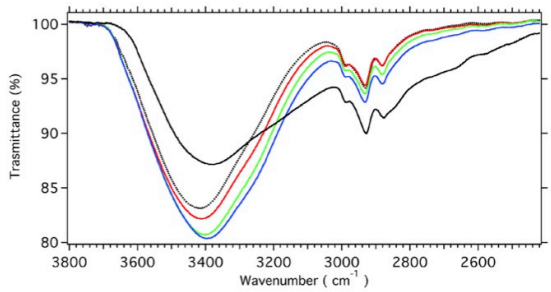

Fig. 5. Attenuated Total Reflection-Fourier Transform Infrared (ATR-FTIR) spectra between 3800 and 2400 cm^{-1} for pure GC (dotted line) and GC + KF solutions at different salt concentration: $7{\cdot}10^{-3}$ M (red), $7{\cdot}10^{-2}$ M (green), 0.21 M (blue), and 0.68 M (black). The whole spectra are shown in Fig. A4 in Appendix D. (For interpretation of the references to colour in this figure legend, the reader is referred to the web version of this article.)

the viscosity data of the pure liquid when an increasing stress is first applied and then reduced. To the best of our knowledge this is the first report on the thixotropic nature of GC due to its intrinsic structuredness. Fig. 3 reports the flow curves for pure GC and with increasing concentrations of KF between 10^{-3} M and 0.68 M.

The viscosity of KF + GC solutions increases as a function of the solute concentration. However, when the KF content is further increased, the viscosity steeply grows and exceeds by >10 times the value found for the pure solvent. This suggests that KF induces a very significant change in the solvent ordering, by forcing the formation of a stronger and more viscous structure in the medium.

The fractions of triple ions, ion pairs and free ions obtained from the conductivity data were used in a modified Jones-Dole equation (Eq. (1)), that describes the variation of the solution viscosity η as a function of the solute concentration c [22], by including two terms that take into account the effect of free ion-solvent and ion pair-solvent interactions [23,24]:

$$\eta = \eta_0 \left[1 + A\sqrt{(\alpha_i + \alpha_t)\, c} + \mathrm{B}_i\,(\alpha_i + \alpha_t)\, c + B_p\,\alpha_p\, c + D\, c^2\right] \qquad (1)$$

here η_0 is the viscosity of the pure solvent at the same temperature, A is the Falkenhagen coefficient that takes into account the electrostatic forces [25], B_i and B_p are the Jones-Dole coefficients that account for the ion-solvent and the ion pair-solvent interactions, respectively, and D is an additional term related to higher order solute-solute interactions. This equation is specifically targeted to fit cases where the salt concentration is relatively high, $c \geq 0.1$ M, and ion pair association is non negligible [23], whereas when $c < 0.1$ M the higher order term Dc^2 is usually overlooked [26–30].

η was recorded at an applied stress of 10 Pa and plotted versus c (see Fig. A3 in Appendix C). The values of A, B_i, B_p and D were calculated by fitting the experimental data according to Eq. (1). We obtained positive values for A and B_p (0.11 $dm^{3/2}$ $mol^{-3/2}$ and 4.22 dm^3 mol^{-1}, respectively); whereas, both B_i and D are negative (−0.92 dm^3 mol^{-1} and −7.67 dm^6 mol^{-2}, respectively). This result and the rise in the viscosity suggest that ion pairs are the most represented species in solution. We recall that the Jones-Dole B coefficient is positive for cosmotropes and negative for chaotropes, e.g., B is 0.127 for F^-, and −0.009 dm^3 mol^{-1} for K^+ (in water, at 25 °C) [31]. Interestingly we note that in the present case B_i, which is due to the free ionic species (mainly K^+, F^-, K_2F^+ and KF_2^-) that singularly destroy the structure of liquid GC, is large and negative. Instead, B_P is positive, suggesting that the ion pairs enhance the order of the solvent molecules.

3.3. Differential scanning calorimetry

The thermal behavior of pure GC and of its KF saturated solution was investigated through Differential Scanning Calorimetry (DSC). The DSC scans are reported in Fig. 4. Glycerol carbonate has a remarkably large range of stability with a high boiling point and a very low melting temperature [3]. From the DSC experiments we detected a glass transition temperature (T_g) at −70.8 °C for the pure GC and at −61.3 °C for the KF saturated solution. A similar behavior was reported for glycerol and

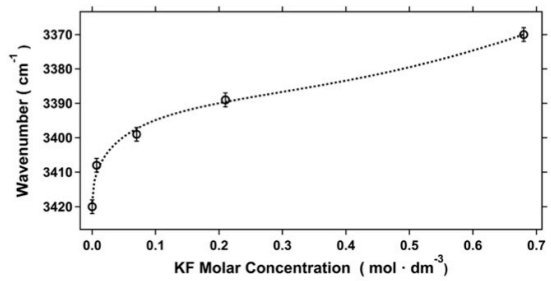

Fig. 6. Shift of the ATR–IR O–H stretching band wavenumber versus the KF concentration. The dotted black line is a guide for the eye.

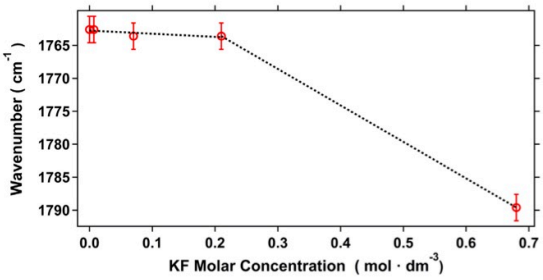

Fig. 7. Shift of the ATR−IR C═O stretching band wavenumber versus the KF concentration. The dotted black line is a guide for the eye.

PC [32,33]. The heat flow signal suggests the presence of an enthalpic recovery associated to the glass transition. The two contributions, namely the ΔC_p at the glass transition temperature (T_g), and the endothermic peak due to the enthalpic recovery process, cannot be separated by standard DSC. The remarkable increment in the T_g of the liquid upon the addition of KF confirms a strong stiffening effect induced by the electrolyte on the solvent molecules structuredness.

3.4. Attenuated total reflection-Fourier transform infrared spectroscopy

The Attenuated Total Reflection-Fourier Transform Infrared Spectroscopy (ATR-FTIR) experiments (see Fig. 5) indicate that an increment in the KF concentration brings about a shift in the O—H stretching band from 3420 cm^{-1} for pure GC, to 3370 cm^{-1} for the 0.68 M KF sample. Most likely this finding reflects the interaction between the hydroxyl moiety and the fluoride anion, that leads to a weakening in the O—H stretching mode. Further addition of KF results in a more significant shift of the band to lower wavenumbers.

Importantly, the addition of KF does not modify the FTIR profile of pure glycerol carbonate (see Fig. A4 in Appendix D). In fact the position of the absorption bands of GC is not affected by the addition of the salt [34,35]. In particular, the CH_2 and CH vibrations of the cyclic carbons remain unaffected (2990–2880 cm^{-1}). The C═O stretching is slightly shifted to lower wavenumbers (from 1791 cm^{-1} for the pure liquid to 1766 cm^{-1} for 0.68 M solution) probably due to the interaction of the carbonyl moiety with the potassium cation. The C—C and C—O stretching of the 2-hydroxyethyl chain appear at 1167 and 1047 cm^{-1} and are not modified by the addition of KF.

The O—H stretching peak decreases as a function of the KF concentration (Fig. 6) due to the stronger solvent-salt interactions while more salt is added.

A lighter and opposite effect was found in the case of the C═O stretching, whose wavenumber increases at high concentrations of KF, as indicated by Fig. 7. We argue that when the concentration of potassium fluoride is large the pristine HB between the carbonyl residue and the primary –OH group is remarkably weakened, as F^- substitutes the carbonyl's O. At the same time the purely electrostatic (ion-dipole) interaction between K^+ and the carbonyl of the GC molecule is weaker than the C═O···H—O hydrogen bonding, resulting in a shift in the infrared peak for the C═O stretching mode. Thus, the basic nature of the fluoride ion seems to be the main driving force that modifies the structuredness of the solvent molecules in ordered domains.

4. Conclusion

In conclusion the experimental results apparently suggest a remarkable strenghtening in the structuredness of liquid glycerol carbonate upon addition of potassium fluoride.

Literature sources on the behavior of fluoride ions in non-aqueous solvents report that F^- is scarcely solvated in aprotic solvents, with a lower basicity and a higher nucleophilicity. On the other hand, in protic solvents F^- greatly interacts with the solvent molecules through HB, leading to a higher basicity [45,46].

The cartoon in Fig. 8 schematically depicts a hypothetical structure of the solution where the solvent molecules are organized in wormlike structures intercalated by KF ion pairs with which they interact through ion-dipole interactions (between K^+ and the C═O residue) and HB between F^- and the –OH moiety of GC. The dissolved KF salt mainly forms ion pairs that are responsible for the remarkable increase in the viscosity of the solution. A similar ordering was proposed by Jones for the dissolution of LiF in EC or PC [2]. Free solvated K^+ and F^- and triple ions are present and contribute to the overall conductivity of the sample.

In the side directions, along the main axis the solvent molecules are oriented in the opposite way, as required by the minimization of the dipoles energy. Such ordered structure would justify the conductivity and viscosity features of this glassy liquid system. Further structural investigations through SAXS and NMR experiments and solubility assessments are currently in progress.

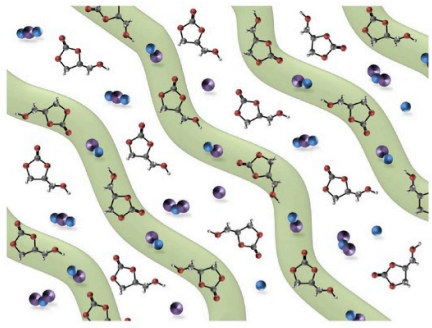

Fig. 8. Schematic cartoon showing the proposed structure that comprises ordered domains of GC molecules with a head-to-tail orientation intercalated by KF ion pairs. In the opposite direction the GC dipoles are inverted. The large purple and the light blue globes represent potassium and fluoride ions, respectively. K^+, F^- and triple ions are dispersed in the solution.

Appendix A. Casteel-Amis Equation and Fuoss-Kraus Formalism

The specific conductivity (κ) was fitted according to the Casteel-Amis model that provides an empirical equation commonly used to describe the conductivity behavior of electrolytes over wide ranges of salt concentration [15,36]. In this model the relation between κ and the concentration m (in molal units) is expressed as:

$$\frac{\kappa}{\kappa_{max}} = \left(\frac{m}{\mu}\right)^{a} exp\left[b(m-\mu)^2 - \frac{a}{\mu}(m-\mu)\right] \quad (A1)$$

where κ_{max} is the maximum value of conductivity, μ is the concentration at which κ_{max} is reached, and a and b are fitting parameters (see Table A1). κ_{max} and μ are mainly determined by the solvent viscosity and the ionic radii [37].

Table A1
The parameters a, b, μ and κ_{max} obtained by fitting the specific conductivity data with the Casteel-Amis equation.

μ	κ_{max}	a	b	χ^2
0.89 ± 0.06	577 ± 4	1.08 ± 0.05	0.316 ± 0.141	375

More recent approaches describe the conductivity of strong electrolyte solutions at moderate-to-high concentrations in polar non-aqueous solvents. The "quasi-lattice theory" or the mean spherical approximation (MSA) method are some examples [17 and references therein]. These models do not fit accurately our data, thus we decided to use a modified semi-empirical version of the Fuoss-Kraus model, which provides a quantitative estimation of the ionic fractions in solution from conductivity measurements [16]. This model is widely used for polyelectrolytes-based systems [38–40]. The method requires the determination of the limiting conductivities, then the calculation of ion pair and triplets conditional formation constants and finally the fractions of triplets, ion pairs and "free" ions as a function of the salt concentration [41].

Assuming that only KF, K^+, F^-, K_2F^+ and K_2F^- are present in the solution (i.e. no quadrupoles or higher charged clusters), the KF ion pair can either dissociate in free ions:

$$KF \rightarrow K^+ + F^-$$

or triplets:

$$3\,KF \rightarrow KF_2^- + K_2F^+$$

From the calculation of the activity coefficients through the extended Debye-Hückel theory and the Bjerrum formula [1a,b] we found that $\gamma_\pm$ ranges between 0.94 and 0.96, thus we used the approximation of unitary coefficients. Moreover, assuming that the concentrations of K_2F^+ and K_2F^- are equal, the corresponding conditional association constants K_I and K_T for ion pairs and triplets are related to the ion fractions in the following manner:

$$K_I = \frac{[KF]}{[K^+][F^-]} = \frac{1-\alpha_I}{\alpha_I{}^2} \quad (A2)$$

$$K_T = \frac{[KF_2^-]}{[KF][F^-]} = \frac{[K_2F^+]}{[KF][K^+]} = \frac{\alpha_T}{\alpha_I c(1-\alpha_I-3\alpha_T)} \quad (A3)$$

where α_I and α_T are the free ions and triplets fractions respectively. From which we obtain:

$$\alpha_I = \frac{-1+\sqrt{1+4K_Ic}}{2K_Ic} \quad (A4)$$

$$\alpha_T = \frac{K_T\alpha_I(1-\alpha_I)c}{1+3K_T\alpha_Ic} \quad (A5)$$

$$\alpha_P = 1-\alpha_I-\alpha_T \quad (A6)$$

α_P is the fraction of ion pairs. If we do not consider the effect of the electrostatic field generated by the ions, the total molar conductivity is expressed as:

$$\Lambda = \alpha_I\Lambda_0{}^I + \alpha_T\Lambda_0{}^T \quad (A7)$$

where $\Lambda_0{}^I$ and $\Lambda_0{}^T$ are the limiting molar conductivities in GC for the free ions and the triple ions respectively. Thus, replacing the expressions for α_I and α_T and rearranging the equation, we obtain:

$$\Lambda\sqrt{c} = \frac{\Lambda_0{}^I}{\sqrt{K_I}} + \frac{\Lambda_0{}^TK_Tc}{\sqrt{K_I}} \quad (A8)$$

In the dilute regime, the plot of $\Lambda\sqrt{c}$ vs. c produces a linear relation with a slope of ${\Lambda_0}^T {K_T} {K_I}^{-1/2}$ and an intercept of ${\Lambda_0}^I {K_I}^{-1/2}$. In order to calculate the values of K_I and K_T, ${\Lambda_0}^I$ and ${\Lambda_0}^T$ must be determined. We assume that ${\Lambda_0}^I = \Lambda_0$, since at infinite dilution ion-ion interactions vanish and triple ions formation can be neglected. The value of Λ_0 from the limiting molar conductivities (λ_i) can be estimated as:

$$\Lambda_0 = \sum_i \nu_i \lambda_i \tag{A9}$$

where ν_i is the number of i ions in the formula unit of the electrolyte.
The limiting molar conductivity λ_i is related to the ionic mobility u_i according to [42]:

$$\lambda_i = z_i F u_i \tag{A10}$$

where F is the Faraday constant and z_i is the charge of the i ion. The ionic mobility is defined as [43]:

$$u_i = \frac{e z_i}{6\pi \eta_0 r_{hi}} \tag{A11}$$

where e is the elementary charge, z_i is the charge of the i ion, η_0 is the solvent viscosity and r_{sol} is the solvated radius of the i ion. Assuming a spherical geometry for the solvated ion, its solvated radius can be calculated as:

$$\frac{4}{3}\pi r_{sol}^3 = \frac{4}{3}\pi r_{cryst,i}^3 + n_s \cdot V_s \tag{A12}$$

where n_s is the number of solvent molecules in the solvation layer around the ion, V_s is the molar volume of a solvent molecule and $r_{cryst,\,i}$ is the crystalline radius of the ion. We calculated the ionic mobilities and the conditional association constants K_I and K_T for n_s values ranging between 1 and 5. The value of n_s has a negligible influence on the ionic mobilities and on the conditional association constants. Moreover, considering also the effects due to the steric hindrance, we assumed an average solvation number of 3. Once Λ_0 is obtained, ${\Lambda_0}^T$ is taken as $2\Lambda_0/3$ (${\Lambda_0}^T$ cannot be determined experimentally) [44].
The values of the ionic mobilities (u, in $A \cdot s^2/kg$) and the limiting molar conductivities (λ and Λ, in $S \cdot m^2/mol$) in GC are shown in Table A2:

Table A2
Calculated ionic mobilities (u, in $A \cdot s^2/kg$) and limiting molar conductivities (λ and Λ, in $S \cdot m^2/mol$) for K^+ and F^- in GC at 25 °C.

u_{K^+}	u_{F^-}	λ_{K^+}	λ_{F^-}	$\Lambda_0 = \lambda_{K^+} + \lambda_{F^-}$
$4.73 \cdot 10^{-10}$	$4.87 \cdot 10^{-10}$	$4.56 \cdot 10^{-5}$	$4.70 \cdot 10^{-5}$	$9.26 \cdot 10^{-5}$

For the triple ions, ${\Lambda_0}^T = \frac{2}{3}\Lambda_0 = 6.17 \cdot 10^{-5}$ S m^2/mol.

The plot of $\Lambda\sqrt{c}$ as a function of c (see Fig. A1) shows a linear trend in the dilute regime, up to approximately 22 mM. The slope and intercept are $2.03 \cdot 10^{-5} \pm 9 \cdot 10^{-7}$ S dm$^{7/2}$ mol$^{-3/2}$ and $5.54 \cdot 10^{-8} \pm 1 \cdot 10^{-8}$ S m$^{1/2}$ mol$^{1/2}$ respectively.

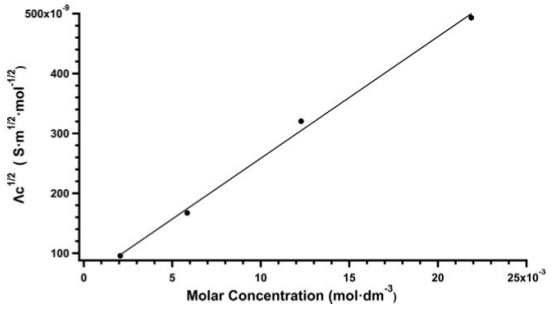

Fig. A1. Plot of $\Lambda\sqrt{c}$ as a function of c.

Eqs. (A2) and (A3) provide the values of K_I and K_T: $K_I = (2.8 \pm 0.4) \cdot 10^6$ and $K_T = 550 \pm 235$, from which the values of α_I, α_T and α_P can be calculated.

Appendix B. Thixotropy in glycerol carbonate

Fig. A2 shows the flow curve of pure glycerol carbonate acquired in two steps: the applied stress was first increased and then restored to the initial value. The hysteresis of the curve reflects the thixotropic nature of the solvent and gives a further evidence of its structuredness.

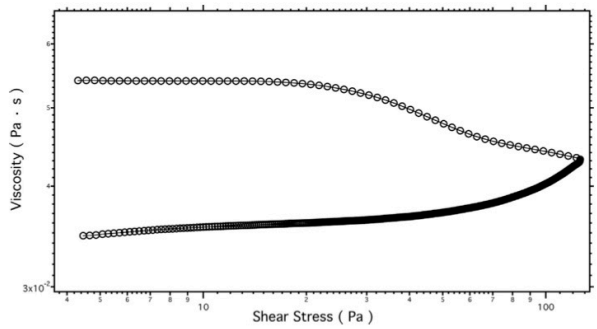

Fig. A2. Thixotropic behavior of pure GC.

Appendix C. Extended Form of the Jones-Dole Equation

The viscosity values at 10 Pa were plotted vs. the KF concentration and fitted with a modified Jones-Dole equation (Fig. A3). Indeed, when ionic association occurs the Jones-Dole B coefficient is split in two different contributions: the first (B_i) is related to the interactions between the solvent and the charged species, whereas the second term (B_p) takes into account the solvent-ion pairs interactions. When the salt concentration exceeds the value of 0.1 M an additional term (D) is added to take into account the solute-solute interactions of higher order [26–29]. The equation then becomes:

$$\eta = \eta_0 \left[1 + A\sqrt{(\alpha_i + \alpha_t)c} + B_i(\alpha_i + \alpha_t)\, c + B_p\, \alpha_p\, c + Dc^2\right] \tag{A13}$$

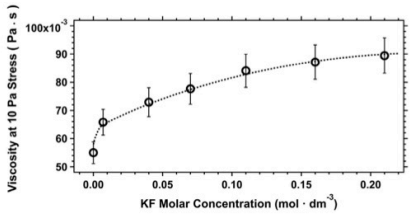

Fig. A3. Viscosity values plotted vs. the salt concentration for KF + GC solutions at 25 °C. The curve is obtained by fitting the experimental data with Eq. (A13) and the fitting parameters are listed in Table S3.

Table S3
Fitting parameters obtained from Eq. (A13).

A	B_i	B_p	D	χ^2
0.11 ± 0.02	−0.92 ± 0.17	4.22 ± 0.72	−7.68 ± 0.97	$3.6{\cdot}10^{-3}$

Moreover, the theoretical Falkenhagen coefficient for GC was calculated as reported by Jenkins and Marcus [24], and compared to the fitting value:

$$A = \frac{A_*}{\eta_0 \cdot \sqrt{\varepsilon_r \cdot T}} \cdot f\left(\lambda_+^\infty, \lambda_-^\infty\right) \tag{A14}$$

where A_* is $1.113{\cdot}10^{-5}$ C (m·K·mol^{-1})$^{1/2}$, ε_r is the dielectric constant of the solvent, T is the absolute temperature, and $f(\lambda_+{}^0, \lambda_-{}^0)$ is the ions infinite dilution equivalent conductivities function that, in the case of symmetrical electrolytes ($z_+ = |z_-| = z$), is defined as:

$$f = \left[\frac{z^2\left(\lambda_+^\infty + \lambda_-^\infty\right)}{4\left(2+\sqrt{2}\right)\left(\lambda_+^\infty \cdot \lambda_-^\infty\right)}\right] \cdot \left[1 - \frac{4\left(\lambda_+^\infty - \lambda_-^\infty\right)^2}{\left(1+\sqrt{2}\right)^2\left(\lambda_+^\infty + \lambda_-^\infty\right)^2}\right] \tag{A15}$$

From Eq. (A14) the calculated value for A comes out to be 0.11 $dm^{3/2}/mol^{3/2}$, in very good agreement with the value obtained from the fitting procedure.

Appendix D. ATR-FTIR Results

The ATR-FTIR spectra acquired in the range 4000–900 cm^{-1} for pure GC and GC + KF solutions at different salt concentration ($7{\cdot}10^{-3}$ M, $7{\cdot}10^{-2}$ M, 0.21 M, and 0.68 M) are reported in Fig. A4.

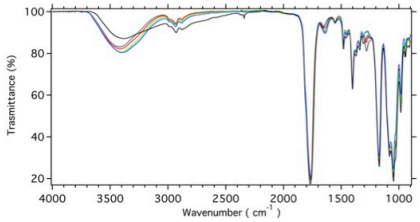

Fig. A4. ATR-FTIR spectra acquired on pure GC (black dotted line) and on KF + GC solutions at different salt concentrations: $7{\cdot}10^{-3}$ M (red), $7{\cdot}10^{-2}$ M (green), 0.21 M (blue), and 0.68 M (black solid line).

References

[1] a) N. Peruzzi, B.W. Ninham, P. Lo Nostro, P. Baglioni, J. Phys. Chem. B 116 (2012) 14398;
b) N. Peruzzi, P. Lo Nostro, B.W. Ninham, P. Baglioni, J. Solut. Chem. 44 (2015) 1224.
[2] J. Jones, M. Anouti, M. Caillon-Caravanier, P. Willmann, D. Lemordant, Fluid Phase Equilib. 285 (2009) 62.
[3] M.O. Sonnati, S. Amigoni, E.P. Taffin de Givenchy, T. Darmanin, O. Choulet, F. Guittard, Green Chem. 15 (2013) 283.
[4] Y. Chernyak, J. Chem. Eng. Data 51 (2006) 416.
[5] X.N. Ying, Phys. Scr. 88 (2013), 025603.
[6] U.R. Pedersen, P. Harrowell, J. Phys. Chem. B 115 (2011) 14205.
[7] K. Koperwas, K. Adrjanowicz, Z. Wojnarowska, A. Jedrzejowska, J. Knapik, M. Paluch, Sci. Rep. 6 (2016) 36934.
[8] R. Zondervan, T. Xia, H. van der Meer, C. Storm, F. Kulzer, W. van Saarloos, M. Orrit, PNAS 105 (2008) 4993.
[9] M. Köhler, P. Lunkenheimer, A. Loid, Eur. Phys. J. E 27 (2008) 115.
[10] Z. Zhang, D.W. Rackemann, W.O.S. Doherty, I.M. O'Hara, Biotechnol. Biofuels 6 (2013) 153.
[11] M. Pagliaro, R. Ciriminna, H. Kimura, M. Rossi, C. Della Pina, Angew. Chem. Int. Ed. 46 (2007) 4434–4440.
[12] J.R. Ochoa-Gómez, O. Gómez-Jiménez-Aberasturi, C. Ramírez-López, M. Belsué, Org. Process. Res. Dev. 16 (2012) 389.
[13] P.U. Okoye, A.Z. Abdullah, B.H. Hameed, J. Taiwan Inst. Chem. Eng. 68 (2016) 51.
[14] P.U. Okoye, A.Z. Abdullah, B.H. Hameed, Energy Convers. Manag. 133 (2017) 477–485.
[15] J.F. Casteel, E.S. Amis, J. Chem. Eng. Data 17 (1972) 55.
[16] C. Kraus, R. Fuoss, J. Am. Chem. Soc. 55 (1933) 21.
[17] K. Izutsu, Electrochemistry in Nonaqueous Solutions, Wiley-VCH, Weinheim, 2002 201–222.
[18] D.J. Darensbourg, A.D. Yeung, Green Chem. 16 (2014) 247.
[19] R. Jan, G.M. Rather, M.A. Bhat, J. Solut. Chem. 43 (2014) 685.
[20] G. Macfie, M.G. Compton, H.R. Corti, J. Chem. Eng. Data 46 (2001) 1300.
[21] D. Aurbach, Nonaqueous Electrochemistry, CRC Press, 1999.
[22] G. Jones, M. Dole, J. Am. Chem. Soc. 51 (1929) 2950.
[23] A. Kacperska, S. Taniewska-Osinska, A. Bald, A. Szejgis, J. Chem. Soc., Faraday Trans. 1 85 (1989) 4147.
[24] H.D.B. Jenkins, Y. Marcus, Chem. Rev. 95 (1995) 2695.
[25] H. Falkenhagen, E.L. Vernon, Phylos. Mag. 14 (series 7) (1932) 537.
[26] R.S. Patil, V.R. Shaikh, P.D. Patil, A.U. Borse, K.J. Patil, J. Mol. Liq. 200 (2014) 416.
[27] N. Martinus, C.D. Sinclair, C.A. Vincent, Electrochim. Acta 22 (1977) 1183.
[28] J.E. Desnoyers, G. Perron, J. Solut. Chem. 1 (1972) 199.
[29] D.S. Viswanath, T. Ghosh, D.H.L. Prasad, N.V.K. Dutt, K.Y. Rani, Viscosity of Liquids, Springer, Berlin, 2007 407–442.
[30] A.A. Zavitsas, Chem. Eur. J. 16 (2010) 5942.
[31] Y. Marcus, Ions in Solution and Their Solvation, John Wiley & Sons, Inc., Hoboken, New Jersey, 2015.
[32] A.G. Lyapin, E.L. Gromnitskaya, I.V. Danilov, V.V. Brazhkin, RSC Adv. 7 (2017) 33278.
[33] J. Geschwind, H. Frey, Macromolecules 46 (2013) 3280.
[34] V. Calvino-Casilda, G. Mul, J.F. Fernandez, F. Rubio-Marcos, M.A. Banares, Appl. Catal., A 409–410 (2011) 106.
[35] J.S. Choi, F.S. Hubertson Simanjuntaka, J. Young Oh, K.I. Lee, S.D. Lee, M. Cheong, H.S. Kim, H. Lee, J. Catal. 297 (2013) 248.
[36] M.S. Ding, J. Chem. Eng. Data 49 (2004) 1469.
[37] K. Izutsu, Electrochemistry in Nonaqueous Solutions, Wiley-VCH, Weinheim, 2002 206–207.
[38] J.R. MacCallum, A.S. Tomlin, C.A. Vincent, Eur. Polym. J. 22 (1986) 787.
[39] L. Niedzicki, M. Kasprzyk, K. Kuziak, G.Z. Zukowska, M. Marcinek, W. Wieczorek, M. Armand, J. Power Sources 196 (2011) 1386.
[40] J. Barthel, Angew. Chem. Int. Ed. Eng. 7 (1968) 260.
[41] L. Niedzicki, M. Kasprzyk, K. Kuziak, G.Z. Zukowska, M. Armand, M. Bukowska, M. Marcinek, P. Szczecinski, W. Wieczorek, J. Power Sources 192 (2009) 612.
[42] R. Haase, Angew. Chem. Int. Ed. Eng. 4 (1965) 485.
[43] J. Cazes, Encyclopedia of Chromatography, CRC Press, Boca Raton, 2001 273.
[44] S. Boileau, P. Hemery, Electrochim. Acta 21 (1976) 647.
[45] J. Clark, Chem. Rev. 80 (1980) 429–452.
[46] I.N. Rozhkov, I.L. Knunyant, Dokl. Akad. Nauk SSSR 199 (1971) 614.

Paper IV

Journal of Molecular Liquids 266 (2018) 711–717

Contents lists available at ScienceDirect

Journal of Molecular Liquids

journal homepage: www.elsevier.com/locate/molliq

Specific ion effects in non-aqueous solvents: The case of glycerol carbonate

Filippo Sarri [a], Duccio Tatini [a], Damiano Tanini [a], Matteo Simonelli [a], Moira Ambrosi [a], Barry W. Ninham [b], Antonella Capperucci [a], Luigi Dei [a], Pierandrea Lo Nostro [a,*]

[a] Department of Chemistry "Ugo Schiff" and CSGI, University of Florence, Via della Lastruccia 3, 50019 Sesto Fiorentino, Firenze, Italy
[b] Department of Applied Mathematics, Research School of Physical Sciences and Engineering, Australian National University, Canberra, ACT 0200, Australia

ARTICLE INFO

Article history:
Received 10 May 2018
Received in revised form 27 June 2018
Accepted 29 June 2018
Available online 2 July 2018

Keywords:
Hofmeister series
Specific ion effect
Ion pairs
Glycerol carbonate

ABSTRACT

The effect of eight potassium salts (KF, K_3PO_4, KOCN, K_2CO_3, KCl, K_2SO_4, KBr and KI) on glycerol carbonate (GC) is studied through NMR, DSC, solubility and ATR-FTIR experiments. From the solubility data, the main thermodynamic functions of solution and solvation are estimated, and the mean molal activity coefficients are calculated. The results suggest that the capability of an anion to establish hydrogen bonds with the solvent molecules (or behave as a base, as in the case of fluoride, phosphate, cyanate and carbonate) is the most important structural feature that determines its effects on the solvent structure. On the other hand potassium iodide behaves in an anomalous way, due to the large polarizability of the anion that can form non-electrostatic, van der Waals dispersive intermolecular interactions.

1. Introduction

In a previous paper [1] we reported some curious effects that followed saturation of glycerol carbonate (GC) with potassium fluoride. The effects were studied at room temperature via conductivity, rheology, differential scanning calorimetry (DSC) and attenuated total reflection Fourier-transform infrared spectroscopy (ATR-FTIR) measurements. We found that KF forms mainly ion pairs, triple ions and larger clusters. Together with a few free ions these impart to the thixotropic solvent a structuredness much stronger than expected for the mixture. Apparently this occurs through the formation of hydrogen bonds (HB) with the fluoride anion and ion-dipole interactions between K^+ and the carbonyl residue [1].

Here we extend the previous work to include the solubility and behavior of a range of other potassium salts in GC. We compare the results with those for other cyclic carbonates previously explored. Since we operate either at the saturation limit or at a moderately high concentration our results are both anion and solvent specific. The aim is to explore the nature of non-aqueous solvent Hofmeister effects systematically. To do so, information on variation of the thermodynamics of solvation across a range of solvents, the effect of ions on solvent structure and on solvent dynamics need to be available to obtain a comprehensive physical picture [2].

Alkylene carbonates such as GC, propylene carbonate (PC) and ethylene carbonate (EC) are non-aqueous associated liquids with strong van der Waals intermolecular interactions as suggested by their structural features (see Scheme 1), and by some of their physico-chemical properties (see Table 1) [3, 4].

All solvents considered in Table 1 possess high dielectric constants and dipole moments. The conventional view is that this explains why alkylene carbonates are suitable solvents for strong electrolytes and therefore widely used in different industrial areas [5, 6]. Solvent-solvent and salt-solvent intermolecular interactions are often depicted in a too simplistic view that derives from an electrostatic (Born energy) interpretation of free energies of ion transfer. We now know that dispersion self-energies provide significant ion specific contributions [14–21].

Alkylene carbonates (glycerol, ethylene and propylene carbonates) also possess high heat capacities and large phase transition parameters that reflect the strong intermolecular interactions.

In the case of GC a terminal primary —OH residue further increases the ordered structure of the solvent and can assist in the ion solvation through hydrogen bonding (HB). Scheme 1 shows the atom numbering and the partial charge on each atom in GC. The presence of a significant negative charge on the carbonyl oxygen (O1) that can strongly interact with the terminal hydroxyl group on the other side of the molecule and build up a robust structuredness in the liquid, as reflected by some solvent properties such as the high enthalpy of vaporization and the relatively low enthalpy of melting. Moreover GC possesses a large static polarizability (about 9.3 $Å^3$, see Ref. 12), larger than that of PC and EC (see Table 1), that – together with the large dipole moment – can justify the existence of important and highly cooperative van der Waals intermolecular interactions [22].

* Corresponding author.
E-mail address: pierandrea.lonostro@unifi.it (P. Lo Nostro).

https://doi.org/10.1016/j.molliq.2018.06.120
0167-7322/

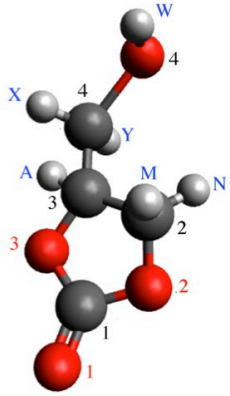

Scheme 1. Minimized chemical structure of GC. Grey, red and white spheres represent carbon, oxygen and hydrogen atoms, respectively. In blue the numbering for hydrogens, in black the numbering for carbons, and in red the numbering for oxygens. Partial charges (calculated with Avogadro 1.1.0): C1: +0.511, C2: +0.135, C3: +0.163, C4: +0.085, O1: −0,203 O2: −0.430, O3: −0.425, O4: −0.391, H_M: +0.074, H_N: +0.074,: H_A: +0.079, H_X: +0.060, H_Y: +0.060, H_W: +0.210.

Another consequence of their ordered structure is that molecular liquids like GC and PC behave as excellent low-molecular-weight organic glass formers [23–25]. In fact these materials show non-liquid-like features, such as the rheological behavior typical of a soft glass, that make them very interesting for fundamental research and technological applications [26, 27]. In spite of the increasing interest in innovative synthetic routes of GC in order to cut the production costs and enhance the yield [28, 29], only few articles on the GC physico-chemical properties have appeared in the literature [30].

Table 1
Physico-chemical properties of glycerol, propylene and ethylene carbonate at 25 °C. In the case of GC the phase change refers to a glass transition.

Property	GC	PC	EC[a]	H_2O
Dielectric constant, ε	109.7	64.9	89.8	80.1
Dipole moment, μ (D)[b]	5.05	5.36	4.81	1.85
Viscosity, η (cP)	85.4[c]	2.53	1.90	0.89
Surface tension, γ (mN/m)	44.2	34.6[d]	50.6[a]	72
Heat capacity, C_p(liquid) (J/mol·K)	201[f]	170[f]	156[g]	75.29
Melting point, *mp* (°C)	(−70.8°)	−52.7°	38.2°	0°
Fusion enthalpy, $\Delta_{fus}H$ (kJ/mol)	(19.6)[h]	8.96[e]	13.02[e]	6.01
Fusion entropy, $\Delta_{fus}S$ (J/mol·K)	(97)	41	43	22
Boiling point, *bp* (°C)	354°	242	248°	100°
Vaporization enthalpy, $\Delta_{vap}H$ (kJ/mol)	78.5	56.3[d]	55.2[d]	40.66
Vaporization entropy, $\Delta_{vap}S$ (J/mol·K)	125	109	107	109
Static polarizability, α_0 (Å^3)[j]	9.3[k]	8.5[k]	6.6[k]	1.5[l]

[a] At 40 °C.
[b] From Ref. [5].
[c] From Ref. [6].
[d] At 150 °C, from Ref. [7].
[e] From Refs. [8] and [9].
[f] At 30 °C from Ref. [5].
[g] At 110 °C from Ref. [5].
[h] Calculated from Ref. [10].
[i] From Ref. [11].
[j] Experimental values obtained from the Lorenz-Lorentz equation.
[k] From Ref. [12].
[l] From Ref. [13].

This is surprising because several applications take advantage of the properties of GC. These include for example the technology of lithium and lithium-ion batteries, cement and concrete industries, sugar cane treatment, cosmetics and detergents [3, 4, 31–33].

Indeed the study of the behavior of salts in organic solvents stands out as a self-evidently important field of research because of the need for better insights into the microscopic mechanisms that determine over specific ion phenomena. In fact the way salts modify the structure and physico-chemical properties of protic and aprotic polar liquids is of great importance to assess whether hydrogen bonding is involved or not. Or indeed whether hydrogen bonding is a meaningful or useful concept on which to build intuition and predictability.

The relative simplicity of aprotic solvents should contribute insights into of the most significant problems related to the universality of Hofmeister effects in aqueous solutions and dispersions, and to the elusive related issues of hydrogen bond clusters and ion specificity of hydration interactions.

In this paper we specifically investigate the effect of HB on the solubility of some salts and more particularly on the thermodynamics and other physico-chemical properties through NMR, DSC and ATR-FTIR measurements. These properties were studied in the presence of different potassium salts to elucidate the interactions between the anions and the solvent. Since the solvent possesses a terminal —OH group, it can establish HB in the pure liquid state, as suggested and confirmed by several peculiar physico-chemical properties and observations. The range of the investigated salts range from potassium halides to phosphate, carbonate, sulfate and cyanate to study the effect of the anion's basicity and of the anion's capability to act as a donor/acceptor for hydrogen bonds. We found that fluoride, phosphate, carbonate and (partly) cyanate do behave as basic anions and are able to interact with the solvent molecules by participating in HB. Chloride and bromide play an intermediate role according to the Hofmeister sequence. Compared to the behavior of iodide in EC and PC, its interactions with GC represent a striking anomaly with respect to what we expected on the basis of our previous studies.

2. Experimental

2.1. Materials

Glycerol carbonate (≥90.0%), potassium fluoride (≥99.5%), potassium chloride (≥99.0%), potassium bromide (≥99.0%), potassium iodide (≥99.0%), potassium carbonate (≥99.0%), potassium phosphate (≥98.0%), potassium cyanate (96%), and potassium sulfate (≥99.0%) were purchased from Sigma-Aldrich (Milan, Italy). The salts were purified, dried and stored under vacuum, according to the standard procedures [3, 4]. Glycerol carbonate was used as received and kept under inert atmosphere to avoid water contamination.

2.2. Solubility

The solubility of salts in GC was measured at different temperatures. A weighted amount of GC was transferred in a test tube and an excess of dry salt was added. The vial was sealed and kept under magnetic stirring for two days in a thermostatted bath at the required temperature (±0.1 °C). The stirring was stopped and the saturated solution was left to equilibrate in the presence of the salt for 24 h, before a certain amount (*b*, in grams) of solution was carefully taken from the top of the solution and transferred to a flask and diluted with water up to a volume *V* (in L). The aqueous mixture was than analyzed through Inductively Coupled Plasma Atomic Emission Spectrometer (ICP-AES) in order to measure the concentration of K^+ (*c*, in mg/L). The calibration curve was built analysing five standard solutions of dry KCl using a water + GC mixture as a solvent with approximately the same composition of the sample under investigation. The calibration data were fitted with a quadratic curve with a correlation coefficient R^2 of 0.99993.

The solubility (m in molal units, i.e. moles of solute per 1 kg of GC) of the salt was then calculated as:

$$m = \frac{1000cV}{1000bM_K - cMV} \quad (1)$$

where M_K is the atomic mass of potassium (39.102 g/mol) and M is the molar mass of the salt.

2.3. Density of glycerol carbonate

The density of GC was measured with an Anton Paar DMA 5000 instrument as a function of temperature between 15° and 50 °C, with an accuracy of $\pm 10^{-5}$ g/mL.

2.4. Nuclear magnetic resonance

1D- and 2D-NMR spectra were recorded with a Bruker 400 Ultrashield spectrometer operating at 400 MHz (for ^{1}H) and 100 MHz (for ^{13}C). All the experiments were carried out in vacuum-dried NMR coaxial tubes. $CDCl_3$ was used as external lock and reference material in the coaxial insert. NMR signals were referenced to nondeuterated residual solvent signals ($CDCl_3$, 7.26 ppm and 77.0 ppm for ^{1}H and ^{13}C, respectively). The monodimensional ^{1}H and ^{13}C NMR spectra for pure GC are shown in Figs. S1 and S2 in the Supporting information. The assignment of the chemical shift to each proton in the pure GC molecule was carried out by performing homo- and heteronuclear 2D-NMR experiments as ^{1}H—^{1}H COSY (homonuclear correlation spectroscopy) and ^{1}H—^{13}C HSQC (heteronuclear single quantum coherence spectroscopy), see Figs. S3 and S4 in the Supporting information.

2.5. Differential scanning calorimetry

Differential Scanning Calorimetry (DSC) runs were carried out on a DSC-Q2000 from TA Instruments (Milan, Italy). The samples were first equilibrated at −30 °C, then cooled from −30 °C to −90 °C at 2 °C/min, and finally heated up to −30 °C at 2 °C/min. The experiments were conducted under N_2 atmosphere with a flow rate of 50 mL/min. The thermograms were analyzed by the TA Universal Analysis software. For all samples the glass transition temperatures (T_g) were obtained from the inflection point in the DSC signal.

2.6. Attenuated total reflection Fourier-transform infrared spectroscopy

Attenuated total reflection Fourier-transform infrared spectroscopy (ATR-FTIR) spectra were acquired using a Thermo Nicolet Nexus 870 FT-IR spectrophotometer, equipped with a liquid nitrogen cooled MCT (mercury cadmium-telluride) detector, by averaging on 128 scans at a resolution of 2 cm^{-1} and with CO_2-atmospheric correction. The spectra were recorded between 4000 and 600 cm^{-1}. For each spectrum the background was recorded and subtracted from the sample profile.

3. Results and discussion

3.1. Nuclear magnetic resonance

The literature offers some reports on the effect of salts or ionic liquids on the NMR spectra of organic molecules, and the study of Hofmeister phenomena by means of NMR techniques is attracting an ever growing attention [34–40]. However a systematic study on specific ion effects induced by a series of selected electrolytes on the NMR spectral properties of glycerol carbonate has not been published yet.

NMR spectra were recorded on saturated solutions of KF, K_2CO_3, K_3PO_4, KCl, KBr, KI, K_2SO_4 and KOCN in GC at room temperature. Fig. 1 shows the NMR of pure GC, and of its saturated solutions of different potassium salts. The individual spectra are reported in the Supplementary material (see Figs. S1–S15).

The change in the shift (δ) of the alcoholic proton was quantified through the shift index I_S defined as:

$$I_S = 100\frac{\delta_{sol} - \delta_0}{\delta_0} \quad (2)$$

where δ_0 (4.42 ppm) and δ_{sol} are the chemical shifts of the —OH in pure GC and in the saturated salt solution, respectively. The values of I_S are reported in Table 2 and follow the trend:

$$KF > K_3PO_4 > KOCN > K_2CO_3 > KCl > K_2SO_4 > KBr > KI$$

These results suggest that the major perturbation in the chemical shift of the —OH proton is produced by anions that behave as strong bases: fluoride, carbonate, phosphate, and cyanate. The deshielding of the hydrogen in the presence of these anions indicates an electron-poor environment around this nucleus. These results suggest that a quite strong interaction (hydrogen bonding) between the basic anion and the —OH group takes place in saturated solutions of KF, K_2CO_3 and K_3PO_4.

This evidence parallels our previous findings that showed the presence of ion pairs, triple ions and higher order clusters in saturated solutions of KF in GC through viscosity and conductivity measurements [1]. A similar study on the viscosity and conductivity of salt solutions in GC as a function of the solute concentration will be performed in a future work in order to detect the presence of ion pairs and higher clusters in GC salt solutions. After some time (about 30 h) saturated solutions of KF or K_3PO_4 slowly became yellowish due to the formation of 2,3-epoxy-1-propanol (glycidol) and CO_2 [41].

On the other hand other anions such as chloride, sulfate and bromide do not alter significantly the chemical environment around the alcoholic proton and/or the structuredness of the solvent.

Concerning the non-hydroxyl protons, all salts left unaltered the NMR spectrum of pure GC with the exception of KI, that produces a small but recordable change. In fact the H_X and H_Y shift from 3.70–3.84 (in pure GC) to 3.56–3.70 ppm, between 2% and 4% compared to pure GC (see Table 3). Due to this effect we recorded HSQC spectra on the GC + KI solution to double check the chemical shift and assignment of each proton (see Fig. S15 in the Supporting information).

Remarkably, KI induces a strong decrement in the value of δ resulting in a negative value of I_s. Since HI is a very strong acid and correspondingly iodide a very weak base, this behavior is rather related to the large polarizability of this anion and to the onset of significant dispersion interactions between the anion and the solvent molecules. We recall that the polarizability of I^- in ethylene carbonate was calculated to be as large as 3 Å^3 [3]. NMR spectra acquired on less concentrated solutions of the same salts did not show any significant variation of the chemical shift respect to δ_0, in fact a clear detectable change in the chemical shift was obtained using salt concentrations near the solubility limit.

Noticeably potassium iodide lowered the chemical shifts of the non-hydroxyl protons (between 2% and 4% respect to pure GC). The other investigated salts did not change the δ of the same nuclei respect to pure GC. We argue that this shielding effect is again due to the large polarizability of iodide that by approaching the GC ring creates an electron-richer environment around these protons.

3.2. Density

The density of pure GC was measured as a function of temperature between 15° and 50 °C (see Table 4).

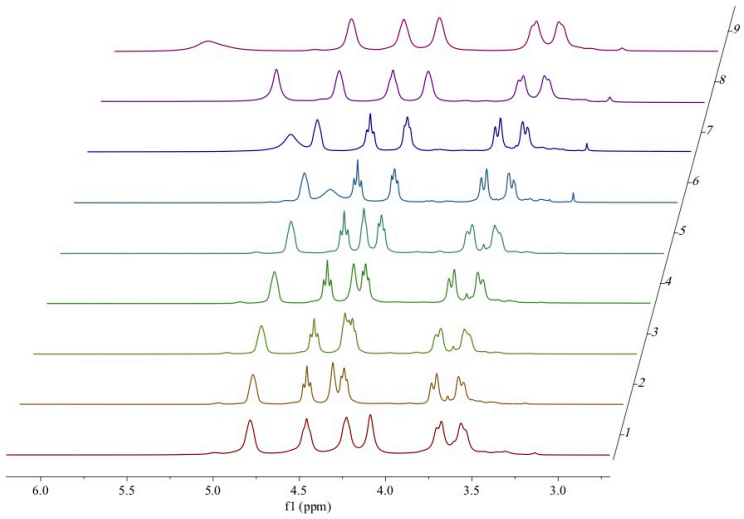

Fig. 1. NMR spectra of pure GC and of its saturated solutions with different potassium salts. 1: KI, 2: KBr, 3: pure GC, 4: K_2SO_4, 5: KCl, 6: K_2CO_3, 7: KCNO, 8: K_3PO_4, 9: KF.

A linear regression was used to fit the data:

$$\rho = 1.6750 - 9.4918 \cdot 10^{-4}\, T \tag{3}$$

To the best of our knowledge this is the first set of density values for GC at different temperatures. The only value we found in the literature was 1.40 g/mL at 25 °C, that agrees with our finding [6, 30].

3.3. Solubility and thermodynamics of solvation

The solubility of salts in GC at different temperatures was measured following the same procedure adopted in previous studies [3, 4]. We observed that potassium phosphate, sulfate and carbonate behave similarly to KF [1], i.e. the solvent can be easily oversaturated with these salts at all temperatures. In our previous study we concluded that this behavior is related to the formation of very stable ion pairs, triple ions (K_2F^+ and KF_2^-) and higher clusters, while the free K^+ and F^- ions represent only a minor fraction of the entire distribution [1]. We also concluded that the ion pairs are intercalated between solvent molecules through ion-dipole interactions between the cation and the carbonyl moiety, and hydrogen bond between the anion and the primary —OH residue. The NMR results reported in Section 3.1 suggest that a similar behavior occurs with phosphate, carbonate and cyanate. As a matter of fact K_3PO_4, K_2CO_3 and KOCN can produce oversaturated solutions in GC.

Such behavior changes when the anion is unable to establish hydrogen bonds with the solvent. Therefore we measured the solubility of KCl, KBr, KI and KOCN as a function of temperature between 25° and 45 °C. Table 5 reports the solubility of these electrolytes expressed in molal units (m) in the equilibrated saturated solutions. The solubility of all salts increases with the temperature, indicating that the dissolution process is endothermic.

From the experimental solubility the enthalpy, Gibbs free energy, and entropy changes of solution can be calculated from Eqs. (4)–(6) [42, 43], assuming that in the investigated temperature range they can be considered constant, and are listed in Table 6:

$$\Delta_{sol}G^0 = -RT\ln K_{sp} = -RT\ln(\gamma_{\pm} m)^2 \tag{4}$$

$$\Delta_{sol}H^0 = -2R\left[\frac{\partial \ln(\gamma_{\pm} m)}{\partial(1/T)}\right] \tag{5}$$

$$\Delta_{sol}S^0 = \left(\Delta_{sol}H^0 - \Delta_{sol}G^0\right)/T \tag{6}$$

$\gamma_{\pm}$ is the mean molal activity coefficient and K_{sp} the solubility product of the salt in GC. The calculation of $\gamma_{\pm}$ is derived from the Debye-Hückel theory and the Bjerrum formula, and outlined in the Appendix A. However imperfect these theories may be, the entropy

Table 2
Chemical shift (δ, in ppm) and shift index ($I_S \pm 0.5\%$) of saturated solutions of KF, KCl, KBr, KI, K_2CO_3, K_3PO_4, K_2SO_4 and KOCN. $CDCl_3$: $\delta = 7.26$ ppm.

Salt	δ	I_S
(Pure GC)	4.40	–
KF	5.66	28.6
K_3PO_4	5.18	17.7
KOCN	5.00	13.6
K_2CO_3	4.71	7.04
KCl	4.44	0.91
K_2SO_4	4.41	0.23
KBr	4.38	−0.34
KI	4.09	−7.05

Table 3
Chemical shifts (δ, in ppm) of the non-hydroxyl protons (see Scheme 1) in pure GC and in its saturated solution of KI.

	B,B′	C	D,D′
GC	3.70–3.84	4.88	4.35–4.57
KI	3.56–3.70	4.79	4.23–4.46

Table 4
Density (ρ, in g/mL) of pure GC as function of temperature (T, in K). σ is the standard deviation for each measured value. $R = 0.99998$.

T(K)	ρ (g/mL)	σ (g/mL)
288.0	1.4017	$1.7512 \cdot 10^{-6}$
293.0	1.3969	$5.0000 \cdot 10^{-7}$
298.0	1.3921	$1.2150 \cdot 10^{-6}$
303.0	1.3873	$8.3666 \cdot 10^{-7}$
308.0	1.3826	$1.2724 \cdot 10^{-6}$
313.0	1.3778	$9.8319 \cdot 10^{-7}$
318.0	1.3731	$9.8319 \cdot 10^{-7}$
323.0	1.3685	$8.9443 \cdot 10^{-7}$

changes are surely positive indicating that the addition of an electrolyte induces a remarkable perturbation in the liquid structure.

The thermodynamic parameters obtained for GC suggest that the dissolution of the electrolyte requires more energy than that involved in the orientation of the solvent dipole around the dissolved ions.

The experimental enthalpy change of solvation, $\Delta_{solv}H^0(exp)$, was calculated as:

$$\Delta_{solv}H^0(\ exp) = \Delta_{sol}H^0 - U \tag{7}$$

where U is the lattice energy of each solid.

For a given ion the Gibbs free energy, the enthalpy, and the entropy changes of solvation can be evaluated according to the modified Born theory that is basically an electrostatic model [45]:

$$\Delta_{solv}G^0 = -\frac{e^2N(\varepsilon-1)}{8\pi\varepsilon_0\varepsilon(r+\tau)} \tag{8}$$

$$\Delta_{solv}H^0 = -\frac{e^2N}{8\pi\varepsilon_0(r+\tau)}\left(1-\frac{1}{\varepsilon}-\frac{T}{\varepsilon^2}\frac{\partial\varepsilon}{\partial T}\right) \tag{9}$$

$$\Delta_{solv}S^0 = \frac{e^2N}{8\pi\varepsilon_0\varepsilon^2(r+\tau)}\left(\frac{\partial\varepsilon}{\partial T}\right) \tag{10}$$

where e is the electron charge, ε the dielectric constant, ε_0 the vacuum permittivity, r_i the crystal radius, T the absolute temperature and τ a fitting parameter. In the derivation of ΔH and ΔS from the derivative of ΔG respect to the temperature, τ is assumed to be temperature independent.

For GC, $(\frac{\partial\varepsilon}{\partial T})$ is about $-0.36\ K^{-1}$, and was estimated from the values of ε reported by Chernyak [5].

The solvation thermodynamic parameters were calculated following the procedure described in a previous work [3] and are listed in Table 7.

As with other polar solvents like dimethylformamide (DMF) or EC, the entropy of solvation change of the ions in GC are all negative and small. Thus, the balance between the disorder induced by the ion in the solvent and the re-ordering of the solvation GC molecules around the ion brings about a (small) lowering in the entropy [3]. The most effective re-structuring ion is K^+, while the anions have a smaller effect.

The values of $\Delta_{soln}S^0$ are quite similar to those that we calculated in ethylene carbonate, indicating a similar perturbation in the liquid structure upon dissolution of the salt [43].

Table 5
Solubility (in molal units, mol/kg) of electrolytes in GC as a function of temperature.

T (°C)	KCl	KBr	KI	KOCN
25°	$2.03 \cdot 10^{-3}$	$2.62 \cdot 10^{-3}$	$7.03 \cdot 10^{-3}$	$2.81 \cdot 10^{-3}$
30°	$4.45 \cdot 10^{-3}$	$5.30 \cdot 10^{-3}$	$13.4 \cdot 10^{-3}$	$3.66 \cdot 10^{-3}$
35°	$9.53 \cdot 10^{-3}$	$10.4 \cdot 10^{-3}$	$20.7 \cdot 10^{-3}$	$6.08 \cdot 10^{-3}$
40°	$19.0 \cdot 10^{-3}$	$19.6 \cdot 10^{-3}$	$24.6 \cdot 10^{-3}$	$14.4 \cdot 10^{-3}$
45°	$41.5 \cdot 10^{-3}$	$39.5 \cdot 10^{-3}$	$99.4 \cdot 10^{-3}$	$21.3 \cdot 10^{-3}$

Table 6
Enthalpy ($\Delta_{sol}H^0$, in kJ/mol), Gibbs free energy ($\Delta_{sol}G^0$, in kJ/mol), entropy ($\Delta_{sol}S^0$, in J/K·mol) changes of solution at 30 °C, lattice enthalpy (U, in kJ/mol), and the experimental enthalpy change of solvation ($\Delta_{solv}H^0(exp)$, in kJ/mol) calculated according to Eq. (7) for the investigated electrolytes in GC.

Salt	$\Delta_{sol}H^0$	$\Delta_{sol}G^0$	$\Delta_{sol}S^0$	U[a]	$\Delta_{solv}H^0(exp)$
KCl	234 ± 5%	27 ± 6%	683 ± 11%	715	−481 ± 5%
KBr	208 ± 5%	26 ± 6%	600 ± 11%	682	−474 ± 5%
KI	203 ± 8%	22 ± 7%	597 ± 15%	649	−446 ± 8%
KOCN	170 ± 11%	28 ± 7%	468 ± 18%	653[b]	−483 ± 11%

[a] See Ref. [44].
[b] Calculated value.

As in the case of EC the solvation process is enthalpy driven and dominated by K^+, while the solvation of anions is weaker (both in enthalpic and entropic terms).

Plotting the value of $\Delta_{solv}H^0$, calculated according to the Born equation (Eq. (9)) [45] as a function of the experimental value $\Delta_{solv}H^0(exp)$ from Eq. (7), we obtain the graph shown in Fig. 2:

The graph shows that the electrostatic Born model works quite well for all salts, except for KI for which there are significant deviations. This occurs also for ethylene carbonate [3]. The deviation is probably related to the non-electrostatic van der Waals interactions that iodide can establish with the solvent molecules due to its soft nature and large polarizability.

3.4. Differential scanning calorimetry

The thermal behavior of pure GC and of its saturated solutions was investigated through Differential Scanning Calorimetry (DSC). The DSC scans are reported in Fig. 3. From the DSC experiments we detected a glass transition temperature (T_g) that strongly depends on the nature of the added salt (see Table 8).

Compared to pure GC ($T_g = -70.8$ °C), KF, K_3PO_4, KOCN and K_2CO_3 induce a significant increment in the glass transition temperature, while KCl, KBr and K_2SO_4 do not modify T_g in a significant manner. A similar behavior was reported for glycerol and PC [46, 47]. The heat flow peak indicates the presence of two contributions, the ΔC_p at the glass transition temperature (T_g), and the endothermic peak related to the enthalpic recovery process. These can be separated by a modulated DSC experiment.

The large increment in the T_g of the liquid upon the addition of KF, K_3PO_4, KOCN and K_2CO_3 confirms a strong stiffening effect induced by the electrolyte on the solvent molecules structuredness as outlined in our previous work [1]. Unexpectedly, KI has the same effect as KF on the glass transition temperature of liquid GC, although it is not able to bind to the —OH group as do the basic anions. We argue that this result and the shielding effect induced by I^- on the protons of the ring may be explained by invoking a partial approach of I^- toward the glycerol carbonate's ring due to non-electrostatic van der Waals forces that involve this anion and the solvent molecules. Probably this phenomenon perturbs the structuredness, reduces the mobility of the solvent molecules and hence increases the glass transition temperature [48]. Further studies are necessary to detail the specific mechanism through which these phenomena occur.

Table 7
Calculated ion solvation free energy (ΔG^{calc}_{solv}, in kJ·mol^{-1}), enthalpy ($\Delta_{solv}H^0$, in kJ·mol^{-1}) and entropy ($\Delta_{solv}S^0$, in J·K^{-1}·mol^{-1}) changes (see Eqs. (8)–(10)) at 30 °C, crystallographic radius (r, in Å), experimental best fitting τ (in Å), for different ions in glycerol carbonate.

Ion	$\Delta_{solv}G^0$	$\Delta_{solv}H^0$	$\Delta_{solv}S^0$	r	τ
K^+	−296	−300	−13	1.33	1.0
Cl^-	−181	−183	−7	1.81	2.0
Br^-	−174	−176	−7	1.96	2.0
I^-	−178	−180	−7	2.16	1.7
OCN^-	−179	−181	−7	2.34	1.5

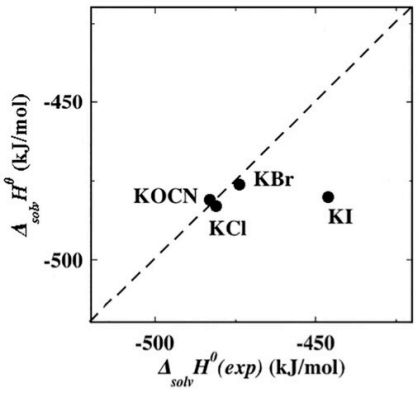

Fig. 2. Calculated $\Delta_{sob}H^0$ versus experimental solvation enthalpy change $\Delta_{sob}H^0(exp)$ at 30 °C for the investigated electrolytes in GC. The calculated value was obtained by summing the two contributions for the cation and the anion.

3.5. Attenuated Total Reflection-Fourier Transform Infrared Spectroscopy

The Attenuated Total Reflection-Fourier Transform Infrared Spectroscopy (ATR-FTIR) experiments indicate a shift of the O—H stretching band from the pristine 3420 cm^{-1} wavenumber that was found for pure GC (see Table 8).

The lowering in the frequency of the O—H signal induced by the presence of KF, K_3PO_4, KOCN and K_2CO_3 reflects the interaction between the hydroxyl moiety and the basic anion, that leads to a weakening in the O—H stretching mode. KI produces an effect comparable to that of KF with a significant shift (from 3420 to 3370 cm^{-1}) in the O—H stretching, indicating a weakening in the strength of the O—H bond. This result parallels the effect that we already recorded in NMR and DSC experiments on KI + GC samples and can be related to the partial adsorption of iodide ions near the GC ring.

Table 8
Glass transition temperature (T_g, in °C) and wavenumber ($\bar{\nu}$ in cm^{-1}) for the O—H stretching absorption in saturated solutions of salts in GC at 25 °C.

Salt	T_g	$\bar{\nu}$
(Pure GC)	−70.8	3420
KF	−61.3	3370
K_3PO_4	−57.4	3398
KOCN	−58.5	3404
K_2CO_3	−62.8	3409
KCl	−70.4	3425
K_2SO_4	−70.0	3428
KBr	−66.5	3408
KI	−61.5	3372

4. Conclusion

The results indicate the dissolution of an electrolyte in glycerol carbonate occurs via two different solvation mechanisms. On one hand the potassium cation interacts with the carbonyl group through simple electrostatic ion-dipole interactions. On the other hand the role played by the anion greatly depends on its nature. If the anion has a strong basic nature, then it interacts with the hydroxyl moiety through hydrogen bonding. This would modify the structuredness of the solvent significantly. Instead, if the anion is not an acceptor, then its interaction with the solvent molecule is minimal. However, in the case of iodide, we recorded a peculiar behavior reminiscent of the effect induced by the very basic fluoride anion. Taking into account the large static polarizability of GC, we discussed this anomaly in terms of polarizability-related non-electrostatic van der Waals interactions that brings the anion close to the GC ring.

In conclusion, if the anion behaves as a strong base in a protic solvent, then the formation of hydrogen bonding is the main feature that determines the behavior of the salt in the solution. On the other hand when the anion cannot participate in a hydrogen bond, then other kinds of interactions, such as van der Waals non-electrostatic forces are at play and in this case specific ion effects emerge.

As a natural extension of this work we envisage the study of the effect induced by more salts (including nitrate, thiocyanate, perchlorate, chlorate, tetrabutylammonium, tetraphenylborate, etc.), the experimental measurements of the activity coefficient, and the acquisition of SAXS profiles on GC solutions in the presence of different salts. We are confident that the new experiments will cast new light on the specific interactions between ions such as iodide and glycerol carbonate molecules.

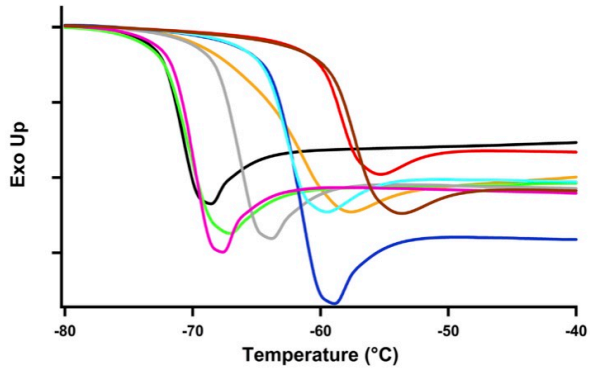

Fig. 3. DSC curves for pure GC (black), KF (orange), KCl (green), KBr (grey), KI (dark blue), KOCN (red), K_2CO_3 (light blue), K_2SO_4 (pink) and K_3PO_4 (brown) saturated solutions.

Appendix A. Mean molal activity coefficient

The mean molal activity coefficient for the free ions ($\gamma_{\pm}$) was estimated through the Debye-Hückel theory as Refs. [3, 49]:

$$log\gamma_{\pm} = -\frac{A\sqrt{m}}{1 + Ba\sqrt{m}} \quad (A1)$$

Here m is the molal concentration of the salt.

$$A = 1.8247 \cdot 10^6 \sqrt{\frac{\rho}{\varepsilon^3 T^3}} \quad (A2)$$

$$B = 50.2901 \sqrt{\frac{\rho}{\varepsilon T}} \quad (A3)$$

where ρ, ε and T are the density and the static dielectric constant of the solvent, and the absolute temperature, respectively. A is in $kg^{1/2} \cdot mol^{-1/2}$ and B in $kg^{1/2} \cdot mol^{-1/2} \cdot Å^{-1}$. a is the distance of closest approach. For fully dissociated 1:1 electrolytes a can be taken as the Bjerrum length q:

$$q = \frac{e^2}{2\varepsilon k_B T} \quad (A4)$$

where e and k_B are the elementary charge and the Boltzmann constant, respectively.

Table A1 shows the values of ε, A, q, and B as a function of temperature that were used for the calculation of the average ionic activity coefficients in GC solutions (see Table A2).

Table A1
Values of ε, A, q, and B as a function of temperature used for the calculation of $\gamma_{\pm}$ in GC solutions.

T	ε	A	q	B
25.1	109.6	0.3642	2.5558	0.3281
30.1	107.8	0.3635	2.5556	0.3276
35.1	106.0	0.3632	2.5569	0.3271
39.7	104.3	0.3631	2.5593	0.3267
45.0	102.4	0.3633	2.5635	0.3264

Table A2
Values of $\gamma_{\pm}$ for the different salts in GC as a function of temperature according to Eqs. (A1)–(A4).

T	$\gamma_{\pm}$ (KCl)	$\gamma_{\pm}$ (KBr)	$\gamma_{\pm}$ (KI)	$\gamma_{\pm}$ (KOCN)
25.1	0.99158	0.98354	0.97187	0.98167
30.1	0.98294	0.97113	0.96241	0.97928
35.1	0.97616	0.96349	0.95443	0.97377
39.7	0.95875	0.93207	0.95093	0.96114
45.0	0.92919	0.90071	0.91333	0.95380

Appendix B. Supplementary data

Supplementary data to this article can be found online at https://doi.org/10.1016/j.molliq.2018.06.120.

References

[1] F. Sarri, D. Tatini, M. Ambrosi, E. Carretti, B.W. Ninham, L. Dei, P. Lo Nostro, J. Mol. Liq. 255 (2018) 397.
[2] V. Mazzini, V.S.J. Craig, Chem. Sci. 8 (2017) 7052.
[3] N. Peruzzi, B.W. Ninham, P. Lo Nostro, P. Baglioni, J. Phys. Chem. B 116 (2012) 14398.
[4] N. Peruzzi, P. Lo Nostro, B.W. Ninham, P. Baglioni, J. Solut. Chem. 44 (2015) 1224.
[5] Y. Chernyak, J. Chem. Eng. Data 51 (2006) 416.
[6] M.O. Sonnati, S. Amigoni, E.P. Taffin de Givenchy, T. Darmanin, O. Choulet, F. Guittard, Green Chem. 15 (2013) 283.
[7] C.S. Hong, R. Wakslak, H. Flnston, V. Fried, J. Chem. Eng. Data 27 (1982) 27 (146.).
[8] M.S. Ding, J. Chem. Eng. Data 49 (2004) 276.
[9] S.P. Verevkin, A.V. Toktonov, Y. Chernyak, B. Schäffner, A. Börner, Fluid Phase Equilib. 268 (2008) 1.
[10] Y. Nannoolal, J. Rarey, J. Ramjugernath, J. Fluid Phase Equilib. 252 (2007) 1.
[11] R. Naejus, C. Damas, D. Lemordant, R. Coudert, J. Chem. Thermodyn. 34 (2002) 795.
[12] R. Bosque, J. Sales, J. Chem. Inf. Comput. Sci. 42 (2002) 1154.
[13] S. Nir, S. Adams, R. Rein, J. Chem. Phys. 59 (1973) 3341.
[14] P. Lo Nostro, B.W. Ninham, Chem. Rev. 112 (2012) 2286.
[15] B.W. Ninham, R.M. Pashley, P. Lo Nostro, Curr. Opin. Colloid Interface Sci. 27 (2016) 25.
[16] T. Duignan, D.F. Parsons, B.W. Ninham, J. Phys. Chem. B 118 (2014) 3122.
[17] T. Duignan, D.F. Parsons, B.W. Ninham, Chem. Phys. Lett. 635 (2015) 1.
[18] B.W. Ninham, P. Lo Nostro, Water, salt and oil, in: P. Lo Nostro, B.W. Ninham (Eds.), An Exploration of the Foundations of mOlecular Forces in "Aqua Incognita: Why Ice Floats on Water and Galileo 400 Years on", Connor Court Publishers, Ballarat 2014, pp. 103–126.
[19] B.W. Ninham, Substantia 1 (2017) 7.
[20] P. Lo Nostro, B.W. Ninham, Curr. Opin. Colloid Interface Sci. 23 (2016) A1.
[21] D.F. Parsons, M. Boström, P. Lo Nostro, B.W. Ninham, Phys. Chem. Chem. Phys. 13 (2011), 12352.
[22] B.W. Ninham, R.A. Sammut, J. Theor. Biol. 56 (1976) 125.
[23] X.N. Ying, Phys. Scr. 88 (2013), 025603.
[24] U.R. Pedersen, P. Harrowell, J. Phys. Chem. B 115 (2011) 14205.
[25] K. Koperwas, K. Adrjanowicz, Z. Wojnarowska, A. Jedrzejowska, J. Knapik, M. Paluch, Sci. Rep. 6 (2016) 36934.
[26] R. Zondervan, T. Xia, H. van der Meer, C. Storm, F. Kulzer, W. van Saarloos, M. Orrit, Proc. Natl. Acad. Sci. U. S. A. 105 (2008) 4993.
[27] M. Köhler, P. Lunkenheimer, A. Loid, Eur. Phys. J. E 27 (2008) 115.
[28] P.U. Okoye, A.Z. Abdullah, B.H. Hameed, J. Taiwan Inst. Chem. Eng. 68 (2016) 51.
[29] P.U. Okoye, A.Z. Abdullah, B.H. Hameed, Energ. Convers, Manage 133 (2017) 477.
[30] Y.M. Delavoux, M. Gilmore, M.P. Atkins, M. Swadzba-Kwasny, J.D. Holbrey, Phys. Chem. Chem. Phys. 19 (2017) 2867.
[31] Z. Zhang, D.W. Rackemann, W.O.S. Doherty, I.M. O'Hara, Biotechnol. Biofuels 6 (2013) 153.
[32] M. Pagliaro, R. Ciriminna, H. Kimura, M. Rossi, C. Della Pina, Angew. Chem. Int. Ed. 46 (2007) 4434.
[33] J.R. Ochoa-Gómez, O. Gómez-Jiménez-Aberasturi, C. Ramírez-López, M. Belsué, Org. Process. Res. Dev. 16 (2012) 389.
[34] A. Strate, V. Overbeck, V. Lehde, J. Neumann, A.M. Bonsa, T. Niemann, D. Paschek, D. Michalik, Ralf Ludwig, Phys. Chem. Chem. Phys. 20 (2018) 5617.
[35] N.O. Johnson, T.P. Light, G. MacDonald, Y. Zhang, J. Phys. Chem. B 121 (2017) 1649.
[36] C. Wiedemann, O. Ohlenschläger, C. Mrestani-Klaus, F. Bordusa, Phys. Chem. Chem. Phys. 19 (2017) 24115.
[37] J.W. Bye, N.J. Baxter, A.M. Hounslow, R.J. Falconer, M.P. Williamson, ACS, Omega 1 (2016) 669.
[38] G. Bekçioğlu-Neff, C. Allolio, Y.S. Desmukh, M. Ryan Hansen, D. Sebastiani, ChemPhysChem 17 (2016) 1166.
[39] J. Shi, J. Wang, J. Phys. Chem. B 118 (2014) 12336.
[40] L.I.N. Tomé, F.R. Varanda, M.G. Freire, I.M. Marrucho, J.A.P. Coutinho, J. Phys. Chem. B 113 (2009) 2815.
[41] D.J. Darensbourg, A.D. Yeung, Green Chem. 16 (2014) 247.
[42] J. Strong, T.R. Tuttle, J. Phys. Chem. 77 (1972) 533.
[43] C.M. Criss, E. Luksha, J. Phys. Chem. 72 (1968) 2966.
[44] C.R. Gopikrishnan, D. Jose, A. Datta, AIP Adv. 2 (2012), 012131.
[45] M. Salomon, J. Phys. Chem. 74 (1970) 2519.
[46] A.G. Lyapin, E.L. Gromnitskaya, I.V. Danilov, V.V. Brazhkin, RSC Adv. 7 (2017) 33278.
[47] J. Geschwind, H. Frey, Macromolecules 46 (2013) 3280.
[48] J.M.G. Cowie, V. Arrighi, Polymers: Chemistry and Physics of Modern Materials, 3rd edition CRC Press, Boca Raton, 2007.
[49] F. Hernández-Luis, M.V. Vazquez, M.A. Esteso, Fluid Phase Equilib. 218 (2004) 295.